THE DEVELOPMENT OF A SOLAR IRRADIANCE NOWCASTING METHOD FOR BUILDINGS

By

LEI CHEN

Supervisors: Prof. Zhiwen Luo
Dr. Du Hu
Dr. Simon Lannon
Prof. Yu-Kun Lai

Thesis submitted in accordance with the requirements of the Cardiff University for the degree of Doctor in Philosophy

In The

Welsh School of Architecture
Cardiff University, United Kingdom

Date of submission: 9th July 2024

Abstract

To control the environmental problems caused by the ever-growing global greenhouse gas emissions, reducing carbon emissions from buildings is necessary. Although solar energy has been widely used in buildings to reduce carbon emissions, its instability poses significant challenges to its utilisation and thus a large number of solar irradiance forecasting methods have been developed to anticipate its fluctuations. However, these methods are usually not customised for buildings and are not developed based on the needs of future building intelligence.

Consequently, the aim of this research is to develop a solar irradiance nowcasting method with high spatial-temporal resolution based on low-cost equipment and user-friendly programming to achieve reliable nowcasting of Global Horizontal Irradiance (GHI), Direct Normal Irradiance (DNI), and Diffuse Horizontal Irradiance (DHI) for buildings and their future development.

In general, this research first applied a clear systematic review methodology to identify appropriate forecasting methods for buildings. Secondly, through using low-cost equipment and user-friendly programming, this research develops a solar irradiance nowcasting method with very short-term forecasting horizons and high spatial-temporal resolution based on a promising Residual Neural Network (ResNet-152) model to achieve 10-sec, 1-min, 5-min, and 10-min nowcasting of GHI, DNI and GHI. Thirdly, a series of comparative tests are conducted to explore the effect of different factors on the nowcasting performance and the results of these comparative tests are verified by selected evaluation metrics. Finally, this research discusses the current and potential applications of the solar irradiance nowcasting method on buildings to demonstrate the practicality this research.

Based on the results verification and analysis of comparative tests, the developed nowcasting method demonstrates evident reliability under the influence of different factors, including various time intervals, forecasting horizons, sky conditions, forecasting models and datasets.

In conclusion, the significance of this research is to innovatively explore a solar irradiance nowcasting method from an architectural perspective and achieve reliable nowcasting of GHI, DNI and DHI for optimising the operational efficiency and safety, occupant comfort and design of buildings. Also, this research establishes an interdisciplinary methodology integrating the knowledge of meteorology, imagery, computer science and architecture, which can increase interdisciplinary communication and cooperation, as well as provide more research directions. Ultimately, the specific approaches, tools and outcomes of the research, as well as the discussion of the possible applications of solar irradiance nowcasting on buildings, provide initial inspiration for future research and the future development of buildings.

Acknowledgments

First of all, I would like to express my sincerest gratitude to my supervisors, Prof. Zhiwen Luo and Dr. Hu Du, who have supported, guided, and encouraged me throughout my PhD journey. Secondly, I would like to thank my second and third supervisors, Dr. Simon Lannon and Prof. Yu-kun Lai, for their specialised advice and comments on my thesis. In addition, I would like to thank Ms. Katrina Leweis, Dr. Zhehao Cui and Ms. Shanshan Liu, who always help me throughout my PhD journey. Finally, I would like to thank my family, especially my wife, Shanshan Liu, for their unconditional love and support during my PhD program.

Table of Contents

List of Figures

List of Tables

Acronyms

ANN	Artificial Neural Network
ANFIS	Adaptive Neuro-Fuzzy Inference System
API	Application Programming Interface
ARIMA	Auto Regressive Integrated Moving Average
ASI	All-Sky Imager
BESS	Battery Energy Storage System
BP	Back Propagation
CNN	Convolutional Neural Network
CPV	Concentrated Photovoltaic
DHI	Diffuse Horizontal Irradiance
DL	Deep Learning
DNI	Direct Normal Irradiance
DRWNN	Deep Recurrent Wavelet Neural Network
EMS	Energy Management System
ESN	Echo State Network
ETS	Ensemble Transform Smoother
FFNN	Feed Forward Neural Network
FS	Forecast Score
GARCH	Generalized Autoregressive Conditional Heteroskedasticity
GHI	Global Horizontal Irradiance
GRU	Gated Recurrent Unit

HDR	High Dynamic Range
HEMS	Home Energy Management System
HSH	Honda Smart Home
HVAC	Heating, Ventilation, and Air Conditioning
GFS	Global Forecast System
kNN	K-Nearest Neighbors
LAD	Least Absolute Deviations
LSTM	Long Short-Term Memory
MAD	Mean Absolute Deviation
MAE	Mean Absolute Error
MAPE	Mean Absolute Percentage Error
MABE	Mean Absolute Biased Error
MBE	Mean Bias Error
MCM	Markov-chain mixture
MeAPE	Median Absolute Percentage Error
ML	Marchine Learning
MLP	Multilayer Perceptron
MPE	Mean Percentage Error
MSE	Mean Squared Error
NAM	North American Mesoscale model
NEO	NASA Earth Observations
NOAA	National Oceanic and Atmospheric Administration
nMAE	Normalized Mean Absolute Error
nMBE	Normalized Mean Bias Error
nRMSE	Normalized Root Mean Squared Error
NWP	Numerical Weather Prediction

PM	Persistence Model
PV	Photovoltaic
R	Correlation Coefficient
R^2	Coefficient of Determination
ResNet	Residual Neural Network
RMSD	Root Mean Square Deviation
RMSE	Root Mean Squared Error
rMAE	Relative Mean Absolute Error
rMBE	Relative Mean Bias Error
RNN	Recurrent Neural Network
rRMSE	Relative Root Mean Squared Error
SDG	Sustainable Development Goal
SS	Skill Score
SVM	Support Vector Machine
SVR	Support Vector Regression
TDA	Topology Data Analysis
TSI	Total Sky Imager
WNN	Wavelet Neural Network
WRF	Weather Research and Forecasting model

Chapter One

1 Introduction

This chapter offers a thorough introduction to this thesis, beginning with an explanation of the research background. Subsequently, the problem statement and the importance of the research are presented. Following this, the aim, focus and scope of this research are proposed. After that, this chapter identifies research gaps, poses research questions, and sets forth research objectives and procedures. Finally, an outline of the thesis is provided

1.1 Research Background

The ever-growing global greenhouse gas emissions will inevitably lead to a series of environmental issues, including the rise of average global temperature, climate changes and other catastrophes. The World Meteorological Organization's (WMO) provisional statement of Global Climate 2023 mentioned concentrations of the three leading greenhouse gases - carbon dioxide, methane, and nitrous oxide - reached record highs in 2022 and continued to increase in 2024 [1]. In this case, global mean temperature likely made the past ten years, 2015 to 2024, the warmest years on record and sea levels reached a new record high in 2023. Thus, reducing carbon emissions from living and production is the inevitable choice for controlling greenhouse gas emissions.

1.1.1 Renewable Energy and Solar Energy

The use of non-renewable energy, particularly fossil fuels such as coal, oil, and natural gas, in living and production is undoubtedly the crucial cause of the increase in carbon emissions [2]. Unlike non-renewable resources, renewable energy such as solar, wind, geothermal, and tidal energy can be continuously replenished from natural processes, and the use of them almost does not produce air pollutants. Therefore, using renewable energy has become a consensus in human society.

Presently, the utilisation of renewable energies has become a global tendency with rapidly growing awareness of sustainable development [3-5]. Meanwhile, more and more international organisations and major players in the world economy have dedicated themselves to enacting policies to control carbon emissions that contribute to utilising renewable energies. For example, the European Union EU aims to reduce greenhouse gas emissions by at least 55% by 2030 by accelerating renewable energy utilisation and become a climate-neutral continent by 2050 [1].

Among the various renewable energies, solar energy undoubtedly plays a crucial role because it has the highest energy potential. At first, solar energy is inexhaustible

as long as the sun exists. Secondly, solar energy is a clean energy source. It generates electricity or heat by converting solar light or thermal energy, a process that does not emit pollutants. In addition, solar energy is also the cause of many other energy sources [6]. For instance, wind energy is a converted form of solar energy. The uneven heating of the earth's surface due to solar radiation leads to an unbalanced pressure distribution in the atmosphere, resulting in the formation of winds. Lastly, solar energy is abundant in most regions of the world. Figure 1.1 shows the long-term average of daily or yearly Global Horizontal Irradiance (GHI) worldwide. It demonstrates the enormous potential of solar energy worldwide. Therefore, solar energy has profound value as a renewable, clean and promising energy resource [7].

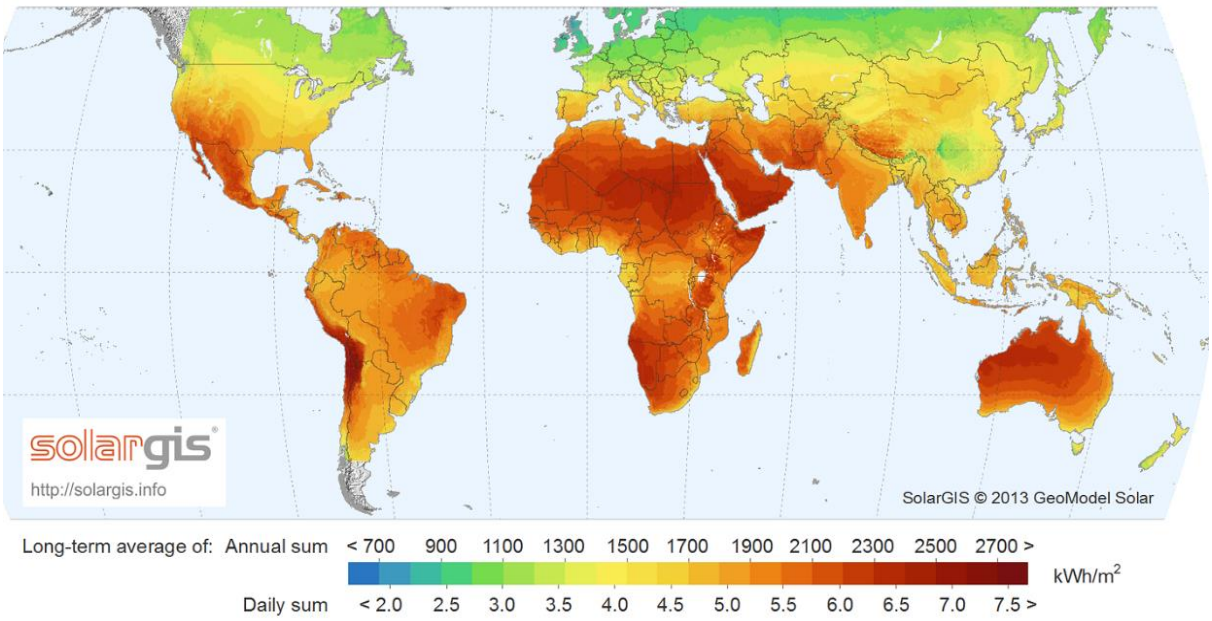

Figure 1.1 The Long-Term Average of Daily or Yearly GHI over The World

(Resource: https://commons.wikimedia.org/wiki/File:SolarGIS-Solar-map-World-map-en.png)

1.1.2 Solar Irradiance Forecasting and Solar Irradiance Forecasting Methods

Although the potential value of solar energy is undoubted, the utilisation of solar energy is often accompanied by a series of challenges due to its instability induced by the dynamic nature of sun movement, cloud transitions, water vapour, and air pollution. Figure 1.2 (a) presents the variation of GHI over a representative day [8, 9]. From an

overall perspective, the variation of GHI follows the diurnal cycle of the sun's movement. GHI starts from zero at sunrise and achieves peak around noon, finally close to zero when sunset arrives. In terms of details, the frequent variation of the relative position between the sun and clouds brings significant fluctuations of GHI, which brings instability to the daily pattern of GHI, as presented in Figure 1.2 (b). Based on the above, understanding the patterns of solar energy variation in advance, especially the variations in solar irradiance, can significantly help the utilisation of solar energy. Thus, a vast number of methods have been explored to achieve reliable solar irradiance forecasting.

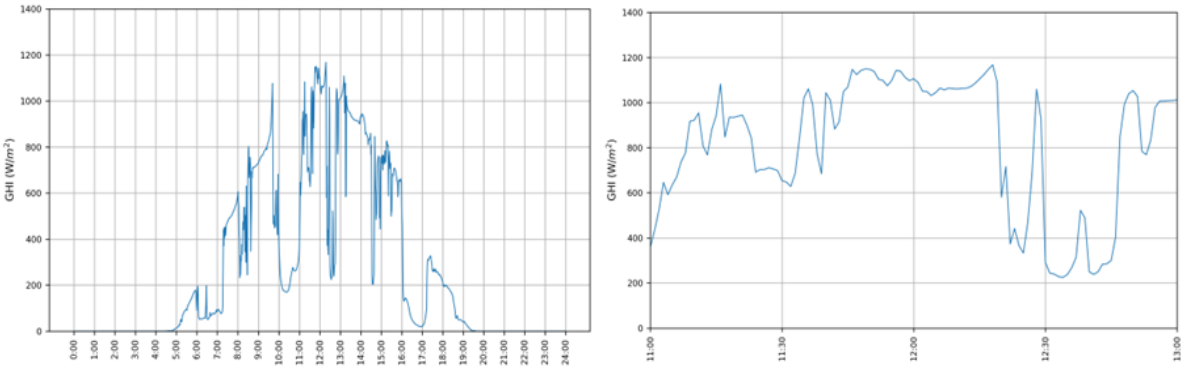

Figure 1.2 (a)The Variation of GHI over A Representative Day. (b) A Zoomed View for 11:00-13:00.

Solar irradiance forecasting methods can be categorised according to different characteristics, including technologies, data acquisition way, forecasting horizons, forecasting parameters, etc. For example, according to the forecasting horizon, solar irradiance forecasting methods can be classified into Day-ahead forecasting methods, Intra-day forecasting methods, Intra-hour forecasting methods and Intra-minute forecasting methods. Among the abovementioned characteristics, forecasting technology is most often used to classify forecasting methods. In this case, a series of comprehensive reviews have proposed their classification of solar irradiance forecasting methods according to different characteristics [10-12]. Refer to their viewpoints, solar irradiance forecasting methods are classified into the following five categories in this research:

- Numerical Weather Prediction methods (NWPs).
- Statistical and Learning methods.
- Top-down forecast methods.
- Bottom-up forecast methods.
- Hybrid methods.

These different solar irradiance forecasting methods were developed according to various forecasting purposes and thus can achieve decent performance in their designated spatial-temporal resolution. A detailed explanation of these forecasting methods will be given in the next chapter.

1.1.3 Solar Irradiance Nowcasting Methods for Buildings

Building is the basis of human living and production. However, about 37% of carbon emissions and 36% of the world's total energy consumption are related to buildings and related construction, according to the 2021 Global Status Report for Buildings and Construction [13]. Therefore, applying renewable energy in buildings is undoubtedly a significant task to reduce conventional fossil energy's cost and carbon emissions[14]. In this context, solar energy has been widely used in buildings, and thus, the value of solar irradiance forecasting for buildings is evident.

At present, solar irradiance forecasting methods are widely used in large regional power grids and infrastructure with solar energy applications for energy conservation, energy management, equipment protection, etc. For example, some solar irradiance forecasting methods were utilised to avoid damage to the system devices of giant electrical grids from sudden changes in unstable solar conditions. In general, extensive areas, low frequency and long forecasting horizons are the main characteristics of these solar irradiance forecasting methods. However, the abovementioned characteristics of solar irradiance forecasting methods are not optimal for specific single buildings or groups of buildings. Fortunately, a series of opportunities have emerged recently to support the development of new solar irradiance forecasting methods for buildings.

First of all, the development of building intelligence, such as the concept of “Smart Building”, aims to utilise environmental information, connected technologies and automated management to enhance buildings’ operational efficiency, safety and occupant comfort [15-17]. Specific technologies of building intelligence may include efficient energy management systems, automated control strategies, and the integration of smart devices and sensors for optimising lighting, temperature control and other building functions. In this context, demand for on-site and high-frequency environmental data environmental information, especially meteorological data (including solar irradiance, temperature, humidity, wind speed, etc.), has increased significantly.

Secondly, the rapid growth of the 5G internet will enormously improve unit data propagation speed and data capacity that thus can construct an advanced infrastructure for linking solar energy forecasting systems (data collection, analysis and prediction) with solar energy application systems (electricity, heating, cooling, lighting). In this case, high-speed and high-capacity interactions between solar energy forecasting systems and solar energy application systems provide the foundation for utilising solar irradiance forecasting on intelligent buildings.

Most importantly, the recent emergence of solar irradiance nowcasting methods contributes to on-site, high-frequency and short to very short-term solar irradiance forecasting, which is very appropriate for intelligent buildings. In meteorological terms, nowcasting refers to the forecast of the time horizons from the next few seconds up to six hours [18].

To sum up, the opportunities and benefits of exploring appropriate solar irradiance nowcasting to develop building intelligence are apparent. Therefore, this research aims to develop a new solar irradiance nowcasting for buildings.

1.2 Statement of Problem

With the development of building intelligence, the link between environmental information and buildings is becoming increasingly strong. One of the most important environmental information is meteorological data. In recent years, it has become common to use the forecasting of meteorological data to predict and optimise the building's performance [19, 20]. Meteorological data in forecasting generally involves a series of weather parameters, such as temperature, humidity, wind speed, air pressure, and solar irradiance. The difficulty of obtaining the forecasting of various weather parameters is very different, as well as the reliability of the forecasting of various weather parameters. For buildings, reliable solar irradiance forecasting is undoubtedly the most difficult to obtain compared to other weather parameters forecasting because of its high instability and a series of specific reasons.

At first, there are relatively fewer sources for obtaining solar irradiance forecasting compared to other weather parameters. In general, the sources of solar irradiance forecasting mainly include national or regional meteorological institutions, commercial companies, and public meteorological stations because only these agencies can utilise sophisticated techniques and afford expensive equipment. In recent years, some have started offering online Weather Application Programming Interfaces (APIs) to provide weather data services to their customers. However, only a few Weather APIs can provide solar irradiance forecasting. Solar irradiance forecasting from the above sources is usually unavailable to the public or requires high purchase prices and is therefore not favourable to the utilisation of specific single buildings or groups of buildings. Thus, exploring appropriate solar irradiance forecasting methods according to the needs of buildings is necessary.

More importantly, the solar irradiance forecasting provided by the abovementioned sources is unreliable for buildings because of the spatial-temporal resolution and forecasting horizon. In this research, spatial resolution refers to the specificity of the forecast areas, and temporal resolution refers to the frequency of the forecast

occurrence. Meanwhile, forecasting horizon refers to how far ahead the forecast predicts the future. Generally, solar irradiance forecasting methods used in the abovementioned sources are usually characterised by low spatial-temporal resolution and medium- to long-term forecasting horizons, which is not ideal for buildings. In this research, low spatial-temporal resolution means wide-area and low-frequency. For example, although some public weather stations can obtain solar irradiance forecasting, the distance between weather stations is often several kilometres or more. As a result, the reliability of solar irradiance forecasting is reduced due to the different locations of a weather station and a specific building. In addition, solar irradiance forecasting from the abovementioned sources can only provide low-frequency and long- to medium-term forecasting on a day or hour scale rather than short- to very short-term nowcasting on a minute or second scale, limiting the future development of more sophisticated building systems operation and management. Emerging solar irradiance nowcasting methods are characterised by short to very short-term forecasting horizons and high spatial-temporal resolution, so it is necessary to study these methods for the future development of buildings.

Apart from spatial-temporal resolution and forecasting horizon, equipment and programming are crucial to utilising solar irradiance forecasting in buildings. Generally, equipment and programming for solar irradiance forecasting used by national or regional meteorological institutions, commercial companies, and public weather stations are expensive and not easy to use for the public. However, low-cost equipment and user-friendly programming are better suited for widespread building use.

In addition, the forecasting parameters are also significant. Most solar irradiance forecasting methods are mainly focused on forecasting Global Horizontal Irradiance (GHI), Direct Normal Irradiance (DNI), Photovoltaic (PV) power, etc. However, Diffuse Horizontal Irradiance (DHI), one of three crucial components of solar irradiance, is usually ignored. In fact, GHI is the sum of DNI and DHI. In many building simulation or system control programs, DNI and DHI need to be used directly, or GHI is converted

to DNI and DHI for use. Thus, forecasting GHI, DNI, and DHI is valuable for buildings.

At last, the possibilities that emerging solar irradiance nowcasting methods bring to the future development of buildings have not yet received attention. Hence, discussing current or potential applications of solar irradiance nowcasting methods in buildings is worthwhile.

1.3 Importance of the Research

Although a large number of solar irradiance forecasting methods have been developed in the last decades, these solar irradiance forecasting methods are usually not tailored for buildings and are not ideal for the potential needs of intelligent buildings for the future. Therefore, the critical purpose of this research is to seize the opportunities presented by the recent development of building intelligence, the 5G internet and the emerging solar irradiance nowcasting methods with high spatial-temporal resolution to develop a suitable solar irradiance forecasting method for buildings and to discuss its possible applications in the present or future.

The importance of this research is to explore a solar irradiance nowcasting method appropriate for buildings and their future development from an architectural perspective and thus achieve reliable nowcasting of GHI, DNI and DHI for optimising building performance. As a result, this research will investigate what solar irradiance forecasting methods are more appropriate for buildings and then combine knowledge of meteorology, imagery, computer science and architecture to develop an interdisciplinary research methodology for solar irradiance nowcasting. Then, this research will apply the developed solar irradiance nowcasting method to achieve GHI, DNI and DHI nowcasting and evaluate the nowcasting reliability. Ultimately, this research attempts to discuss the potential value of solar irradiance nowcasting to buildings and the development of future buildings, which provides initial inspiration for subsequent research.

In this case, the main concerns of this research will address the following aspects:

- Exploring an appropriate solar irradiance forecasting method for buildings to move away from the limitations of the current sources of solar irradiance forecasting.
- Developing a solar irradiance nowcasting method to meet the potential needs of buildings for high spatial-temporal resolution and short to very short-term forecasting.

- Studying low-cost equipment and user-friendly programming for the developed solar irradiance nowcasting method to increase its building practicality.
- Nowcasting GHI, DNI and DHI to provide the three most critical foundational data of solar irradiance for the applications of buildings.
- Evaluating the nowcasting results to verify the reliability of the developed solar irradiance nowcasting method.
- Discussing possible applications of the developed solar irradiance nowcasting methods in buildings, thus stimulating more researchers' interest.

1.4 Research Aim

This research aims to develop a solar irradiance nowcasting method with high spatial-temporal resolution based on low-cost equipment and user-friendly programming to achieve reliable GHI, DNI and DHI nowcasting for buildings and their future development.

Specifically, this research will first conduct desktop and field studies to quantify the impact of unstable solar irradiance on building performance and review the research of solar irradiance forecasting methods; then develop an appropriate and reliable solar irradiance nowcasting method for buildings, combining multiple forecasting methods, low-cost equipment and user-friendly programming; finally use the proposed solar irradiance nowcasting methods to achieve the nowcasting of three critical solar irradiance components involving GHI, DNI and DHI and discuss their current and potential applications in buildings.

1.5 Research Focus and Scope

1.5.1 Research Focus

This research is centred on developing a solar irradiance nowcasting method for buildings. In this case, the major concerns of this research include:

- The review of solar irradiance forecasting methods.
- The nowcasting horizon and the spatial-temporal resolution of the solar irradiance nowcasting method.
- Equipment and programming for implementing the solar irradiance nowcasting method.
- The nowcasting of GHI, DNI and DHI and the verification of the nowcasting.
- The discussion of possible building applications of GHI, DNI and DHI nowcasting.

1.5.2 Area and Generalisation

Due to the influence of COVID-19 and parenting responsibility, this research has

been conducted in Shanghai, China, since 2021. Thus, the research area is Shanghai, China. Despite this, this research applies to most regions of the world except for some areas with an extreme lack of sunlight because the proposed solar irradiance nowcasting method in this research is linked only with solar irradiance. In other words, this research is not region-specific but general.

1.5.3 Nowcasting Horizon and Spatial-Temporal Resolution

The term 'nowcasting' in this research mainly covers the forecast of the time horizons from 10 seconds to 10 minutes, also known as ‘very short-term forecasting’. Specifically, this research's nowcasting horizons include 10 seconds, 1 minute, 5 minutes, and 10 minutes.

In addition, this research’s spatial resolution of the nowcasting is from 1 metre to 2 kilometres. The temporal resolutions of the nowcasting, like nowcasting horizons, are 10 seconds, 1 minute, 5 minutes, and 10 minutes.

1.5.4 Nowcasting Parameters

The three most critical foundational solar irradiance data are GHI, DNI, and DHI. GHI, DNI and DHI can not only be used directly in building simulation programs but can also be used to calculate PV power. Thus, this research only focuses on nowcasting GHI, DNI and DHI.

1.5.5 Building Applications of GHI, DNI and DHI Nowcasting.

The purpose of this research is to give initial inspiration for subsequent research by discussing current and potential applications of GHI, DNI and DHI nowcasting. Thus, this research will not present the specific content of applications.

1.6 Research Gaps

A series of literature reviews of solar irradiance forecasting methods have exhaustively presented various aspects of this field, including data acquisition methods, forecasting methods, forecasting parameters, evaluation metrics, etc [3, 10, 21-26]. Based on these literature reviews and architectural perspectives, several significant research gaps were summarised as follows:

1. Most literature reviews of solar irradiance forecasting methods tend to focus on the forecasting methods themselves. However, very few researchers have reviewed solar irradiance forecasting methods suitable for buildings from an architectural perspective. Besides, most research tend to lack a clear methodology for literature review.
2. Little research has been done to consider what kind of nowcasting horizons and spatial-temporal resolution are appropriate for the building. More importantly, only a very few research have explored the potential value of emerging solar irradiance nowcasting methods with short- to very short-term forecasting horizons and high spatial-temporal resolution for buildings and their future development.
3. Further, little attention has been paid to what kind of equipment and programming for solar irradiance forecasting methods are suitable for the utilisation of buildings. In terms of equipment, purchase costs, installation conditions and operating difficulty are critical. In the case of programming, ease of learning and use, variability, and extensibility are necessary.
4. At present, most solar irradiance forecasting methods mainly focus on GHI forecasting, and a relatively small number of forecasting methods are also concerned with DNI forecasting. However, forecasting methods for DHI are very rare. In fact, GHI, DNI and DHI are three equally critical parameters of the necessary weather files for most building simulation programs. Thus, the forecasting of DHI is valuable.
5. Few studies have comprehensively explored the effects of diverse factors on the

reliability of solar irradiance forecasting. These factors include various time intervals and horizons of forecasting, different sky conditions, forecasting models, and datasets.

6. Little attention has been paid to the study of evaluation metrics for solar irradiance forecasting methods, resulting in the selection of evaluation metrics often chosen without a clear reason. In this case, it is valuable to screen and use appropriate and diverse evaluation metrics to evaluate solar irradiance forecasting methods from various perspectives.
7. Only a few studies have discussed what current or potential building applications of solar irradiance forecasting methods can be used from an architectural perspective, especially those solar irradiance nowcasting methods that have emerged in recent years.

1.7 Research Questions

Based on the above research gaps, several research questions were proposed:

1. How can a literature review be conducted based on a clear methodology to screen the solar irradiance forecasting methods appropriate for buildings?
2. How can a solar irradiance nowcasting method appropriate for buildings be developed?
3. How can the results of solar irradiance nowcasting be generated?
4. How can the reliability of solar irradiance nowcasting be verified?
5. What current or potential building applications can the proposed solar irradiance nowcasting method be applied to?

In order to answer the above research questions and achieve the research aim, a series of research objectives were proposed in the following section.

1.8 Research Objectives and Procedures

1. To conduct a systematic review of current solar irradiance forecasting methods and identify the forecasting methods appropriate for buildings according to the characteristics of forecasting methods.
    a) Determining a well-defined methodology for literature review.
    b) Conducting a systematic literature review of current solar irradiance forecasting methods.
    c) Identifying critical characteristics of solar irradiance forecasting methods appropriate for buildings, such as nowcasting horizon, spatial-temporal resolution, equipment, programming, etc.
    d) Collating and analysing solar irradiance forecasting methods suitable for buildings based on the critical characteristics of forecasting methods.
2. To develop a solar irradiance nowcasting method with very short-term forecasting horizons and high spatial-temporal resolution using low-cost equipment and user-friendly programming to achieve the nowcasting of GHI, DNI and GHI.
    a) Proposing a methodology for GHI, DNI, and GHI nowcasting with very short-term nowcasting horizons and high spatial-temporal resolution.
    b) Establishing a system of low-cost equipment for GHI, DNI, and GHI nowcasting.
    c) Selecting user-friendly programming to implement the nowcasting procedures of GHI, DNI, and GHI nowcasting.
3. To apply the proposed irradiance nowcasting method to achieve the nowcasting of GHI, DNI, and GHI in a series of comparative tests.
    a) Applying the developed low-cost equipment to obtain ground-based cloud images and measurement of GHI and DHI with high spatial resolution (2km) and temporal resolution (10-sec, 1-min, 5-min, and 10-min).
    b) Training solar irradiance nowcasting models using cloud images and

measurement of GHI and DHI based on the selected user-friendly programming.

c) Designing a series of comparative tests according to various factors, including time intervals, nowcasting horizons, sky conditions, forecasting models, and datasets.

d) Using trained solar irradiance models and cloud images to generate 10-sec, 1-min, 5-min, and 10-min nowcasting of GHI and DHI in different comparative tests.

e) Calculating 10-sec, 1-min, 5-min, and 10-min nowcasting of DNI using the nowcasting of GHI and DHI generated from different comparative tests based on the mathematical relation equation among GHI, DNI and DHI.

4. To utilise appropriate evaluation metrics to evaluate the reliability of the GHI, DNI, and DHI nowcasting from various perspectives.

   a) Assessing the characteristics and popularity of evaluation metrics, including MAE, RMSE, nMAE, nRMSE, skill score (SS), r, etc.

   b) Selecting appropriate evaluation metrics to evaluate the reliability of GHI, DNI and DHI nowcasting obtained from different comparative tests.

5. To discuss current and potential building applications of the proposed solar irradiance nowcasting method.

   a) Discussing current building applications of the proposed solar irradiance nowcasting method according to current building applications of solar irradiance nowcasting methods.

   b) Discussing potential building applications of the proposed solar irradiance nowcasting method according to the future trends of building development.

1.9 Thesis Outline

This thesis is organised into six chapters. In Chapter 1, a thorough introduction involving the research background, statement of problem, importance of research, research aim, research focus and scope, research gaps, research questions, research objectives and methods, and thesis outline are presented. Chapter 2 conducts a systematic review of current solar irradiance forecasting methods and identifies the appropriate forecasting methods for buildings according to the characteristics of forecasting methods. Subsequently, a comprehensive research methodology involving data collection and processing, nowcasting models, equipment and programming, evaluation metrics, and comparative tests of GHI, DNI and DHI nowcasting is articulated in Chapter 3. In Chapter 4, the results verification and analysis of GHI, DNI and DHI nowcasting in different comparative tests of various factors, including time intervals, nowcasting horizons, sky conditions, forecasting models, and datasets, are displayed. Chapter 5 articulates the advantages and limitations of this research and discusses current and potential building applications of the proposed solar irradiance nowcasting method. Finally, the conclusion and possible directions for further work are given in Chapter 6.

Chapter Two

2 Literature Review with Systematic Review Methodology

The purpose of Chapter 2 is to respond to the first research question in Chapter 1 - “How can a literature review be conducted based on a clear methodology to screen the solar irradiance forecasting methods appropriate for buildings?”. Therefore, the crucial task of this chapter is to achieve the first research objective - to develop a well-defined review methodology to review current solar irradiance forecasting methods systematically and identify the forecasting methods appropriate for buildings according to the characteristics of forecasting methods.

In specific, this chapter deals with a series of main sections. Firstly, the potential of solar energy in different regions of the world is introduced to demonstrated the value of this research for most regions of the world. Secondly, a series of background information, such as building energy demand, building energy benchmarks, is discussed to clarify the link between building and solar irradiance forecasting. Thirdly, a brief introduction of diverse solar irradiance forecasting methods is presented. After that, current review methodologies of solar irradiance forecasting methods and their limitations are demonstrated.

Subsequently, the developed systematic review methodology for solar irradiance forecasting methods and its relationship with research methodology of solar irradiance nowcasting are articulated. And then, a systematic review of current solar irradiance forecasting methods based on the proposed systematic review methodology is conducted to provide a comprehensive review of different forecasting methods and their characteristics, including forecasting horizons, spatial-temporal resolution, data acquisition ways, forecasting parameters, equipment and programming, etc.

On this basis, a series of research gaps are identified based on the needs of building applications and a further specific review of the emerging solar irradiance nowcasting methods is carried out to explore how these methods can address the

research gaps. In this case, the aim of this research and the characteristics of solar irradiance nowcasting methods needed for this research are demonstrated. Afterwards, the specific characteristics of solar irradiance nowcasting methods chosen for this research and the reasons for their selection are articulated. Finally, the conceptualisation of solar irradiance nowcasting method is discussed to inform the development of the research methodology in Chapter 3.

2.1 Potential of Solar Energy in Different Regions of The World

Solar Radiation is a free resource available in more or less quantities anywhere on the planet. In the current era of global climate change, the application of solar energy offers an opportunity for countries and communities to transform or develop their energy infrastructure and step up their low-carbon energy transition. However, what is the potential of solar energy in a specific region? This is a question often asked by policymakers and businesses alike. In this context, a report - Global Photovoltaic Power Potential by Country - has been developed by Solargis under contract to the World Bank, which effectively clarifies the potential of solar energy in different regions of the world [27].

In the report, the long-term average of daily or yearly GHI and DNI worldwide are respectively shown in Figure 2.1 and Figure 2.2, which demonstrate the theoretical potential of solar energy in different regions of the world. The theoretical potential for of solar energy merely depends on the long-term distribution of solar resource and thus allows for the comparison of the conditions between different regions without considering any solar energy system configuration. On the contrary, the report also proposes the practical potential of solar energy in different regions of the world based on their level of development and technological conditions, as shown in Figure 2.3.

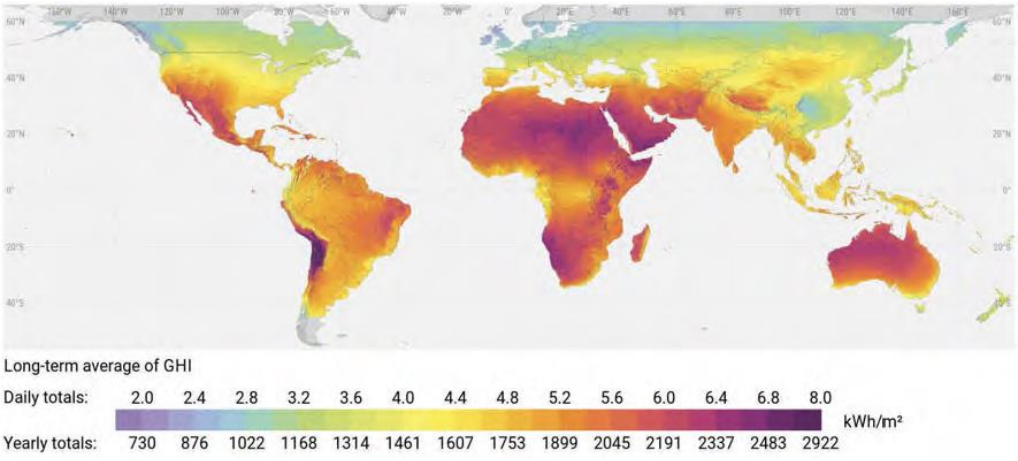

Figure 2.1 The Long-Term Average of Daily or Yearly GHI over The World

(Resource: Energy Sector Management Assistance Program, Global photovoltaic power potential by country, World Bank, (2020).)

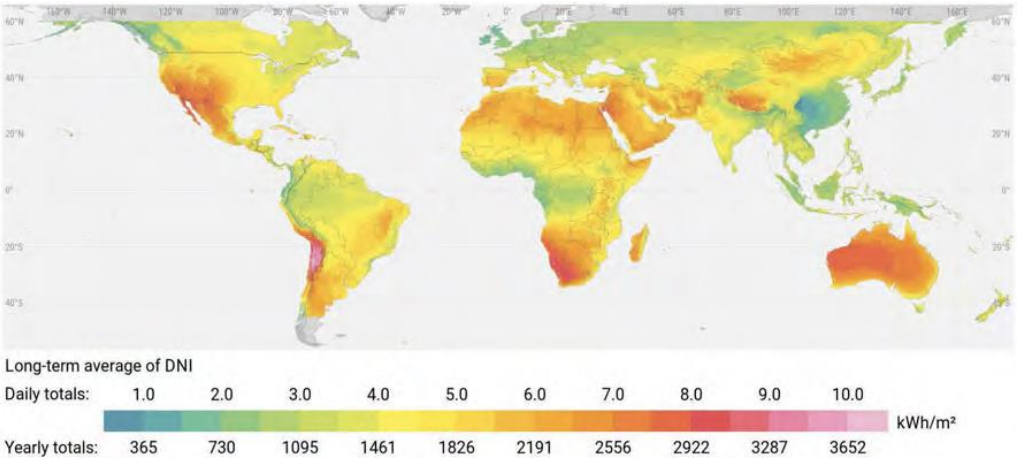

Figure 2.2 The Long-Term Average of Daily or Yearly DNI over The World

(Resource: Energy Sector Management Assistance Program, Global photovoltaic power potential by country, World Bank, (2020).)

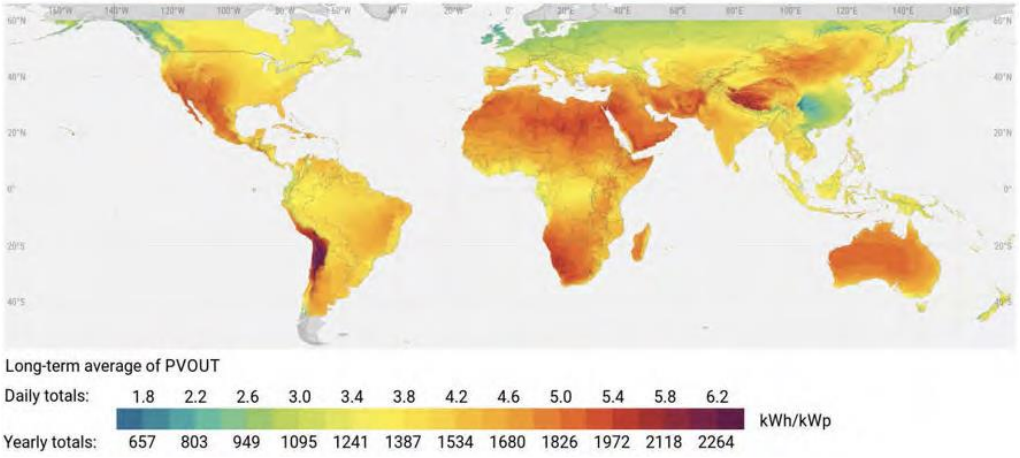

Figure 2.3 The Long-Term Average of Daily or Yearly Practical Solar Power Potential over The World

(Resource: Energy Sector Management Assistance Program, Global photovoltaic power potential by country, World Bank, (2020).)

In summary, around 20% of the global population lives in the regions with excellent conditions for solar energy application, where long-term daily PVOUT averages exceed 4.5 kWh/kWp. In addition, regions in the favourable mid-range between 3.5 and 4.5 kWh/kWp account for 71% of the global population. These include five of the six most populous countries (China, India, the United States, Indonesia, and Brazil) and 100 others (Canada, the rest of Latin America, southern Europe, and African countries around the Gulf of Guinea, as well as central and southeast Asia). In the end,

regions accounting for 9% of the global population score an average PVOUT below 3.5 kWh/kWp, dominated by European - except those in southern Europe. However, the potential is not dramatically lower compared to the top-performing group. To sum up, most regions of the world have solar energy potential.

According to the above, the main research sites of this research – Cardiff, UK, and Shanghai, China – both have good potential for solar energy, which confirms the basic value of this study. At the same time, the above report also proves the value of this research for most regions of the world.

2.2 The Link between Building and Solar Irradiance Forecasting

As mentioned in section 1.1.3, buildings are a major part of global energy consumption, estimated to account for about 36% of total energy use, primarily for heating, cooling, lighting, and operating appliances.

2.2.1 Building Energy Demand

Building energy demand refers to the total amount of energy required to maintain a comfortable indoor environment, equipment power supply and operation. It depends on the size, design, construction materials, insulation quality, and the habits of its occupants of the building. In specific, energy demand involves the following aspects:

- Heating Demand.
  a) Space Heating.

     Space Heating is the process of maintaining a comfortable indoor temperature in building spaces, especially in colder climates. It involves heating the air within the building to make the environment comfortable for occupants.

  b) Passive Heating.

     Passive heating refers to the design approach that utilizes the natural environment to maintain comfortable indoor temperatures without the use of mechanical systems.

  c) Active Heating.

     Active heating involves mechanical or electrical systems to generate and distribute heat throughout a building.

- Cooling Demand.
  a) Space Cooling.

     Space cooling is the process of lowering the indoor temperature of a building to maintain a comfortable living or working environment, particularly in hot climates. It involves managing the temperature and humidity of the

air inside a building to prevent overheating and discomfort.

b) Passive Cooling.

Passive cooling refers to techniques and building designs that naturally reduce the heat inside a building without the use of mechanical or electrical systems. It relies on the environment, building orientation, and materials to minimize the need for energy-intensive cooling.

c) Active Cooling.

Active cooling involves mechanical systems that use energy to reduce indoor temperatures. These systems actively cool the air and are used when passive methods are not sufficient to maintain comfort.

- Electricity Demand.

a) Lighting.

This refers to the energy used for illumination within a building. It includes all types of lighting systems such as incandescent bulbs, fluorescent lamps, LED lights, and other specialized lighting technologies.

b) Appliances and Equipment.

This refers to the energy consumption of various devices, appliances, and office equipment within a building. It includes everything from kitchen appliances (like refrigerators and microwaves) to office equipment (computers, printers, and copiers), as well as heating, ventilation, and air conditioning (HVAC) systems.

- Ventilation Demand and Hot Water Demand.

a) Mechanical ventilation.

This refers to the use of mechanical systems to circulate and exchange indoor air in a building. Unlike natural ventilation, which relies on outdoor air and wind to ventilate a space, mechanical ventilation actively moves air in and out of buildings to ensure proper air quality, temperature, and humidity levels.

b) Hot Water Supply.

Hot Water Supply refers to the process of providing heated water for various uses within a building, such as for bathing, cooking, cleaning, and heating.

In conclusion, each of the abovementioned aspects has different strategies and technologies to optimize energy use and reduce overall consumption, which is crucial for energy efficiency and sustainability in building management.

2.2.2 Building Energy Benchmarks

Building energy benchmarks are reference standards or benchmark values set based on the energy performance of buildings. These benchmarks are often based on historical data from similar types of buildings or industry standards, and are used to assess building energy demand. By comparing the actual energy demand of a building to industry benchmarks, it can be determined whether the building is performing efficiently or requires improvements in its energy usage. In practice, different countries and regions have formulated different building energy benchmarks based on their respective energy resources, climatic conditions, levels of economic development and environmental protection needs. Below are some widely used building energy benchmarks:

- Building Research Establishment Environmental Assessment Method (BREEAM).

  BREEAM is a British environmental performance assessment standard, and one of the most widely used green building certification systems globally. BREEAM considers not only energy efficiency but also factors like building materials, waste management, and overall sustainability. The ratings range from Pass to Outstanding, based on a building's performance in areas like energy efficiency and resource management.

- Leadership in Energy and Environmental Design (LEED).

  LEED is an international certification system developed by the U.S. Green Building Council (USGBC) to assess the sustainability and environmental

performance of buildings, including energy efficiency. LEED offers various levels of certification, from Certified to Gold, Silver, and Platinum, based on the building's performance in energy management, water use, material selection, and indoor environmental quality.

- ISO 50001 Energy Management Systems Standard.

  ISO 50001 is an international standard developed by the International Organization for Standardization (ISO) for energy management systems (EnMS).

- ASHRAE 90.1 Standard.

  ASHRAE 90.1 is a building energy standard published by the American Society of Heating, Refrigerating, and Air-Conditioning Engineers (ASHRAE), primarily focused on commercial buildings. The standard includes energy performance requirements for heating, cooling, lighting, ventilation, and air-conditioning systems.

- China's Green Building Evaluation Standard.

  In China, the energy performance of buildings is often assessed using the Green Building Evaluation Standard (GB/T 50378), which focuses on energy efficiency, water conservation, and waste management. The evaluation of energy performance under this standard includes both the design phase and the operational phase of the building.

To sum up, building energy benchmarks vary widely, and different certification systems and standards emphasize different aspects depending on the region or country. By using energy benchmarks, buildings can optimize energy use, reduce costs, and enhance environmental sustainability.

2.2.3 The Value of Solar Irradiance Forecasting for Buildings

To achieve building energy benchmarks, a series of software tools have been developed. The most representative tools involve building simulation programs and building control programs.

- Building Simulation Programs.

  Building simulation programs are primarily used to simulate the energy performance of buildings during their design and operational phases. This software predicts the energy demand of a building under different climatic conditions, using different materials and technological solutions to ensure that the design and operation of buildings meet specific energy benchmarks. Common building simulation programs include:

  1. EnergyPlus.

     EnergyPlus is a comprehensive and flexible energy simulation tool used to model heating, cooling, lighting, ventilating, and other energy flows in buildings.

  2. DesignBuilder.

     This is a user-friendly interface for EnergyPlus, offering detailed building energy, lighting, and comfort analysis, well-suited for the design and optimisation of complete buildings and their systems.

  3. Transient System Simulation Tool (TRNSYS).

     TRNSYS is a flexible, graphically based software environment used to simulate the behaviour of transient systems, particularly where heat transfer is involved, widely used in building energy simulations.

  4. eQUEST:

     EQUEST is a widely used graphical interface for building energy performance simulation. It is suitable for both detailed and simplified energy analysis.

  5. Integrated Environmental Solutions Virtual Environment (IES VE).

     This is a suite that offers detailed analysis tools for optimizing the sustainable performance of buildings, including energy modeling, thermal simulations, and daylight analysis.

- Building Control Programs.

  Building control programs are used for real-time monitoring and controlling various systems in a building (such as HVAC, lighting systems, etc.), to improve operational efficiency of buildings, dynamically adjusting and optimising the operation of building systems to reduce unnecessary energy demand. Representative building control programs include:

  1. Honeywell Building Management Systems.

     Honeywell offers advanced control systems for managing and optimising building operations and energy efficiency.

  2. Johnson Controls Metasy.

     This is a comprehensive, scalable building management system that provides extensive monitoring and optimization of building performance.

  3. Siemens Desigo CC.

     Siemens' Desigo CC is an integrated building management platform that supports a wide range of automation and control functions.

  4. Matrix Laboratory (MATLAB).

     MATLAB is a high-level programming and numeric computing platform used widely across various industries for data analysis, algorithm development, and modeling and simulation.

  5. OpenModelica.

     OpenModelica is a comprehensive, open-source modeling and simulation environment based on the Modelica modeling language. The primary goal of OpenModelica is to create a freely available system modeling platform that supports simulation and model-based design of complex systems, spanning mechanical, electrical, hydraulic, thermodynamic, robotic, and other interconnected physical domains.

In summary, building simulation software and building control software play crucial roles in achieving and maintaining building energy benchmarks, thereby realising

overall energy efficiency and sustainable development goals.

The critical input parameters for building simulation and control programs usually include a series of detailed and critical data that are essential for accurately simulating the energy performance and other related performance of the building. These data commonly include climate and environmental data, the dimensions, layout and orientation of buildings, materials and building components, Internal Loads, HVAC systems, operation and usage patterns. Among these data, climate and environmental data is the most basic and important and thus building simulation and control programs usually require high-quality weather files. These weather files commonly include diverse weather data, such as temperature, humidity, air pressure, solar irradiance.

In recent years, the use of weather data for simulating and predicting building energy demand has become increasingly common, which helps building managers, facility operators, and designers better understand and optimise the energy efficiency of buildings. [28] investigates the effects of using weather nowcasting within dynamic building simulations, particularly focusing on its influence on predicting indoor temperatures for buildings without heating or cooling systems (free float buildings), as well as on the prediction of heating loads and energy usage for buildings with heating systems. Based on the occupancy behaviour pattern detection and local weather forecasting, [29] develops a methodology for integrated building heating and cooling control to reduce energy consumption and maintain indoor temperature set-point. [30] discusses the importance of accurate solar forecasting in the application of Model Predictive Control (MPC) for achieving Net Zero Energy Buildings (NZEBs) and communities. [31] discusses the use of Model Predictive Control (MPC) and weather forecasting to improve the energy efficiency of Integrated Room Automation (IRA), while ensuring occupant comfort. IRA involves the simultaneous control of heating, ventilation, and air conditioning (HVAC), as well as shading and lighting in a building zone, to ensure that room temperature, CO2 levels, and brightness remain within specified comfort ranges.

In summary, these studies are representative for understanding how weather forecasting can enhance the accuracy and efficiency of building management systems. Among various weather data forecasting, solar irradiance forecasting is very critical but also very difficult to obtain, mainly for the following reasons:

- Availability and Coverage

  At first, compared to common data like temperature and humidity, solar irradiance is generally harder to access because measuring solar irradiance requires specialised instruments such as pyranometers, which may not be installed at all weather stations. In addition, solar irradiance is often available only at certain research institutions, universities, or specialised meteorological stations, limiting its coverage and widespread availability.

- Accuracy and Resolution

  The accuracy of solar irradiance depends on the maintenance and calibration of the instruments, which can lead to lower data quality in resource-poor areas. Common weather data such as temperature and precipitation, although also requiring proper calibration, are more mature and standardised, typically offering higher accuracy. Besides, solar irradiance requires high-frequency recording, such as every minute or hour, to accurately reflect changes in sunlight conditions. In contrast, other weather data like temperature and humidity might also be recorded at a high frequency, but for most applications, daily averages or maximum and minimum values are sufficient.

- Cost

  On the one hand, pyranometers and other solar irradiance measuring devices are expensive, including not only the initial purchase cost but also maintenance and calibration costs. On the contrary, general meteorological measuring equipment is usually cheaper and easier to maintain. Moreover, accessing high-quality solar radiation data might require licensing fees, especially when the data comes from specialised institutions or is needed at high resolutions.

For common weather data like temperature and wind speed, due to their wide availability, it is generally possible to obtain them for free or at a low cost from common weather stations.

Based on the above, to utilise building simulation and control programs for optimising building energy efficiency, solar irradiance forecasting is critical. In practice, the aforementioned building simulation and control programs all support the use of solar irradiance forecasting data for effective building performance simulation and system control. For example, Johnson Controls Metasy can integrate GHI forecasting into the HVAC control system. When predicted GHI are high, the cooling demand in a building usually rises. The system can use this information to dynamically adjust the operating mode of air conditioning and refrigeration equipment in advance. Thus, this research aims to explore an effective solar irradiance forecasting method for buildings.

2.3 Introduction of Solar Irradiance Forecasting Methods

The dynamic nature o movement, cloud transitions, water vapour, and air pollution leads to the high instability of solar energy f sun, which brings significant difficulty to its application. With the growing demand for renewable energy and the development of solar energy technologies, accurate solar irradiance forecasting has become a key way for optimising the design and operation of solar energy systems. Thus, a large number of solar irradiance forecasting methods have been developed over recent decades.

In order to quickly establish a preliminary understanding of solar irradiance forecasting methods, a series of crucial information must be introduced concisely. The information involves the classification of solar irradiance forecasting methods, data acquisition ways, forecasting parameters, etc.

2.3.1 Classification of Solar Irradiance Forecasting Methods

In the last several decades, a large number of diverse methods have been proposed for solar irradiance forecasting, which relates to complex disciplines such as mathematics, physics, statistics, etc [32]. Thus, the first step of solar irradiance forecasting method research is to explore the approaches of classification. One of the earliest and most popular classifications of solar irradiance forecasting methods was published in 2013 [33]. According to the author's discourse, solar irradiance forecasting methods were classified into five groups, including regressive methods, artificial intelligence, remote sensing network (based on the utilisation of satellite), Numerical Weather Prediction (NWP) and local sensing (based on the utilisation of total sky imager, Wireless sensor network). Besides this paper, other representative papers, which also discussed the classification of solar forecasting methods, were published in later years [12, 34]. [10] also proposed a persuasive classification that divided solar irradiance forecasting methods into five classes, including time series, regression, Numerical Weather Prediction (NWP), machine learning and image-based forecasting. In terms of the forecasting horizons, solar power forecasting methods were classified into four classes, including long-term, mid-term, short-term and intra-hour forecasting

[35]. [36] categorised solar irradiance and photovoltaic power forecasting methods using ML and DL algorithms into meso-scale, micro-scale, and building-scale forecasting in urban environments from a multi-scale perspective. Based on the above research, solar irradiance forecasting methods in this paper are classified into five categories:

- Numerical Weather Prediction methods (NWPs).
- Statistical and Learning methods.
- Top-down forecast methods.
- Bottom-up forecast methods.
- Hybrid methods.

As mentioned at the beginning of Chapter 1, different solar irradiance forecasting methods were developed according to various forecasting purposes and thus can achieve decent performance in their designated spatial-temporal resolution.

2.3.2 Numerical Weather Prediction (NWP) Methods

2.3.2.1 The State of The Art of Numerical Weather Prediction (NWP) Methods

As the earliest applied weather forecast method, Numerical Weather Predictions (NWPs) use mathematical models of the atmosphere and oceans to predict the weather in the future [10]. This method relies heavily on the computational ability of large computers and knowledge of hydromechanics and thermodynamics [37]. Due to the giant scale of the atmosphere and ocean, the analysis of NWPs method is mainly based on a national or regional level [12]. In this case, NWP models are unable to provide an accurate weather forecast for the precise position based on micro-scale physics. Modern NWP models may be classified into two main types: global models, such as Global Forecast System (GFS), or regional models, including North American Mesoscale (NAM), European Centre for Medium-Range Weather Forecasts (ECMWF), Weather Research and Forecasting (WRF) [12]. In recent years, a lot of researchers have expressed their interest in the WRF model because it is open-source and can be configured by the user to a high resolution over a specific region [38]. In general, the

strict requirement of highly specialised skills, knowledge, and equipment is not conducive to universal research.

In the paper [39], a comparative study of NAM/GFS/ECMWF was presented to introduce the respective features of these representative methods and contrast their performance for global solar irradiance forecasting. In recent years, a lot of researchers have expressed their interest in the WRF model because it is open-source and can be configured by the user to have a high resolution over a specific region [40-42]. The representative studies of NWP methods are listed in Table 2.1.

Table 2.1 NWP methods for solar irradiance forecasting

Article	Parameter	Forecasting Horizon	Data Source	Method
[39]	GHI	Intra-day	Public Meteorological Observations	NAM/GFS /ECMWF
[40]	GHI	Intra-day	Public Meteorological Observations	WRF
[41]	GHI	Day Ahead/Intra-day /Intra-hour	Public Meteorological Observations Public Meteorological Satellites	WRF-CLDDA
[42]	GHI + DNI	Hourly	Public Meteorological Systems	WRF

Parameter: Forecasting Parameter, Frequency: Time-interval
GHI: Global Horizontal Irradiance, DNI: Direct Normal Irradiance, DHI: Diffuse Horizontal Irradiance

2.3.2.2 Data Acquisition of Numerical Weather Prediction Methods (NWP)

In general, the data for NWP methods comes from the database of public meteorological observations, such as the National Oceanic and Atmospheric Administration of the USA (NOAA), the Meteorological Office of the UK (Met Office), Bureau of Meteorology of AUS (BOM), which can offer comprehensive and complex data and environmental information. Recently, an ascendant approach, which utilises Application Programming Interface (API) to provide accurate meteorological data, has expressed its potential as a data resource for NWP methods. Table 2.2-2.3 shows available data types from various APIs.

Table 2.2 Parameters available from APIs

APIS	Temp	RH	Wind Spd	Wind Dir	Pres	UV
Weather Bit 2.0	√	√	√	√	√	√
Solcast	√	√	√	√	√	X
AccuWeather	√	√	√	√	√	√
Foreca	√	√	X	√	√	X
Dark Sky	√	√	√	√	√	√
Datapoint	√	√	√	X	√	√
Open Weather Map	√	√	√	√	√	√

Temp: Temperature, RH: Relative Humidity, Pres: Pressure, UV: UV Index

Table 2.3 Parameters available from APIs

APIS	Weather	PoP	Cloud	Solar Rad	GHI	DNI	DHI
Weather Bit 2.0	√	√	√	√	√	√	√
Solcast	X	√	√	√	√	√	√
AccuWeather	√	√	√	√	√	√	√
Foreca	√	√	X	√	X	X	X
Dark Sky	√	√	√	X	X	X	X
Datapoint	√	√	X	X	X	X	X
Open Weather Map	√	√	√	X	X	X	X

Weather: Weather Type, Pop: Probability of Precipitation, Cloud: Cloud Coverage, Solar Rad: Estimated Solar Irradiance, GHI: Global Horizontal Irradiance, DNI: Direct Normal Irradiance, DHI: Diffuse Horizontal Irradiance

2.3.3 Statistical and Learning Methods

2.3.3.1 The State of The Art of Statistical and Learning Methods

Due to the rapid development of computer techniques, Statistical and Learning methods of solar irradiance forecasting have been widely applied, which contributes to more research publications against other forecasting methods in the last two decades. The essence of Statistical and Learning methods is to conduct the collection, analysis, and conclusion of historical data based on mathematical methods that eventually contribute to the prediction of data performance in the future. Statistical and Learning methods for solar irradiance forecasting can be divided into two categories: Model-driven methods and Data-driven methods.

Model-driven methods essentially utilise statistical models to determine the interdependent quantitative relationship among variables. In this case, a determined statistical model can obtain forecast data based on historical data. Model-driven

methods tend to require rich statistical experience of researchers and thus it is not very user-friendly to the public. Typical Model-driven methods include an autoregressive integrated moving average (ARIMA), exponential smoothing (ETS), generalised autoregressive conditional heteroskedasticity (GARCH) and so on [10]. In general, ARIMA holds the best performance. It has been a common choice for a reference method and can be supported by a wide range of software applications.

In the recent decade, learning methods have gradually been the most popular approach in the field of solar irradiance forecasting because of a large number of available methods and variants in machine learning (ML), as well as the full range of applications it supports, including classification, regression, and clustering. Unlike Model-driven methods, which tend to require researchers' mastery of empirical models, Data-driven methods rely on the principle of ML and thus emphasise self-learning of models from ample data samples, where learning implies classification, regression, and prediction. Once the training and testing stages are completed, the “black box” models can apply historical data to forecast future data. The most typical learning method is undoubtedly an artificial neural network (ANN). A good deal of research papers work on basic ANN models, its optimised algorithms, such as BP and LM, and its advanced models, such as DRWNN and WNN [43, 44]. The optimization of models not only increases the accuracy of forecasting but also expands the forecasting types of solar irradiance (from GHI to DNI) and shrinks the forecasting intervals (from monthly, daily, hourly to min-ahead) [28]. Besides the ANN method, other popular Data-driven methods, including SVM and kNN, were also employed for solar forecasting [45, 46]. The typical challenges of these methods are the selection, operation and optimisation of statistical models. Table 2.4 lists research papers on various Statistical and Learning methods for solar irradiance forecasting.

Table 2.4 Statistical and Learning methods for solar irradiance forecasting

Article	Parameter	Forecasting Horizon	Data Source	Method
Model-Driven Methods				
[47]	GHI	Monthly	Public Meteorological Observations	ARMA
[48]	GHI	Monthly	Public Meteorological Observations	GARHA
[49]	GHI	Hourly	Public Meteorological Observations	ETS
[50]	GHI/DHI/DNI	Hourly	Public Meteorological Observations	ARIMA
Data-Driven Methods				
[51]	GHI	Monthly	Public Meteorological Observations	RBF/MLP
[52]	GHI	Daily	Privately-owned Equipment	SOM
[53]	DNI	Daily/Hourly	Privately-owned Equipment	MLP/BP /LM
[54]	GHI	Hourly	Public Meteorological Observations	BP/LM/RBF /ANFIS
[43]	GHI	Hourly	Public Meteorological Observations	DRWNN
[55]	GHI	Hourly	Public Meteorological Observations	SVM
[56]	DNI	5/10/15/20 Mins	Privately-owned Equipment	kNN

Parameter: Forecasting Parameter, Frequency: Time-interval
GHI: Global Horizontal Irradiance, DNI: Direct Normal Irradiance, DHI: Diffuse Horizontal Irradiance

2.3.3.2 Data Acquisition of Statistical and Learning Methods

In general, Statistical and Learning methods tend to utilise measured data, which can be mainly obtained from several channels: public meteorological observation stations of public organisations, such as Airports, the Centre for Environmental Data Analysis and Met Office in the UK, National Oceanic and Atmospheric Administration in the US; laboratory of academic and research institution, such as Welsh School of Architecture; privately-owned weather stations. Among these channels, public meteorological observation organisations can often offer the most comprehensive and long-term meteorological data types, such as temperature, wind direction, wind speed, relative humidity, and air pressure. However, it is worth noting that available solar irradiance data are very seldom measured, even though various meteorological data types can be obtained.

2.3.4 Top-down Forecast Methods

2.3.4.1 The State of Art of Top-down Forecast Methods

The principle of Top-down forecast methods is to analyse satellite cloud images obtained from the atmosphere above. By examining two consecutive images captured by the meteorological satellite, cloud motion can be tracked based on a statistical algorithm. Finally, cloud motion accompanied by cloud cover information is translated into the solar irradiance forecast based on specific mathematic models. Due to the particular characteristics of meteorological satellites, satellite images can usually be produced with broad coverage, low resolution, and longer intervals for taking images. In this case, Top-down forecast method can provide reliable accuracy for solar irradiance forecasts in comparative large spatial and temporal horizons only. The disadvantages of these methods include unreliable forecasting accuracy for specific locations caused by the coarse resolution of satellite cloud images and limited forecasting intervals resulting from the photographic period of satellites [10].

An early approach using the satellite cloud image method for solar irradiance forecasting was proposed in 1999 [57]. In [58, 59], the authors presented the better forecasting performance of the satellite cloud image method against NWP methods for specific forecast horizons. In 2014, a study [60] proposed an optimised satellite cloud image method for solar irradiance forecasting, which was based on satellite images and ground measurements without other inputs and with low computation costs. The typical Top-down forecast methods have been listed in Table 2.5.

Table 2.5 Top-down methods for solar irradiance forecasting

Article	Parameter	Forecasting Horizon	Data Source	Method
[59]	GHI	6 Hours	Public Meteorological Satellites	Satellite Cloud Image Analysis
[60]	GHI	1/2/3 Hours	Public Meteorological Satellites	Satellite Cloud Image Analysis
[58]	GHI	30 Mins-6 Hours	Public Meteorological Satellites	Satellite Cloud Image Analysis
[57]	GHI	30 Mins-2 Hours	Public Meteorological Satellites	Satellite Cloud Image Analysis

Parameter: Forecasting Parameter, Frequency: Time-interval

GHI: Global Horizontal Irradiance, DNI: Direct Normal Irradiance, DHI: Diffuse Horizontal Irradiance

2.3.4.2 Data Acquisition of Top-down Forecast Methods

Satellite images, as the uppermost data for Top-down forecast methods, mainly come from the database of public meteorological observation organisations, such as NASA Earth Observations (NEO), USSG Earth explorer, National Oceanic and Atmospheric Administration (NOAA). Different meteorological satellites are used by various organisations that contributes to different characteristics of obtained satellite images, such as coverage area, image resolution, and photograph intervals. In addition, some APIs, such as OpenWeather, can also provide free satellite images. Table 2.6 shows different characters of satellite images from various sources.

Table 2.6 Different characters of satellite images obtained from various sources

Satellites Name	Operation Organization	Parameter	Spatial Resolution	Frequency
METEOSAT Satellite	EUMETSAT	Satellites Cloud Image	2.5 x 2.5/4.5 Km	30 Mins
GOES-West Satellite	NOAA	Satellites Cloud Image	1/4/16 Km	15 Mins
GOES-East Satellite	NOAA	Satellites Cloud Image	1/4/16 Km	15 Mins
GOES-16 Satellite	NOAA	Satellites Cloud Image	2 Km	15 Mins
Himawari-8	NOAA	Satellites Cloud Image	1 Km	10 Mins

2.3.5 Bottom-up Forecast Methods

2.3.5.1 The State of Art of Bottom-up Forecast Methods

The research of Bottom-up forecast methods, which have gradually become popular in recent years, has presented promising potential to overcome the limitations induced by the low spatial and temporal resolution of NWP and Top-down forecast methods [12]. Similar to Top-down forecast method, the key of the TSI method is to analyse the advection of clouds through consecutive cloud images observed with ground-based all-sky cameras called “sky imager” (TSI) [61]. By combining a series of image processing technologies with statistical methods, cloud cover information and cloud motion can be extracted from grounded sky images [62]. It can be used to generate solar irradiance forecasts at the sky imager location. Although the spatial resolution of the TSI method is comparatively limited because of the ability of the

camera, it provides advanced cloud information at a lead time of several minutes to hours, which contributes to a short-term forecast of solar irradiance. Various researchers have explored the typical procedure of the TSI method and its optimisation through improving hardware, software and cooperation of multiple sky-imagers. The biggest challenges of these methods involve the selection and protection of equipment and errors caused by using two-dimensional cloud images to represent actual three-dimensional features of clouds.

The paper [63] proposed a typical working procedure for TSI methods. Some other authors explored the forecasting performances in various short-term forecast intervals (minutes to hours). In addition, some studies expressed their interest in DNI forecasting rather than universal GNI forecasting. With the development of technologies, some papers also presented some low-cost equipment and optimised software applications for TSI methods. In 2015, a method using multiple sky-imagers to analyse three-dimensional features of clouds contributed to an innovative approach for improving the limitation of two-dimensional cloud image analysis based on a single sky imager. Table 2.7 presents typical Bottom-up forecast methods.

Table 2.7 Bottom-up methods for solar irradiance forecasting

Article	Parameter	Forecasting Horizon	Data Source	Method
[64]	GHI	Intra-hour	Public Met Observations + Grounded Sky Imagers	Ground Cloud Image Analysis
[65]	GHI	Intra-hour	Public Met Observations + Grounded Sky Imagers	Ground Cloud Image Analysis
[66]	GHI	30s-15 Mins	Public Met Observations + Grounded Sky Imagers	Ground Cloud Image Analysis
[63]	DNI	3-15 Mins	Public Met Observations + Grounded Sky Imagers	Ground Cloud Image Analysis
[61]	DNI	5 Mins	Public Met Observations + Grounded Sky Imagers	Ground Cloud Image Analysis
[67]	GHI	1/5/10/15 Mins	Public Met Observations + Grounded Sky Imagers	Ground Cloud Image Analysis

Parameter: Forecasting Parameter, Frequency: Time-interval, Met: Meteorological
GHI: Global Horizontal Irradiance, DNI: Direct Normal Irradiance, DHI: Diffuse Horizontal Irradiance

2.3.5.2 Data Acquisition of Bottom-up Forecast Methods

Grounded sky imagery, as the crucial data for Bottom-up forecast method, is generally generated by various “Sky Imagers”. The performance of different “Sky

Imagers" is relevant to various characters, including equipment composition, resolution, environmental adaption, size, cost and associated software application. In this case, different types of "Sky Imagers", such as Yankee TSI 880 sky imager, ASI-16 All Sky Imager, etc, tend to be invented by various research groups according to their specific research purposes.

2.3.6 Hybrid Methods

Hybrid methods usually consist of any two or more of the methods described previously. In recent years, several Hybrid methods have presented their superior performance for forecasting high-quality solar irradiance [68]. By taking advantage of the strengths of each methodology, Hybrid methods can increase forecasting accuracy efficiently. For instance, by utilising cloud cover information derived from satellite images instead of common weather data, such as temperature and humidity, as the input of ANNs, research can achieve accurate solar irradiance forecasts in some remote areas without meteorological observations [69]. Another reason for developing Hybrid methods is to overcome the limitations of each forecasting method in the various spatial and temporal horizons. Due to none of the individual methods spanning all relevant areas of interest, Hybrid methods, which incorporate the advantages of several methods, obviously need to be developed. Table 2.8 shows typical Hybrid methods for solar irradiance forecasting.

Table 2.8 Hybrid methods for solar irradiance forecasting

Article	Parameter	Forecasting Horizon	Data Source	Method
[70]	GHI	24 hours	Public Met Observations	ANN + WRF
[71]	GHI	30/60/90/120 mins	Public Met Observations + Satellite	ANN + Satellite Image
[72]	GHI	Hourly	Public Met Observations	ARMA + TDNN
[68]	GHI	Hourly	Public Met Observations	NWP + ANN + ARMA + Time Series
[69]	DNI	5/10 mins	Public Met Observations + Private Equipment	ANN + TSI

Parameter: Forecasting Parameter, Frequency: Time-interval

GHI: Global Horizontal Irradiance, DNI: Direct Normal Irradiance, DHI: Diffuse Horizontal Irradiance

2.3.7 Comparison of Different Solar Irradiance Forecasting Methods

Table 2.9 lists the various spatial-temporal horizons where different methods can achieve good performance. All of them have respective advantages and limitations according to the different spatial-temporal horizons. In this case, Hybrid methods can integrate the strengths of different methods that thus can perform well in the widest spatial and temporal horizon once the suitable combination of different methods is utilised. As a result, various Hybrid methods can flexibly meet the needs of different application purposes, such as building simulation.

Table 2.9 Performance of different methods in various forecasting horizons and spatial resolutions

Methods	NWP Method	Statistical Method	Top-Down Method	Bottom-Up Method	Hybrid Method
Spatial Horizon	5-20 km	1 m-2 km	1-10 km	1 m-2 km	1 m-20 km
Temporal Horizon	4-36 hours	1 second -1 month	30 mins -6 hours	5-30 mins	1 second -1 month

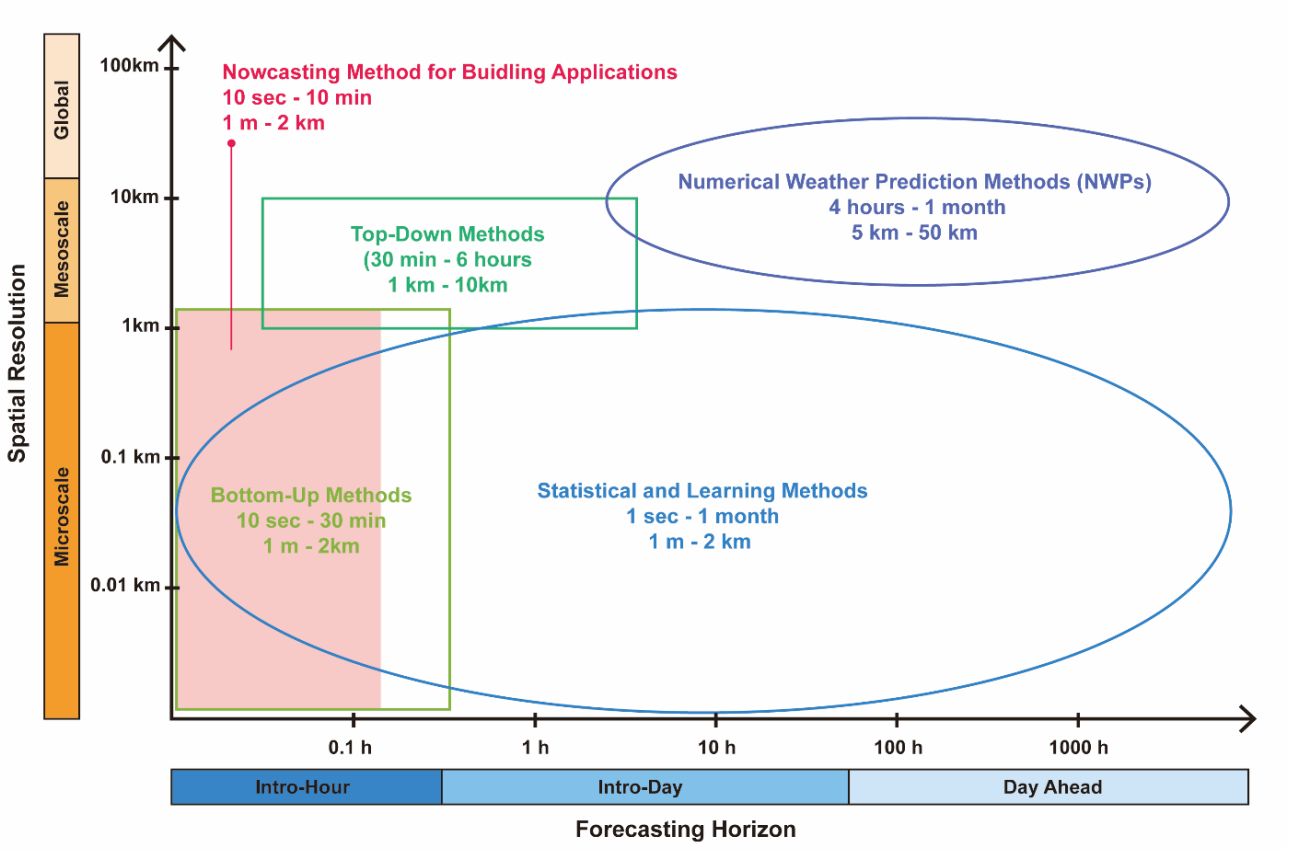

Figure 2.4 Classification of various models based on spatial-temporal resolution.

In summary, different solar irradiance forecasting methods can achieve decent

performance in their designated forecasting horizons and spatial-temporal resolution. Figure 2.4 demonstrates the current limits of different forecasting methods in various forecasting horizons and spatial resolution, as well as the specific forecasting horizons and spatial resolution of the conceived solar irradiance nowcasting method (red zone).

2.3.8 Parameters of Solar Irradiance Forecasting

Solar radiation is the basis for the utilisation of solar energy. One of the most important ways to measure the quantity of solar radiation is solar irradiance, which is the radiant flux received by a surface per unit area (W/m2). The ultimate purpose of solar irradiance forecasting is to achieve reliable predictions of different types of solar irradiance. Typical types of solar irradiance include:

1. Total Solar Irradiance. It is a measure of the solar power over all wavelengths per unit area incident on the Earth's upper atmosphere.
2. Extraterrestrial Irradiance. Extraterrestrial irradiance is a measure of the power of the sun incident outside the earth's atmosphere. It varies throughout the year because of the Earth’s elliptical orbit, which results in the Earth-Sun distance varying during the year in a predictable way.
3. Global Horizontal Irradiance (GHI). It is the total irradiance from the sun on a horizontal surface on Earth. Most existing research tended to focus on the prediction of GHI.
4. Direct Normal Irradiance (DNI). It is measured at the surface of the Earth at a given location with a surface element perpendicular to the Sun. More and more research on solar irradiance forecasting has started to explore both GHI and DNI in recent years.
5. Diffuse Horizontal Irradiance (DHI). It is the radiation at the Earth's surface from light scattered by atmospheric components, such as molecules and particles. Currently, there is very little research that pays attention to the research of DHI forecasting.

In general, the relationship between GHI, DNI and DHI can be expressed as:

$$GHI = DHI + DNI \times cos(\theta) \quad (2.1)$$

Where θ is the solar zenith angle, which is the angle of the sun relative to a line perpendicular to the earth's surface. The solar zenith angle is significantly associated with GHI, DNI, and DHI because it is a key parameter used to describe the sun's path across the sky. Figure 2.5 demonstrates the relationship between DNI, DHI and θ.

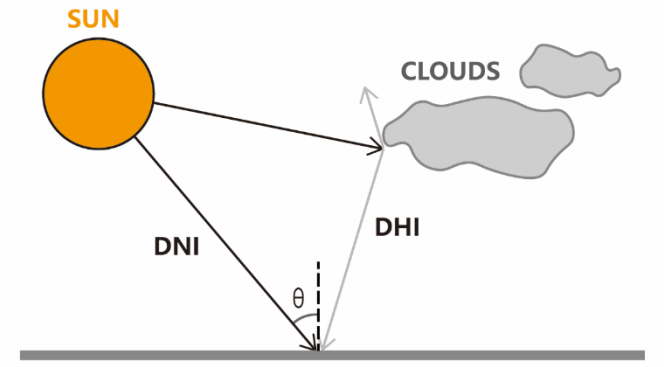

Figure 2.5 The relationship between DNI, DHI and θ.

Among typical types of solar irradiance, GHI, DNI, and DHI are the three major types that most solar irradiance forecasting methods focus on, along with three critical weather parameters needed for building applications. Thus, this research pays attention to the forecasting of GHI, DNI, and DHI.

2.4 Current Reviews of Solar Irradiance Forecasting Methods

A great number of literature reviews of solar irradiance forecasting methods have been published in the last decades. These reviews have efficiently contributed to familiarising students and researchers with developing new topics and facilitating the utilisation of new and powerful tools. These reviews produce significant contributions to the research of solar irradiance forecasting methods, including compilation, summary, critiques and synthesis of the available information on the subject.

2.4.1 Representative Types of Current Review Methodologies

In general, current reviews can be divided into two representative types according to their methodologies – conventional review method and computer review method.

- Conventional Review Method.

  This method refers to traditional, human-centred approaches to reviewing. In this method, a reviewer manually reads through materials or documents to assess content quality, accuracy, relevance, and other criteria. It relies heavily on human judgment and expertise, making it suitable for subjective analysis that requires context understanding, interpretation, or creativity.

- Computer Review Method.

  In this method, computer technology, typically using machine learning algorithms, is employed to execute the classification, filtering and evaluation of materials or documents. The advantage of this method is its ability to handle large amount of materials efficiently, without being influenced by personal bias.

Table 2.10 shows the typical reviews of solar irradiance forecasting methods and their review method.

Table 2.10 Representative reviews of solar irradiance forecasting methods.

Review	Title	Journal	Review Method	Citations
[10]	History and trends in solar irradiance and PV power forecasting: A preliminary assessment and review using text mining	Solar Energy	Computer	123
[73]	Machine learning methods for solar irradiance forecasting: A review	Renewable Energy	Convention	414
[34]	Review of photovoltaic power forecasting	Solar Energy	Convention	432
[74]	On recent advances in PV output power forecast	Solar Energy	Convention	166
[23]	Direct normal irradiance forecasting and its application to concentrated solar thermal output forecasting—A review	Solar Energy	Convention	113
[12]	Review of solar irradiance forecasting methods and a proposition for small-scale insular grids	Renewable & Sustainable Energy Reviews	Convention	426
[33]	Solar forecasting methods for renewable energy integration	Progress in Energy and Combustion Science	Convention	624
[75]	Solar energy forecasting and resource assessment	Book	Convention	295

2.4.2 Limitations of Current Review Methodologies

Although the benefits of current reviews are undoubted, several main drawbacks of their methodologies tend to exist:

1. Most of the reviews based on conventional methods haven't proposed well-defined methodologies of literature review, which define clear searching boundary engines, publications, key words, literature type, systematic selection process (identification, screening, eligibility, inclusion) and qualificative and quantitative analysis for information extraction and insights generation.

2. Most current reviews based on computer analysis tend to be limited by the number and characteristics of searching engines that thus lack comprehensive utilisation and comparative analysis of various databases. Most importantly, complex applications of computer skills on literature review are not friendly to every researcher.

3. A lot of crucial characteristics of solar irradiance forecasting methods have not been reviewed and analysed, such as the various data acquisition way for various solar irradiance forecasting methods. For example, a rising and potential data acquisition way - Weather API (Weather Application Programming Interface) - has been applied in recent years and thus it is worthing to be systematically reviewed.

In general, the above three major drawbacks are regarded as the main research gaps of current reviews of solar irradiance forecasting methods. Thus, the first significant step of this research is to explore an appropriate review method of solar irradiance forecasting methods for filling the above research gaps.

2.5 Systematic Review Methodology for Solar Irradiance Forecasting Methods

Countless studies on solar irradiance forecasting have been published in the last decades; thus, the total number of articles about solar irradiance forecasting methods is enormous. For example, Google Scholar merely searches for “solar irradiance forecasting” and “PV power forecasting” and returns 8760 and 9350 results for the year 2019 alone. However, this research focuses on exploring a solar irradiance nowcasting method with specific characteristics suitable for buildings and their future development, such as forecasting horizons, spatial-temporal resolution, equipment and programming, etc. Therefore, a more targeted literature review with a clear review methodology needs to be conducted to achieve the research aim.

Literature review is the most crucial foundation in any field of academic research. Apart from the articles that explore approaches and techniques for specific topics, a great deal of literature review articles has also been written to summarise abundant approaches and techniques. With the growth of literature review articles, mature methodologies of literature review are developed progressively. In recent years, more and more review methodologies have been developed to conduct literature review systematically [10, 76]. In terms of the limitations mentioned in section 2.4.2 and the huge number of articles on solar irradiance forecasting methods, this research develops a systematic review methodology for solar irradiance forecasting methods based on the review methodology proposed in [76]. In general, the process of systematic review in this research involves four major procedures: identification, screening, eligibility and inclusion.

2.5.1 Significance of The Systematic Review

In general, systematic review methodology for the literature review of solar irradiance forecasting methods and research methodology of solar irradiance nowcasting are both the crucial contributions of this research. There is a strong

relationship between systematic review methodology and the research methodology, as presented in the Figure 2.6 below:

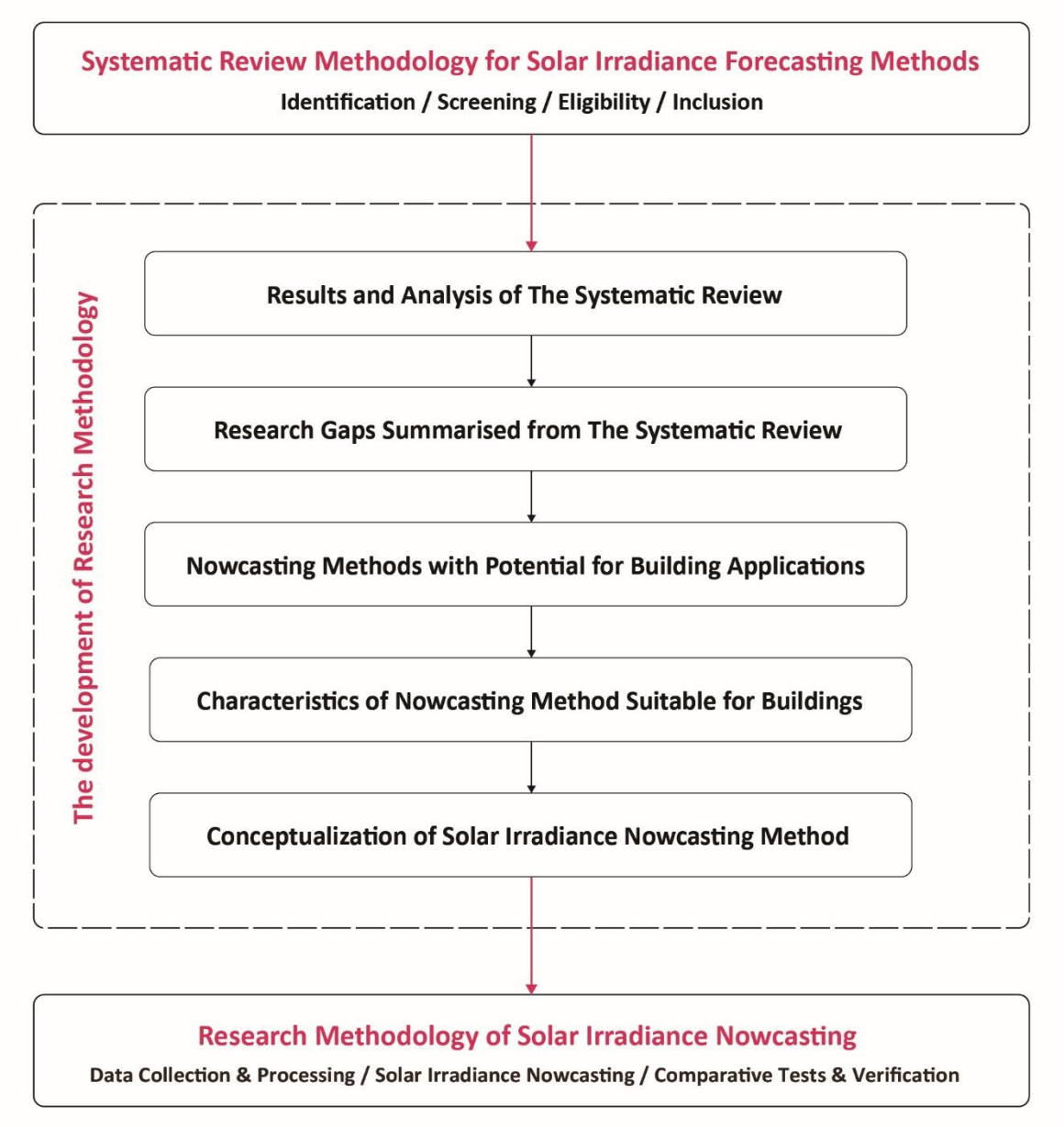

Figure 2.6 The relationship between systematic review methodology and research methodology

In summary, both systematic review methodology and research methodology are the critical research process of this research. The systematic review methodology is the foundation of research methodology. Based on the systematic review methodology discussed in this chapter, a clear research methodology is developed and presented in detail in Chapter 3.

2.5.2 Goals of The Systematic Review

Before starting the systematic review, several major questions are hierarchically proposed and the corresponding goals of this literature review are defined in response to these questions:

1. What review methods are easy to use by most people and suitable for conducting a systematic review?

Literature review is undoubtedly the foundation of academic research. It helps new researchers to understand the state of the art of specific subjects involving social, environmental, and economic background, popular researchers and publications, methodologies, data acquisition and processing, equipment and programming, etc. Conventionally, researchers conduct literature reviews based on individual experience, popular research, relevant references in popular research and other random searching of research. In this way, conventional approaches tend to lack a clear methodology of literature review and limit the total number of research reviewed. Therefore, conventional approaches are no longer suitable for the subjects that have been studied for a long time and thus have countless research results, such as solar irradiance forecasting methods. In recent years, a series of emerging methods have been developed to conduct literature reviews with a clear methodology and process countless academic resources using computer science, such as text mining. However, the adaptability of various databases to computer-based methods and the in-depth requirement of computer skills are two major challenges.

In this case, a particular review methodology is developed based on the review methodology proposed in [76] to conduct a literature review in a systematic way that mainly involves four steps:

1. Identification of review articles based on search strategies and selection of databases.
2. Screening of review articles according to languages, authority and topic relevance.

3. Eligibility of review articles through full-text articles assessed that excludes unnecessary articles with articulated reasons, such as specific spatial and temporal horizon of forecasting methods.
4. Inclusion of review articles that classifies, analyses and summaries the final included articles.

In this case, this systematic review method articulates the boundary of data searching, the total amount of articles, the logic of screening and a summary of comprehensive analysis that is friendly to most researchers. Thus, the development of this systematic review method is the first goal of this literature review.

2.What are the types of solar irradiance forecasting methods suitable for buildings?

As mentioned above, solar irradiance forecasting methods can be classified into five major types: Numerical Weather Prediction (NWP) Method, Statistical and Learning Method, Top-down Forecast Method, Bottom-up Forecast Method, and Hybrid Method.

These methods utilise various forecasting models, data acquisition ways, equipment and programming that determine their different spatial and temporal resolution of solar irradiance forecasting. In this research, the critical aim is to explore a solar irradiance forecasting method appropriate for buildings and their future development. Thus, the systematic review focuses on exploring the methods that have appropriate characteristics, such as forecasting horizon, spatial-temporal resolution, equipment and programming, for matching the requirements of building applications. In this case, the second goal of this literature review is to comprehensively review all types of solar irradiance forecasting methods and identify suitable methods for buildings based on the distinct characteristics of these methods.

3. What equipment and programming of solar irradiance forecasting methods are suitable for building applications?

Most of the previous review articles pay less attention to the equipment and programming that are two actual crucial factors of the research of solar irradiance

forecasting methods. For example, emerging researches have started to use weather application programming interfaces (APIs) that are offered by various institutions or organisations for collecting data in recent years. A series of advantages of APIs, including accessibility, laboursaving and timeliness, undoubtedly present their potential for data collection. In addition, different features of the equipment of solar irradiance forecasting methods, such as accessibility, adaptability, convenience, and cost, are also worth to be discussed for further researchers. Thus, the third crucial goal of this literature review is to classify, analyse and summarise various equipment and programming of current research.

2.5.3 Search Strategies of The Systematic Review

- Academic Resources and Search Engines.

  The first step of the literature review is to identify appropriate academic resources and corresponding search engines. In this research, diversified academic resources are considered for acquiring a broad horizon. In general, the types of articles include academic journals, conference papers, Ph.D. thesis and books. In the field of solar irradiance forecasting methods, academic journals are mainly published by Elsevier, Springer, Taylor & Francis, Sage, Wiley and (Multidisciplinary Digital Publishing Institute) MDPI. The Above publishers commonly have corresponding search engines, such as ScienceDirect, SpringerLink, Taylor & Francis Online, SAGE journals and Wiley Online Library. Among these search engines, ScienceDirect covers the largest number of high-quality articles. Apart from these search engines, Google Scholar, Web of Science, Microsoft Academic and IEEE Xplore are also representative search engines. The biggest advantage of Google Scholar is that it covers almost all articles. However, its update rate of publications is comparatively slow and search results tend to vary in quality. Thus, Google Scholar are suitable as a reference for other search engines. Web of Science also has a comparative board database and thus its database covers a series

of articles from the above publishers. Unlike Google Scholar and Web of Science which provides rough and broad search results, Microsoft Academic uses its special search algorithm that is contributed to narrowed but more accurate search results. Through fast browsing in Google Scholar, abundant conference papers related to solar irradiance forecasting methods are covered in IEEE Xplore. Taking into account the quantity and quality of articles, literature relevance and accessibility of different databases, this research finally determines five major search engines involving ScienceDirect, Microsoft Academic, IEEE Xplore, Wiley Online Library and Taylor & Francis Online. Table 2.11-2.12 shows the relationship between publishers and search engines.

Table 2.11 The relationship between publishers and search engines

Publishers / **Search Engines**	Elsevier	Taylor & Francis	Sage	MDPI
Google Scholar	Covered	Covered	Covered	Covered
Science Direct	Covered	No	No	No
Web of Science	Covered	Covered	Covered	Covered
Microsoft Academic	Covered	Covered	Covered	Covered
Wiley Online Library	No	No	No	No
IEEE Digital Library	No	No	No	No
Taylor & Francis Online	No	Covered	No	No
Sage journals	No	No	Covered	No
Springer Link	No	No	No	No

Table 2.12 The relationship between publishers and search engines

Publishers / **Search Engines**	Wiley	Springer	IEEE	IET
Google Scholar	Covered	Covered	Covered	Covered
Science Direct	No	No	No	No
Web of Science	No	Covered	Covered	Covered
Microsoft Academic	Covered	Covered	Covered	Covered
Wiley Online Library	Covered	No	No	No
IEEE Digital Library	No	No	Covered	Covered
Taylor & Francis Online	No	No	No	No
Sage journals	No	No	No	No
Springer Link	No	Covered	No	No

- Search Term.

  The search terms were derived from a series of trials on Google Scholar. Firstly, “Solar” and “Forecasting” as two crucial key words are used in Google Scholar

for searching all relevant topics excluding citations and patents. In this case, 1,220,000 results were returned if “solar” and “forecasting” were searched directly in Google Scholar because of countless research on this subject. In this case, a search strategy that searches more accurate keywords in the titles of articles is used to narrow the results into a reasonable quantity. The search term consists of two groups of keywords.

1. The first group includes “Solar” or “Photovoltaic” or “PV”.
2. The second group includes “Forecast” or “Nowcast” or “Predict”.

Table 2.13 presents the two groups of keywords.

Table 2.13 The key words used in advanced search

First Key Words	Second Key Words
Solar	Forecast
Photovoltaic	Nowcast
PV	Predict

2.5.4 Execution of The Systematic Review

The execution of the systematic review is shown in Figure 2.7. The main process includes four steps: identification, screening, eligibility and inclusion.

1. Identification

   In the field of solar irradiance forecasting methods, academic journals are mainly published by Elsevier, Springer, Taylor & Francis, Sage, Wiley and MDPI. The Above publishers commonly have corresponding search engines, including ScienceDirect, SpringerLink, Taylor & Francis Online, SAGE journals, Wiley Online Library. Following the above search strategies, various combinations of keywords are used to search articles. Thesis articles from various databases are merged to remove duplicates that produce initial records.

2. Screening

   The records identified are screened by their languages, authority, titles and abstracts. According to the author’s ability, only English and Chinese articles

are reserved. In addition, articles published before 2004 were excluded due to their generally low quality. Besides, some irrelevant themes, such as forecasting of solar flares, activities, and particles, are excluded. Finally, the articles without peer-review are excluded. However, some specific articles are considered according to their comprehensive quality, such as Ph.D. thesis.

3. Eligibility

   The screened records are assessed for eligibility through full text. Firstly, the articles do not focus on the forecasting of GHI, DNI and DHI were excluded. Then, the articles with unclear descriptions of research methods were excluded. Finally, the articles without appropriate forecasting horizons and spatial-temporal resolutions according to the needs of buildings were excluded. Specifically, the review excluded articles that describe forecasting methods with forecasting horizons longer than 6 hours, spatial resolution exceeding 10 km, and temporal resolution more than 1 hour. Based on the above, the rest of the articles are included.

4. Inclusion

   All the included articles are classified, analysed and summarised according to forecasting methods, data acquisition way, equipment and programming and evaluation metrics, etc. Also, the statistical analysis for the research quantity and performance data of solar irradiance forecasting methods is produced based on the articles included.

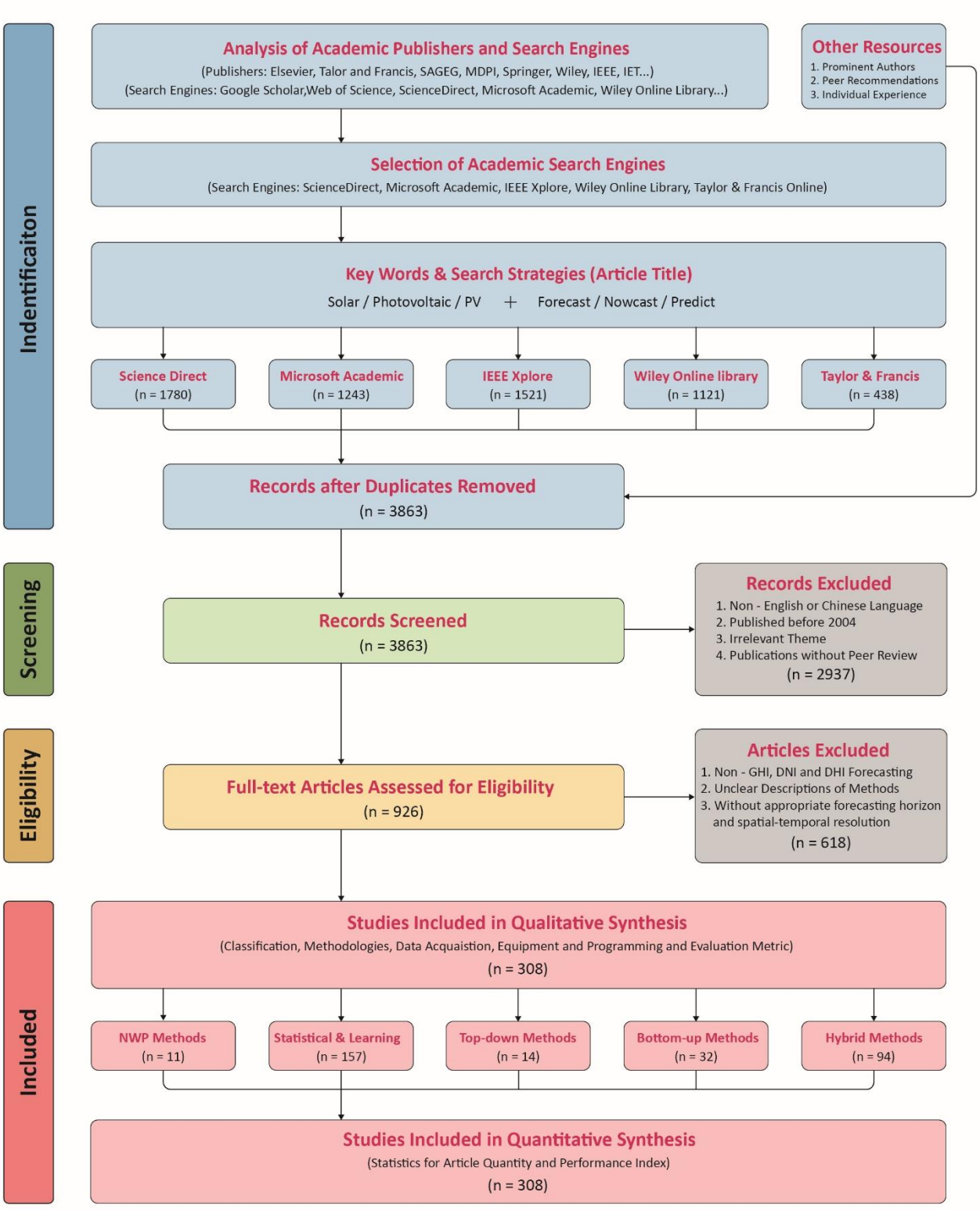

Figure 2.7 Methodology of systematic review

2.6 Results and Analysis of The Systematic Review

Based on the systematic review methodology, 308 articles on solar irradiance forecasting methods are included in the crucial literature review list and analysed. In general, the included articles mainly involve five types of solar irradiance forecasting methods, including NWP methods, Statistic and Learning methods, Top-down forecast methods, Bottom-up forecast methods and Hybrid methods. In the following analysis, Statistical and Learning methods will be further divided into two types: Data-driven and Model-driven. According to the systematic review, the forecasting horizons of all included solar irradiance nowcasting methods vary from 1 second to 6 hours.

2.6.1 Popular Journals and Conferences for Solar Irradiance Forecasting Methods

Figure 2.8 presents the top 10 popular journals and conferences of solar irradiance forecasting methods according to the included articles.

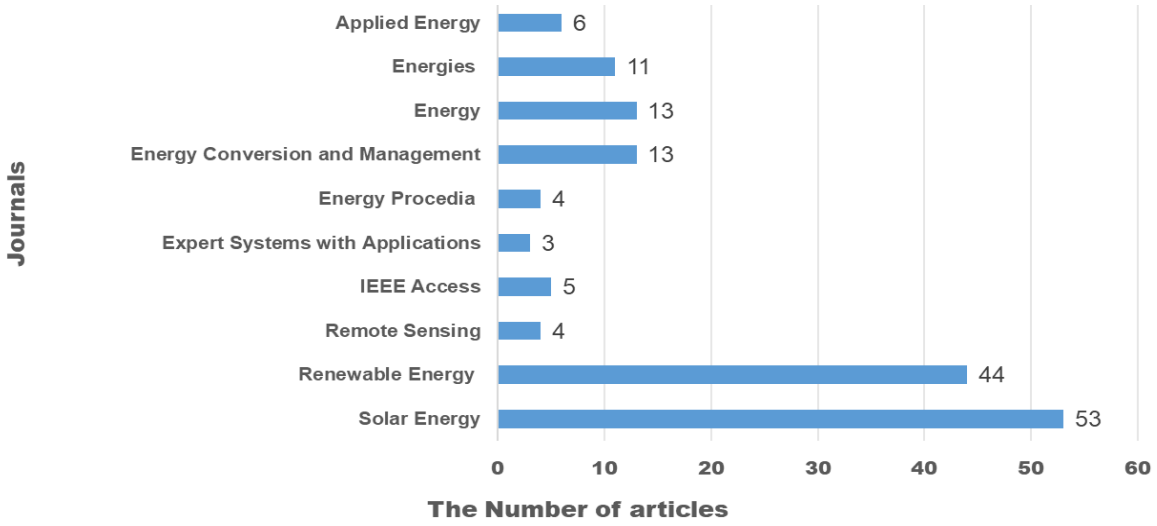

Figure 2.8 Top 10 popular journals and conferences of solar irradiance forecasting methods

In general, Solar Energy and Renewable Energy are the most popular journals, and both have relatively high impact factors. First of all, the highest number of articles published in Solar Energy, which is one of the leading journals in the field of solar energy, focusing on solar energy technology, applications, and scientific research

related to solar energy, with a very high degree of specialization. Secondly, Renewable Energy covers the research on all types of renewable energy sources and it is also an important journal in the field of solar energy research. The number of articles published in Energy Conversion and Management and Energy is tied for third place. Energy Conversion and Management specialises in energy conversion technologies and management strategies, while Energy focuses on multiple energy technologies and strategies. The number of remaining journals and conferences is relatively small, but they are also authoritative. Energies and Applied Energy are the top journals in the field of energy, covering a wide range of energy technologies and energy policy research. IEEE Access and Expert Systems with Applications focus on applied science and engineering technologies, including intelligent management and optimization of energy systems. Remote Sensing mainly publishes research on remote sensing technology and its application in earth science and environmental monitoring, which is equally important for resource assessment and environmental impact analysis in the field of energy. Energy Procedia, an open-access journal primarily for energy science conferences, covers a range of recent advances in energy management.

2.6.2 Popular researchers of Solar Irradiance Forecasting Methods

The top 10 popular researchers of solar irradiance forecasting methods are presented according to the included articles, as shown in Figure 2.9. It's worth noting that they are not necessarily the first authors of the article.

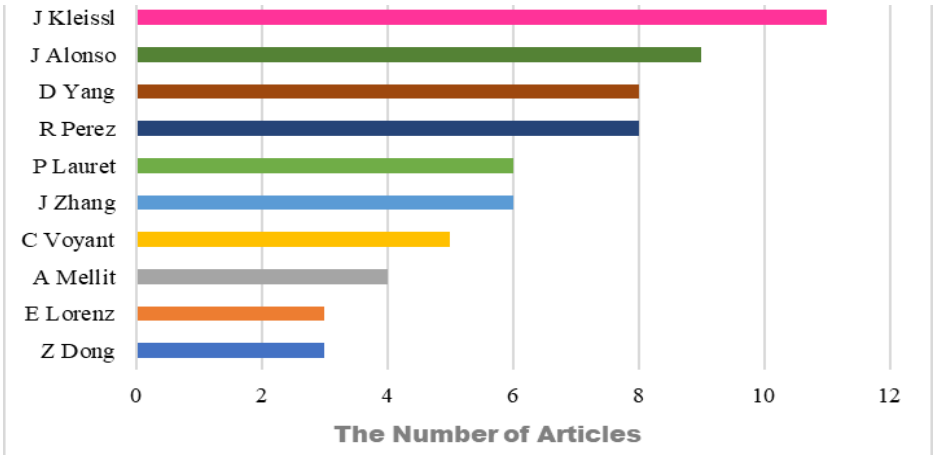

Figure 2.9 Top 10 popular researchers of solar irradiance forecasting methods

2.6.3 The Number of Articles of Solar Irradiance Forecasting Methods

Figure 2.10 shows the trend in the number of published articles on solar irradiance nowcasting methods from 2007 to 2024. The number continually increases each year from a shallow level in 2007 (only 1 article) to a peak in 2019 (43 articles), after which it begins to decline from 2019 to 2024 gradually. That reflects the growth of research interest in this field, which started in 2007 and will become mature and stable in 2019. In addition, since the methods used for solar irradiance forecasting are similar to those used for PV power forecasting, the focus of solar irradiance forecasting is likely to shift from the forecasting of solar irradiance to PV power.

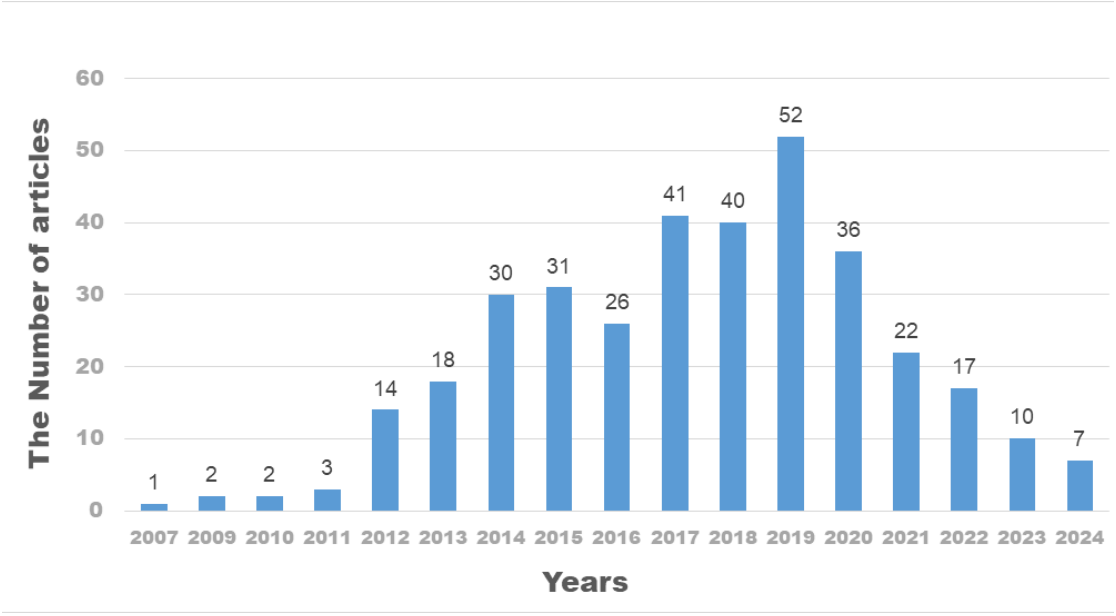

Figure 2.10 The number of published articles on solar forecasting methods from 2007 to 2024

2.6.4 The Number of Articles of Different Solar Irradiance Forecasting Methods

Figure 2.11 depicts the total number of articles of different solar irradiance forecasting methods. At first, the limited number of articles of Numerical Weather Prediction (NWP) methods and Top-Down forecast methods indicates that these methods are not ideal for the forecasting from 1 second to 6 hours. The major reason is the low spatial-temporal resolution of Numerical Weather Prediction (NWP) methods

and Top-Down forecast methods. In contrast, the number of articles of Data-driven methods and Hybrid methods is very large, which implies that they are well suited for the above forecasting horizons. This is because both Data-driven methods and Hybrid methods usually depend on the conditions of datasets, and thus can achieve ideal forecasting results as long as the conditions of datasets meet requirements. Moreover, although both Model-Driven methods and Data-driven methods are Statistical and Learning methods, Model-Driven methods are used less often because they require a depth level of understanding of the statistical models. At last, despite Bottom-up forecast methods are developed specifically for very short and short-term forecasting, the number of articles on them are relatively small due to the late emergence of them. Based on the above, Bottom-up forecast methods, Data-driven methods and Hybrid methods will be the focus of this research.

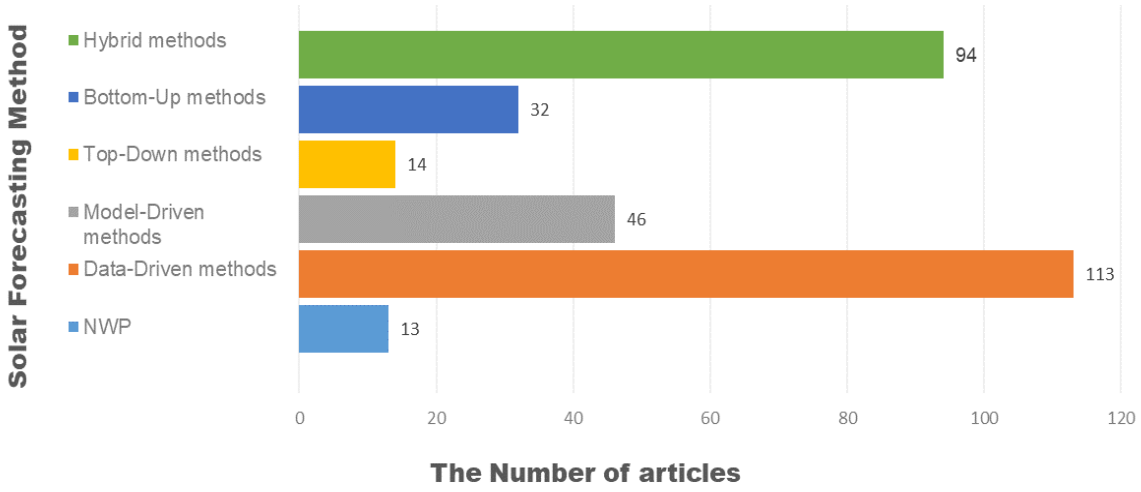

Figure 2.11 The total number of articles on different solar forecasting methods

Trends in the development of different solar irradiance forecasting methods over the past few years are shown in Figure 2.8. According to Figure 2.8, the number of articles on Numerical Weather Prediction (NWP) methods and Top-Down forecast methods were mainly published between 2013 and 2020 and have been absent in recent years. The article number of Bottom-up forecast methods reaches its peak in 2017 and significantly declines after that time. The explosion of Bottom-up forecast methods in 2017 is attributed to the development of total sky imager and image

processing techniques. On the other hand, the decline of Bottom-up forecast methods might be a result of the development of hybrid methods, as hybrid methods are often composed of Bottom-up forecast methods and Data-driven methods. Similar to Bottom-up forecast methods, Model-driven methods show a similar downward trend. Trends in the number of articles of Data-driven methods and Hybrid methods evidently demonstrate they are widely used in this field. However, the article number of Hybrid methods has decreased in recent years relative to Data-driven methods, except for 2024 probably induced by the rapid development of Deep Learning (DL) and computer hardware. In general, Figure 2.12 implies that Data-driven and Hybrid methods are the future direction of this field.

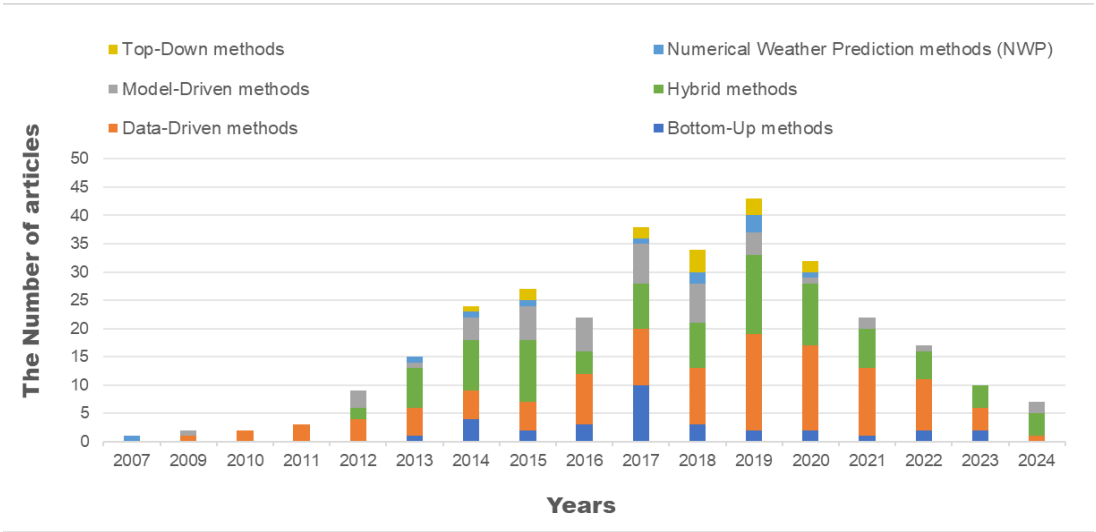

Figure 2.12 The number of articles of different solar forecasting methods in different years

2.6.5 Data Acquisition Ways of Solar Irradiance Forecasting Methods

Figure 2.13 describes the number of articles on different data acquisition ways for solar irradiance forecasting methods. As mentioned before, data acquisition ways mainly involve five types: Public Weather Observation, Privately-owned Equipment, Meteorological Satellites, Grounded Sky Imagers and Weather APIs.

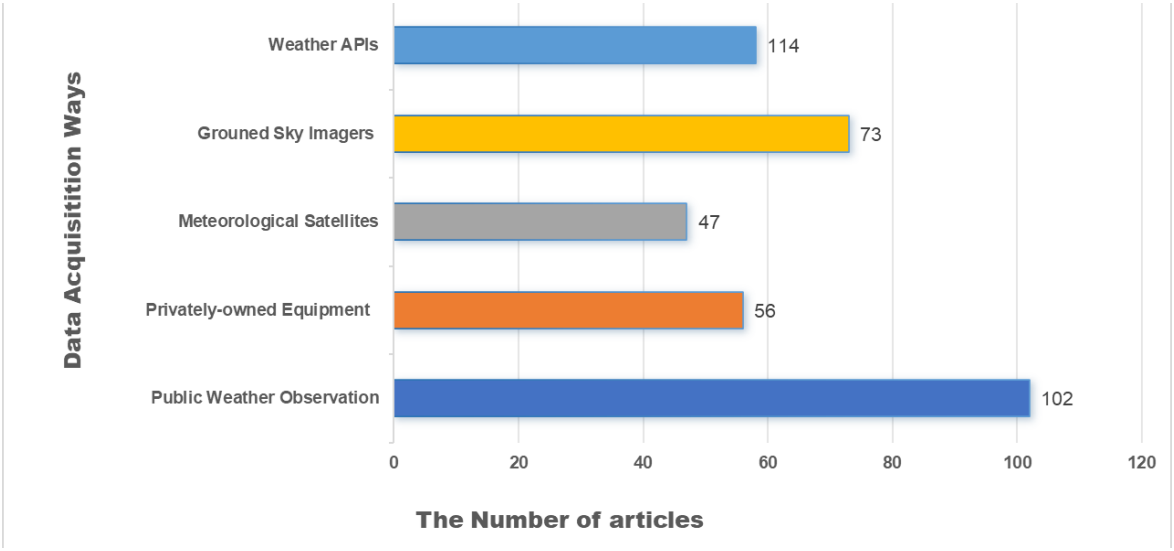

Figure 2.13 The number of articles of different data acquisition ways

In general, as the most conventional and stable data acquisition way, public weather observation shows obvious advantages in terms of article number. It includes several advantages, such as easy access, low cost, high stability, and is therefore particularly suitable for studies requiring medium to long-term weather data. In contrast, privately-owned equipment is typically used by individual researchers or small research organisations for special studies. Thus, its article number is relatively small. The cost of privately-owned equipment depends on the device type and configuration. Its initial investment may be high, but it can save the cost of data acquisition in the long term. The article's number of meteorological satellites is the smallest, which is usually induced by its low spatial-temporal resolution and fewer satellite resources. The high article number of ground sky imagers demonstrates its popularity in recent years because of their late emergence. The crucial advantage of ground sky imagers is high spatial-temporal resolution. Thus, they are well suited for collecting on-site and high-frequency sky image data. The cost of the ground sky imager also depends on the device type and configuration and sometime there will be maintenance issues. Weather APIs, as another emerging data acquisition, have also become popular recently in terms of the number of articles. Although some basic weather data is available for free, high-quality and hard-to-obtain data, such as solar irradiance, may require payment. In summary, the choice of each method depends on specific

application requirements, budgetary constraints and other factors. Thus, researchers need to consider the cost, accessibility, accuracy, and spatial-temporal resolution of data. Considering that building applications usually require on-site and high-frequency data, privately-owned equipment and ground sky imagers will be the focus of this research implies the potential of Bottom-up forecast methods, Data-driven methods and Hybrid methods for buildings.

2.6.6 Forecasting Horizons and Temporal Resolutions of Solar Irradiance Forecasting Methods

Figure 2.14 demonstrates the proportion and the number of articles with different forecasting horizons.

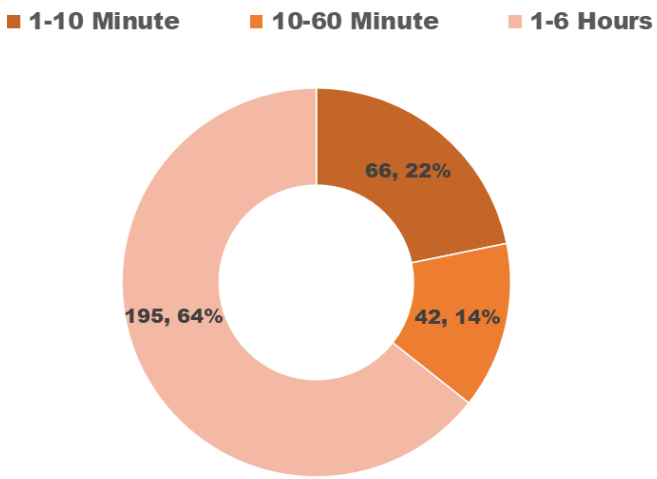

Figure 2.14 The proportion and number of articles with different forecasting horizons

In general, forecasting horizons from 1 to 6 hours account for 64% of the total articles, with a total number of 195. This indicates that hourly nowcasting is more common than minutely nowcasting because of its relative lower difficulty of forecasting and wide applications. Specifically, hourly nowcasting has been widely used for daily energy management and scheduling, which helps grid operators, energy markets or buildings to predict energy demand and supply conditions for the coming hours. In contrast, intra-hour nowcasting from 10 to 60 minutes is relatively less. However, intra-hour nowcasting, especially 1-sec to 10-min nowcasting, has the potential to provide

real-time or near-real-time solar irradiance data, which is promising for the more fine-grained management and regulation of building energy systems in the future. Figure 2.15 indicates the research on intra-hour nowcasting was mainly published between 2017 and 2022 and declined in the last year but grew again in 2024. In summary, the research of solar irradiance nowcasting methods is still promising.

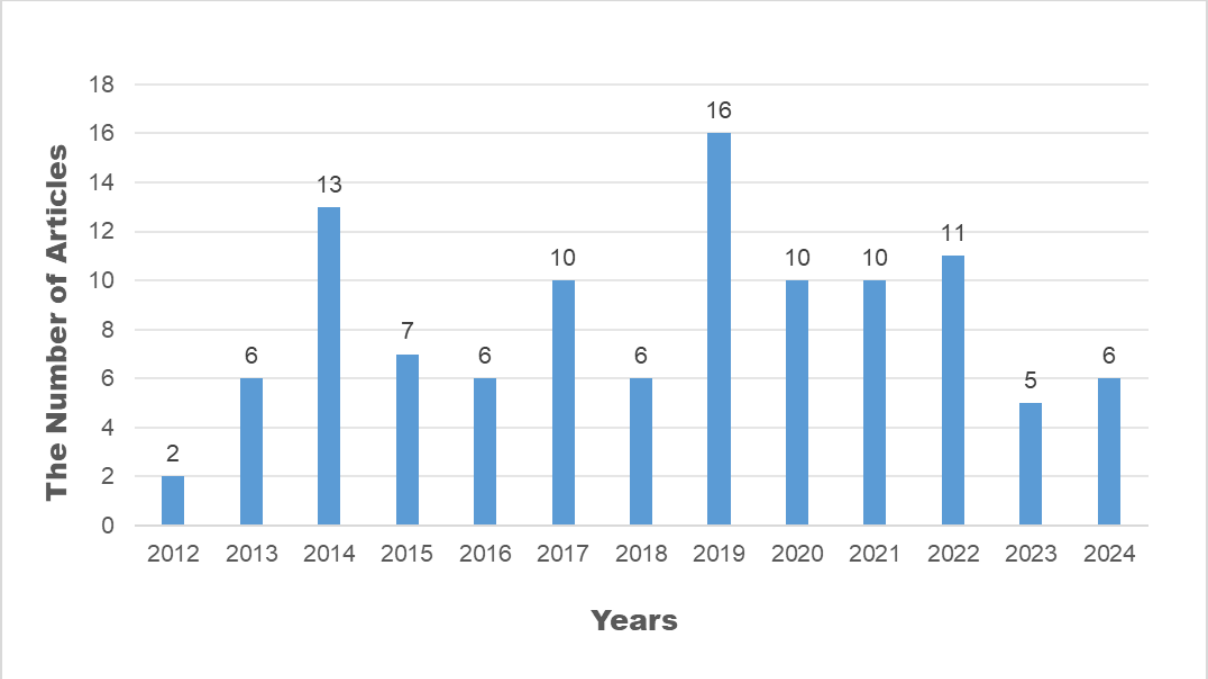

Figure 2.15 The articles with forecasting horizons from 1 to 60 minutes in different years

Figure 2.16 displays the proportion and the number of articles with various temporal resolutions. It is evident that the temporal resolution of solar irradiance nowcasting is mainly distributed under ten minutes and over one hour. Temporal resolution directly determines the frequency of solar irradiance nowcasting, and it thus impacts the applications scenarios of solar irradiance forecasting. In addition, intra-hour temporal resolution accounts for 76% which indicates high temporal resolution is in high demand in the field of solar irradiance nowcasting.

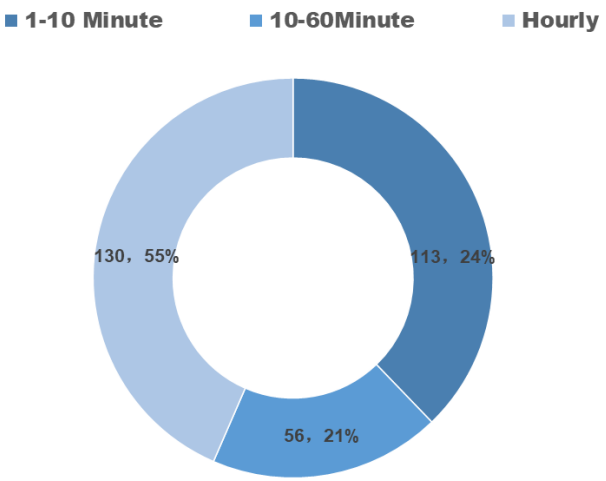

Figure 2.16 The proportion and number of articles with different temporal resolution

In addition, Figure 2.17 shows that fewer studies have paid attention to multiple temporal resolutions, which merely account for 26.8%. In this case, future research is necessary to investigate the effects of multiple temporal resolutions on solar irradiance forecasting methods.

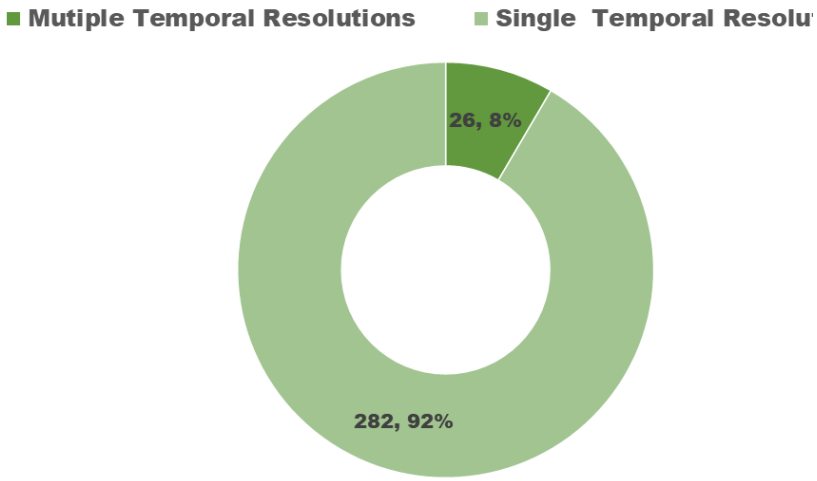

Figure 2.17 The proportion and number of articles with single interval and multiple intervals

2.6.7 Forecasting Parameters of Solar Irradiance Forecasting Methods

Figure 2.18 describes the proportion of three critical parameters of solar irradiance forecasting in the included articles, including GHI, DNI and DHI. At first, GHI has the largest share at 80%. Secondly, DNI accounts for 15%, significantly less than GHI. At

last, DHI has the smallest share at 5%. This distribution of GHI, DNI, and DHI shows that GHI is the most common focus of solar irradiance forecasting methods. This is because GHI is the sum of the DNI and DHI and can be used directly in solar applications. Although DNI and DHI are also crucial for specific applications, they are not major forecasting parameters in solar irradiance forecasting, especially DHI. In this case, the forecasting of DHI is an evident research gap.

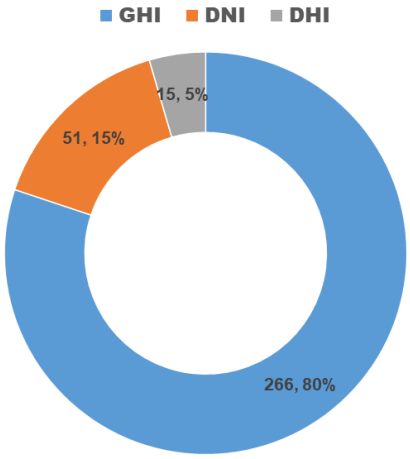

Figure 2.18 The proportion of articles for GHI, DNI and DHI forecasting

2.6.8 Evaluation Metrics of Solar Irradiance Forecasting Methods

Evaluation metrics is a significant solution to measure forecasting accuracy. In specific, these metrics aim to judge the error between predicted value and actual value. Figure 2.19 presents the number of times various evaluation metrics were used. It is obvious that the Root Mean Squared Error (RMSE) is used far more often than other metrics and the Mean absolute error (MAE) is the second. After RMSE and MAE, the Normalized Root Mean Square Error (nRMSE) and the Mean Absolute Percentage Error (MAPE) are also very popular. In addition, the Mean Bias Error (MBE), the Correlation Coefficient (r) and the Coefficient of Determination (r^2) are also relatively popular. In addition to the common evaluation metrics, there are some specific indicators, such as the Forecast Skill Score (SS), and others specifically designed for some studies. The above evaluation metrics can be divided into two categories: absolute indicator and relative indicator. Absolute indicators provide specific values

that directly reflect the reality of a phenomenon or data and thus are Ideal for comparison on the same or similar datasets. Conversely, relative indicators are indicators relative to other benchmarks or ratios and are often used to compare and assess relationships or trends between data. Thus, they are usually used to compare different datasets. A few common evaluation metrics will be explained in detail below.

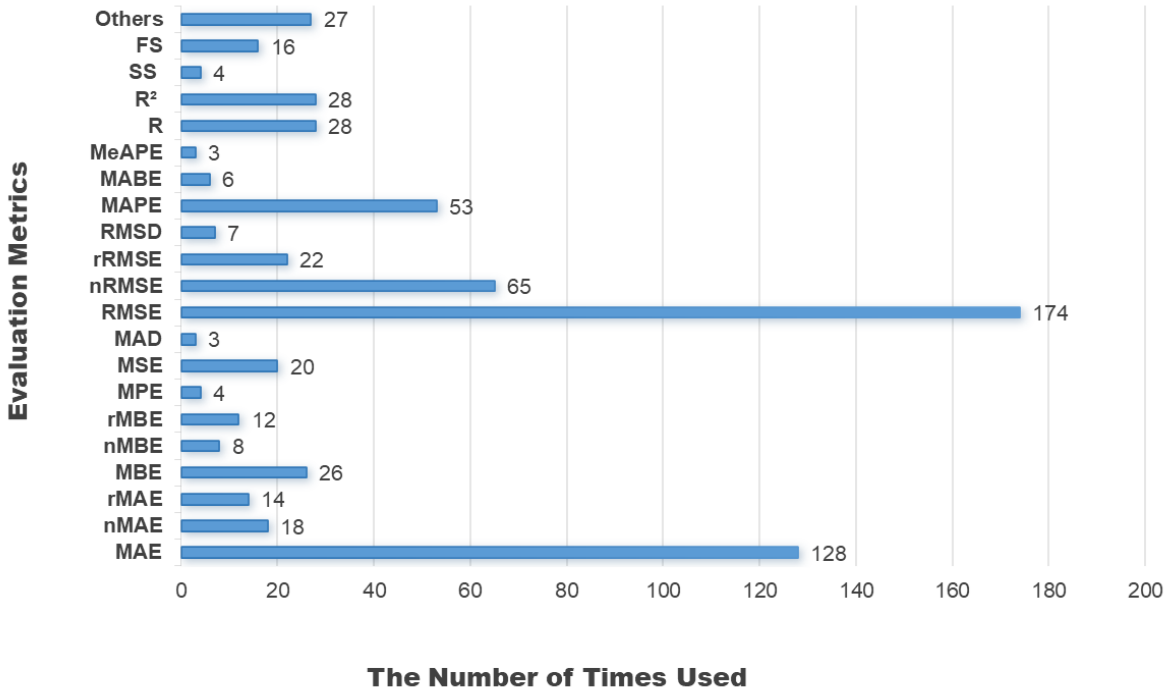

Figure 2.19 The number of articles on various evaluation metrics

In the following equations, p_i represents the nowcasting values, m_i represents the measurements, $\bar{m}$ represents the averaged measurements, $\hat{m}$ represents the i-th value predicted from the regression model.

- Root Mean Squared Error (RMSE)

  The root mean squared error is a representative absolute indicator. It is calculated based on the difference between the predicted value and the true value. It can be expressed as:

$$RMSE = \sqrt{\frac{1}{N}\sum_{i=1}^{N}(p_i - m_i)^2} \tag{2.2}$$

  The critical advantage of RMSE is that it is highly sensitive to large prediction

errors, making it suitable for situations where the effects of large errors need to be emphasised. In addition, the square root keeps it at the same magnitude as the original data and thus improves its interpretability. However, the drawbacks of RMSE are apparent. First of all, RMSE is susceptible to extreme values, which means that if there are some abnormal values leading to large deviations, the RMSE will be larger and thus impact the overall judgement of the model. Meanwhile, RMSE could only assess the different model performances under the same basic dataset. In other words, it is meaningless to compare the predicted performance of diverse models based on different datasets because the original data is distinct.

- The Normalised Root Mean Square Error (nRMSE)

  The normalised root mean square error is a relative indicator. The "normalized" aspect of NRMSE refers to the scaling of the error based on the range or standard deviation of the observed data, which makes the measure dimensionless and allows for the comparison between different datasets or models with different scales. It can be expressed as:

$$nRMSE = RMSE / \overline{m} \tag{2.3}$$

  The critical advantage of nRMSE is that it is possible to more accurately understand and compare the performance of different models when datasets are very different. The purpose of nRMSE is to restrict the deviation result in the range of 0 to 1. As a result, the final calculated value is often expressed as a percentage, where lower values indicate higher accuracy. Figure 2.20 evidently indicates that the nRMSE for most studies ranged from 9.29% to 28.37%. The lowest nRMSE is 0.1%, which means that the accuracy is extremely high. However, there are some studies with the lowest nRMSE OF 56.4%. Nevertheless, it is worth noting the accuracy of the forecasting model is influenced by multiple factors and thus the model with the highest precise may not suited for all datasets. To sum up, based on the nRMSE of all articles,

an nRMSE between 9.49% to 29.43% would be considered as the qualified accuracy for this research.

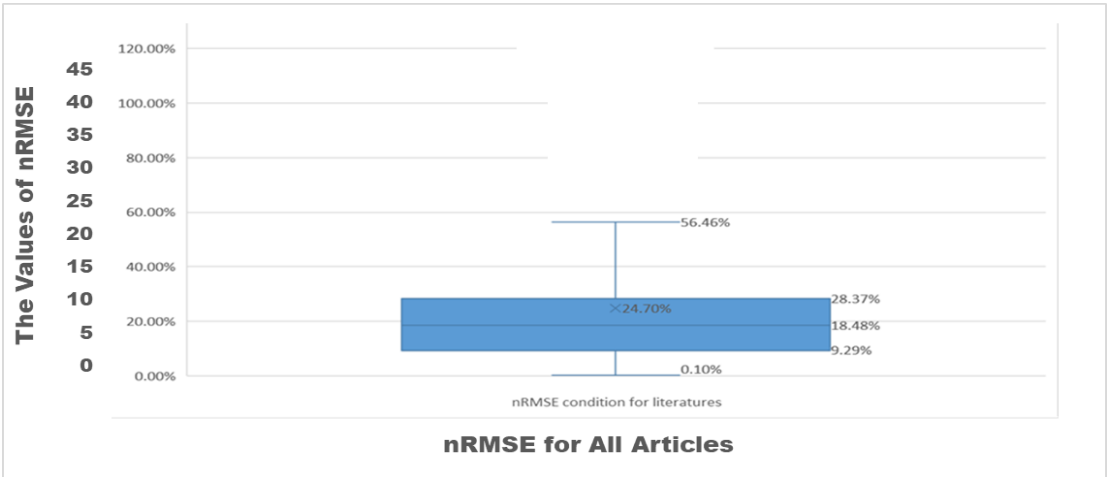

Figure 2.20 The distribution of nRMSE across all articles.

- The Mean Absolute Error (MAE)

  The mean absolute error is a basic absolute indicator to measure the average absolute error between predicted and actual values. It can be expressed as:

$$MAE = \frac{1}{N}\sum_{i=1}^{N}|p_i - m_i| \tag{2.4}$$

  The MAE and RMSE are generally similar, but the MAE is less sensitive to abnormal values because it does not take into account the direction and magnitude of the error squared. To sum up, the choice of MAE or RMSE depends on the sensitivity of abnormal values and the size of the error.

- The Normalised Mean Absolute Error (nMAE).

  Similar to nRMSE, the normalised mean absolute error is a relative indicator. It can be expressed as:

$$nMAE = MAE / \bar{m} \tag{2.5}$$

  Figure 2.21 depicts the values of nMAE for all articles. It can be obtained that currently, the nMAE value mainly distributes between 6.36% and 28.94%, and the average term is 16.53%. The maximum and minimum nMAE are 2.38% and 46.37% respectively. Thus, the nMAE for this research is ideal as long as it is less than 16.53%.

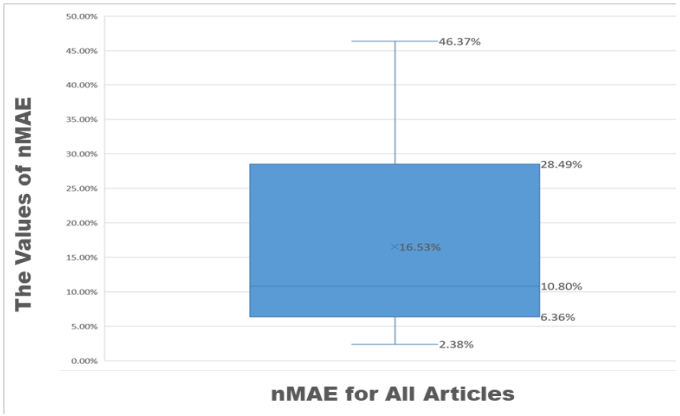

Figure 2.21 The distribution of nMAE across all articles.

- Coefficient of Determination (R^2)

  The coefficient of determination is a relative indicator. It is used to measure the reliability of the change in the dependent variable. The value of R^2 varies between 0 and 1. The closer R^2 is to 1, the higher the accuracy. In contrast, when R^2 is closer to 0, the accuracy is worse. It can be expressed as:

$$R^2 = 1 - \frac{\sum_{i=1}^{N}(m_i - \hat{m})^2}{\sum_{i=1}^{N}(m_i - \bar{m})^2} \tag{2.6}$$

  Figure 2.22 presents R^2 for all included articles. Most articles have R^2 between 0.86 and 0.98, demonstrating that the differences between prediction and actual observations are minor, indicating that forecasting can capture the trends of data variation accurately.

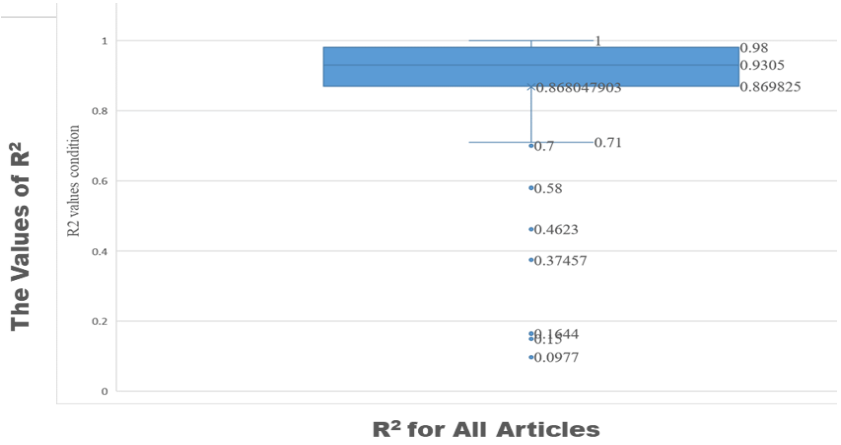

Figure 2.22 The distribution of R^2 across all articles.

To sum up, during the process of systematic literature review, it was found that most studies do not articulate specific reasons for the selection of evaluation metrics

and analyse these metrics in detail, so this is a rewarding research gap that needs to be addressed.

2.6.9 Application of Solar Irradiance Forecasting Methods

Figure 2.23 indicates most studies are concerned about the application of solar irradiance forecasting. However, most studies have focused only on PV-related applications rather than other possible other applications. Therefore, the potential applications of solar irradiance nowcasting are worth being discussed in this research.

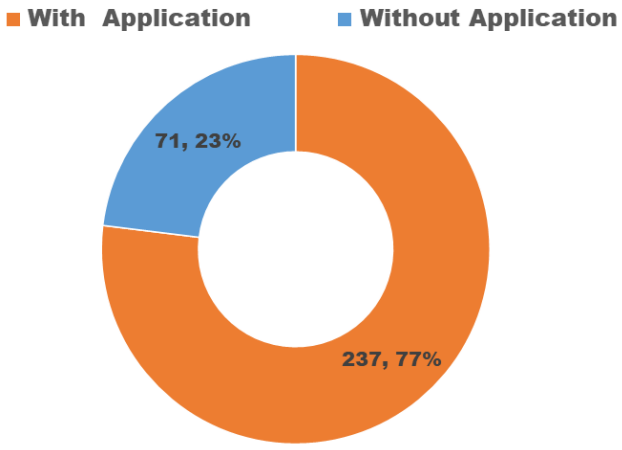

Figure 2.23 The proportion of articles proposing applications of solar irradiance nowcasting

2.7 Research Gaps Summarised from The Systematic Review

Based on the systematic literature view, the main research gaps are summarised as follows:

1. Very few studies pay attention to nowcasting horizons and spatial-temporal resolution appropriate for building applications. The potential value of emerging solar irradiance nowcasting methods to buildings and their future development has not yet gotten a high profile.
2. Few studies have articulated the equipment and programming used for solar irradiance forecasting methods in conjunction with the needs of buildings.
3. The nowcasting of DHI has received little attention despite being one of three critical parameters of solar irradiance, which is valuable to building simulation programs.
4. The impact of diverse factors, including forecasting horizons, time intervals, sky conditions, forecasting models and datasets, on the forecasting performance has not been investigated comprehensively.
5. Little research pays attention to the study and selection of evaluation metrics for solar irradiance forecasting methods.
6. The prospective applications of solar irradiance forecasting methods on buildings have not been discussed from an architectural perspective.

2.8 Nowcasting Methods with Potential for Building Applications

After a comprehensive analysis of the results from the systematic literature review, it is essential to specifically explore the potential of different solar irradiance nowcasting methods for buildings.

Based on the meteorological term, forecasting with forecasting horizons from 1 second to 6 hours is defined as nowcasting in this research. As mentioned above, solar irradiance forecasting methods can be classified into five types: Numerical Weather Prediction (NWPs), Statistical and Learning, Top-down, Bottom-up, and Hybrid. Although these methods have very different forecasting horizons and spatial-temporal resolutions, portions of each method fulfil the definition of nowcasting.

Since this research aims to explore solar irradiance nowcasting methods with very short-term forecasting horizons and high spatial-temporal resolution potential for building applications, an in-depth review of nowcasting methods from the five types is necessary.

- Numerical Weather Prediction methods (NWPs)

  Due to the spatial-temporal resolution of NWP methods always being very low, it is rarely used for solar irradiance nowcasting. [77] utilised an improved WRF model, which is a common model used in NWP methods, to achieve 1-hour nowcasting of GHI. [78] presented several NWP models used for forecasting, including ECMWF, NAM, GFS, RAP and used those models to obtain 3-hour GHI nowcasting. Table 2.14 summarises the studies of NWP methods for nowcasting and evidently demonstrates NWP methods is not used in any intra-hour nowcasting.

Table 2.14 NWP methods for solar irradiance nowcasting.

Nowcasting Horizons (1sec-10min)	Nowcasting Horizons (10min-60min)	Nowcasting Horizons (1-6hour)
/	/	[77-87]

- Statistical and Learning Methods

  Data-driven methods are one of the main types of Statistical and Learning methods and are commonly used for solar irradiance nowcasting. First, some studies enable solar irradiance nowcasting with innovative machine learning models. [88] is a representative Data-driven method which utilised semi-real-time decision tree ensemble algorithms to achieve reliable 15-sec and 30-sec GHI nowcasting by using only historical data of GHI. This method not only has a low computational cost but also achieves effective forecasting without the need for external information. In addition, the combination of multiple machine learning models is also a way to develop effective nowcasting methods. A representative Data-driven method proposed in 2024 utilised GHI, DNI, DHI and other diverse weather data as model input to train a hybrid deep learning model - TLD and ultimately acquired 10-min and 15-min nowcasting of DNI [89]. The TLD model integrates topological features captured by Topology Data Analysis (TDA) with temporal features captured by LSTM. [90] also developed a WPD-CNN-LSTM-MLP model, which combines several types of deep learning models to predict GHI for one hour ahead based on the use of GHI and different weather data acquired from a weather API. In summary, Data-driven methods are well suited for solar irradiance nowcasting. However, those methods tend to require permanent use of solar irradiance data and diverse weather data, which might lead to high purchase and maintenance costs of equipment or difficulty of data access. This is not ideal for building applications. More studies of Data-driven methods for nowcasting are summarised in Table 2.15. It is obvious Data-driven methods are more often used for 1 to 6-hour nowcasting.

Table 2.15 Data-driven methods for solar irradiance nowcasting.

Nowcasting Horizons (1sec-10min)	Nowcasting Horizons (10min-60min)	Nowcasting Horizons (1-6hour)
[44, 79, 91-101]	[44, 79, 89, 92, 98, 102-113]	[44, 45, 48, 73, 79, 90, 92, 98, 102, 105, 108-185]

Although the total number of Model-driven methods is significantly lower than Data-driven methods that enable the achieve solar irradiance nowcasting, some studies still demonstrate their ability for nowcasting. Based on Markov-chain mixture (MCM) model, [186] successfully achieved 1 to 5 min nowcasting of GHI. The forecasting method proposed in this study is a typical Model-driven method. ARIMA, as a representative statistical model for time series forecasting, is applied to achieve 15-min, 30-min, 45-min, and 1 to 3-hour nowcasting [187]. Table 2.16 summarises the studies of Model-driven methods for nowcasting. The number of distributions in different forecasting horizons of Model-driven methods is relatively similar.

Table 2.16 Model-driven methods for solar irradiance nowcasting.

Nowcasting Horizons (1sec-10min)	Nowcasting Horizons (10min-60min)	Nowcasting Horizons (1-6hour)
[88, 186, 188-191]	[50, 187, 191-199]	[49, 124, 187, 192, 194, 197, 200-227]

- Top-down forecast methods

  Similar to NWP methods, Top-down forecast methods is also not ideal for solar irradiance nowcasting because of their low spatial-temporal resolutions. Based on the visible and near-infrared channels (AGRI) onboard the FengYun-4A (FY-4A) geostationary satellite, [228] utilised an algorithm to obtain 30 to 180-min nowcasting of GHI and DNI. [229] successfully predicted from 15 to 180 minutes by using satellite images. The articles on Top-down forecast methods are summarised in Table 2.17, which intuitively shows only several articles have utilised the Top-down forecast methods to obtain intra-hour nowcasting.

Table 2.17 Top-down forecast methods for solar irradiance nowcasting.

Nowcasting Horizons (1sec-10min)	Nowcasting Horizons (10min-60min)	Nowcasting Horizons (1-6hour)
/	[228-230]	[228-241]

- Bottom-up forecast methods

  Unlike NWP methods and Top-down forecast methods, Bottom-up forecast methods have a significant advantage for solar irradiance nowcasting due to their high spatial-temporal resolutions. [242] published in 2013, it is the earliest to use Total Sky Imager (TSI) and image processing techniques to predict 3 to 15-min DNI. The study innovatively predicts 3-hour GHI, DNI and DHI by using the conversion between digital image levels and solar irradiances, as well as the maximum cross-correlation method [233]. Based on a developed All-Sky Imager (ASI) nowcast, [243] proposed a real-time capable nonparametric probabilistic quantile nowcasting method which successfully achieve 1 to 20 min nowcasting of GHI and DNI. Table 2.18 summarises the articles of Top-down forecast methods for nowcasting, as well as explicitly demonstrates Bottom-up forecast methods have a significantly higher number of articles for the intra-hour nowcasting, especially from 1 second to 10 minutes.

Table 2.18 Bottom-up methods for solar irradiance nowcasting.

Nowcasting Horizons (1sec-10min)	Nowcasting Horizons (10min-60min)	Nowcasting Horizons (1-6hour)
[66, 242-253]	[66, 242, 250, 254-263]	[64, 232, 233, 264-268]

- Hybrid methods

  Hybrid methods combine the advantages of different forecasting methods and are therefore well suited for solar irradiance nowcasting. Based on weather data from NWP forecast models and two designed ANN models, [269] achieves 10-min nowcasting of DNI. [270] proposed a hybrid method which utilised satellite data and a machine learning regression model to conduct hourly GHI

nowcasting. The study respectively utilised four groups of cloud images captured from four ASIs and different cloud detection methods, including clear sky library, Neural Network, Red/Blue ratio and deep learning, to obtain GHI nowcasting from 1 to 20 minutes and compared the results of different groups. [271] used TSI and two CNN models - AlexNet and ResNet-101 to predict GHI from 1 to 15 minutes. [272] used CNN to extract the spatial features of infrared cloud images and a prevalent deep learning model - Long Short-Term Memory (LSTM) networks to capture the temporal dynamics of solar irradiance data that thus effectively predict GHI in 15 minutes. The studies of Hybrid methods are summarised in Table 2.19, which shows Hybrid methods are widely used for 1-sec to 6-hour nowcasting.

Table 2.19 Hybrid methods for solar irradiance nowcasting.

Nowcasting Horizons (1sec-10min)	**Nowcasting Horizons (10min-60min)**	**Nowcasting Horizons (1-6hour)**
[65, 69, 251, 269, 271-287]	[251, 271, 282, 283, 285-308]	[64, 110, 130, 202, 214, 269, 270, 274, 275, 286, 291, 301, 306, 309-348]

Considering the trend towards building intelligence, very short-term forecasting horizons and high spatial-temporal resolutions will be the crucial characteristics of solar irradiance nowcasting methods appropriate for buildings. According to Figure 2.1 in section 2.1.7, the red zone demonstrates the specific forecasting horizons and spatial resolution of the conceived solar irradiance nowcasting method.

Based on the above, Data-driven methods, Bottom-up forecast methods and Hybrid methods are potential for solar irradiance nowcasting. In this case, it is necessary to investigate the specific techniques and approaches associated with the aforementioned methods more thoroughly.

2.9 Characteristics of Nowcasting Method Suitable for Buildings

Based on the above, this section examines the characteristics of Data-driven methods, Bottom-up forecast methods and Hybrid methods in terms of their suitability for buildings. Since the Hybrid methods tend to consist of Statistical and Learning methods, Bottom-up forecast methods, this section provides a targeted study on some specific characteristics of Data-driven methods and Bottom-up forecast methods. These characteristics involve image processing techniques, low-cost equipment, deep learning models and user-friendly programming.

- Image Processing Techniques of Bottom-up Forecast Methods

  Image processing techniques are the critical characteristic of Bottom-up forecast methods. First, cloud images are the crucial data of Bottom-up forecast methods and thus the first step is to process captured images. Common data processing techniques involve image calibration, image masking, exposure adjustment, cloud pixels identification, cloud movement vector calculation, etc.

  Some studies will first take image correction techniques to ensure that each point in the image correctly reflects its actual position. This step is important because the angle of the sky camera, its position, or the distortion of the camera lens can lead to image distortion. After that, an essential masking step is used to eliminate unnecessary elements in the image, including buildings, trees, streets, etc. Thirdly, some techniques are applied to adjust image exposure for the following cloud pixel identification. Next, a key step of image processing is conducted to extract the red-green-blue (RGB) value of each image pixel and use diverse approaches to complete cloud pixel recognition. At last, based on the identified cloud pixels in two consecutive images, the movement vector is calculated and thus can achieve the motion trajectory of the pixel, which is then used to predict the position of the pixel in the next

timestep. In addition to the key steps mentioned above, different studies will propose unique image processing steps or optimised solutions according to actual circumstances.

[249] was a representative study applying a series of comprehensive image processing techniques to achieve 1 to 10-min GHI nowcasting. Another article achieved 5-min DNI nowcasting based on very complex image processing techniques with a unique Lucas-Kanade optical flow method, which was used to track the feature points of cloud images [349]. [263] utilised a novel object oriented approach with four spatially distributed ASIs to achieve 15-min nowcasting of DNI. [287] developed a hybrid method which used CNN-LSTM to learn cloud features and thus obtain 4 to 20-min nowcasting.

In summary, the choice of image processing techniques is one of the key factors affecting this research and it thus needs to be fully considered in the development of the methodology.

- Equipment for Bottom-up Forecast Methods

  Apart from image processing techniques, equipment is also the core of Bottom-up Forecast Methods because all this type of methods relies on grounded sky cameras. There are very many different forms and configurations of grounded sky cameras. Some studies use expensive high-resolution specialised Total Sky Imager (TSI), but others tend to develop special camera systems by innovatively using some low-cost equipment. In addition, a grounded sky camera does not have to work alone. Some studies have compensated for the limitations of a single camera by using multiple cameras together.

  [250] compared several popular grounded sky cameras and utilised two sky cameras located in two different sites to achieve 1 to 15-min GHI nowcasting. [255] innovatively developed a sun-tracking imaging system which can effectively minimise the circumsolar image distortion and thus improve the

nowcasting method. Some other studies focused on the exploration of low-cost ground sky cameras and achieved reliable nowcasting successfully [61, 64, 274]. Recently, [286] achieved 10-min to 2-hour nowcasting by using a public webcam.

To sum up, low-cost equipment is very promising considering the generalisation of solar irradiance nowcasting methods on buildings.

- Machine Learning Models of Data-driven Methods

  Machine Learning models are the foundation of Data-driven Methods. Representative Machine Learning models and some statistical models are summarised from the systematic literature review, as shown in Figure 2.20.

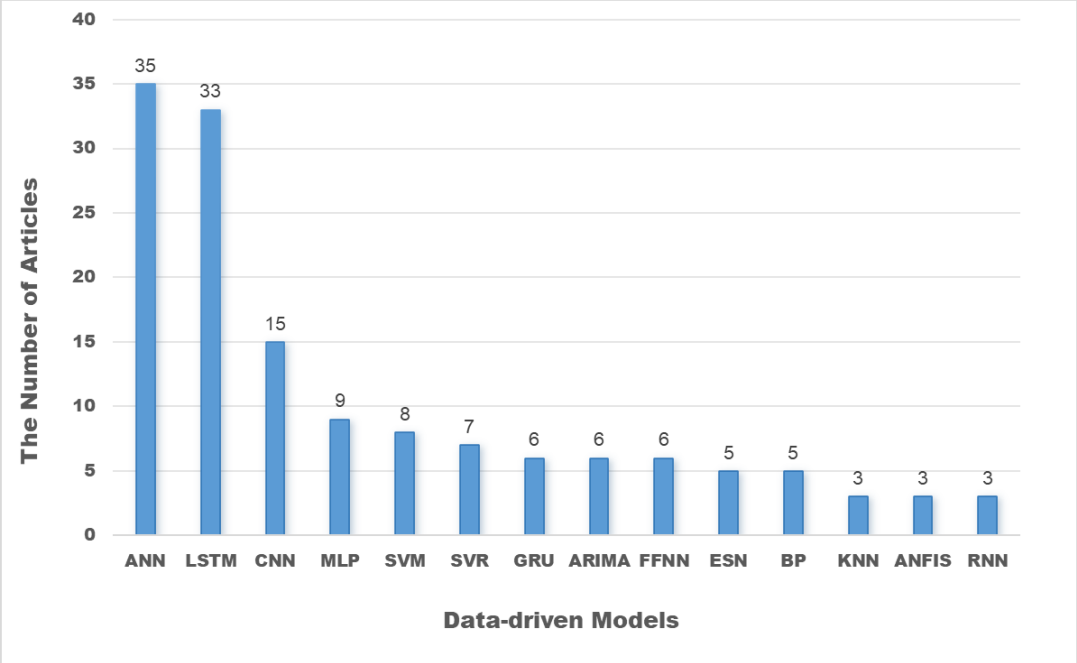

Figure 2.24 The number of articles used different forecasting models

It is evident that basic ANN and CNN models, as well as LSTM are widely used for solar irradiance nowcasting. ANN is the most basic form of neural network and is suitable for simple or moderately complex classification and regression, but it is not good with data that is spatially and temporally correlated. The crucial advantage of ANN is simple and flexible. CNN is designed to process data with a grid-like structure, such as images. In this

case, CNNs are well suited for processing data with strong spatial or temporal proximity and thus can achieve higher accuracy in image or video recognition tasks. LSTM is a particular type of Recurrent Neural Network (RNN) that specialises in processing and predicting time series data. However, the training of LSTMs is usually more time-consuming than ANNs and simple CNNs. In recent years, these models have also been used in combination to develop more advanced models for optimising solar irradiance forecasting methods.

Two ANNs were employed with cloud images to achieve 1 to 5-min nowcasting of GHI by [350]. [182] respectively utilised CNN, LSTM, ConvLSTM to achieve the nowcasting of GHI. The nowcasting performance of LSTM and FFNN is compared by [166]. Recently, [271] developed a hybrid method, which used the grounded cloud image and two representative deep learning model - AlexNet and ResNet-101, to achieve 1 to 15-min GHI nowcasting.

In summary, the selection of nowcasting model is also the core of this research. A combination of model characteristics, such as learning ability, time consumption, extensibility, etc, are needed to be considered.

- Programming for Data-driven Methods

  Programming tools and language are the basics of Machine Learning models. However, the selection of programming tools and language is rarely articulated in most studies. The diverse toolbox of MATLAB can help developers quickly implement complex algorithms, and thus, it has been widely used in past decades. However, MATLAB is commercial software that requires the purchase of a license to use and thus increases the cost of use. In this case, more and more studies use Python to execute Data-driven model due to a series of user-friendly features, including open-source, free, abundant libraries and extensive community support.

MATLAB was applied to execute SVM for hourly GHI nowcasting in 2013 by [119]. [343] proposed a multi-timescale ESN (MTS-ESN) model to achieve hourly nowcasting of GHI based on Python in 2019. Based on both MATLAB and Python, [156] successfully achieved hourly GHI nowcasting using SOM and deep learning algorithms.

On this basis, the selection and application of programming tools and languages also needed to be explored in this research.

In conclusion, the abovementioned characteristics involving image processing techniques, machine learning models, equipment and programming will be considered in conjunction with the needs of buildings to develop a hybrid methodology for this research.

2.10 Conceptualisation of Solar Irradiance Nowcasting Method

The importance of this research is to explore a solar irradiance nowcasting method from an architectural perspective and achieve reliable GHI, DNI and DHI nowcasting to optimise the operational efficiency and safety, occupant comfort and design of buildings.

Based on the importance of this research and systematic literature review, the proposed solar irradiance nowcasting method should have the following characteristics:

- Very Short-term Nowcasting Horizons and High Spatial-Temporal Resolution

  Single building or several buildings need on-site and real-time weather data to achieve precise regulation and management of building systems and thus optimise the building performance. Therefore, a very short-term nowcasting horizon range from several seconds to a few minutes is valuable. In addition, high spatial resolution ranging from 1 meter to 2 kilometers and high temporal resolution on a minute scale are necessary.

- Appropriate Image Processing Techniques and Reliable Nowcasting Model

  The balance between the utilisation of image processing techniques and machine learning models should be considered carefully to maximise the advantages of each and improve the accuracy and efficiency of solar irradiance nowcasting.

- Low-cost Equipment and User-friendly Programming.

  In this research, low-cost equipment and user-friendly programming will be prioritised to lower the cost and difficulty of building applications.

- Nowcasting Capabilities of GHI, DNI and DHI.

  Considering different types of solar systems and applications, the methodology of this research should achieve the nowcasting of GHI, DNI and DHI.

2.11 Chapter Summary

In summary, this chapter begins with a concise introduction of background information including the potential of solar energy in different regions worldwide, building energy demand, building energy benchmarks, the link between building and solar irradiance forecasting. And then, five representative solar irradiance forecasting methods, their data acquisition ways, forecasting horizons and spatial resolution are articulated briefly. Moreover, current literature reviews of solar irradiance forecasting methods and the limitations of their methodologies are demonstrated.

In this case, a systematic review methodology for solar irradiance forecasting methods is proposed and its relationship with the research methodology of solar irradiance nowcasting is articulated. Based on the methodology of systematic review, a comprehensive literature review is conducted and a large number of articles are reviewed and analysed.

After that, a series of research gaps are summarised, leading to the selection of promising solar irradiance forecasting methods, including Bottom-up forecast methods, Data-driven methods and Hybrid methods and the further investigation of their characteristics appropriate for building application. On this basis, a special solar irradiance nowcasting method is conceptualised, which informs the development of the research methodology of solar irradiance nowcasting in the next chapter.

Chapter Three

3 Research Methodology

Chapter 3 is dedicated to addressing the second research question proposed in Chapter 1 - “How can a solar irradiance nowcasting method appropriate for buildings be developed?” In this case, the primary purpose of this chapter is to fulfil the second research objective - to develop a solar irradiance nowcasting method with very short-term forecasting horizons and high spatial-temporal resolution using low-cost equipment and user-friendly programming to achieve the nowcasting of GHI, DNI and GHI.

The methodology of this research is developed based on the literature review and the exploration of previous research. According to Chapter 2, the literature review indicates a number of characteristics of solar irradiance nowcasting methods valuable for buildings, including very short-term nowcasting horizons, high spatial-temporal resolutions, equipment and programming, forecasting parameters, etc. Along with the development of building intelligence, solar irradiance nowcasting methods with the above characteristics will be promising in improving the building's operational efficiency, safety and occupant comfort. In this case, this research builds on the solar irradiance nowcasting methods in the literature review and previous research to develop a Hybrid solar irradiance nowcasting method with high spatial-temporal resolution for potential building applications.

This chapter first presents the comprehensive research methodology workflow. In general, this research mainly includes three crucial stages, each consisting of several steps involving a series of specific approaches. The three crucial stages involve data collection and processing, solar irradiance nowcasting, comparative tests and verification. Subsequently, the specific research methods and procedures for every step in each stage are described in detail.

3.1 The Workflow of Research Methodology

The most crucial purpose of this research is to develop a low-cost and user-friendly solar irradiance nowcasting method with a high spatial-temporal resolution to achieve reliable GHI, DNI and DHI nowcasting for buildings. In this case, the workflow of the research methodology is developed in Figure 3.1.

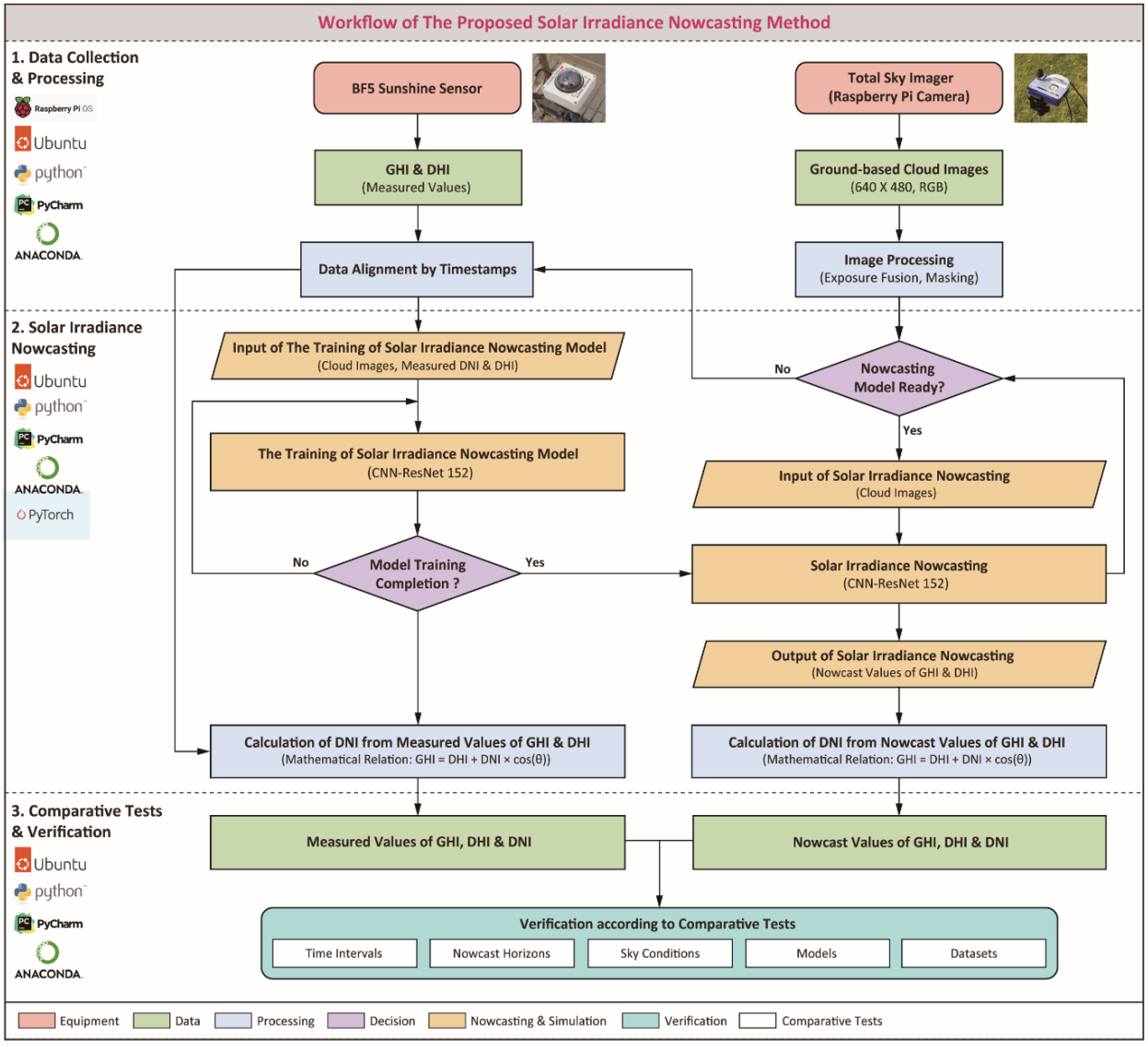

Figure 3.1 The workflow of research methodology

In Figure 3.1, the main stages of this research and their specific research contents, as well as the corresponding equipment and software are demonstrated.

The main equipment includes BF5 Sunshine Sensor and Total Sky Imager (Raspberry Pi Camera), which are described in detail in Section 3.2.2.

The main software tools used in this research are shown on the left side of Figure 3.1, these tools involve:

- Raspberry Pi OS

  Raspberry Pi OS is the official operating system for Raspberry Pi computers. It is based on Debian Linux and provides a user-friendly interface along with a wide range of pre-installed software, making it an ideal platform for hobbyists, educators, and developers alike.

- Ubuntu 20.04 OS

  Ubuntu is a popular, user-friendly Linux distribution (OS) based on Debian. It's known for its ease of use, strong community support, and a wide range of applications available through its software repositories. Ubuntu is often recommended for people new to Linux due to its simplicity, but it's also powerful enough for developers, IT professionals, and enthusiasts.

- Python

  Python is a high-level, interpreted programming language that is widely recognized for its simplicity, readability, and versatility. It is commonly used in diverse fields such as web development, data science, automation and artificial intelligence.

- Pycharm

  PyCharm is a popular Integrated Development Environment (IDE) used for programming in Python. Developed by JetBrains, PyCharm is designed to provide developers with a feature-rich and efficient environment for writing, testing, and debugging Python code.

- Anaconda

  Anaconda is an open-source distribution of the Python and R programming languages, primarily aimed at scientific computing, data science, machine learning, and large-scale data processing. It simplifies the installation and management of packages, environments, and tools that are commonly used

in data science workflows.

- PyTorch

  PyTorch is an open-source machine learning framework used primarily for deep learning applications. Developed by Facebook's AI Research lab (FAIR), PyTorch provides a flexible and efficient platform for building, training, and deploying machine learning models.

As shown in the figure, the above software tools are used in different stages of this research, their specific application are described in Section 3.4.6.

According to Figure 3.1, three main stages incorporate data collection and processing, solar irradiance nowcasting, comparative tests and verification.

The first stage - data collection and processing - mainly provides the basis for the development of the solar irradiance nowcasting model. Thus, it presents the location and devices for data collection, the types of collected data and a series of data processing approaches.

The second stage - solar irradiance nowcasting - is the critical stage which focus on the development of the proposed solar irradiance nowcasting model. Therefore, it articulates the background, the dataset collation, and the training and testing of the nowcasting model. In addition, the nowcasting of GHI and DHI, as well as the calculation of DNI, are demonstrated.

The third stage - comparative tests and verification - concentrates on the experiments and verification of the proposed solar irradiance nowcasting model. Consequently, a seris of specific setup involving time intervals, nowcasting horizon, classification of sky conditions, comparative models and evaluation metrics for comparative tests are described.

In summary, a range of specific approaches involved in each critical step of each stage is articulated in Figure 3.1. In addition, Figure 3.1 presents the equipment and relavent software tools used in each stage. At last, the different coloured legends at the bottom of Figure 3.1 identify the different research contents.

3.2 Data Collection and Processing

This section is mainly concerned with data collection and data processing. First, the location and devices for data collection, as well as collected data and datasets, are introduced. Then, the major data processing methods involving exposure fusion, masking, and data alignment are presented. As shown in Figure 3.1, red symbols represent specific devices used for data collection, Green symbols represent data types, and Blue symbols represent data processing procedures.

3.2.1 Location for Data Collection

All data for solar irradiance nowcasting were collected on the roof of the Department of Computer Science and Technology building, Tongji University, Shanghai, China (31.3° N, 121.2° E), which has an essentially subtropical monsoon climate, characterised by mild weather that is often cloudy, wet, and windy. The reason for selecting this location was the absence of tall buildings and trees nearby that could cause shade, ensuring a complete capture of the sky and clouds in the centre of the image.

The reason for selecting Shanghai, China, as the location for data collection was the impact of the lockdown policy induced by COVID-19 in the UK and the responsibility of parenting. However, it is worth noting the data collection activities at Tongji University, Shanghai, were also limited due to the administrative policy of Tongji University for non-members of the University. In this case, the dates of data collection were not completely consecutive.

3.2.2 Devices for Data Collection

There are two crucial devices for data collection, including a low-cost Raspberry Pi total sky imager and a Delta-T Device BF5 sunshine sensor, as shown in Figure 3.1. The low-cost Raspberry Pi total sky imager was mounted at a distance of approximately 5 meters to the Delta-T Device BF5 sunshine sensor.

- Low-cost Raspberry Pi total sky imager

  The low-cost Raspberry Pi total sky imager consisted of a Raspberry Pi 4 single-board computer equipped with a WAVESHARE OV5647 fisheye lens (5 megapixels OV5647 sensor, 180° field of view, 0.87 focal length) and was used to capture ground-based cloud images. Each 10-sec, a written Python program controlled the Raspberry Pi total sky imager to capture three different levels of exposure values and keep other photographic parameters consistent, such as ISO, saturation, brightness, contrast, etc.

  Unlike versatile and extremely expensive commercial total sky imager, which usually costs at least £20,000, Raspberry Pi total sky imager costs only around £150. In this case, the cost of capturing ground-based cloud images is significantly reduced, which is more affordable for the application on single or several buildings. The cost details of the Raspberry Pi total sky imager are shown in Table 3.1.

Table 3.1 Cost details of Raspberry Pi total sky imager.

Device Names	Raspberry Pi 4 Single-Board Computer	WAVESHARE OV5647 fisheye lens	Memory Card	Total
Cost	£80	£30	£40	£150

- Delta-T Device BF5 sunshine sensor

  The Delta-T Device BF5 sunshine sensor is a versatile, multi-purpose, and easy-to-use solar radiation sensor that can measure GHI, DHI, and sunshine state without the need for routine adjustment or polar alignment. In this research, the Delta-T Device BF5 sunshine sensor recorded GHI and DHI each 10-sec, synchronised with the frequency of Raspberry Pi total sky imager capturing cloud images.

  There are several main reasons for choosing the Delta-T Device BF5 sunshine sensor in this research. Firstly, the cost of Delta-T Device BF5 sunshine sensor is relatively lower compared to other similar productions.

For example, as the office website of Delta-T Devices described, the BF5 sunshine sensor is a more affordable alternative to the high-performance SPN1 sunshine pyranometer. Secondly, the Delta-T Device BF5 sunshine sensor is easier to use because it does not need routine adjustment or polar alignment. At last, it can simultaneously measure GHI and DHI with relatively high accuracy.

The equipment cost for solar irradiance nowcasting, which includes the cost of Raspberry Pi Total Sky Imager, Delta-T Device BF5 sunshine sensor and other accessories, is shown in Table 3.2. In general, the total cost of the equipment used in this research is lower compared to other similar studies. More importantly, BF5 Sunshine Sensor are only needed in the training stage of solar irradiance nowcasting model that implies only the purchase and maintenance costs of the Raspberry Pi need to be afforded in daily use after the training of the nowcasting model is completed, which might merely cost a few hundred GBPs. In summary, this research provides a low-cost equipment solution that is very beneficial for daily applications in buildings.

Table 3.2 Equipment cost for solar irradiance nowcasting.

Device Names	Raspberry Pi Total Sky Imager	Delta-T Device BF5 Sunshine- Sensor	Data Logger	Other Accessories	Total
Cost	£150	£3,000	£200	£150	£3,500

Figure 3.2 Raspberry Pi total sky imager (Left 1 and 2), BF5 sunshine sensor (Right).

3.2.3 Collected Data

Collected data in the stage of solar irradiance nowcasting involves three types: ground-based cloud images, GHI and DHI. All data were collected between October 2020 and January 2021 and between April and September 2021. However, data collection had several limitations. Firstly, due to the administrative policy of Tongji University for non-members of the University, the dates of data collection were not completely consecutive. In addition, solar irradiance nowcasting for rainy days was excluded from the scope of this research, and thus, the data on rainy days were not collected. At last, those dates which collected low-quality and incomplete data due to ambient factors or human factors were also excluded. In this case, a total of 60 days of data from April to September were used in this research due to the high quality, integrity and diverse sky conditions represented by these data. In addition, these data were only recorded from 9:00 am to 5:00 pm each day because of the restrictions on the opening hours of the rooftop terrace. In specific, all collected data included 518400 ground-based cloud images, 172800 GHI values and 172800 DHI values.

- Ground-based cloud images

  As mentioned above, ground-based cloud images were regularly captured by the low-cost Raspberry Pi total sky imager every 10 seconds. The resolution of ground-based cloud images was 640 x 480 pixels, and all images were colour images with RGB channels. Every 10 seconds, the Raspberry Pi total sky imager captured three cloud images with high, medium, and low levels of exposure values (and other constant photographic parameters. Different levels of exposure values allow the Raspberry Pi Total Sky Imager to capture a greater dynamic range than what is possible with a single image, where the image intensity is proportional to the exposure time. Finally, three cloud images with different exposure values were used to synthesise a well-exposed High Dynamic Range (HDR) image.

- GHI and DHI

  GHI and DHI were recorded by the Delta-T Device BF5 sunshine sensor every 10 seconds with units in watt per square meter (W/m^2). The time step of recorded GHI and DHI was consistent with the time step of captured ground-based cloud images.

3.2.4 Data Processing

Data processing in the stage of solar irradiance nowcasting mainly involves two processing methods for ground-based cloud images and the data alignment of ground-based cloud images, GHI and DHI.

- High Dynamic Range (HDR) Synthesis: The first step of cloud image processing.

  In this research, ground-based cloud images were captured using a Raspberry Pi total sky imager. Due to the image sensor of the Raspberry Pi Total Sky Imager lacking the ability of the dynamic range of the human eye, cloud images taken from the Raspberry Pi Total Sky Imager tend to be over-exposed in the position of the sun and areas surrounding the sun while under-exposed in regions of dark shade. To deal with this challenge, the most representative way, according to the literature review in Chapter 2, is to capture several cloud images in quick succession with various exposure values and then fuse them into one single HDR cloud image. In this case, a series of Python programs were applied to capture three cloud images at three different levels of exposure values every 10 seconds and fuse them together to generate an HDR image which presents well-exposed.

  In this research, the image processing method of this step was named 'HDR Synthesis' in this research which consists of two specific HDR image synthesis methods called the Robertson Method and the Mertens method. These two methods were originally presented in two articles [351, 352]. In

Python, the Robertson Method and Mertens method were written as *cv2.createMergeRobertson* function and *cv2.createMergeMertens* function in the Open Computer Vision (OpenCV) package and these two functions were used to perform HDR Synthesis in this research. In principle, *cv2.createMergeRobertson* function firstly merge exposed image sequence into one HDR image, which is of type float32. In order to save or display the results, *cv2.createMergeMertens* function was then applied to map the 32-bit float HDR data into the range [0..1], which helps convert the data into 8-bit integers in the range of [0..255]. Based on HDR Synthesis, only the "best" parts in the different exposed image sequences were retained, and image sequences with multiple exposure values were fused into one single HDR image containing more detail, content, and higher quality.

Figure 3.3 presents a typical HDR Synthesis process. In Figure 3.3, three consecutive raw ground-based cloud images with different exposure values are fused to generate a well-exposed HDR image.

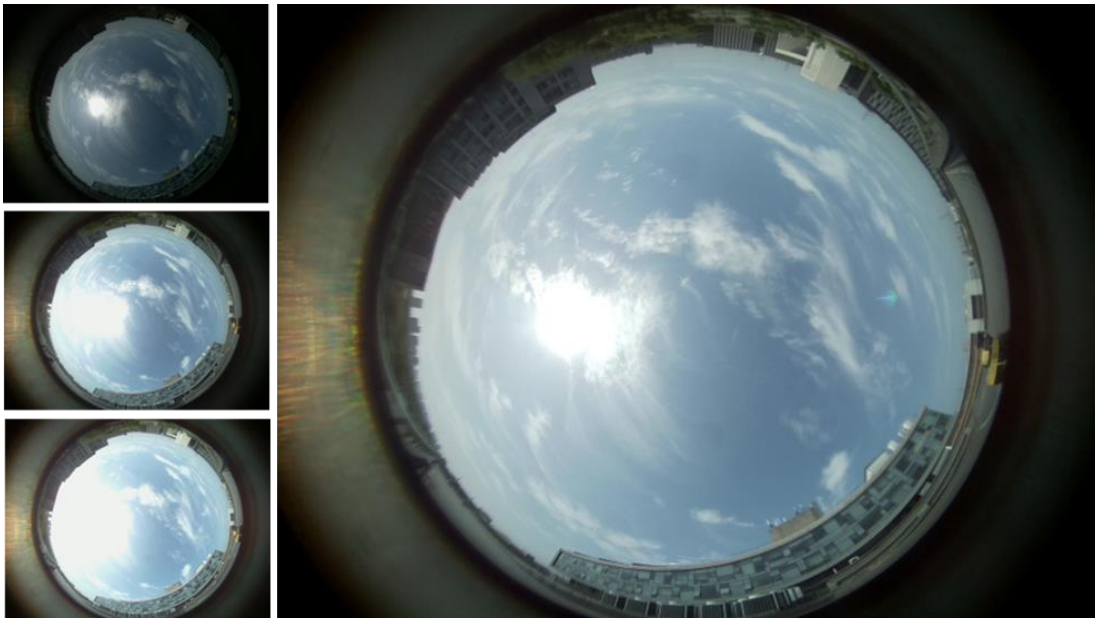

Figure 3.3 Exposure fusion of ground-based cloud images.

- Masking: The second step of cloud image processing.

  Once an HDR cloud image is achieved, the next step is to remove

unnecessary information included in the image. Due to the features of the WAVESHARE OV5647 fisheye lens, a series of unnecessary information involving buildings, trees, and terrain usually exists at the edge of the image. Thus, a mask is used to eliminate unnecessary information for acquiring the pure information of clouds and the sky.

After Exposure Fusion, a mask was used to cover unnecessary information, including buildings, trees, and terrain existing on the edge of the HDR image. This image processing step was named 'Masking' in this research. The first step of Masking was to convert an RGB colour image to a grayscale image using *cv2.cvtColor* function in OpenCV. Then, a proper threshold was selected to distinguish the pixels of clouds and the sky from the pixels of other elements, such as buildings and trees. This step was based on *cv2.threshold* function. Based on the above two steps, a black mask was generated. Finally, the black mask was used to cover the original RGB colour image using *cv2.bitwise* function. The key to the above steps is to select a proper threshold to generate an accurate mask that can cover the unnecessary information precisely. In this research, several thresholds between 0-255 were tested manually in several cloud images, and an appropriate threshold was finally determined, which efficiently covered unnecessary information.

Based on the step of Masking, the pure information of clouds and the sky in an HDR image can be achieved, as shown in Figure 3.4.

Figure 3.4 Masking of a ground-based cloud image.

- Data alignment.

  Once the processing of cloud images is completed, cloud images and corresponding GHI data and DHI data are aligned following a fixed timestep H, which is equivalent to the nowcasting horizon. In this research, a past sequence of the cloud images is aligned and denoted as $X = [X_1, \ldots, X_T]$, and a recent sequence of the GHI data and DHI data is aligned following the fixed timestep H and denoted $G= [G_{1+H}, \ldots, G_{T+H}]$ and $F= [F_{1+H}, \ldots, F_{T+H}]$. X_T denotes the cloud image at the T timestep; G_{T+H} is the GHI data at the T+H timestep; F_{T+H} is the DHI data at the T+H timestep. In addition, t denotes the time interval, which represents the sampling and nowcasting frequency of the solar irradiance nowcasting model, and H denotes the length of time into the future for which the nowcasting is to be prepared. In this research, H is always greater than t or sometimes aligns with H. More detailed definitions of H and t are presented in section 3.4.1.

3.3 Solar Irradiance Nowcasting

Solar irradiance nowcasting is the most crucial section of this research, and the solar irradiance nowcasting model is the key to this section. Based on the solar irradiance nowcasting model, a series of critical steps were conducted to achieve reliable GHI, DNI and DHI nowcasting. These steps include dataset collation, the training of solar irradiance nowcasting model, the nowcasting of GHI and DHI, and the calculation of DNI.

3.3.1 Convolutional Neural Networks (CNNs)

As one of the most representative algorithms of Deep Learning (DP), CNN was applied to construct the solar nowcasting model in this research. It has been proved that CNN has enabled great success in many research fields, such as image recognition, speech recognition (Krizhevsky, Sutskever, & Hinton, 2012), natural language processing (Ronan & Jason, 2008), etc.

A typical CNN typically consists of three parts: convolution layers, pooling layers, and fully connected layers. In brief, convolution layers are responsible for extracting local features in an image. The pooling layers are used to significantly reduce the magnitude and dimensionality of data information, which is also called downsampling. Fully connected layers are similar to the part of a conventional neural network and are used to output the desired results. In general, a CNN contains a series of convolution stages, and each stage includes multiple convolution layers and pooling layers. Each convolution stage learns about the features of the input image and generates a series of outputs called feature maps, which understand the input image at a higher level. The essence of each convolution stage is to downsample the feature maps generated in the previous convolution stage that thus compress and generalise the feature representations. In this case, multiple convolution stages process feature maps in sequence and, finally, output feature maps that capture high-level information of the input image. Fully connected layers usually appear at the end of a CNN, and

multiple fully connected layers might be stacked together. The role of a fully connected layer is to take the image features consolidated by previous convolution stages as input to establish the mapping relation with output. In this research, the input of CNN is cloud images and the output is solar irradiance. Thus, solar irradiance can be achieved by analysing cloud images. A more detailed description of each part of CNN is presented as follows.

- Convolution Layer.

  The process of convolution uses a convolution kernel (also called a filter) to filter individual small regions of the image to obtain the feature values of these regions. The filter is usually a 2-D matrix that is applied on the input image pixels or feature maps from the previous convolution stage. The size of the filter is also called the receptive field, which means how large a portion of the image can be seen at a time. In the process of convolution, the filter moves step by step from left to right and top to bottom in sequence. The essence of each movement is to use the filter to multiply the input pixels and then sum up the result. In general, multiple filters are applied to the same input that produces multiple feature maps. These feature maps are stacked together as one tensor and pass on to the next convolution stage as input. In this research, cloud images with RGB colour are the input of CNN. In terms of structure, the number of pixels controls the size of the image and RGB channels form the entire image colour. If a right-angle coordinate system is established, axis X and Y present the size of a cloud image under a horizontal plane and axis Z presents the vertical information about RGB channels. In this case, the same filter is applied simultaneously on three channels with RGB (Red, Green, Blue) and then synthesises a final feature map after convolution. In other words, 2-D filters on three colour channels constitute a 3-D filter in the process of convolution of a cloud image.

  The final step of convolution is activation. After the process of convolution,

an activation function is introduced to calibrate the convolution results for each pixel. The application of activation function is to increase the non-linearity in the output. Representative activation functions include the ReLu function, sigmoid function, tanh function, etc.

- Pooling Layer.

  Similar to convolution, the pooling process also applies a filter. It essentially involves sliding this filter over sequential patches of the image and processing pixels caught in the kernel in some kind of way. The process of pooling intends to decrease the magnitude and dimensionality of feature maps because the feature maps still have too complex pixel information after convolution. Pooling helps to extract more informative representations and reduce computational costs. Commonly used pooling methods involve max pooling and average pooling. Max pooling means the filter simply chooses the maximum pixel value in the receptive field to replace the original feature value. Average pooling refers to calculating the average value of pixel values in the receptive field.

- Fully Connection Layer.

  Fully connection layer in CNN is used to aggregate information for making a global prediction, such as classification or regression. The feature maps generated from the previous convolution stages are flattened to a vector. Then this vector is fed to a fully connected layer so that it captures complex relationships among high-level features. The output of this layer is a one-dimensional feature vector. In other words, convolution layer and pooling layer are responsible for extracting efficient information from cloud images, while fully connection layer is used for achieving the prediction. In this research, the feature maps of cloud images are extracted by a series of convolution stages. In the end, fully connection layer establishes the connecting bridge between these feature maps and the nowcasting values

of solar irradiance. As a result, the proposed CNN can use cloud images as input to output the nowcasting values of solar irradiance.

3.3.1.1 ResNet-152 Model

The CNN used in this research is known as Residual Neural Network (ResNet). ResNet was introduced by Microsoft Labs in 2015, and it broke a series of records when it was first proposed in a paper [353]. The emergence of ResNet is a milestone in CNN history because it can train deeper CNN models and thus achieve higher accuracy.

Theoretically, a deeper neural network with more layers has stronger learning capabilities. However, the degradation problem gradually emerges as the increase of CNN layers significantly affects the accuracy of results. The degradation problem refers to the problem of the final accuracy gradually becoming saturated and then degrading rapidly as the depth of the network increases. In other words, the accuracy of a CNN model decreases when the number of model layers reaches a threshold value. Meanwhile, once the network has too many layers, the weight values for different neurons tend to be an oversized or undersized condition as an accumulation effect along with layers.

ResNet can overcome the two issues mentioned above by increasing the number of layers without limitation while maintaining precision. To solve the degradation problem, ResNet integrates a residual learning block that can enhance the layers of the neural network via residual learning, which allows backpropagation to be effectively carried out even when certain neurons are saturated. This design allows ResNet to efficiently train deeper neural networks and thus outperform other CNN models. The key to residual learning is the “shortcuts or skip connection” between the front and back layers, which helps the backpropagation of gradients during model training and thus can train deeper CNN. A typical residual learning block is shown in Figure 3.5. In Figure 3.5, x denotes the input, and *F*(x) denotes the output of the

residual learning block before the activation function in the second layer. $F(x)=W_2\sigma(W_1x)$, where W_1 and W_2 denote the weights of the first and second layers, σ denotes the ReLU activation function. The final output of residual learning block is $\sigma(F(x) + x)$. When there is no shortcut (the curved arrow from x to $\oplus$), the residual learning block is a normal 2-layer network. Setting the output of the second layer network before the activation function as $H(x)$. For a network without a shortcut, if the optimal output of this 2-layer network is the input x, it needs to be optimised as $H(x) = x$; For a network with a shortcut, that is, residual learning block, then it is sufficient to optimise $F(x) = H(x) - x$ to zero.

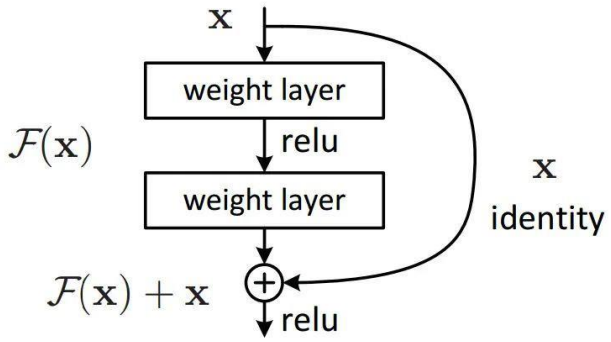

Figure 3.5 A typical residual learning block.

- Diverse Structures of ResNet.

  There are several classical network structures of ResNet: ResNet-18, ResNet-34, ResNet-50, ResNet-101, ResNet-152. Among these structures, ResNet-18 and ResNet-34 are relatively shallow networks, while ResNet-50, ResNet-101 and ResNet-152 belong to deeper networks. Regardless of the number of layers in ResNet, they all have the following common features.

  a) The network contains a total of 5 convolutional groups, each with one or more basic convolutional computation processes.

  b) Each convolutional group contains one operation of downsampling to halve the size of the feature maps, and downsampling is achieved in two ways involving convolution and pooling.

  c) The first convolutional group contains only one convolutional computation

operation, and the first convolutional group is the same as the five typical ResNet structures mentioned above.

d) The second to fifth convolutional groups all contain multiple identical residual units and these groups are usually called stage1, stage2, stage3 and stage4, respectively.

- The Advantages of ResNet-152.

  In general, ResNet-152 has obvious advantages for the crucial task of this research - cloud images recognition. These advantages include:

  a) Advanced Feature Learning Capabilities.

     The deep structure of ResNet-152 enables it to learn complex features of cloud images, including cloud textures, lighting variation, and colour gradients. ResNet-152 can effectively learn and extract useful information from these features.

  b) Residual Learning Mechanism.

     The residual learning mechanism employed by ResNet-152 helps maintain the flow of information, reducing information loss during training. This means that even in a deep network of 152 layers, gradients can be effectively propagated, thus maintaining the performance and stability of the network. This is especially beneficial for sky image recognition because the model needs to capture subtle changes of clouds and the sky meticulously.

  c) Effective Transfer Learning.

     Due to the widespread availability of pretrained models of ResNet-152 for various image recognition tasks, it can be transferred to specific application scenarios easily, such as cloud image recognition. The pretrained model can serve as a basis, and through fine-tuning, adapt to specific sky image datasets, which helps reduce training time and improve recognition accuracy.

d) Generalisation Capability.

ResNet-152 has been proven to have good generalisation capabilities, which is particularly important for recognising cloud images under different weather conditions. The network can handle images from clear, overcast to cloudy, maintaining high accuracy in recognition.

e) Ability to Handle Imbalanced Data.

Sky image datasets may exhibit class imbalance, such as having more clear cloud images than overcast or cloudy ones. The strong feature extraction ability of ResNet-152 helps the model learn robust features from less represented categories, thereby improving overall recognition performance.

3.3.1.2 The Selection of ResNet-152 as Nowcasting Model.

Based on the above, the ResNet-152 is used as the solar irradiance nowcasting model for this research due to the following main reasons. First, ResNet-152 is well suited to handle image recognition tasks, while this research involves a large number of cloud image recognition tasks. In addition, the performance of ResNet-152 is more balanced in terms of accuracy, computational time consumption and number of parameters compared to other CNNs, as shown in Figure 3.6. Figure 3.6 comes from an article published in 2016 [354]. The vertical axis of Figure 3.6 represents the accuracy, the horizontal axis represents computational time consumption, and the size of the circle represents the number of parameters. Finally, although ResNet-152 has been widely used in different fields, it has hardly been used to achieve solar irradiance nowcasting.

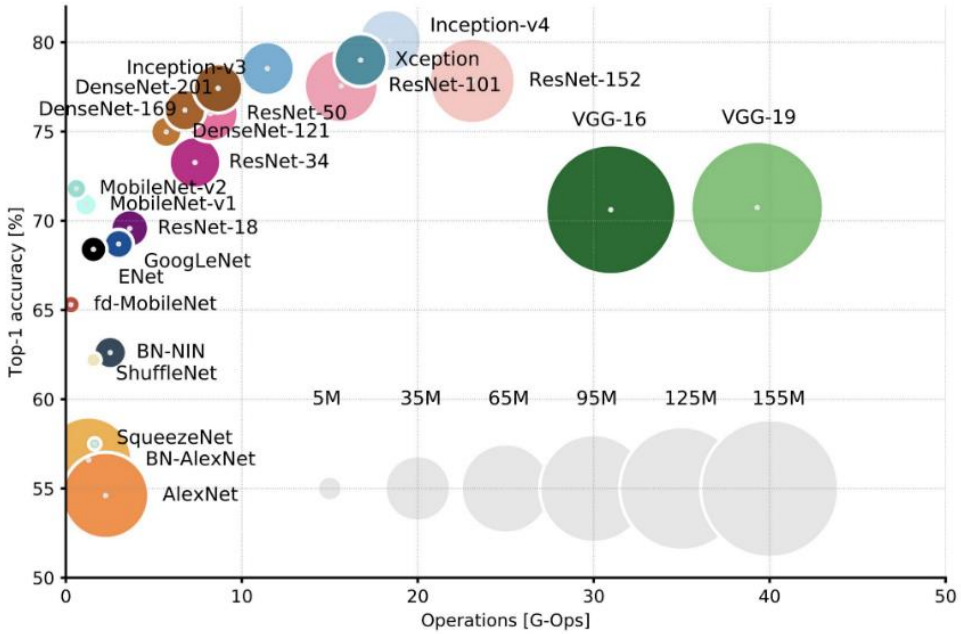

Figure 3.6 Comparison among different CNNs.

(Resource: A. Canziani, A. Paszke, E. Culurciello, An analysis of deep neural network models for practical applications, arXiv preprint arXiv:1605.07678, (2016).)

Figure 3.7 presents the structure of ResNet-152 applied in this research. The ResNet-152 model consists of 5 convolutional groups, 50 convolution blocks, 152 convolution layers, 2 max pooling layers, 2 averaged pooling layers and 1 fully connection layer.

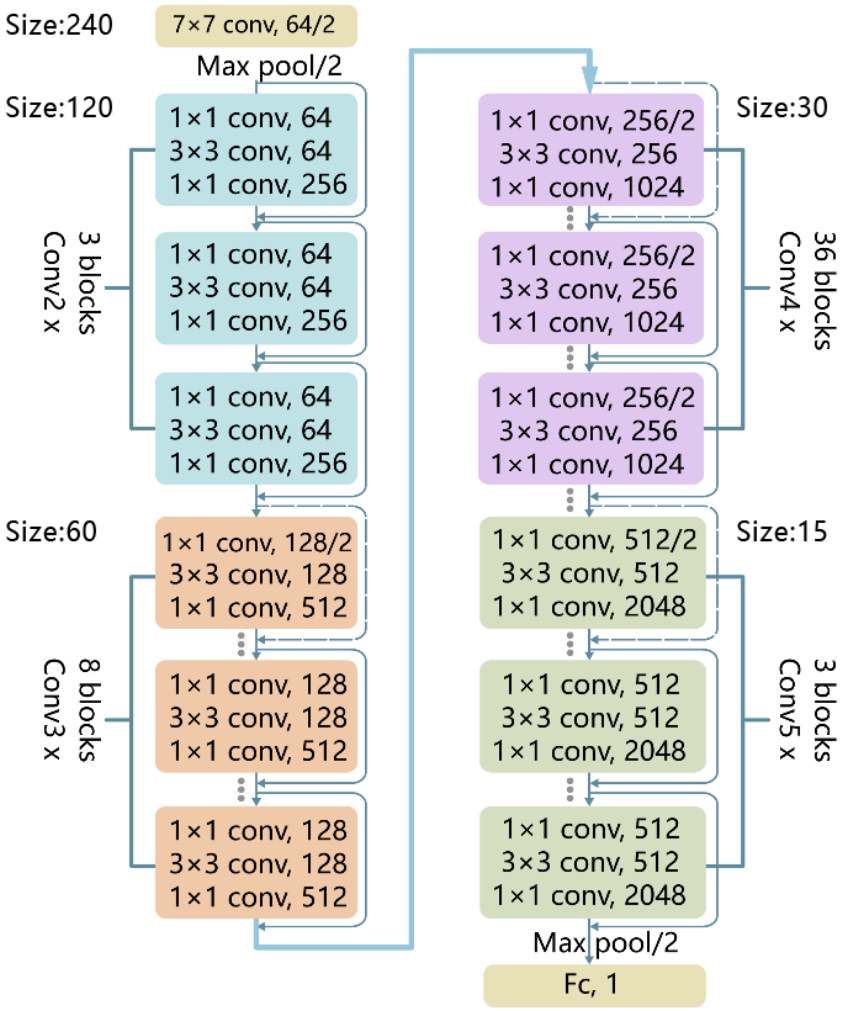

Figure 3.7 Structure of the proposed ResNet-152 model.

3.3.2 Dataset Collation for Solar Irradiance Nowcasting

Dataset collation is the first step of solar irradiance nowcasting. In general, collected data described in section 3.3.13 are divided into two types of datasets: the dataset for the training of solar irradiance nowcasting models and the dataset for the testing of solar irradiance nowcasting models, as shown in Figure 3.8. It is worth noting that the specific data in these two types of datasets changes depending on the different purposes of comparative tests presented in later sections.

Figure 3.8 Datasets of the proposed solar irradiance nowcasting method.

As mentioned above, a total of 60 days of data were used in this research. This research adopted an 8:2 ratio to partition the training set and testing set. Therefore, the training set consisted of 48 days of data and the testing set consisted of 12 days of data.

- The dataset for the training of solar irradiance nowcasting models.

  The dataset for the training of solar irradiance nowcasting models consists of 48 days of data from April to September. These data were daily recorded from 9:00 am to 5:00 pm. In specific, it included 138240 ground-based cloud images and a corresponding number of GHI and DHI values. In this research, 48 days of data were redistributed into two subsets on a daily unit using cross-validation. These two subsets were respectively used as train set and validation set. This research adopted a 3:1 ratio to partition the train set and validation set. Thus, the train set, including 36 days of data was used to train the nowcasting models and the validation set including 12 days of data, was used to adjust model parameters.

- The dataset for the testing of solar irradiance nowcasting models.

  The dataset for the testing of solar irradiance nowcasting models, also known as test set, consisted of 12 days of data from April to September. These data were recorded daily at the same time step as the dataset for the training of solar irradiance nowcasting models. Total 34560 ground-based cloud images and corresponding GHI and DHI values were included in this

dataset. Test dataset was used for evaluating the performance of solar irradiance nowcasting.

3.3.3 The Training of Solar Irradiance Nowcasting Model

In this section, the dataset for the training of solar irradiance nowcasting models mentioned above were used to train the solar irradiance nowcasting models. In this research, ResNet-152 model was used as solar irradiance nowcasting model. Based on the data alignment, both a past sequence of the cloud images $X = [X_1, \ldots, X_T]$ as input and a recent sequence of the GHI data $G= [G_{1+H}, \ldots, G_{T+H}]$ as output was used to train a ResNet-152 model for nowcasting GHI. In the meanwhile, the same operation was also implemented on a past sequence of the cloud images $X = [X_1, \ldots, X_T]$ and a recent sequence of the DHI data $F= [F_{1+H}, \ldots, F_{T+H}]$ to achieve DHI nowcasting. Using various time intervals, nowcasting horizons and other test conditions, a series of the ResNet-152 models were trained to obtain the nowcasting of GHI and DHI according to the different purposes of comparative tests. Figure 3.9 demonstrates the process of the training of solar irradiance nowcasting model.

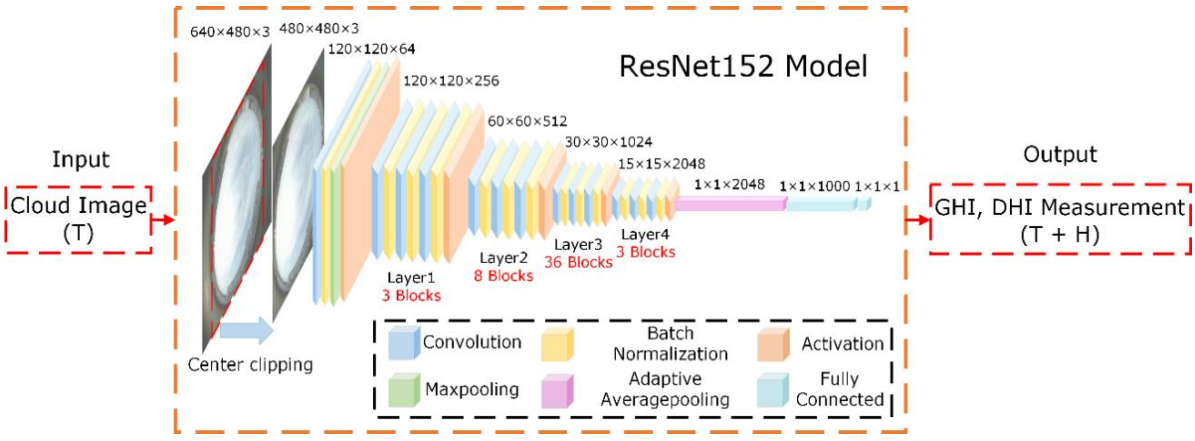

Figure 3.9 The training of solar irradiance nowcasting models.

- Optimisation of solar irradiance nowcasting models.

  The training of solar radiation nowcasting models needs to be continuously adjusted to achieve the optimal solar radiation nowcasting models. In this research, two main means for the optimisation of model training are the selection of loss functions and the adjustment of hyperparameters.

a) The Selection of Loss Function.

Loss function is necessary to evaluate the degree of convergence of the training of solar irradiance nowcasting model. In deep learning, L1 function and L2 function are the most common loss functions. The L1 loss function, also known as Least Absolute Deviations (LAD) or Manhattan Loss, calculates the sum of the absolute differences between the predicted and actual values. The L2 loss function, also known as Mean Squared Error (MSE), is one of the most commonly used loss functions in regression tasks. It calculates the mean of the squared differences between the predicted and actual values. In general, L1 function is used for simple models, while L2 function is more commonly used in neural networks, especially in CNNs, which are usually used to solve complex problems.

In this research, the L2 loss function was utilised for the training of the ResNet-152 models. The L2 loss function, which minimises the mean of the squared differences between the predicted and actual values, inherently penalizes larger errors more severely than smaller ones, thereby ensuring that the model pays more attention to significant errors during training. Unlike other loss functions that might be prone to dramatic shifts due to outlier influence, the L2 loss ensures smoother gradient descent, which is vital given the deep nature of ResNet-152 that is susceptible to fluctuations in gradient updates. Thus, the application of the L2 loss function in training the ResNet-152 model can help the model preventing overfitting, improving training stability and generalisation.

b) Hyperparameter Adjustment.

Optimising hyperparameters is crucial for achieving the best performance from deep neural networks. In this research, two key hyperparameters - the learning rate and epochs - are tuned manually and systematically.

Learning Rate: When training deep neural networks like ResNet-152,

adjusting the learning rate is crucial for achieving efficient training and good model performance. The goal of learning rate adjustment is to control the speed at which model weights are updated during training. Optimising the learning rate can help the model converge more quickly and enhance the final accuracy and stability of the model.

In this research, the learning rate is adjusted manually through trial and error. First, a small range of learning rates are selected, and then gradually increased or decreased, observing the training loss and validation accuracy of the model to select the optimal learning rate. In general, the learning rate is usually set to a small value because an excessively large learning rate may cause the model to fail to converge. After a series of trial and error, the learning rate of 0.001 are finally determined for training the solar irradiance nowcasting model in this research.

Epochs: When training deep neural networks like ResNet-152, adjusting the number of training epochs is an important aspect of optimising model performance. Proper adjustment of training epochs not only ensures that the model sufficiently learns features from the data but also prevents overtraining and wastage of time resources.

This research starts with a number of training epochs based on past experience, and then adjust through repeated trials, adjusting the number of epochs based on the results of each training session. Although this method is time-consuming, it helps identify the most suitable number of epochs for the different solar irradiance nowcasting models precisely.

In summary, the training of solar radiation nowcasting models is considered complete only after the optimal nowcasting models has been obtained through repeated optimisation experiments using the validation set mentioned in section 3.3.2. On this basis, the next stage of solar radiation nowcasting can be performed.

3.3.4 Nowcasting of GHI and DHI

In this section, the dataset for the testing of solar irradiance nowcasting models mentioned in 3.3.2.3 was used to achieve solar irradiance nowcasting of GHI and DHI. Once the training of the Resnet-152 nowcasting models was completed, the nowcasting of GHI and DNI at the T+H timestep can be achieved by importing the ground-based cloud image at the T timestep into the Resnet-152models, as shown in Figure 3.10. In terms of the different purposes of comparative tests, a series of GHI and DHI nowcasting were achieved. Figure 3.10 demonstrates the process of solar irradiance nowcasting.

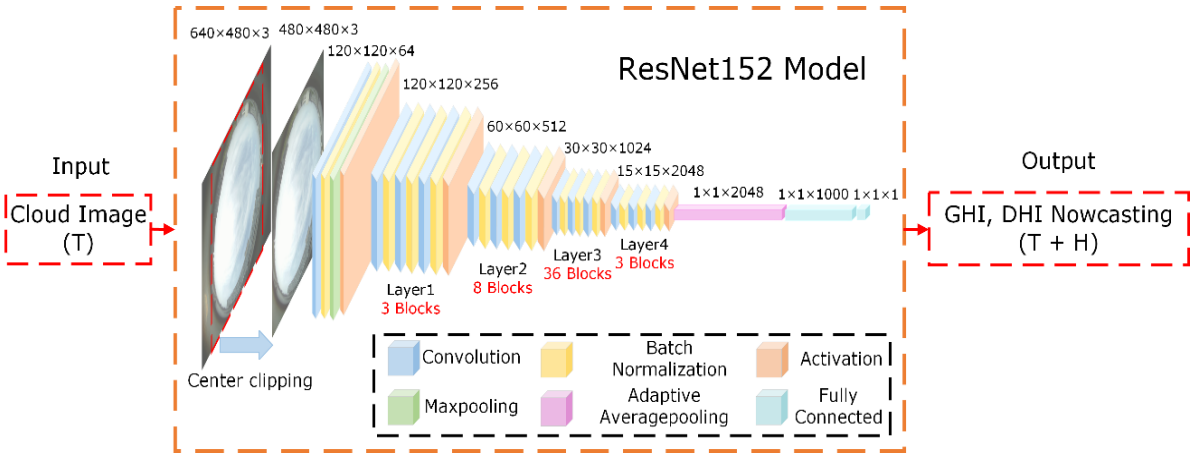

Figure 3.10 The nowcasting of GHI and DHI.

3.3.5 Calculation of DNI from Nowcast Values of GHI and DHI

After the GHI and DNI at the T+H timestep are obtained, the DNI at the T+H timestep can be calculated using GHI and DHI according to the expression shown in Eq. (X):

$$GHI = DHI + DNI \times cos(\theta) \tag{3.1}$$

Where θ is the solar zenith angle.

The solar zenith angle is the angle of the sun relative to a line perpendicular to the earth's surface. The solar zenith angle can be calculated based on the expression shown in Eq. (X):

$$\theta = cos^{-1}\left(sin(\phi) \times sin(\delta) + cos(\phi) \times cos(\delta) \times cos(H)\right) \quad (3.2)$$

Where ϕ is the geographical latitude of the location; δ is the current declination of the sun; H is the hour angle.

The current declination of the sun is the angle between the equatorial plane and the line formed by the sun's position relative to the Earth's centre. It can be calculated by the following expression:

$$\delta = 23.45sin(\frac{360}{365}(n + 10)) \quad (3.3)$$

Where n refers to the nth day of the year.

The hour angle is the measure of time since solar noon. It can be calculated by the following expression:

$$H = 15 \times (Local\ Solar\ Time - 12) \quad (3.4)$$

In this research, an *ephemeris* function developed based on PVLIB, a popular Python library for calculating solar zenith, is applied to calculate the solar zenith angle at specific timesteps.

Based on the above, the calculated DNI at the T+H timestep is exactly the nowcasting of DNI because is calculated from the nowcasting of GHI and DHI. In this case, the nowcasting of three critical solar irradiance parameters - GHI, DNI and DHI - is achieved.

3.4 Comparative Tests and Verification

In the stage of solar irradiance nowcasting, five sets of different comparative tests were conducted to evaluate its performance. Each set of comparative tests was designed with a specific objective. On this basis, the five objectives of the stage of solar irradiance nowcasting include:

- Evaluating the nowcasting performance at various time intervals.
- Evaluating the nowcasting performance for various nowcasting horizons.
- Evaluating the nowcasting performance in different sky conditions.
- Evaluating the nowcasting performance among different models.
- Evaluating the nowcasting performance based on different datasets.

To address the five objectives mentioned above, the following five sets of comparative tests were specifically conducted:

- Nowcasting performance at various time intervals.
- Nowcasting performance for various nowcasting horizons.
- Nowcasting performance in different sky conditions.
- Nowcasting performance among different models.
- Nowcasting performance based on different datasets.

Before presenting the results of comparative tests, a series of basic settings for comparative tests need to be clarified, including time intervals, nowcasting horizons, the classification of sky conditions, comparative models and evaluation metrics for verification.

3.4.1 Time Intervals and Nowcasting Horizons

Time interval refers to the sampling frequency of input data for the training and testing of a nowcasting model. The sampling frequency of input data determines the nowcasting frequency of the solar irradiance nowcasting model. The nowcasting frequency defines the nowcasting temporal resolution of the solar irradiance nowcasting model. The nowcasting horizon refers to how far ahead a nowcasting

model predicts the future. For a solar irradiance nowcasting model, nowcasting horizons are always greater than or equal to time intervals. In this research, the effect of 10-sec, 1-min, 5-min, and 10-min time intervals and nowcasting horizons on nowcasting performance are explored. The relationship between time interval and nowcasting horizon is shown in Figure 3.11.

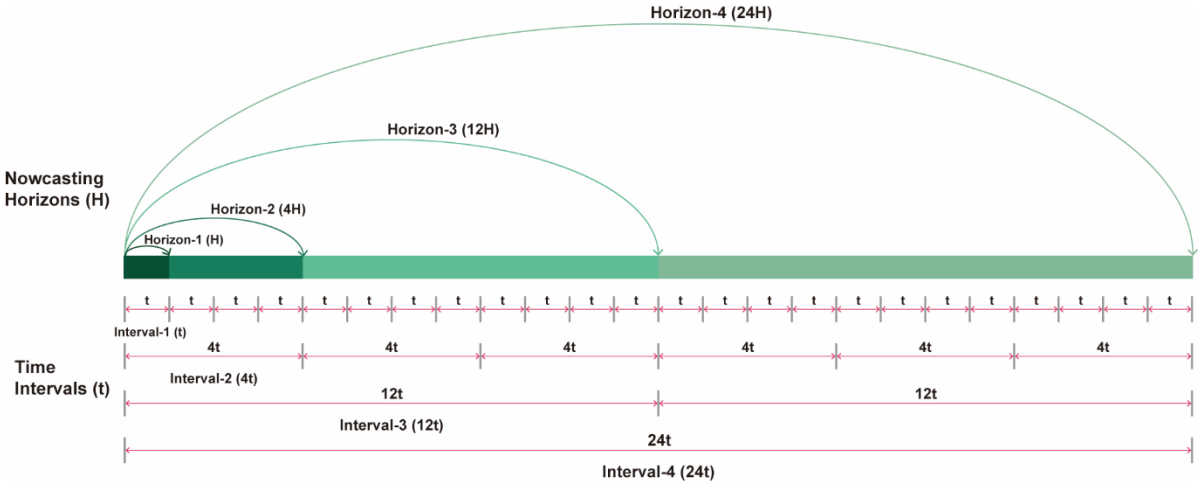

Figure 3.11 The relationship between time interval and nowcasting horizon.

In terms of different solar irradiance components, time intervals and nowcasting horizons, a total 20 nowcasting models are trained and tested in this section. These models are divided into three groups according to 1-min, 5-min and 10-min nowcasting horizons comparison. In addition, these models are only used for nowcasting GHI and DHI rather than DNI, which needs to be calculated from GHI and DHI. Table 3.3 presents the basic information of 20 nowcasting models. In Table 3.3, “G” of model name represents GHI, “D” of model name represents DHI, “I” of model name represents interval, “H” of model name represents horizon, the number in front of “I” and “H” represents the time scale in seconds, and “Total Images” represents the total number of cloud images used for the training and testing of solar irradiance nowcasting models.

Table 3.3 20 trained Solar irradiance nowcasting models.

Model Name	Components	Intervals	Horizons	Total Images
G-10I-10H	GHI	10s	10s	178517
D-10I-10H	DHI	10s	10s	178517
G-10I-60H	GHI	10s	60s (1mins)	178222
D-10I-60H	DHI	10s	60s (1mins)	178222
G-60I-60H	GHI	60s (1mins)	60s (1mins)	29752
D-60I-60H	DHI	60s (1mins)	60s (1mins)	29752
G-10I-300H	GHI	10s	300s (5mins)	176806
D-10I-300H	DHI	10s	300s (5mins)	176806
G-60I-300H	GHI	60s (1mins)	300s (5mins)	29516
D-60I-300H	DHI	60s (1mins)	300s (5mins)	29516
G-300I-300H	GHI	300s (5mins)	300s (5mins)	5950
D-300I-300H	DHI	300s (5mins)	300s (5mins)	5950
G-10I-600H	GHI	10s	600s (10mins)	175036
D-10I-600H	DHI	10s	600s (10mins)	175036
G-60I-600H	GHI	60s (1mins)	600s (10mins)	29221
D-60I-600H	DHI	60s (1mins)	600s (10mins)	29221
G-300I-600H	GHI	300s (5mins)	600s (10mins)	5891
D-300I-600H	DHI	300s (5mins)	600s (10mins)	5891
G-600I-600H	GHI	600s (10mins)	600s (10mins)	3026
D-600I-600H	DHI	600s (10mins)	600s (10mins)	3026

3.4.2 Classification of Sky Conditions

In this research, different sky conditions are defined according to the proportion of cloud pixels to sky pixels in a cloud image. The sky condition is defined as clear when the proportion is less than 25% for most of the time. In contrast, it is defined as overcast when the proportion is greater than 75%. When the proportion is between 25% - 50%, the sky condition is defined as light cloudy. At last, the sky condition is defined as heavy cloudy when the proportion is between 50% - 75%. The definitions of sky conditions are presented in Table 3.4.

Table 3.4 The definition of weather conditions.

Weather Conditions	Clear Sky	Light Cloudy	Heavy Cloudy	Overcast
Proportion of Cloud Pixels	< 25%	25% - 50%	50% - 75%	> 75%

In this case, the recognition of cloud pixels and sky pixels is the basis for the classification of sky conditions. In a cloud image, cloud and the sky are often significantly different in colour. Clouds typically appear white or grey, while the sky often displays hues of blue or presents orange and red during sunrise or sunset. Thus, a single pixel can be defined as cloud pixels or sky pixels by setting a colour range for the sky and the cloud based on a series of colour thresholds, including hue, saturation, and brightness. In this research, these colour thresholds are set manually by repeated tests at different times of the day due to the small sample size of the testing dates. Based on the set thresholds, this research employs an image processing library in Python - Pillow, to identify cloud pixels and sky pixels and calculate their proportion. The specific process of pixel recognition is to load an image, and convert it to HSV colour (Hue, Saturation, Brightness), and traverse each pixel of the cloud image to set thresholds to determine if the pixel belongs to the sky or cloud.

3.4.3 Comparative Models

Two comparative models were used in this research: Multilayer Perceptron (MLP) and Persistence Model (PM). The former is the simplest and most basic Artificial Neural Network (ANN) and simplest forecasting model, and the latter is the simplest forecasting model. In this research, MLP is used as a baseline model because it represents the simplest machine learning model. In contrast, although PM is the simplest forecasting model, its accuracy increases significantly as the nowcasting horizons decrease. Thus, PM can achieve extremely high accuracy in very short-term forecasting that outperforms most solar irradiance forecasting models. In this case, PM is used as a benchmark model because this research focuses on 10-sec, 1-min, 5-min, and 10-min nowcasting of GHI, DNI and DHI.

- Baseline Model - Multilayer Perceptron (MLP)

  Multilayer Perceptron (MLP) with feed-forward back propagation is usually used in solar irradiance estimation and forecasting. An MLP usually includes at least three layers of nodes: an input layer, a hidden layer, and an output layer. Different layers are fully connected. The basic operation of MLP is that the hidden layer receives input data and sends an output signal to the output layer. Apart from the input nodes, each node is a neuron that uses a nonlinear activation function, usually a sigmoid or ReLU function. In addition, A neuron receives signals from other previous neurons or input data unidirectionally for a feed-forward MLP configuration.

  In general, MLP is usually used in classification and regression problems. In classification problems, the output layer usually has several neurons and each neuron corresponds to a category. In this case, the output of the output layer is the probability value of each category. In regression problems, the output layer has only one neuron, and the output value is the predicted value. The training process usually uses loss functions such as L1 and L2 to update the weights and thresholds through gradient descent and backpropagation algorithms.

  The MLP used in this research only takes ground-based cloud images as input to achieve the nowcasting of GHI and DHI. Its structure is shown in Figure 3.12. This MLP consists of one input layer, two hidden layers, and one output layer and the number of neurons in the four layers are k, m, n and o. After experiments, the number of inputs merely has a subtle effect on the network effectiveness. In this research, the input layer of MLP is set up with 6 inputs that are the solar irradiance in advance of 6 moments, noted k = 6. Each hidden layer contains 64 neurons, that is m = n = 64. Since solar irradiance nowcasting belongs to the regression problem, the number of neurons in the output layer o = 1, which is the final output of solar irradiance.

The ReLU functions is used for activations function and L2 function is used for the loss function. Figure 3.12 shows the structure of MLP.

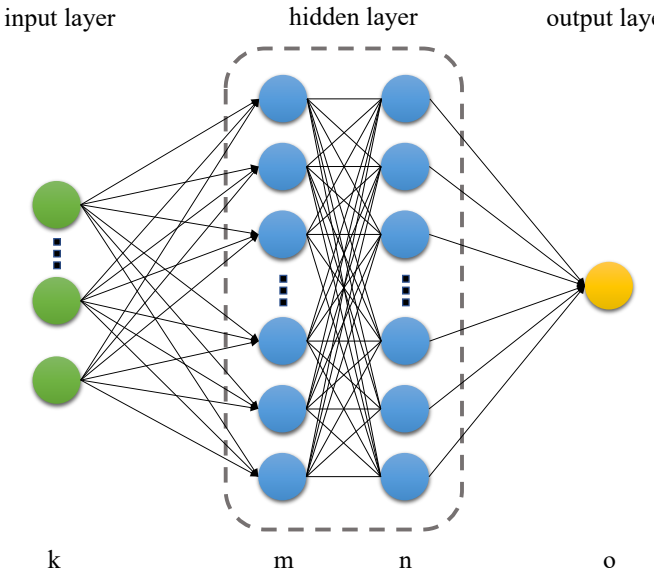

Figure 3.12 The structure of MLP.

- Benchmark Model - Persistence Model (PM)

  The principle of persistence model assumes that the previous value is the same as the previous one. In this case, persistence model is very effective for very short-term solar irradiance forecasting due to the sky conditions and solar irradiance would usually not change dramatically, especially on clear or overcast days. However, its accuracy decreases significantly with forecasting horizon for the same reasons. Persistence model is given by:

$$\hat{X}_{t+H} = X_t \tag{3.5}$$

  Where X is the solar irradiance, including GHI, DNI and DHI. $\boldsymbol{X_t}$ denotes the solar irradiance at time t and H is the duration of a time interval.

3.4.4 Evaluation Metrics for Verification

A series of evaluation metrics are used to compare the nowcasting values of GHI, DNI and DHI with their measurements. The measurements of GHI and DHI are obtained directly by Delta-T Device BF5 sunshine sensor, and the measurements of

DNI are calculated based on the measured GHI and DHI. The nowcasting values of GHI and DHI are generated from the proposed solar irradiance nowcasting models and the nowcasting values of DNI are calculated from the nowcasting values of GHI and DHI.

In the stage of solar irradiance nowcasting, eight evaluation metrics was used to verify the performance of solar irradiance nowcasting from multiple perspectives. These evaluation metrics include MAE, nMAE, RMSE, nRMSE, MAPE, r, SS-MAE and SS-RMSE. The selection of these evaluation is based on the statistical analysis of evaluation metrics presented in literature review. Among these metrics, MAE, nMAE, RMSE, nRMSE are the most common metrics used for evaluating solar irradiance forecasting, according to the literature review in Chapter 2. MAPE is always used to evaluate the prediction accuracy of a forecasting method and is suitable for comparisons between different studies because it is an indicator of relative error. In contrast, r is less used but suitable for demonstrating the correlation between nowcasting and measurement. Lastly, SS-MAE and SS-RMSE are usually the best choices for comparing the performance of different models. In this research, a series of evaluation metrics that have been widely chosen in literature reviews is mainly selected to facilitate direct comparison with most studies. These metrics consist of absolute indicators, including MAE and RMSE, and relative indicators, such as nMAE, nRMSE, MAPE, r, and SS. In the following equations, p_i represents the nowcasting values, m_i represents the measurements, $\bar{m}$ represents the averaged measurements.

- The Mean Absolute Error (MAE).

  The mean absolute error (MAE) is the average absolute deviation of the predicted values from their measured values, which is the most basic evaluation metric for prediction evaluation. MAE can reflect the actual error of prediction because the deviations are absolutised. Its equation can be expressed as:

$$MAE = \frac{1}{N}\sum_{i=1}^{N}|p_i - m_i| \tag{3.6}$$

Where N is number of data points, p_i and m_i respectively denote the actual value and the predicted value of solar irradiance. A larger MAE means a larger prediction error.

- The Normalised Mean Absolute Error (nMAE).

  The normalised mean absolute error (nMAE) is used to facilitate the comparison between models with different scales. The averaged measured value of solar irradiance is generally used as a reference in the normalisation. It can be expressed as:

$$nMAE = MAE / \bar{m} \tag{3.7}$$

  Where $\bar{m}$ is the mean of the actual values of solar irradiance m. When nMAE is closer to 0, the prediction accuracy is higher, while a value closer to 1 indicates a larger error.

- The Root Mean Square Error (RMSE).

  The root mean square error (RMSE), as the most widely-used metric for evaluating prediction, represents the square root of the differences between predicted values and observed values. Thus, RMSE is more sensitive to significant prediction error than MAE. It can be expressed as:

$$RMSE = \sqrt{\frac{1}{N}\sum_{i=1}^{N}(p_i - m_i)^2} \tag{3.8}$$

  Where N is number of data points, p_i and m_i respectively denote the actual value and the predicted value of solar irradiance. A larger RMSE means a larger prediction error.

- The Normalised Root Mean Square Error (nRMSE).

  The normalised root mean square error (nRMSE) is used to facilitate the comparison between models with different scales. The averaged measured

value of solar irradiance is generally used as a reference in the normalisation. It can be expressed as:

$$nRMSE = RMSE / \bar{m} \tag{3.9}$$

Where $\bar{m}$ is the mean of the actual values of solar irradiance m. Similar to nMAE, the closer the RMSE is to 0, the higher the prediction accuracy, and conversely, the closer the RMSE is to 1, the larger the error.

- The Mean Absolute Percentage Error (MAPE).

  The mean absolute percentage error (MAPE) is one of the most popular metrics used to evaluate prediction performance because of its very intuitive interpretation in terms of relative error. Unlike MAE and RMSE, MAPE can directly compare various models between different datasets. Its equation can be expressed as:

$$MAPE = \frac{100\%}{N} \sum_{i=1}^{N} \left| \frac{p_i - m_i}{m_i} \right| \tag{3.10}$$

  Where N is number of data points, p_i and m_i respectively denote the actual value and the predicted value of solar irradiance. A larger MAPE means a larger prediction error.

- The Correlation Coefficient (r).

  The correlation coefficient (r) is used to evaluate how strong a relationship is between two variables. In this research, it is used to judge the correlation between nowcasting values and measurements. It can be expressed as:

$$r = \frac{\sum_{i=1}^{N}(p_i - \bar{p})(m_i - \bar{m})}{\sqrt{\sum_{i=1}^{N}(p_i - \bar{p})^2} \sqrt{\sum_{i=1}^{N}(m_i - \bar{m})^2}} \tag{3.11}$$

  Where N is number of data points, p_i and m_i respectively denote the actual value and the predicted value of solar irradiance, $\bar{p}$ is the mean of the predicted values of solar irradiance p, and $\bar{m}$ is the mean of the actual values of solar irradiance m. The larger r denotes stronger correlation between the

predicted value and the actual value that means higher prediction accuracy.

- The Forecast Skill Score (SS).

  The forecast skill score (SS) is used to compare performance between two models, and it is given by:

$$SS = \left(1 - \frac{\mathcal{E}_{prediction}}{\mathcal{E}_{benchmark}}\right) \times 100\% \quad (3.12)$$

  where $\mathcal{E}_*$ is any evaluation metric that is used to evaluate performance for every model. If the "prediction" model performs equally well as the comparative model, the skill score will be 0. A higher skill score thus means that the "prediction" model outperforms the comparative model. The comparative models used in this research are presented in the following section.

3.4.5 Comparative Tests

3.4.5.1 Comparison of Nowcasting Performance at Various Time Intervals

The object of this set of comparative tests is to explore the impact of various time intervals on the performance of GHI, DNI and DHI nowcasting for a series of fixed nowcasting horizons. In this section, these tests were divided into three groups based on 1-min, 5-min, and 10-min nowcasting horizons. Thus, these three groups of tests were:

- Nowcasting performance at various time intervals for 1-min nowcasting horizon.
- Nowcasting performance at various time intervals for 5-min nowcasting horizon.
- Nowcasting performance at various time intervals for 10-min nowcasting horizon.

For 1-min nowcasting horizon, GHI, DNI and DHI nowcasting were respectively conducted at 10-sec and 1-min time intervals. Consequently, a total of six sub-groups

of nowcasting results were achieved. For 5-min nowcasting horizon, GHI, DNI and DHI nowcasting were respectively conducted at 10-sec, 1-min and 5-min time intervals. Therefore, a total of nine sub-groups of nowcasting results were achieved. For 10-min nowcasting horizon, GHI, DNI and DHI nowcasting were respectively conducted at 10-sec, 1-min, 5-min and 10-min time intervals. As a result, a total of twelve sub-groups of nowcasting results were achieved. After obtaining the above nowcasting results, these nowcasting results were evaluated by six metrics including MAE, nMAE, RMSE, nRMSE, MAPE and r.

3.4.5.2 Comparison of Nowcasting Performance for Various Nowcasting Horizons

This set of comparative tests aims to understand the impact of various nowcasting horizons on the performance of GHI, DNI and DHI nowcasting. Due to 10 seconds being the smallest time interval achievable in this research, it is used as the sole fixed time interval in this set of comparative tests to compare the performance of GHI, DNI and DHI nowcasting for 1-min, 5-min, and 10-min nowcasting horizons. Consequently, a total of twelve groups of nowcasting results were achieved. As with the comparative tests of nowcasting performance at various time intervals, the nowcasting results in this set of comparative tests were also evaluated by six metrics, including MAE, nMAE, RMSE, nRMSE, MAPE and r.

3.4.5.3 Comparison of Nowcasting Performance in Different Sky Conditions

The purpose of this set of comparative tests is to investigate the effect of different sky conditions on the performance of GHI, DNI and DHI nowcasting. In this section, the crucial variables are sky conditions and thus this set of comparative tests used fixed 1-min time interval and 1-min nowcasting horizon.

Sky conditions were classified into four types, including clear sky, less cloudy, heavy cloudy and overcast. A particular Resnet-20 model was developed for the classification of sky conditions. For a single cloud image, if the proportion of cloud

pixels to the total image pixels is less than 25%, the sky condition represented by this image is defined as clear. When this proportion is greater than 25% but less than 50%, the sky condition is defined as light cloudy. Similarly, if the proportion of cloud pixels to the total image pixels is greater than 50% but less than 75%, the sky condition is defined as heavy cloudy. Finally, the sky condition is defined as overcast when this proportion is greater than 75%.

Based on the above, when the number of cloud images representing a specific sky condition is the highest among all collected cloud images on a particular date, that date is defined as the corresponding sky condition. For instance, if the number of cloud images representing overcast is the highest among all collected cloud images on a particular date, that date is defined as a overcast day.

In this section, two groups of comparative tests respectively were implemented:

- Nowcasting performance of 12 testing days in different sky conditions.
- Nowcasting performance at several moments under different sky conditions of a representative date.

Firstly, a total of 12 testing days with four types of sky conditions including clear, less cloudy, heavy cloudy and overcast were used in this set of comparative tests. Among these 12 testing days, the days with each type of sky condition were 3 days. In this case, a total of twelve groups of nowcasting results were achieved and evaluated to explore the performance of GHI, DNI and DHI nowcasting on days with different sky conditions. The evaluation metrics used in this set of comparative tests were MAE, nMAE, RMSE, nRMSE, MAPE and r.

Then, a representative date - June 25, 2021, which respectively presented three different sky conditions during morning, noon, and afternoon of the day, was used in this section to analyse the performance of GHI, DNI and DHI nowcasting at several moments under different sky conditions. Specifically, a detailed analysis was conducted for a total of nine specific moments within the aforementioned three periods.

3.4.5.4 Comparison of Nowcasting Performance among Different Models

The goal of this set of comparative tests is to compare the GHI, DNI and DHI nowcasting performance of the proposed ResNet-152 solar irradiance nowcasting model with a baseline model - Multilayer Perceptron (MLP) and a benchmark model - Persistence Model (PM). In this section, these tests were conducted with the same 10-sec time interval and were divided into three groups based on 1-min, 5-min, and 10-min nowcasting horizons. These three groups of tests were:

- Nowcasting performance at 1-min time interval for 1-min nowcasting horizon among different models.
- Nowcasting performance at 1-min time interval for 5-min nowcasting horizon among different models.
- Nowcasting performance at 1-min time interval for 10-min nowcasting horizon among different models.

Due to GHI, DNI and DHI nowcasting were respectively achieved by three different nowcasting models including ResNet-152, PM and MLP, a total of nine sub-groups of nowcasting results were achieved in each group mentioned above. Then, all nowcasting results were evaluated by eight metrics including MAE, nMAE, RMSE, nRMSE, MAPE, r, SS-MAE and SS-RMSE.

3.4.5.5 Comparison of Nowcasting Performance Based on Different Datasets

This set of comparative tests aims to understand the influence of different datasets on the performance of GHI, DNI and DHI nowcasting. In this section, the GHI, DNI and DHI nowcasting was conducted with fixed 1-min time interval and various nowcasting horizons. The variables of this section were the total size of the datasets and the seasonality of the datasets. In this case, this set of comparative tests was divided into two groups, which were:

- Nowcasting performance between the solar irradiance nowcasting models trained with 34 days of data and 48 days of data.

- Nowcasting performance based on different seasonal testing dates.

In the first group of comparative tests, the effect of the total size of datasets on the performance of GHI, DNI and DHI nowcasting was explored. In this section, a dataset consisting of 48 days of data from April to September and a dataset consisting of 34 days of data from April to July were respectively used to achieve GHI, DNI and DHI nowcasting. Both these two datasets consisted of days with four types of sky conditions, with an equal number of days for each type of sky condition. On this basis, 8 identical days of data from the two above datasets were selected as testing set. Every 2 days within these 8 days had one type of sky condition. In this case, the only difference between the solar irradiance nowcasting models trained with 34 days of data and 48 days of data was the total number of days in training set. Consequently, a total of eighteen sub-groups of nowcasting results were achieved. Then, all nowcasting results were evaluated by six metrics including MAE, nMAE, RMSE, nRMSE, MAPE and r.

In the second group of comparative tests, the impact of the seasonality of datasets on the performance of GHI, DNI and DHI nowcasting was investigated. Using the same training set selected from the dataset consisting of 48 days of data, the nowcasting results based on 12 testing dates with various sky conditions from April to September and 4 testing dates in December were achieved and compared. Consequently, a total of forty-eight sub-groups of nowcasting results were achieved and evaluated by the same metrics as the first group.

3.4.6 Hardware and Software

The core hardware for data pre-processing, the training and testing of solar irradiance nowcasting models and comparative tests are an Intel(R) Core(TM) i9-10900X CPU@3.70GHz and an NVIDIA GeForce RTX 3090 graphic card.

In terms of software, the programming of this research is implemented on the Raspberry Pi OS and Ubuntu 20.04 OS using Python as the programming language

and Pycharm as IDE. Anaconda is used to manage the Python environment and PyTorch, as an open-source machine learning framework, is used to execute the training and testing of the proposed solar irradiance nowcasting model. In addition, the programming for capturing cloud images is implemented on the Raspberry Pi OS using Python as the programming language.

In general, the programming of this research is mainly based on Python because it is very user-friendly. First, Python is an open-source language, which means its source code is open to all and free to use and distribute. For individuals, students, and startups with limited budgets, Python offers a cost-effective alternative. Moreover, Python has a huge and continuously growing of libraries covering a wide range of areas such as data analytics, machine learning, image processing, etc. For example, the NumPy libraries provide mathematical and scientific computing capabilities similar to MATLAB, while the Pandas library is an indispensable tool for data analysis. Finally, Python has a large global community, which means that the researcher can easily find solutions, documentation, and tutorials for common problems and challenges.

Based on the above, this research applies user-friendly programming which is more conducive to its popularity in building applications.

3.5 Chapter Summary

In summary, Chapter 3 elaborately demonstrates the development of a solar irradiance nowcasting method involving data collection and processing, solar irradiance nowcasting, comparative tests and verification. The developed solar irradiance nowcasting method is well suited for building applications based on its following critical characteristics.

- Low-cost Equipment

  The equipment cost of this research is around £3,500, which mainly consists of the purchase cost of Raspberry Pi Total Sky Imager and Delta-T Device BF5 sunshine sensor. Due to BF5 Sunshine Sensor are not necessary after the training stage of solar irradiance nowcasting model completed, only very low maintenance cost of Raspberry Pi Total Sky Imager needs to be considered in the long-term daily use of buildings.

- User-friendly Programming

  A great deal of programming work in this research is entirely based on Python because of its user-friendly features, which include open-source, free, extensive libraries and broad community support.

- ResNet-152 Nowcasting Model

  By applying ResNet-152 as nowcasting model to learn the relationship between cloud images and solar irradiance, this research can utilise consecutive cloud images to achieve reliable nowcasting of GHI, DNI and DHI with very short-term forecasting horizons and high spatial-temporal resolution, which is ideal for buildings and their future development.

Chapter Four

4 Results Verification and Analysis of Solar Irradiance Nowcasting

The goal of Chapter 4 is to answer the third and fourth research questions in Chapter 1 - “How can the results of solar irradiance nowcasting be generated?” and “How can the reliability of solar irradiance nowcasting be verified?” Therefore, the main tasks of this chapter are to achieve the third research objective - to apply the proposed irradiance nowcasting method to achieve the nowcasting of GHI, DNI, and GHI in a series of comparative tests, as well as the fourth research objective - to utilise appropriate evaluation metrics to evaluate the reliability of the GHI, DNI, and DHI nowcasting from various perspectives.

In general, Chapter 4 demonstrates the results of verification and analysis of solar irradiance nowcasting. Five groups of comparative tests were conducted to investigate the effect of different factors on solar irradiance nowcasting, involving time intervals, nowcasting horizons, sky conditions, forecasting models and datasets. First of all, the results of comparative tests of nowcasting performance for various time intervals were presented. Secondly, the effect of various nowcasting horizons was investigated. Thirdly, a series of comparative tests were conducted to explore the nowcasting performance under different sky conditions. Fourthly, the performance of the proposed solar irradiance nowcasting method is evaluated by comparing the proposed nowcasting model with a benchmark model and a baseline model. Fifthly, the nowcasting performance of the proposed solar irradiance nowcasting method based on different datasets was articulated. In the end, the results of the above five groups of comparative tests are summarised at the end of this chapter.

4.1 Results Verification and Analysis of Solar Irradiance Nowcasting

To verify the reliability of the proposed solar irradiance nowcasting method, it is necessary to explore the performance of solar irradiance nowcasting based on different circumstances and its performance relative to other models. Thus, a series of comparative tests are implemented.

4.1.1 Comparison of Nowcasting Performance at Various Time Intervals

In this section, the nowcasting performance at various time intervals for 1-min, 5-min and 10-min nowcasting horizons are respectively compared. Since the total number of ground-based cloud images in datasets is a certain amount, larger time intervals mean lower sampling frequency, which results in fewer images for the training and testing of solar irradiance nowcasting models. Thus, various time intervals determine that the number of cloud images used for training and testing of different nowcasting models are varied. The maximum and minimum number of cloud images used for training and testing are 178517 and 3026. Nevertheless, even the solar irradiance nowcasting model using the minimum number of cloud images achieves a convergence situation in terms of the loss function that indicates the model is reliable.

4.1.1.1 Nowcasting Performance at Various Time Intervals for 1-Min Nowcasting Horizon

Table 4.1 presents the nowcasting performance of GHI, DNI and DHI at various time intervals for 1-min nowcasting horizon. In general, the nowcasting of DHI apparently performs better than the nowcasting of GHI and DNI with respect to MAE and RMSE because the DHI is less sensitive to meteorological changes and sky conditions. In contrast, the nowcasting of DNI shows the largest MAE and RMSE due to its high sensitivity to meteorological changes and sky conditions, such as the relative position of clouds and the sun. For example, the DNI dramatically descends

when clouds block the sun for a moment. Specifically, the MAE of GHI and DNI nowcasting are close to 60 and the MAE of DHI nowcasting are close to 20. The RMSE of GHI and DNI nowcasting are close to 100 and the RMSE of DHI nowcasting are lower than 30. Apart from MAE and RMSE, the MAPE of GHI are lower than 15% and the MAPE of DHI are lower than 8%. In terms of r, the r of GHI, DNI and DHI nowcasting are higher than 0.93. Typically, MAPE less than 30% indicates the forecasting models are high quality and r greater than 0.7 indicates a strong correlation between the two variables. Thus, the above evaluation metrics demonstrate the high reliability of GHI, DNI and DHI nowcasting at various time intervals for 1-min nowcasting horizon.

Table 4.1 Nowcasting performance at various time intervals for 1-min nowcasting horizon.

Components	Total Images	Intervals	MAE	nMAE	RMSE	nRMSE	MAPE	r
GHI	178222	10s	60.48	0.1	97.77	0.17	13.40%	0.949
	29752	1 min	58.82	0.1	98.66	0.17	13.53%	0.9481
DHI	178222	10s	20.06	0.07	27.75	0.09	7.64%	0.9769
	29752	1 min	19.17	0.07	27.51	0.09	7.54%	0.9782
DNI	/	10s	63.9	0.18	104.27	0.29	/	0.9353
	/	1 min	62.74	0.18	106.61	0.3	/	0.9324

Comparing the nowcasting at 10-sec time interval with the nowcasting at 1-min time interval, the nowcasting at 1-min time interval demonstrates slight advantage according to the MAE. The nowcasting at 1-min time interval achieves the lower MAE of 58.82 for GHI, 19.17 for DHI, 62.74 for DNI. However, the nowcasting at 10-sec time interval achieves the lower RMSE of 97.77 for GHI, and 104.27 for DNI. In terms of MAPE and r, the nowcasting at 10-sec time interval performs close to the nowcasting at 1-min time interval. Figure 4.1 presents the comparison of MAE and RMSE among the nowcasting at 10-sec and 1-min time interval for 1-min nowcasting horizon.

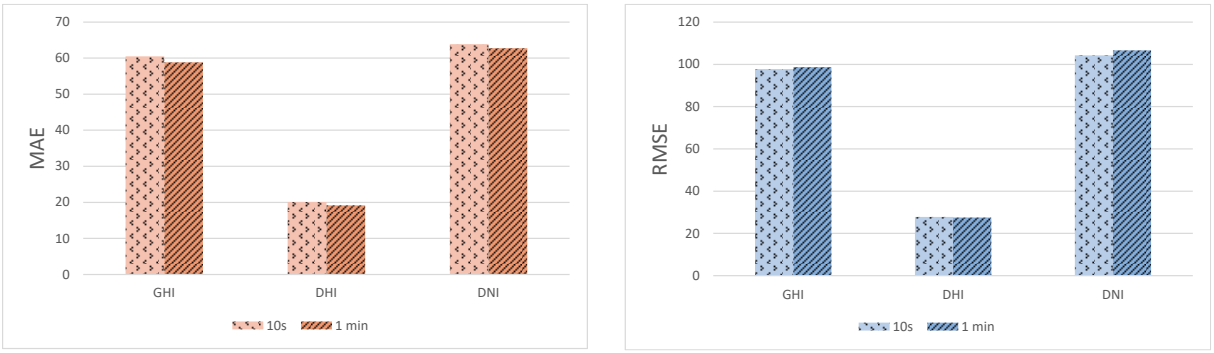

Figure 4.1 The comparison of MAE and RMSE among the nowcasting at 10-sec and 1-min time intervals for 1-min nowcasting horizon.

Considering the high variability and higher values of GHI and DNI, the nowcasting performance of GHI and DNI is used as the critical factor to judge the nowcasting performance at various time intervals. For 1-min nowcasting horizon, the nowcasting at 10-sec time interval have very close accuracy to the nowcasting at 1-min time interval according to the evaluation metrics presented in Table 4.1.

4.1.1.2 Nowcasting Performance at Various Time Intervals for 5-Min Nowcasting Horizon

The nowcasting performance of GHI, DNI and DHI at various time intervals for 5-min nowcasting horizon are presented in Table 4.2. Similar with the nowcasting for 1-min nowcasting horizon, DHI nowcasting for 5-min nowcasting horizon significantly present higher accuracy compared to GHI and DNI nowcasting. In specific, the MAE of GHI and DNI nowcasting are close to 100 and the MAE of DHI nowcasting are close to 34. The RMSE of GHI and DNI nowcasting are close to 150 and the RMSE of DHI nowcasting are close to 50. Besides MAE and RMSE, the MAPE of GHI are lower than 26% and the MAPE of DHI are lower than 23%. In addition, most r of GHI, DNI and DHI nowcasting are higher than 0.86. Thus, the nowcasting of GHI, DNI and DHI at various time intervals for 5-min nowcasting horizon are generally reliable.

Table 4.2 Nowcasting performance at various time intervals for 5-min nowcasting horizon.

Components	Total Images	Intervals	MAE	nMAE	RMSE	nRMSE	MAPE	r
GHI	125502	10s	92.37	0.16	147.21	0.25	23.13%	0.8832
	20952	1 min	94.39	0.16	144.36	0.25	13.53%	0.8839
	4224	5 min	100.47	0.17	151.39	0.26	25.70%	0.8733
DHI	125502	10s	34.21	0.12	51.36	0.18	23.13%	0.9198
	20952	1 min	33.99	0.12	49.21	0.17	14.53%	0.9231
	4224	5 min	33.3	0.11	49.69	0.17	13.07%	0.9221
DNI	/	10s	106.2	0.3	157.38	0.44	/	0.8598
	/	1 min	97.47	0.27	147.98	0.42	/	0.8648
	/	5 min	114.61	0.32	163.56	0.46	/	0.8346

Comparing the nowcasting at 10-sec, 1-min, 5-min time interval for 5-min nowcasting horizon, the nowcasting at 1-min time interval demonstrates obvious advantages according to various evaluation metrics. In terms of MAE, the MAE of GHI nowcasting at 10-sec and 1-min time interval are lower and close 93 and all MAE of DHI nowcasting at 10-sec, 1-min, 5-min time interval are very close to 33. However, the MAE of DNI nowcasting at 1-min time interval achieves 97.47 which outperforms significantly than the MAE of DNI nowcasting at 10-sec and 5-min time intervals. For RMSE, GHI, DNI and DHI nowcasting at 1-min time interval achieves the lowest RMSE of 144.36 for GHI, 49.21 for DHI and 147.98 for DNI. Apart from MAE and RMSE, the MAPE of GHI nowcasting at 1-min time interval are much lower than others and the MAPE of DHI nowcasting at 1-min and 5-min time interval are much lower and close. In addition, GHI, DNI and DHI nowcasting at 1-min time interval achieves the highest r of 0.8839 for GHI, 0.9231 for DHI, 0.8648 for DNI. Figure 4.2 shows the comparison of MAE and RMSE among the nowcasting at 10-sec, 1-min, 5-min time interval for 5-min nowcasting horizon.

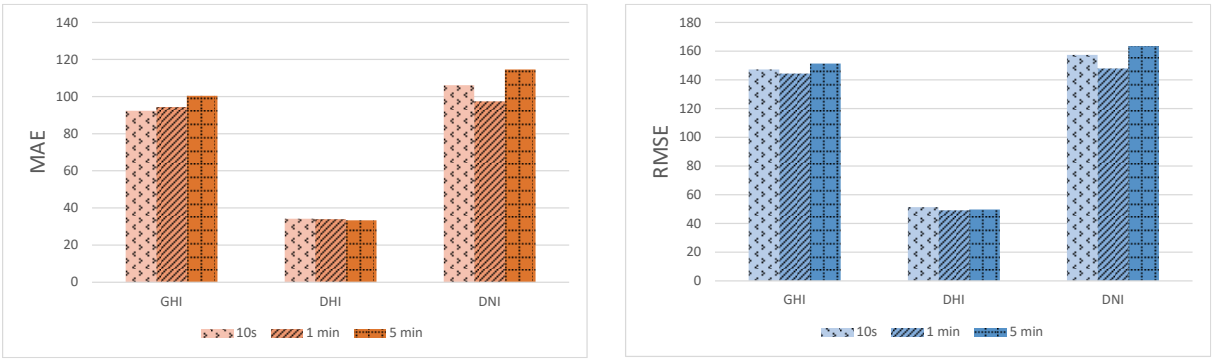

Figure 4.2 The comparison of MAE and RMSE among the nowcasting at 10-sec, 1-min, 5-min time intervals for 5-min nowcasting horizon.

To sum up, GHI, DNI and DHI nowcasting at 1-min time interval achieves the lowest RMSE and the highest r. In the meanwhile, the MAE and the MAPE of GHI, DNI and DHI nowcasting at 1-min time interval also present lower values. Thus, GHI, DNI and DHI nowcasting at 1-min time interval present the best performance for 5-min nowcasting horizon.

4.1.1.3 Nowcasting Performance at Various Time Intervals for 10-Min Nowcasting Horizon

Table 4.3 presents the nowcasting performance of GHI, DNI and DHI at various time intervals for 10-min nowcasting horizon. DHI nowcasting for 10-min nowcasting horizon are far more accurate than GHI and DNI nowcasting according to MAE and RMSE. In specific, most MAE of GHI and DNI nowcasting are lower than 116 and the MAE of DHI nowcasting are close to 45. Most RMSE of GHI and DNI nowcasting are close to 165 and the RMSE of DHI nowcasting are close to 61. In addition, most MAPE of GHI are close to 27% and the MAPE of DHI are lower than 20%. In terms of r, most r of GHI, DNI and DHI nowcasting are higher than 0.8. The MAPE and the r indicate the nowcasting of GHI, DNI and DHI at various time intervals for 10-min nowcasting horizon are generally reliable.

Table 4.3 Nowcasting performance at various time intervals for 10-min nowcasting horizon.

Components	Total Images	Intervals	MAE	nMAE	RMSE	nRMSE	MAPE	r
GHI	175036	10s	107.85	0.19	156.33	0.27	26.21%	0.8657
	29221	1 min	104.42	0.18	164.71	0.28	27.01%	0.8585
	5891	5 min	114.82	0.2	163.32	0.28	30.09%	0.8503
	3026	10 min	114.52	0.2	161.37	0.28	26.12%	0.8633
DHI	175036	10s	44.1	0.15	60.71	0.21	19.05%	0.8867
	29221	1 min	42.37	0.15	61.09	0.21	17.22%	0.8785
	5891	5 min	44.02	0.15	60.83	0.21	17.20%	0.8844
	3026	10 min	45.92	0.16	63.66	0.22	18.37%	0.872
DNI	/	10s	115.78	0.33	164.83	0.46	/	0.8372
	/	1 min	113.98	0.32	176.24	0.5	/	0.8203
	/	5 min	130.19	0.37	180.01	0.51	/	0.7976
	/	10 min	115.28	0.32	164.56	0.46	/	0.8335

Comparing the nowcasting at 10-sec, 1-min, 5-min, 10-min time interval for 10-min nowcasting horizon, the nowcasting at 1-min time interval performs better than others according to MAE. The nowcasting at 1-min time interval achieves the lowest MAE of 104.42 for GHI, 42.37 for DHI and 113.98 for DNI. However, the nowcasting at 10-sec time interval achieve the lowest RMSE of 156.33 for GHI, 60.71 for DHI and almost the lowest RMSE of 164.83 for DNI. In terms of MAPE, the MAPE of GHI nowcasting at 10-sec, 1-min, 10-min time interval are lower and the MAPE of the DHI nowcasting at 1-min, 5-min time interval are lower. With respect to r, the nowcasting at 10-sec time interval achieves highest r for GHI, DNI and DHI. However, most r of the nowcasting at various time intervals are very close apart from the r of DNI nowcasting at 5-min time interval. Figure 4.3 demonstrates the comparison of MAE and RMSE among the nowcasting at 10-sec, 1-min, 5-min, 10-min time interval for 10-min nowcasting horizon.

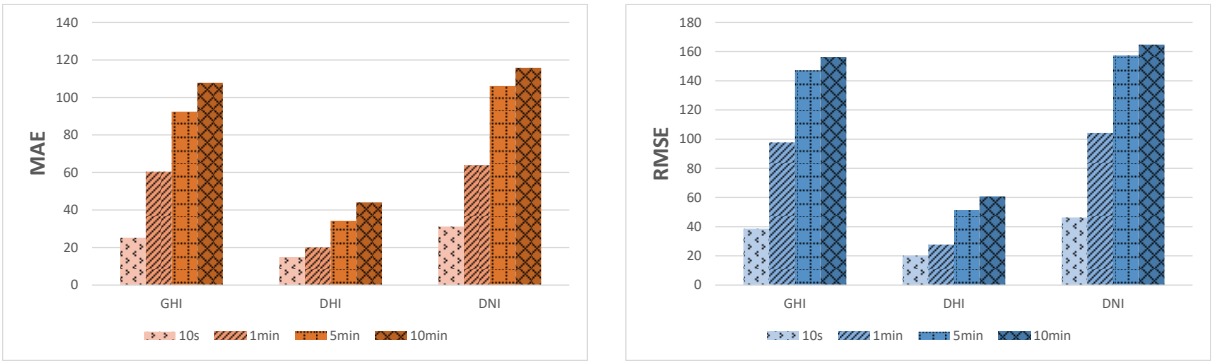

Figure 4.3 The comparison of MAE and RMSE among the nowcasting at 10-sec, 1-min, 5-min, 10-min time intervals for 10-min nowcasting horizon.

In light of the above, the GHI, DNI and DHI nowcasting at 10-sec and 1-min time interval present higher accuracy compared to the GHI, DNI and DHI nowcasting at 5-min and 10-min time intervals for 10-min nowcasting horizon. However, considering the time consumption of computer operation, data transmission, system response and other factors, the GHI, DNI and DHI nowcasting at 1-min time interval is obviously more in line with the requirements of the practical application. In this case, the GHI, DNI and DHI nowcasting at 1-min time interval outperform the GHI, DNI and DHI nowcasting at other time intervals for 10-min nowcasting horizon.

In summary, the GHI, DNI and DHI nowcasting at 10-sec and 1-min time interval outperform the nowcasting at 5-min and 10-min time interval for various nowcasting horizons. However, there is no clear correlation between time intervals and nowcasting accuracy. Nevertheless, the nowcasting of GHI, DNI and DHI at 1-min time interval achieves the best performance for 1-min, 5-min and 10-min nowcasting horizon in terms of evaluation metrics and is optimal for the requirements of the practical application.

4.1.2 Comparison of Nowcasting Performance for Various Nowcasting Horizons

In practice, different application objectives obviously require various nowcasting horizons. Therefore, it is worth to investigate the effect of various nowcasting horizons on nowcasting performance. In this section, the nowcasting performance at 10-sec,

1-min, 5-min and 10-min time intervals for various nowcasting horizons are compared to investigate the impact of nowcasting horizons on the nowcasting performance.

Table 4.4 gives the GHI, DNI and DHI nowcasting performance at 10-sec time interval for various nowcasting horizons. In general, DHI nowcasting always achieves the highest accuracy in terms of MAE and RMSE, while DNI nowcasting is the opposite. Most MAPE of GHI, DNI and DHI nowcasting are lower than 20% and the largest MAPE are lower than 27% which indicates the nowcasting is reliable. The r of GHI, DNI and DHI nowcasting are higher than 0.83 which demonstrates the high agreement between nowcasting and measurement.

Table 4.4 Nowcasting performance at 10-sec time intervals for various nowcasting horizons.

Components	Total Images	Horizons	MAE	nMAE	RMSE	nRMSE	MAPE	r
GHI	175036	10s	25.17	0.04	38.64	0.07	5.38%	0.9921
	29221	1 min	60.48	0.1	97.77	0.17	13.40%	0.949
	5891	5 min	92.37	0.16	147.21	0.25	23.13%	0.8832
	3026	10 min	107.85	0.19	156.33	0.27	26.21%	0.8657
DHI	175036	10s	14.95	0.05	20.17	0.07	5.71%	0.9888
	29221	1 min	20.06	0.07	27.75	0.09	7.64%	0.9769
	5891	5 min	34.21	0.12	51.36	0.18	12.29%	0.9198
	3026	10 min	44.1	0.15	60.71	0.21	19.05%	0.8867
DNI	/	10s	31.18	0.09	46.27	0.13	/	0.9878
	/	1 min	63.9	0.18	104.27	0.29	/	0.9353
	/	5 min	106.2	0.3	157.38	0.44	/	0.8598
	/	10 min	115.78	0.33	164.83	0.46	/	0.8372

Comparing the nowcasting performance at 10-sec time interval for 10-sec, 1-min, 5-min and 10-min nowcasting horizons, it is evident that the nowcasting for shorter nowcasting horizon presents higher accuracy in terms of all evaluation metrics because the position of the sun, cloud appearance and sky conditions are more stable over a shorter horizon. The nowcasting for 10-sec nowcasting horizon achieves the lowest MAE of 25.17 for GHI, 14.95 for DHI, 31.18 for DNI and the lowest RMSE of 38.64 for GHI, 20.17 for DHI, 46.27 for DNI. In contrast, the nowcasting for 10-min

nowcasting horizon achieves the highest MAE of 107.85 for GHI, 44.1 for DHI, 115.78 for DNI and the highest RMSE of 156.33 for GHI, 60.71 for DHI, 164.83 for DNI. The MAE and RMSE of GHI nowcasting for 10-min nowcasting horizon are higher than GHI nowcasting for 10-sec nowcasting horizon by 328.5% and 304.6%. In addition, the MAE and RMSE of the nowcasting for 10-min nowcasting horizon are respectively higher than the nowcasting for 10-sec nowcasting horizon by 195.0% and 201% in terms of DHI. According to DNI, the MAE and the RMSE of the nowcasting for 10-min nowcasting horizon is higher than the nowcasting for 10-sec nowcasting horizon by 271.3% and 256.2%. The comparison of MAE and RMSE among the nowcasting at 10-sec time interval for 10-sec, 1-min, 5-min and 10-min nowcasting horizons are shown in Figure 4.4.

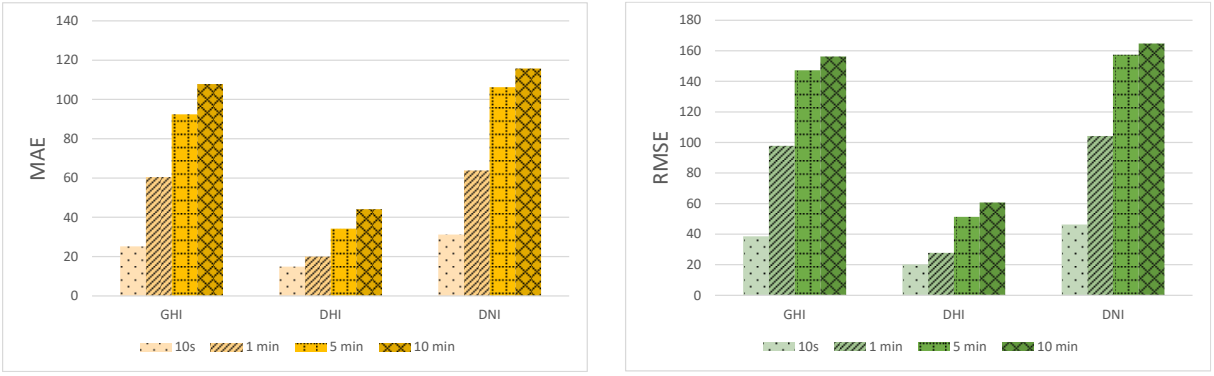

Figure 4.4 The comparison of MAE and RMSE among the nowcasting at 10-sec time interval for 10-sec, 1-min, 5-min and 10-min nowcasting horizon.

The GHI, DNI and DHI nowcasting performance at 1-min and 5-min time interval for various nowcasting horizons are present in Table 4.4. To sum up, the accuracy of GHI, DNI and DHI nowcasting decreases as nowcasting horizons increase. The nowcasting of GHI, DNI and DHI for 10-sec and 1-min nowcasting horizons achieves very high accuracy that as demonstrated in Figure 4.4. However, the nowcasting performance of GHI and DNI for 5-min and 10-min nowcasting horizons are less sensitive when GHI and DNI dramatically raise or drop that is evidently shown in Figure 4.4.

4.1.3 Comparison of Nowcasting Performance in Different Sky Conditions

In this section, the effect of different sky conditions on nowcasting performance is explored. On the one hand, the nowcasting performance of 12 testing days in different sky conditions is investigated. On the other hand, the nowcasting performance at several moments under different sky conditions of a representative date is analysed.

4.1.3.1 Nowcasting Performance of 12 Testing Days in Different Sky Conditions

In this research, 12 testing days are pre-selected according to four types of sky conditions including clear, less cloudy, heavy cloudy and overcast. In specific, the days with each type of sky condition are 3 days. The four types of sky conditions are classified according to the proportion of cloud pixels to sky pixels in an image, which is presented in Chapter 3.

Table 4.5 Nowcasting performance in different sky conditions.

Components	Sky Conditions	Interval	Horizon	MAE	nMAE	RMSE	nRMSE	MAPE	r
GHI	Clear	1 min	1 min	52.53	0.07	91.94	0.13	8.53%	0.9358
	Light Cloudy			52.14	0.08	90.15	0.14	11.32%	0.9484
	Heavy Cloudy			86.46	0.14	133.75	0.22	18.64%	0.9083
	Overcast			44.14	0.13	66.85	0.2	15.62%	0.9541
DHI	Clear	1 min	1 min	12.23	0.05	16.68	0.07	5.75%	0.9858
	Light Cloudy			16.76	0.05	22.56	0.07	5.25%	0.9806
	Heavy Cloudy			19.61	0.06	25.97	0.08	7.67%	0.9789
	Overcast			28.07	0.1	39.58	0.14	11.48%	0.9667
DNI	Clear	1 min	1 min	70.68	0.11	109.88	0.17	/	0.8551
	Light Cloudy			59.84	0.16	99.39	0.26	/	0.887
	Heavy Cloudy			93.84	0.27	141.94	0.41	/	0.8544
	Overcast			26.6	0.49	58.01	1.06	/	0.8857

Table 4.5 presents the nowcasting performance in different sky conditions. In general, the MAPE of GHI, DNI and DHI nowcasting are lower than 20% and the r of GHI, DNI and DHI nowcasting are higher than 0.85 which indicates the nowcasting

has a reliable accuracy. Compared to GHI and DHI nowcasting, the accuracy of DNI nowcasting is relatively lower in terms of MAE, RMSE and r.

Comparing the nowcasting performance in different sky conditions, it is evident that GHI and DNI nowcasting on heavy cloudy days always present the lowest accuracy according to all evaluation metrics, especially MAE and RMSE. That is because the relative position between the sun and cloud usually varies dramatically on heavy cloudy days. In contrast, GHI and DNI nowcasting on overcast days achieves the best performance because the sun is almost completely covered by clouds. GHI and DNI nowcasting performance in clear days and light cloudy days are similar because the sun is usually only briefly obscured by fewer or thinner clouds. According to MAE and RMSE, DHI nowcasting performance on clear days is the best but decreases as cloud increases. In this case, DHI nowcasting accuracy in overcast days are the lowest. That is because the increase of clouds leads to a more complex distribution of air molecules, cloud droplets, and aerosols in the atmosphere, increasing the variability of DHI. Figure 4.5 presents the nowcasting performance of 4 days in four different sky conditions. The above findings are visualised clearly in these figures. For example, it is evident that GHI and DNI measurements on heavy cloudy day have very high fluctuations and thus increase the difficulty of GHI and DNI nowcasting in Figure 4.6. In case of a dramatic decrease or increase of GHI and DNI, the nowcasting models are not sensitive enough. In addition, the decline of DHI nowcasting performance with increasing clouds is also demonstrated clearly in Figure 4.7. In this section, only the nowcasting at 1-min time interval for 1-min nowcasting horizon in different sky conditions are presented. Despite this, the nowcasting at various time intervals for various nowcasting horizons in different sky conditions also achieves a similar conclusion. Relevant Tables are shown in the Appendices.

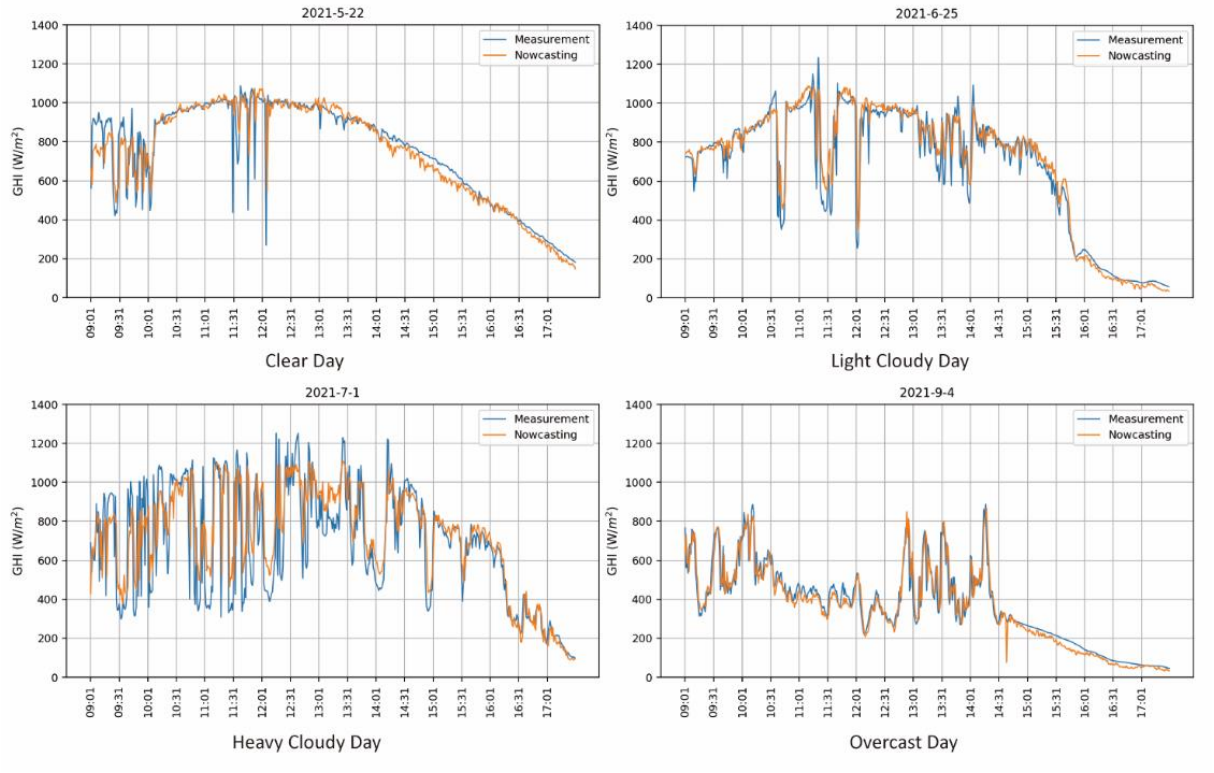

Figure 4.5 GHI nowcasting performance of 4 days in four different sky conditions

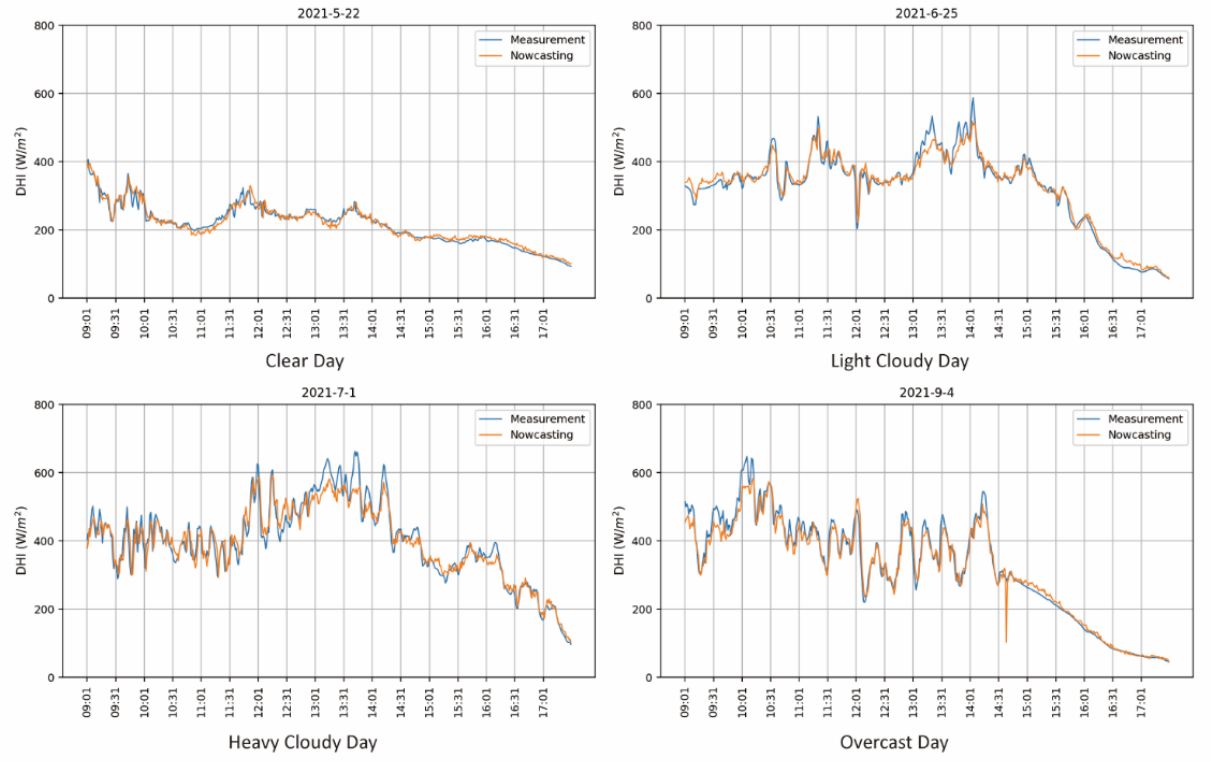

Figure 4.6 DHI nowcasting performance of 4 days in four different sky conditions.

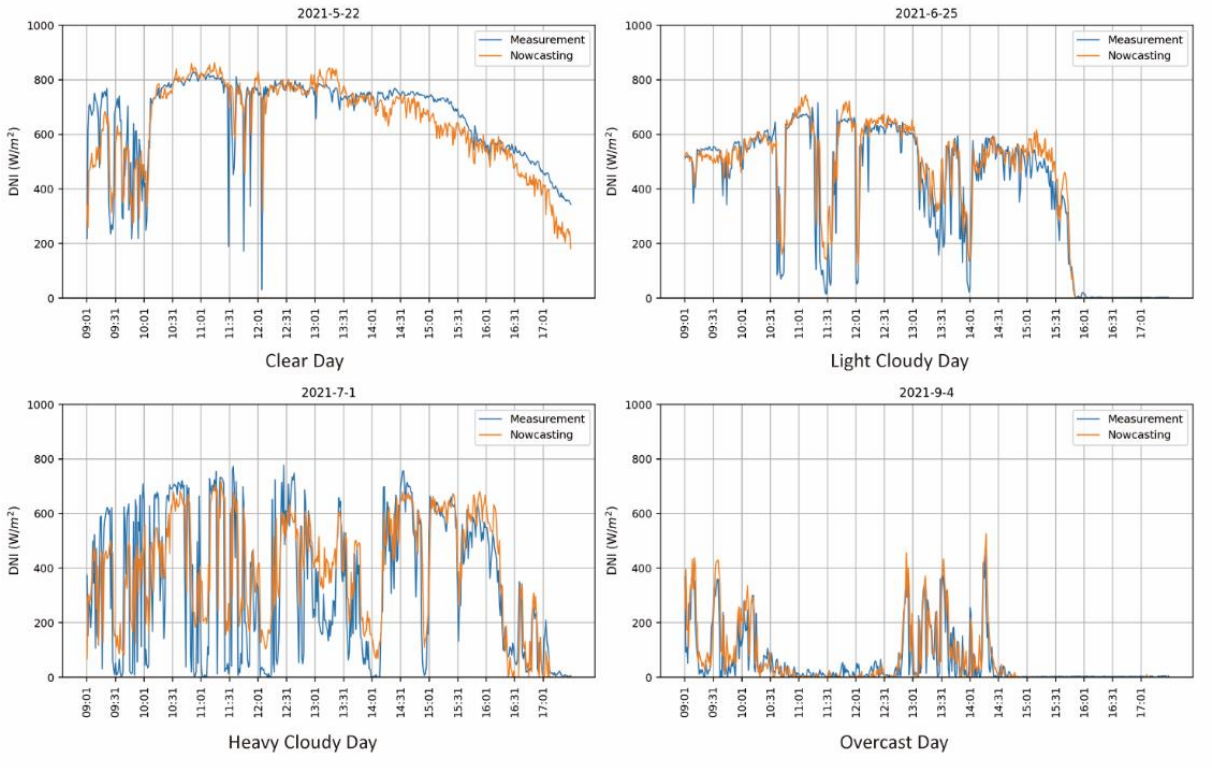

Figure 4.7 DNI nowcasting performance of 4 days in four different sky conditions.

4.1.3.2 Nowcasting Performance at Several Moments under Different Sky Conditions of A Representative Date

In this section, the nowcasting of GHI, DNI and DHI at 1-min time interval for 1-min nowcasting horizon on a representative date are used to demonstrate the nowcasting performance under different sky conditions. This representative date is June 25, 2021, which presented three different sky conditions at different times of the day. Between 9 am to 11 am, the sky condition was mainly clear sky. From 11 am to 4 pm, the sky condition was mostly cloudy sky and finally changed to overcast sky after 4 pm. Figure 4.8 presents the nowcasting of GHI, DNI and DHI for the whole day on June 25, 2021 at the top. In addition, the nowcasting performance and corresponding cloud images at a series of specific moments in different sky conditions are shown at the middle and the bottom of Figure 4.8. Although only the nowcasting performance in different sky conditions on June 25, 2021 is presented in this section, the nowcasting performance among different sky conditions of other testing dates

also achieves a similar conclusion.

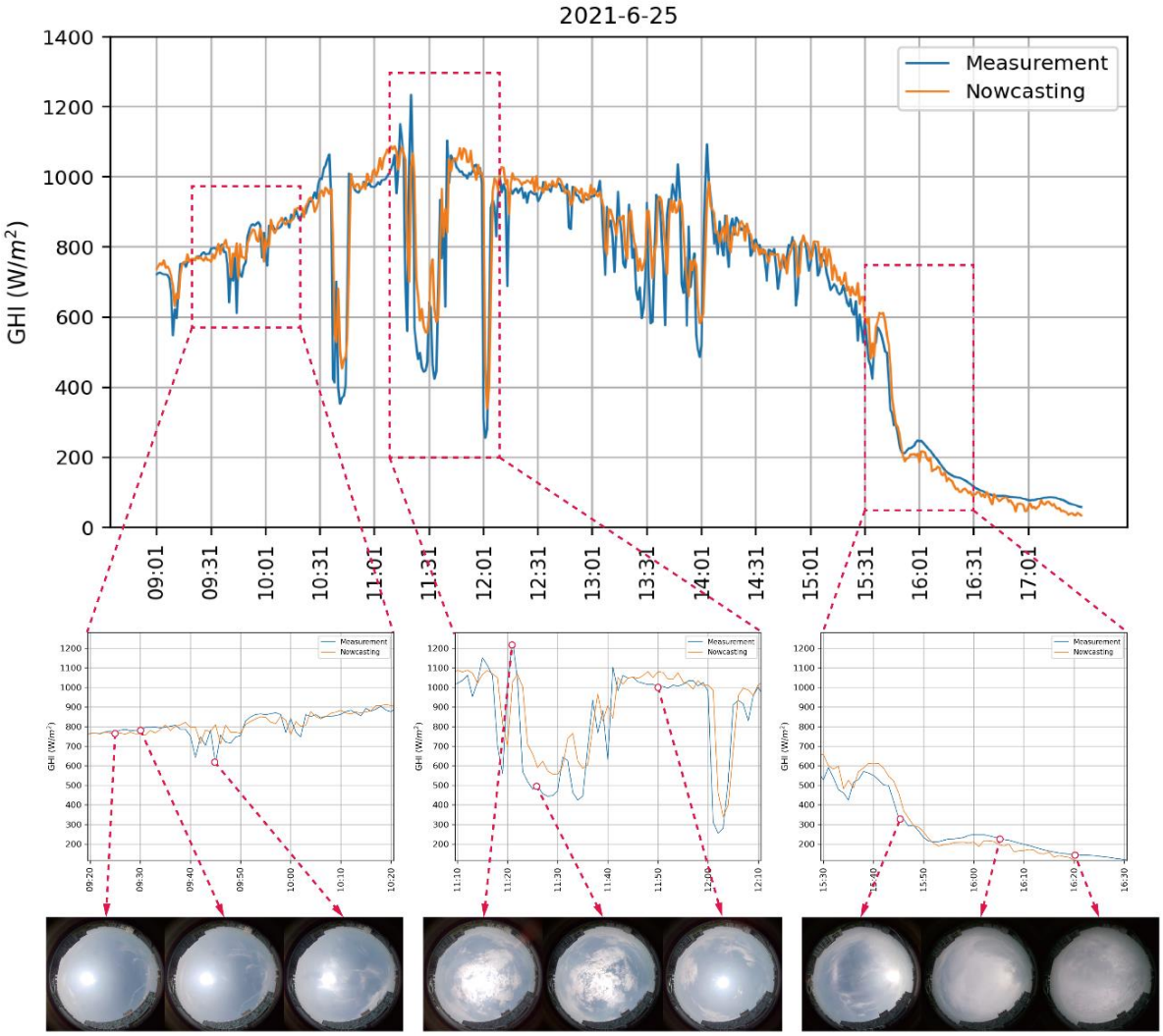

Figure 4.8 The performance of GHI nowcasting at 1-min time interval for 1-min nowcasting horizons in clear sky, cloudy sky and overcast sky.

As the middle left and bottom left of Figure 4.9 shows, nowcasting values and measured values of GHI both are very stable in clear sky from 9:20 am to 9:35 am and the errors between them are very small, usually less than 20 W/m^2. However, the errors between nowcasting and measurement dramatically raise more than 100 W/m^2 or more at a few moments, such as 9:45 am, when the sun is suddenly obscured by clouds or emerges from them (as shown in the third cloud image from the left at the bottom of Figure 4.9.

According to the centre and bottom middle of Figure 4.9, nowcasting values and

measured values of GHI both present sharp fluctuations under cloudy sky and the errors between them are obvious. Comparing the GHI nowcasting performance under heavy cloudy sky from 11:20 am to 11:40 am (as shown in the first two cloud images at the bottom middle of Figure 9) with its performance under light cloudy sky from 11:40 am to 12:00 am (as shown in the last cloud image at the bottom middle of Figure 15), it is obvious that heavy cloudy sky leads to greater errors because of more frequent and dramatic position variations between the sun and clouds. The errors are often more than 100 W/m^2 or more in heavy cloudy sky but less than 100 W/m^2 in light cloudy sky. Nevertheless, it is worth noting that the curves of nowcasting and measurement present very similar trends, indicating high agreement between nowcasting and measurement.

The middle right and bottom right of Figure 4.9 present the change of sky conditions from cloudy sky to overcast sky. Unlike the dramatic variations of the nowcasting performance under cloudy sky, nowcasting values and measured values of GHI are also very stable under overcast sky from 3:40 pm to 4:30pm and the errors between them are very small due to the sun being almost completely blocked (as shown in the first and second cloud images from the right at the bottom of Figure 4.9).

To sum up, very small errors of GHI nowcasting under clear sky and overcast sky indicate that solar irradiance nowcasting models perform best in these sky conditions. In the meanwhile, although GHI nowcasting under cloudy sky has larger errors than GHI nowcasting under clear sky and overcast sky, the high agreement of the curves of GHI nowcasting and GHI measurement indicates that the proposed solar irradiance nowcasting method is also reliable under cloudy sky.

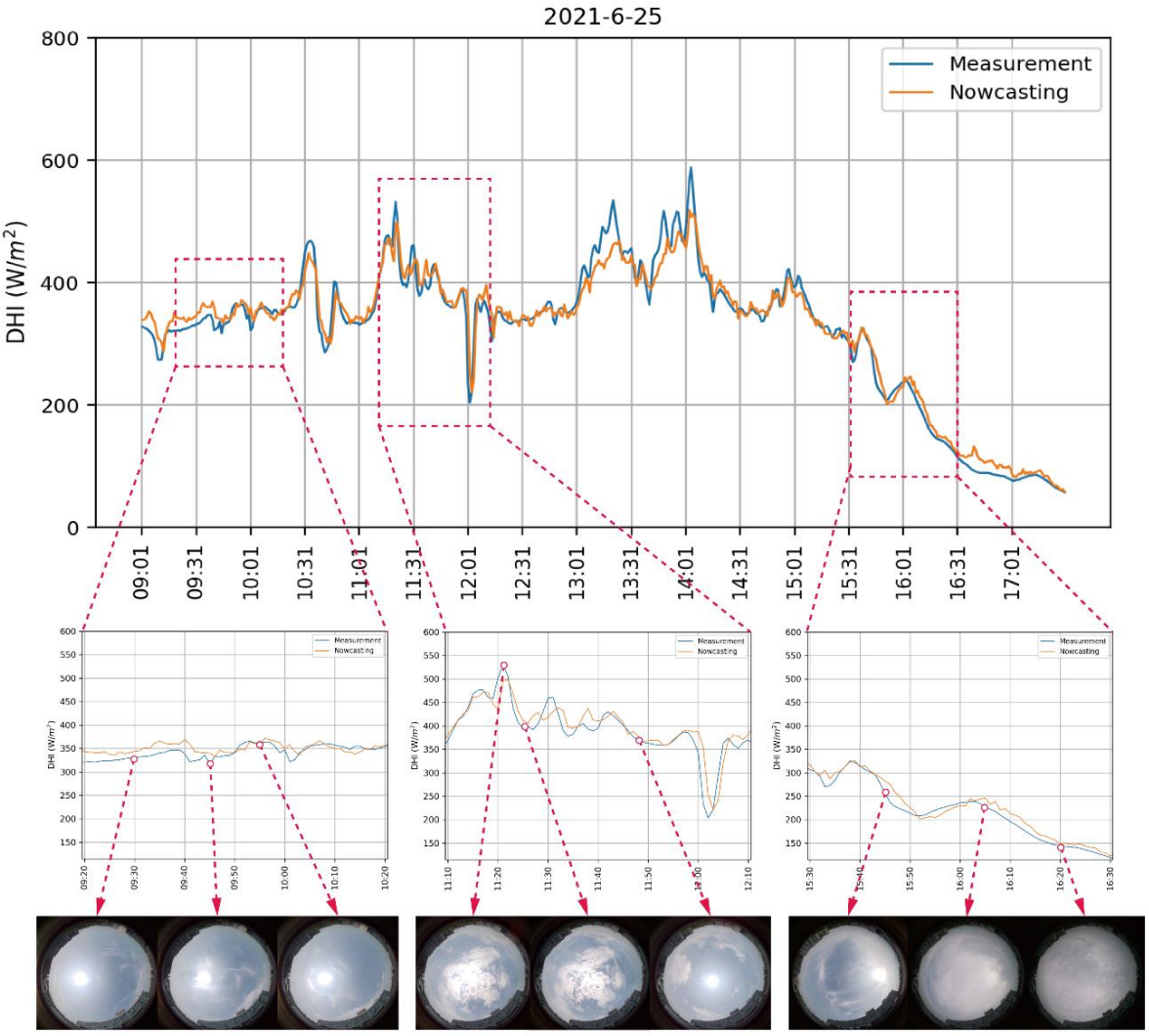

Figure 4.9 The performance of DHI nowcasting at 1-min time interval for 1-min nowcasting horizons in clear sky, cloudy sky and overcast sky.

According to Figure 4.10, the effect of different sky conditions on DHI nowcasting and GHI nowcasting are similar, but it is worth noting that the effect of cloudy sky on the errors of DHI nowcasting is not very significant. In specific, although the DHI nowcasting under cloudy sky shows more fluctuations and larger errors compared to the DHI nowcasting under clear and overcast sky, the errors between nowcasting values and measured values of DHI are usually less than 50 W/m^2 with only very few cases greater than 100 W/m^2. That is because the actual values of DHI is normally small compared to the actual values of GHI and DNI. Apart from that, the variation of DHI is less affected by the change of relative position between the sun and clouds.

Meanwhile, the curves of DHI nowcasting and DHI measurement evidently present a high agreement. In this case, DHI nowcasting always has high accuracy regardless of sky conditions.

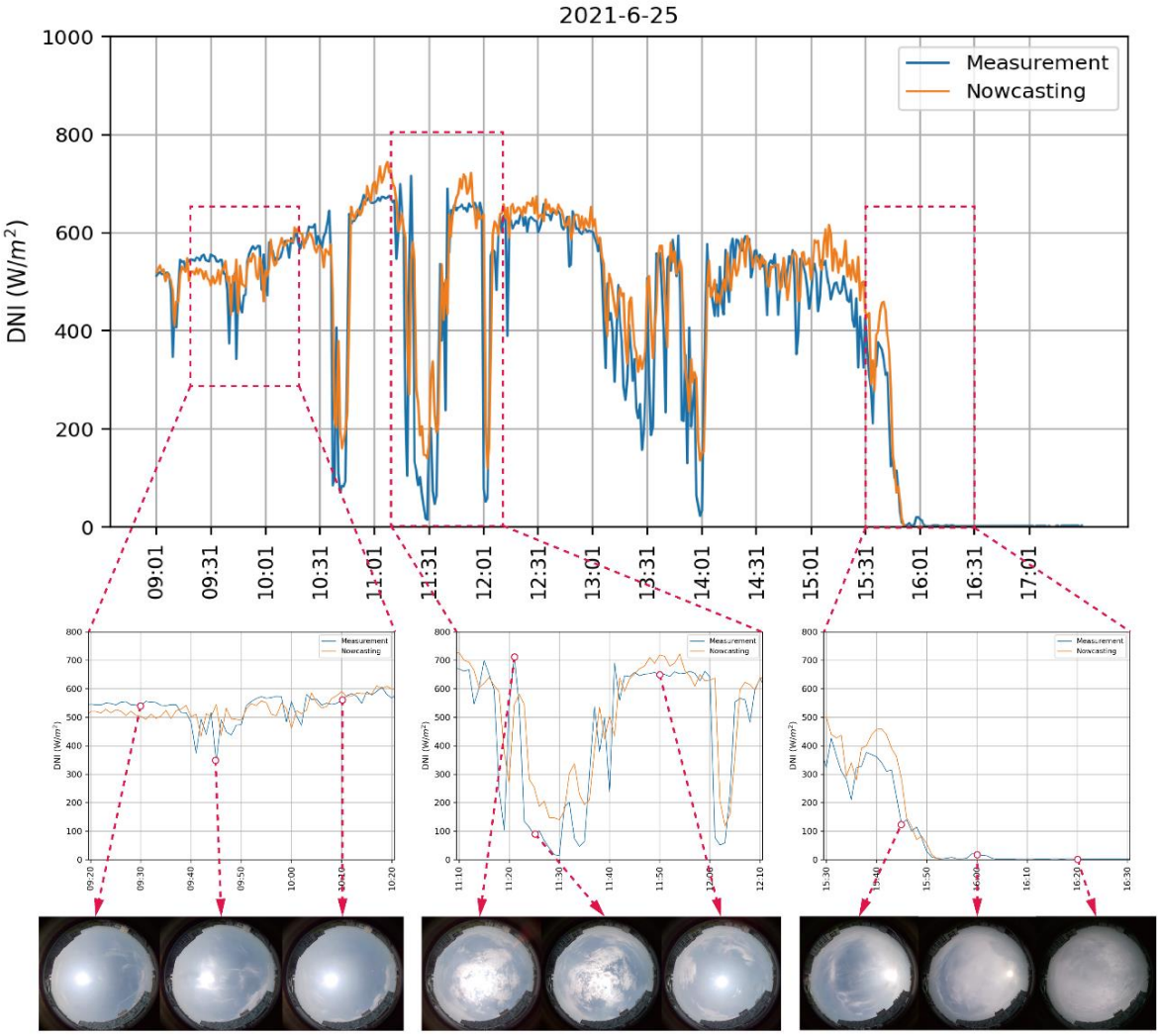

Figure 4.10 The performance of DNI nowcasting at 1-min time interval for 1-min nowcasting horizons in clear sky, cloudy sky and overcast sky.

Contrary to DHI nowcasting, although the effect of different sky conditions on DNI nowcasting is also similar to their effect on GHI and DHI nowcasting, DNI nowcasting under cloudy sky always presents more significant fluctuations and greater errors, as shown in Figure 4.10. That is because the variation of DNI is highly correlated with the relative position of the sun and clouds. Once the sun is suddenly obscured by clouds or emerges from them, the DNI sharply drops or rises. The errors of DNI

nowcasting are often more than 150 W/m^2 or more under cloudy sky. Nevertheless, the errors of DNI nowcasting are normally less than 60 W/m^2 under clear and overcast sky and the curves of DNI nowcasting and DNI measurement also present clear agreement. To sum up, the DNI nowcasting under clear and overcast sky has high accuracy and apparently outperforms the DNI nowcasting under cloudy sky. Although the accuracy of DNI nowcasting under cloudy sky is unable to achieve the level under clear and overcast sky, the DNI nowcasting under cloudy sky is still reliable.

4.1.4 Comparison of Nowcasting Performance among Different Models.

In this section, the GHI, DNI and DHI nowcasting performance of the proposed ResNet-152 solar irradiance nowcasting models are compared with a baseline model and a benchmark model, including Multilayer Perceptron (MLP) and Persistence Model (PM). As described in the previous section, the nowcasting of GHI, DNI and DHI at 1-min time interval usually achieves the best performance. Thus, all comparative tests of GHI, DNI and DHI nowcasting in this section are based on 1-min time interval.

Table 4.6 Nowcasting performance at 1-min time interval for 1-min nowcasting horizon among different models.

Components	Model	MAE	nMAE	RMSE	nRMSE	MAPE	r
GHI	ResNet-152	58.82	0.1	98.66	0.17	13.53%	0.9481
	PM	46.98	0.08	105.99	0.18	8.89%	0.9407
	MLP	65.59	0.11	111.64	0.19	16.38%	0.9331
DHI	ResNet-152	19.17	0.07	27.51	0.09	7.54%	0.9782
	PM	10.5	0.04	19.09	0.07	3.60%	0.9887
	MLP	21.12	0.07	32.09	0.11	8.44%	0.9692
DNI	ResNet-152	62.74	0.18	106.61	0.3	/	0.9324
	PM	47.2	0.13	110.74	0.31	/	0.9291
	MLP	68.54	0.19	113.15	0.32	/	0.9253

Table 4.6 presents the nowcasting performance at 1-min time interval for 1-min nowcasting horizon among different models. In general, the r of ResNet-152, PM and MLP for GHI, DNI and DHI nowcasting are very close and higher than 0.9 which

indicates very high agreement between nowcasting and measurement. PM demonstrates an absolute advantage for DHI nowcasting according to all evaluation metrics and an obvious advantage for GHI and DNI nowcasting according to MAE, nMAE, MAPE and r. In contrast, MLP shows the worst performance for GHI, DNI and DHI nowcasting in terms of all evaluation metrics. Thus, PM is the best nowcasting model at 1-min time interval for 1-min nowcasting horizon, while Resnet-152 is the second best.

Table 4.7 Nowcasting performance at 1-min time interval for 5-min nowcasting horizon among different models.

Components	Model	MAE	nMAE	RMSE	nRMSE	MAPE	r
GHI	ResNet-152	94.39	0.16	144.36	0.25	23.13%	0.8839
	PM	98.1	0.17	177.81	0.31	21.01%	0.8335
	MLP	108.16	0.19	163.91	0.28	28.12%	0.8487
DHI	ResNet-152	33.99	0.12	49.21	0.17	14.53%	0.9231
	PM	31.03	0.11	50.01	0.17	11.32%	0.9225
	MLP	35.35	0.12	51.46	0.18	14.59%	0.9161
DNI	ResNet-152	97.47	0.27	147.98	0.42	/	0.8648
	PM	89.4	0.25	174.39	0.49	/	0.8252
	MLP	103.93	0.3	156.29	0.45	/	0.8501

Table 4.7 presents the nowcasting performance at 1-min time interval for 5-min nowcasting horizon among different models. Comparing the nowcasting performance for 1-min nowcasting horizon with 5-min nowcasting horizon, the overall r of GHI, DNI and DHI nowcasting decreases but is still higher than 0.8. The overall MAPE of GHI, DNI and DHI nowcasting increase but is lower than 30%. For GHI nowcasting, ResNet-152 significantly outperform PM and MLP according to all evaluation metrics besides MAPE. In actual, the MAPE of ResNet-152 and PM are also very close. In terms of DHI nowcasting, the nowcasting performance of ResNet-152, PM and MLP are very close. For DNI nowcasting, PM demonstrates an advantage according to MAE and nMAE, while ResNet-152 shows an advantage according to RMSE, nRMSE and r. That indicates the nowcasting of ResNet-152 has larger errors overall, but the

nowcasting of PM has the largest errors at some specific moments. In this case, the nowcasting performance of ResNet-152 and PM are close. Considering the overall nowcasting performance of GHI, DNI and DHI , ResNet-152 is the optimal nowcasting model at 1-min time interval for 5-min nowcasting horizon.

Table 4.8 Nowcasting performance at 1-min time interval for 10-min nowcasting horizon among different models.

Components	Model	MAE	nMAE	RMSE	nRMSE	MAPE	r
GHI	ResNet-152	104.42	0.18	164.71	0.28	27.01%	0.8585
	PM	119.52	0.21	200.05	0.35	27.15%	0.7901
	MLP	123.42	0.21	177.5	0.31	32.86%	0.8208
DHI	ResNet-152	42.37	0.15	61.09	0.21	17.22%	0.8785
	PM	41.52	0.14	62.52	0.21	15.98%	0.8792
	MLP	43.82	0.15	61.32	0.21	18.74%	0.8788
DNI	ResNet-152	113.98	0.32	176.24	0.5	/	0.8203
	PM	108.04	0.31	196.44	0.56	/	0.7796
	MLP	129.49	0.37	180.56	0.51	/	0.7953

Table 4.8 presents the nowcasting performance at 1-min time interval for 10-min nowcasting horizon among different models. In general, the overall r of GHI, DNI and DHI nowcasting for 10-min nowcasting horizon is lower compared to 5-min nowcasting horizon but are still higher than 0.77. The overall MAPE of GHI, DNI and DHI nowcasting for 10-min nowcasting horizon are higher compared to 5-min nowcasting horizon but are lower than 33%. In terms of GHI nowcasting, it is evident that ResNet-152 achieves the best performance according to all evaluation metrics. In contrast, DHI nowcasting of PM outperforms ResNet-152 with respect to all evaluation metrics besides RMSE. Despite this, ResNet-152, PM and MLP have very close accuracy of DHI nowcasting in actual. For DNI nowcasting, the nowcasting performance of PM is better according to MAE and nMAE but worse than ResNet-152 according to RMSE, nRMSE and r. Therefore, like the nowcasting performance for 5-min nowcasting horizon, ResNet-152 presents the best performance at 1-min time interval for 10-min nowcasting horizon.

Apart from the evaluation metrics presented in Table 4.6-4.8. SS-MAE and SS-RMSE are also effective and straightforward evaluation metrics for the comparison of different nowcasting models. The comparison of SS-MAE and SS-RMSE are shown in Figure 4.11-4.13.

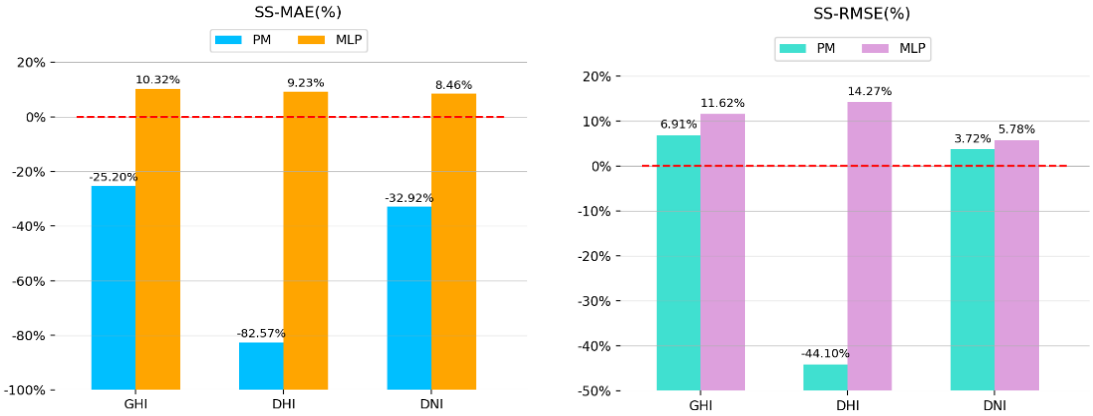

Figure 4.11 SS-MAE and SS-RMSE of PM and MLP for GHI, DNI and DHI nowcasting at 1-min time interval for 1-min nowcasting horizon.

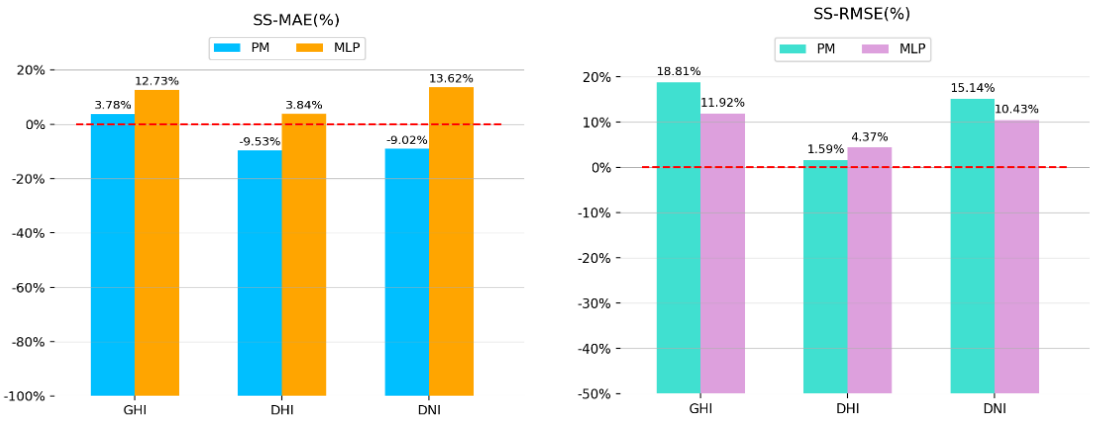

Figure 4.12 SS-MAE and SS-RMSE of PM and MLP for GHI, DNI and DHI nowcasting at 1-min time interval for 5-min nowcasting horizon.

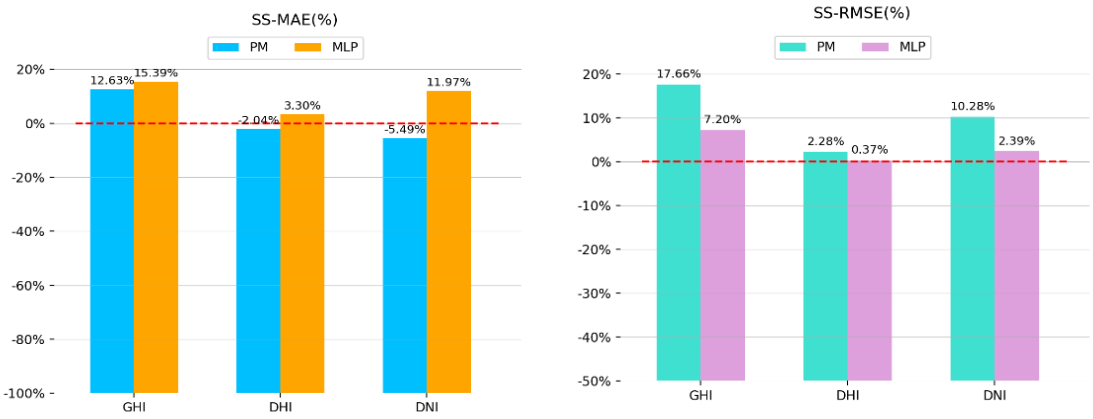

Figure 4.13 SS-MAE and SS-RMSE of PM and MLP for GHI, DNI and DHI nowcasting at 1-min time interval for 10-min nowcasting horizon.

According to Figure 4.11, SS-MAE(PM) are all negative and SS-MAE(MLP) are all positive that indicates the nowcasting performance of MLP ResNet-152 is better than MLP but not as good as PM. However, ResNet-152 presents more strengths on SS-RMSE because SS-MAE(PM) and SS-MAE(MLP) are almost positive in Figure 4.12. Due to PM achieves very large SS-MAE(PM) of -25% for GHI, -83% for DHI and -33% for DNI. Thus, PM achieves the best performance at 1-min time interval for 1-min nowcasting horizon but merely outperforms ResNet-152 slightly. However, ResNet-152 gradually outperforms PM as the nowcasting horizon increases in terms of Figure 4.13. SS-MAE(PM) of DHI and DNI are still negative, but the values are very small, indicating very close nowcasting performance between ResNet-152 and PM. In the meanwhile, the nowcasting performance of MLP is always the worst. In practical applications, PM and MLP require solar data obtained from a permanent set-up and expensive solar sensor for solar irradiance nowcasting, while ResNet-152 proposed in this research merely requires ground-based cloud images captured by a low-cost Raspberry Pi camera. In this case, both the equipment itself and its long-term maintenance costs are greatly reduced.

4.1.5 Comparison of Nowcasting Performance Based on Different Datasets.

In this section, the effect of different datasets on nowcasting performance is

evaluated. In previous sections, a total of 60 days of data from April to September are used for the training and the testing of solar irradiance nowcasting models. Of these 60 days, the training set is 48 days, and the testing set is 12 days. In this case, this section first respectively uses 48 days of data from April to September, as mentioned above, to train a series of solar irradiance nowcasting models. Then, 34 days of data from April to July were used to train a series of solar irradiance nowcasting models. Finally, 8 identical testing days from April to July are input into two abovementioned groups of nowcasting models to compare the nowcasting performance between the solar irradiance nowcasting models trained with 34 days of data and 48 days of data. In addition, the solar irradiance nowcasting models trained with 48 days of data from April to September are used to test the nowcasting performance for 3 days in December to investigate the generality of the solar irradiance nowcasting models.

4.1.5.1 Nowcasting Performance between The Solar Irradiance Nowcasting Models Trained with 34 Days of Data and 48 Days of Data

To investigate the effect of different datasets on nowcasting performance, 34 days of data from April to July and 48 days of data from April to September are respectively used to train two groups of solar irradiance nowcasting models. The results of 8 testing days generated from the nowcasting models trained with 34 days of data and 48 days of data are evaluated using the evaluation metrics presented before, as shown in Table 4.9.

Table 4.9 Nowcasting performance for 8 testing days between the solar irradiance nowcasting models Trained with 34 days of data and 48 days of data.

Components	Datasets	Intervals	Horizons	MAE	nMAE	RMSE	nRMSE	MAPE	r
GHI	48 days	1 min	1 min	58.26	0.1	96.98	0.16	12.64%	0.9514
	34 days			57.36	0.09	94.31	0.15	11.49%	0.9532
DHI	48 days			19.67	0.07	28.81	0.1	7.42%	0.9723
	34 days			21.73	0.07	30.86	0.1	19.69%	0.9704
DNI	48 days			59.79	0.16	102.28	0.28	/	0.932
	34 days			63.16	0.17	99.65	0.27	/	0.9372

GHI	48 days	1 min	5 min	89.42	0.15	136.15	0.22	20.49%	0.9
	34 days			92.04	0.15	141.03	0.23	20.34%	0.8931
DHI	48 days			35.09	0.12	51.6	0.17	14.57%	0.9067
	34 days			35.51	0.12	52.34	0.17	14.27%	0.9019
DNI	48 days			90.78	0.25	136.07	0.37	/	0.8765
	34 days			90.65	0.25	140.7	0.38	/	0.8702
GHI	48 days	1 min	10 min	99.92	0.16	157.44	0.26	24.55%	0.8725
	34 days			102.27	0.17	150.92	0.25	26.33%	0.8764
DHI	48 days			42.07	0.14	61.82	0.21	17.31%	0.8618
	34 days			45.7	0.15	65.88	0.22	20.18%	0.841
DNI	48 days			105.13	0.29	166.42	0.45	/	0.8211
	34 days			100.69	0.27	151.53	0.41	/	0.846

According to Table 4.9, the nowcasting performance for 8 testing days between the solar irradiance nowcasting models trained with 34 days of data and 48 days of data are very close. In general, the maximum error of MAE is less than 100 and RMSE is less than 150. However, the solar irradiance nowcasting model trained with 48 days of data performs slightly better than those trained with 34 days of data for DHI nowcasting. Since the 48-day dataset mainly adds the data from August to September compared to the 30-day dataset, the above findings indicate adding the extra training dataset from different months to solar irradiance nowcasting models does not significantly affect the nowcasting accuracy of the original testing dataset. In addition, based on the nowcasting model trained with 48 days of data, the nowcasting performance for 8 testing days significantly outperforms the nowcasting performance for 12 testing days. That might imply the accuracy of a solar irradiance nowcasting model based on a larger time span of testing dataset is reduced.

4.1.5.2 Nowcasting Performance Based on Different Seasonal Testing Dates

To explore the generality of the solar irradiance nowcasting models trained with 48 days of data, the results of the 4 testing days in December generated from the nowcasting models are compared with the results of the 12 testing days from April to September. However, it is worth noting that since the sky is dark after 3:30 pm in

December, the data from 3:30 pm to 5:30 pm are excluded from the calculation of the evaluation metrics of the 4 testing days in December. Thus, the total amount of data used to calculate the evaluation metrics of 4 testing days in December and the 12 testing days from April to September are different. The results of each day are evaluated through a series of evaluation metrics, as shown in Table 4.10.

Table 4.10 GHI Nowcasting performance at 1-min time interval for 1-min nowcasting horizon based on the 12 testing dates from April to September.

Dates	Sky Conditions	MAE	nMAE	RMSE	nRMSE	MAPE	r
2021-05-22	Clear	43.95	0.06	82.26	0.11	7.06%	0.9463
2021-06-21	Clear	69.17	0.09	104.65	0.14	10.05%	0.9287
2021-08-31	Clear	44.47	0.06	87.42	0.13	8.49%	0.938
2021-05-09	Light Cloudy	32.57	0.05	58.23	0.09	6.88%	0.9742
2021-05-30	Light Cloudy	58.72	0.08	94.91	0.13	10.91%	0.9305
2021-08-28	Light Cloudy	72.27	0.12	117.75	0.2	15.85%	0.893
2021-06-25	Heavy Cloudy	51.57	0.08	84.4	0.13	16.76%	0.9665
2021-07-01	Heavy Cloudy	117.38	0.17	167.67	0.24	20.49%	0.8265
2021-08-29	Heavy Cloudy	83.28	0.18	128.64	0.28	24.50%	0.9244
2021-04-25	Overcast	53.12	0.12	82.38	0.19	12.89%	0.9525
2021-05-20	Overcast	39.57	0.2	55.74	0.28	21.59%	0.9077
2021-09-04	Overcast	39.72	0.11	59.27	0.16	12.37%	0.959

In terms of the GHI nowcasting performance based on the 12 testing days from April to September, as shown in Table 4.11, the GHI nowcasting in overcast days obviously achieves the best performance. In contrast, the GHI nowcasting in heavy cloudy days always has higher errors. The nowcasting accuracy in clear days and light cloudy days are similar. The above findings are especially reflected in MAE and RMSE. The higher errors of the GHI nowcasting in heavy cloud days is mainly caused by the sharp and frequent variation of the relative position between the sun and clouds.

Table 4.11 GHI Nowcasting performance at 1-min time interval for 1-min nowcasting horizon based on the 4 testing dates in December.

Dates	Sky Conditions	MAE	nMAE	RMSE	nRMSE	MAPE	r
2021-12-04	Clear	59.35	0.15	73.13	0.19	22.55%	0.9021
2021-12-11	Light Cloudy	44.37	0.13	56.78	0.16	14.24%	0.926
2021-12-07	Heavy Cloudy	31.67	0.09	40.74	0.12	10.45%	0.9695
2021-12-08	Overcast	30.19	0.13	38.98	0.17	14.68%	0.9085

Comparing the GHI nowcasting performance based on the 12 testing days from April to September with the GHI nowcasting performance based on the 4 testing days in December according to Table 10-15, it is evident that the GHI nowcasting based on the 4 testing days in December achieves very high accuracy in different sky conditions. The nowcasting performance is close in different sky conditions but slightly increases with the increase of clouds according to MAE and RMSE. The GHI nowcasting performance in December presents a very different pattern compared to the GHI nowcasting performance from April to September. That is because the values of GHI in winter are very low and stable, unlike in other seasons.

Table 4.12 DHI Nowcasting performance at 1-min time interval for 1-min nowcasting horizon based on the 12 testing dates from April to September.

Dates	Sky Conditions	MAE	nMAE	RMSE	nRMSE	MAPE	r
2021-05-22	Clear	9.41	0.04	12.47	0.06	4.42%	0.9763
2021-06-21	Clear	14.53	0.05	20.33	0.07	4.76%	0.9841
2021-08-31	Clear	12.75	0.08	16.3	0.1	8.06%	0.9703
2021-05-09	Light Cloudy	13.62	0.04	17.12	0.05	4.74%	0.987
2021-05-30	Light Cloudy	14.24	0.05	18.58	0.06	4.73%	0.9745
2021-08-28	Light Cloudy	21.69	0.06	28.46	0.08	5.52%	0.9792
2021-06-25	Heavy Cloudy	14.97	0.05	20.59	0.06	5.49%	0.9856
2021-07-01	Heavy Cloudy	24.52	0.06	31.93	0.08	6.08%	0.9628
2021-08-29	Heavy Cloudy	20.06	0.08	25.65	0.1	12.22%	0.9846
2021-04-25	Overcast	29.18	0.08	39.95	0.12	7.76%	0.9839
2021-05-20	Overcast	36.89	0.19	48.91	0.25	21.37%	0.934
2021-09-04	Overcast	18.15	0.06	26.68	0.08	5.30%	0.9869

According to Table 4.13, the DHI nowcasting always keeps a high accuracy but the nowcasting accuracy gradually decreases as clouds increase in the sky. In this case, the DHI nowcasting achieves the best performance in clear days and the worst in overcast days.

Table 4.13 DHI Nowcasting performance at 1-min time interval for 1-min nowcasting horizon based on the 4 testing dates in December.

Dates	Sky Conditions	MAE	nMAE	RMSE	nRMSE	MAPE	r
2021-12-04	Clear	12.42	0.07	16.08	0.1	8.65%	0.8109
2021-12-11	Light Cloudy	18.34	0.08	22.88	0.1	7.90%	0.9255
2021-12-07	Heavy Cloudy	24.14	0.1	27.66	0.11	9.81%	0.9671
2021-12-08	Overcast	24.27	0.11	29.39	0.13	10.97%	0.9812

In terms of Table 4.14, the DHI nowcasting based on the 4 testing days in December has very good performance regardless of different sky conditions. Contrary to the GHI nowcasting, the DHI nowcasting slightly decreases as the cloud increases, according to all evaluation metrics. In general, since the values of DHI are smaller in winter compared to other seasons, the errors of DHI nowcasting thus are also smaller.

Table 4.14 DNI Nowcasting performance at 1-min time interval for 1-min nowcasting horizon based on the 12 testing dates from April to September.

Dates	Sky Conditions	MAE	nMAE	RMSE	nRMSE	MAPE	r
2021-05-22	Clear	60.51	0.09	95.43	0.14	/	0.8205
2021-06-21	Clear	86.73	0.16	125.54	0.24	/	0.8622
2021-08-31	Clear	64.79	0.09	106.54	0.15	/	0.791
2021-05-09	Light Cloudy	38.33	0.09	68.51	0.16	/	0.9124
2021-05-30	Light Cloudy	65.48	0.14	101.7	0.22	/	0.8551
2021-08-28	Light Cloudy	91.03	0.3	134.39	0.44	/	0.7406
2021-06-25	Heavy Cloudy	50.17	0.13	82.97	0.21	/	0.9454
2021-07-01	Heavy Cloudy	130.36	0.38	175.41	0.51	/	0.7581
2021-08-29	Heavy Cloudy	85.67	0.35	139.04	0.56	/	0.8892
2021-04-25	Overcast	41.45	0.39	76.58	0.12	/	0.9093
2021-05-20	Overcast	5.31	1.31	16.49	0.05	/	0.099
2021-09-04	Overcast	33.03	0.63	62.91	0.19	/	0.8199

As presented in Table 4.15, the DNI nowcasting achieves the highest accuracy in overcast days because the values of DNI are very low and stable in this sky condition. In general, the conclusions of the DNI nowcasting are similar to GHI nowcasting.

Table 4.15 DNI Nowcasting performance at 1-min time interval for 1-min nowcasting horizon based on the 4 testing dates in December.

Dates	Sky Conditions	MAE	nMAE	RMSE	nRMSE	MAPE	r
2021-12-04	Clear	109.88	0.26	143.93	0.34	/	0.6082
2021-12-11	Light Cloudy	104.26	0.49	130.17	0.62	/	0.8532
2021-12-07	Heavy Cloudy	99.91	0.48	119.09	0.57	/	0.9017
2021-11-08	Overcast	75.48	5.53	103.76	0.76	/	0.9472

Unlike the very high accuracy of the GHI and DHI nowcasting, the DNI nowcasting in winter presents obvious errors in terms of MAE and RMSE. The nowcasting performance increases with the increase of clouds, according to MAE and RMSE. However, the nMAE, the nRMSE and the r of the DNI nowcasting even show abnormal. The reasons for this circumstance involve the adaptability of solar irradiance nowcasting models, larger solar zenith angle, very low DNI in winter, etc. In specific, the nowcast value of DHI is calculated from the nowcast values of GHI and DHI according to equation 2.1 in section 2.3.8. Since the solar irradiance nowcasting model used in this set of tests is trained using 48 days of data in the summer, while the input of this set of tests is the data from 4 testing dates in the winter, the nowcasting model may not be adaptable enough. In this case, the nowcasting of GHI and DHI both shows obvious errors, especially GHI, as shown in Figure 4.14-4.15. In addition, due to the solar zenith angle θ in winter is larger, the value of $cos(\theta)$ becomes smaller, resulting in larger nowcast values of DNI. In contrast, the measured values of DNI in winter are generally very low. Therefore, the errors between the nowcast values and measured values become larger. With the accumulation of the above errors, the difference between the nowcast values and measured values of DNI gradually increase, as shown in Figure 4.16. In this case, the reliability of the DNI

nowcasting needs to be further investigated.

To sum up, the solar irradiance nowcasting models based on 48 days of data from April to September present good performance for the GHI, DNI and DHI nowcasting from April to September and the GHI, DHI nowcasting in December. However, the performance of these nowcasting models on the DNI nowcasting in December is uncertain.

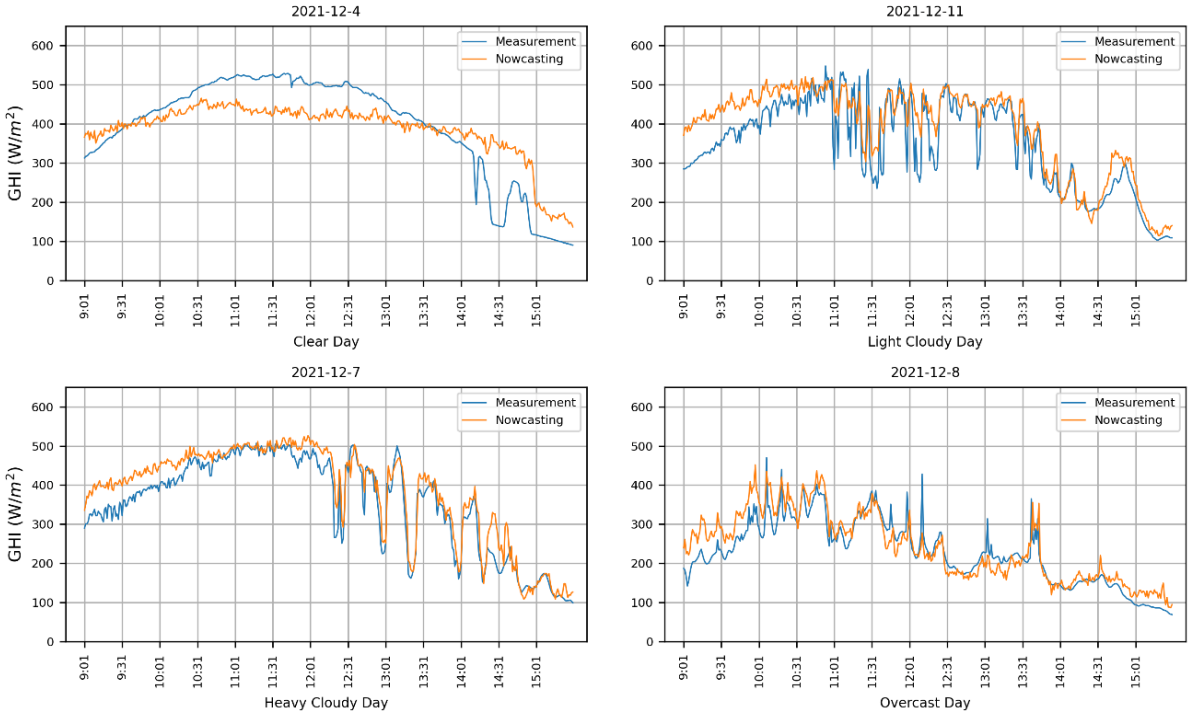

Figure 4.14 GHI Nowcasting performance at 1-min time interval for 1-min nowcasting horizon based on the 4 testing dates in December.

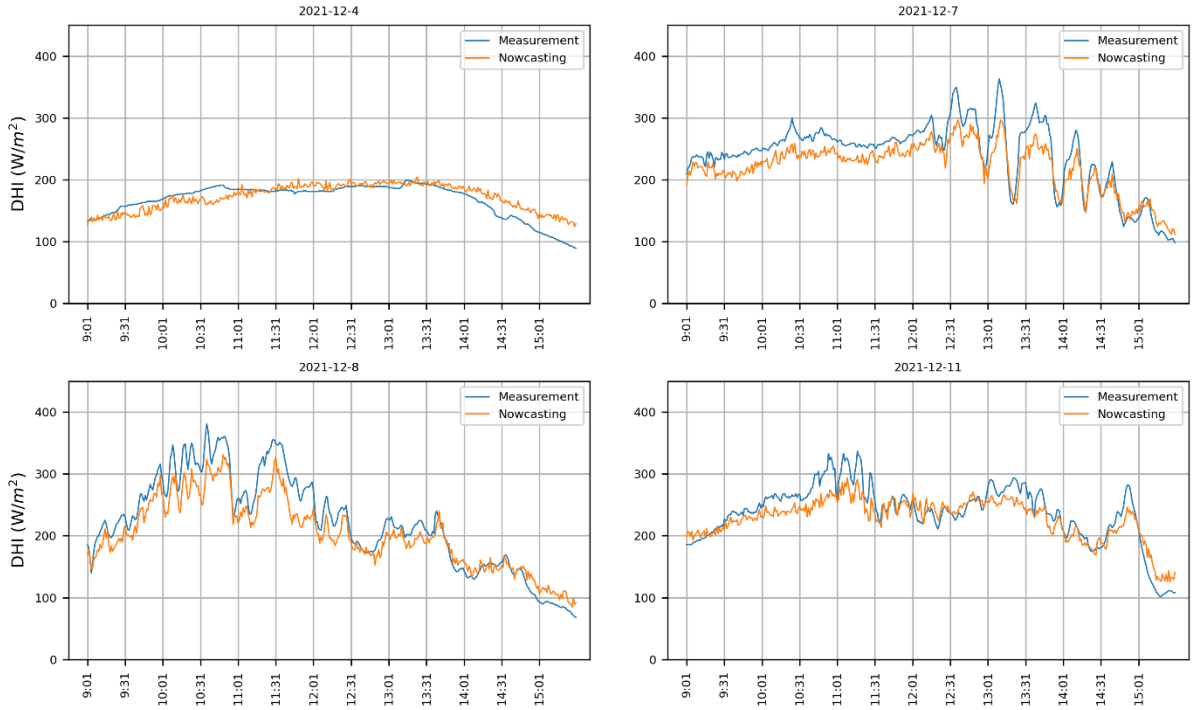

Figure 4.15 DHI Nowcasting performance at 1-min time interval for 1-min nowcasting horizon based on the 4 testing dates in December.

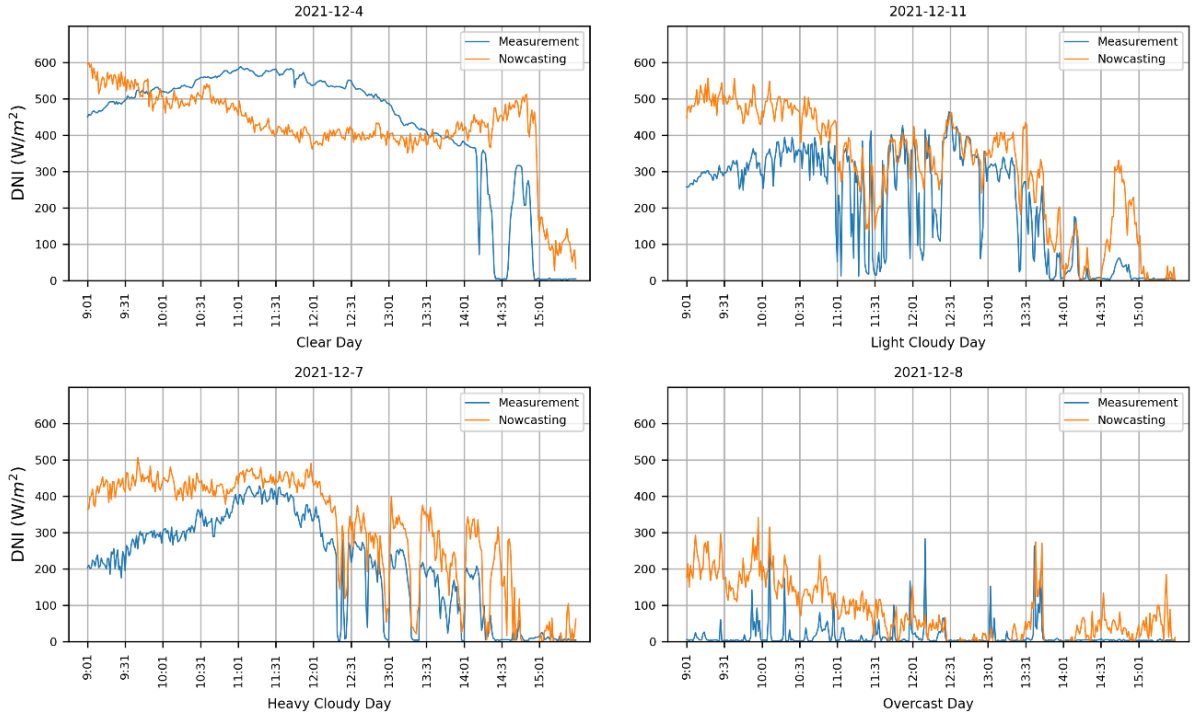

Figure 4.16 DNI Nowcasting performance at 1-min time interval for 1-min nowcasting horizon based on the 4 testing dates in December.

4.2 Chapter Summary

This chapter presents the results of verification and analysis of solar irradiance nowcasting. Based on the nowcasting objectives, a series of comparative tests are implemented to evaluate the effect of various factors on the nowcasting performance of GHI, DNI and DHI. These factors include time intervals, nowcasting horizons, sky conditions, benchmark models, and datasets. The main findings are summarised as follows:

- The effect of various time intervals on nowcasting performance.

  In general, the correlation between time intervals and corresponding nowcasting accuracy is unclear. However, it is worth noting that nowcasting at shorter time intervals has a higher probability of achieving better performance for various nowcasting horizons compared to nowcasting at longer time intervals, especially for GHI and DNI nowcasting. Moreover, although the nowcasting performance at 10-sec and 1-min time intervals are very close, the nowcasting performance at 1-min time interval presents more advantages according to evaluation metrics. Based on the above, the nowcasting of GHI, DNI and DHI at 1-min time interval consistently achieves the best performance for various nowcasting horizons. Among the nowcasting of GHI, DNI and DHI, the nowcasting of DHI achieves very high accuracy, which performs much better than the nowcasting of GHI and DNI. Compared to the nowcasting of DNI, the nowcasting of GHI performs slightly better.

- The effect of various nowcasting horizons on nowcasting performance.

  Unlike time intervals, the effect of various nowcasting horizons on nowcasting performance is very evident. Nowcasting accuracy of GHI, DNI and DHI improves significantly with the shortening of nowcasting horizons. Differences in the nowcasting performance of GHI, DNI, and DHI are similar

to those described above.

- The effect of different sky conditions on nowcasting performance.

  For the days with different sky conditions, it is evident that the GHI and DNI nowcasting performance are the worst on heavy cloudy days. In contrast, the GHI and DNI nowcasting can achieve the highest accuracy on overcast days. The nowcasting accuracy of GHI and DNI are similar on clear days and light cloudy days. Unlike GHI and DNI, the nowcasting performance of DHI presents a clear pattern. The accuracy of DHI nowcasting decreases with the increase of clouds. Thus, the DHI nowcasting consistently achieves the best accuracy on clear days and the worst on overcast days.

  For a representative date with different sky conditions at several moments, GHI and DNI nowcasting accuracy are the lowest under cloudy sky and the highest under clear sky and overcast sky. However, DNI nowcasting shows more dramatic errors than GHI nowcasting. Contrary to DNI, DHI nowcasting always keep high accuracy no matter what sky conditions. In summary, the proposed solar irradiance nowcasting method performs well for the nowcasting of GHI and DNI under clear and overcast sky and the nowcasting of DHI under all sky conditions. Although the nowcasting of GHI and DNI under cloudy sky sometimes show relatively large errors, they are still reliable due to the high agreement between nowcasting and measurement.

- The influence of different models on nowcasting performance.

  As the representative benchmark model, PM presents significant advantages for shorter nowcasting horizons compared to ResNet-152 and MLP. However, the nowcasting performance of ResNet-152 is gradually beyond PM as nowcasting horizons are increased. In this research, ResNet-152 achieves better nowcasting performance for 5-min and 10-min nowcasting horizons. Compared to PM and ResNet-152, the nowcasting

performance of MLP is always unsatisfactory. In addition, unlike PM and MLP, ResNet-152 merely relies on low-cost equipment to achieves solar irradiance nowcasting and thus is more appropriate for practical applications.

- The influence of different datasets on nowcasting performance.

  The comparison between solar irradiance nowcasting models trained with 34 days of data and 48 days of data demonstrates the nowcasting accuracy of the original testing dataset is less affected by the addition of extra training datasets from different months in the solar irradiance nowcasting models. Besides, the larger time span of the testing dataset might decrease the accuracy of a solar irradiance nowcasting model.

  In addition, the nowcasting results of 4 testing days in December generated from the solar irradiance nowcasting models trained with 48 days of data from April to September indicate the nowcasting models are very suitable for GHI and DHI nowcasting, but the ability of these models for DNI nowcasting is less than ideal.

To sum up, the performance of the developed solar irradiance nowcasting method demonstrates evident reliability under the influence of diverse factors.

Chapter Five

5 Discussion

The purpose of Chapter 5 is to initiate an expansive discussion on the results from the nowcasting of solar irradiance and answer the last research question in Chapter 1 - “What current or potential building applications can the proposed solar irradiance nowcasting method be applied to?”. In this case, the main task of this chapter is to interpret the results of solar irradiance nowcasting and complete the fifth research objective - to discuss current and potential building applications of the proposed solar irradiance nowcasting method.

This chapter begins with an interpretation of the results of this research. Firstly, comparative tests of solar irradiance nowcasting in this research are introduced briefly. Secondly, the major findings of this research, the reasons for the findings and the potential effects of the findings are demonstrated. Thirdly, the comparison of nowcasting performance between the proposed method and contemporary state-of-the-art methods is presented. After that, the limitations of this research are articulated. At last, the implications of this research and a series of current and potential applications of solar irradiance nowcasting are discussed to envision the value of this research for buildings in the future and provide initial sights for subsequent research.

5.1 Interpretation of the Results

The results verification and analysis of solar irradiance nowcasting presented in Chapter 4 respond to one of the crucial research questions posed in Chapter 1: How can the reliability of solar irradiance nowcasting be verified? Fundamentally, verifying the reliability of solar irradiance nowcasting in this research is based on two main aspects: the evaluation of the impact of different factors on solar irradiance nowcasting, including time intervals, nowcasting horizons, sky conditions, forecasting models and datasets, and the evaluation metrics for evaluating the nowcasting accuracy. Unlike evaluation metrics, which are only used for verifying the results of solar irradiance nowcasting, different effective factors are directly linked to the nowcasting results. Consequently, a series of comparative tests were performed to generate different nowcasting results.

Based on the above, a brief introduction to comparative tests is presented first in this section. Subsequently, the findings of this research, the reasons for the findings and the potential effects of the findings are articulated. It is also worth reminding that Chapter 4 presents only a portion of this research's results because of the thesis's length limitations, and more results will be presented in the appendix.

5.1.1 Brief Introduction to Comparative Tests

This research explored the effects of different factors on the reliability of solar irradiance nowcasting through a series of comparative tests. Some of these factors are common, such as forecasting horizons, sky conditions, and forecasting models, but others, including datasets and time intervals, are rarely explored. Overall, the comparative tests include the following five:

- Comparison of Nowcasting Performance at Various Time Intervals.

  This test was designed to explore the impact of various time intervals on the nowcasting of GHI, DNI and DHI, and thus, the only variable for this test was the time interval. The nowcasting performance of GHI, DNI and DHI at 10-sec,

1-min, 5-min and 10-min time intervals for 1-min, 5-min , and 10-min nowcasting horizons were respectively compared, which totally involved 27 sets of solar irradiance nowcasting.

- Comparison of Nowcasting Performance for Various Nowcasting Horizons.

  The objective of this test was to investigate the effect of various nowcasting horizons on the nowcasting of GHI, DNI and DHI. Therefore, the only variable for this test was the nowcasting horizon. The nowcasting performance of GHI, DNI and DHI for 1-min, 5-min and 10-min nowcasting horizons at fixed 1-min time interval were compared. A total of 12 sets of solar irradiance nowcasting were conducted in this test.

- Comparison of Nowcasting Performance in Different Sky Conditions.

  This test used only sky conditions as variables to study the influence of different sky conditions on the nowcasting of GHI, DNI and DHI. Firstly, the nowcasting performance of GHI, DNI and DHI under four kinds of sky conditions, including clear, less cloudy, heavy cloudy and overcast, in 12 days were compared, which involved a total of 36 sets of solar irradiance nowcasting. Then, 3 sets of solar irradiance nowcasting were used to articulate the nowcasting performance of GHI, DNI and DHI at several moments under different sky conditions on a representative date.

- Comparison of Nowcasting Performance among Different Models.

  The goal of this test was to compare the GHI, DNI and DHI nowcasting performance of three models for 1-min, 5-min and 10-min nowcasting horizons at fixed 1-min time interval. These three models included the proposed ResNet-152 solar irradiance nowcasting model, a baseline model - Multilayer Perceptron (MLP), and a benchmark model - Persistence Model (PM). In this test, a total of 7 sets of solar irradiance nowcasting were involved.

- Comparison of Nowcasting Performance Based on Different Datasets.

  This test aimed to study the impact of different datasets on the nowcasting performance of GHI, DNI and DHI. Consequently, the total size and seasonality of the datasets were used as variables. This test first compared the performance of two solar irradiance nowcasting models trained with 34 days of data and 48 days of data, involving 18 sets of solar irradiance nowcasting. Then, the nowcasting performance based on different seasonal testing dates was compared, involving 48 sets of solar irradiance nowcasting.

5.1.2 Major Findings of the Research

The major findings of this research, the reasons for the findings and the significance of the findings are presented in the following:

Firstly, the critical finding on the effect of various time intervals on nowcasting performance is that the nowcasting of GHI, DNI and DHI at 1-min time interval achieves the best performance, regardless of the nowcasting horizons. One potential reason is that the nowcasting models at 10-sec time interval is overfitted, and 5-min and 10-min time intervals are underfitted. This finding implies that 1-min time interval may be the optimal temporal resolution for solar irradiance nowcasting. In fact, 1-min time interval is more appropriate than 10-sec time interval for practical applications considering the time consumption of computer operation, data transmission, system response and other factors. However, solar irradiance nowcasting at 1-min time interval is still high-frequency, requiring a certain amount of device computing power and stability. Nevertheless, high-frequency solar irradiance nowcasting is valuable for buildings and their future development. For instance, grid operators or energy companies can utilise high-frequency solar forecasts nowcasting to activate fast-responding energy storage systems or backup generation systems, ensuring grid reliability and efficiency when a "ramp event" occurs. "Ramp event" refers to an event in which there is a rapid change in solar power generation.

Secondly, the effect of various nowcasting horizons on nowcasting performance demonstrates a clear trend. As the nowcasting horizons increase, the nowcasting of GHI, DNI and DHI decrease significantly. The crucial reason for this is that clouds are more likely to vary dramatically over a longer horizon. Despite this, the nowcasting of GHI, DNI and DHI for 10-sec, 1-min, 5-min and 10-min nowcasting horizons achieves reliable accuracy, especially 10-sec and 1-min. Therefore, the proposed solar irradiance nowcasting method demonstrates its robust ability to achieve very short-term nowcasting of GHI, DNI and DHI. Similarly mentioned above, the 1-min nowcasting horizon of solar irradiance nowcasting is very suitable for responding to "ramp events". In addition, solar irradiance nowcasting for 5-min and 10-min nowcasting horizons are potentially valuable for building comfort adjustment, such as shading control, thermal and lighting control, etc.

Thirdly, the effect of different sky conditions on nowcasting performance varies significantly. In general, the nowcasting of GHI and DNI achieves high accuracy under clear, light cloudy and overcast sky conditions. However, the nowcasting of GHI and DNI exhibits large errors under heavy cloudy sky conditions. That is because GHI and DNI, especially DNI, are sensitive to the changes in the relative position between the sun and clouds. Unlike GHI and DNI, the nowcasting of DHI always achieves very high accuracy regardless of sky conditions because the values of DHI usually are minor, and DHI are less affected by the changes in the relative position between the sun and clouds. Based on the above, the key finding of the effect of different sky conditions on nowcasting performance is the proposed solar irradiance nowcasting method performs well for the nowcasting of GHI, DNI and DHI under most of sky conditions. Although the performance of the proposed solar irradiance nowcasting method for DNI nowcasting is not stable enough under heavy cloudy sky conditions, it can still successfully predict the overall trend of the DNI. Consequently, the proposed solar irradiance nowcasting method can be adapted under different sky conditions, which meets the needs of the building's daily applications.

Fourthly, the crucial finding of the influence of different models on nowcasting performance is the proposed solar irradiance nowcasting model, ResNet-152, performs better than the baseline model - Multilayer Perceptron (MLP) and the benchmark model - Persistence Model (PM) for 5-min and 10-min nowcasting horizons. Although PM achieves the best nowcasting performance for 1-min nowcasting horizon, utilising PM requires much higher equipment costs and complex practical operations. That is because the utilisation of PM generally requires continuous solar irradiance or other weather parameters, such as temperature and humidity, as input of PM. The acquisition of these continuous data requires the long-term use of expensive and complex solar pyranometers or weather stations. Unlike PM, although a solar pyranometer is also needed at the beginning to collect solar irradiance as training data, ResNet-152 only requires a very low-cost and user-friendly Raspberry Pi camera to collect continuous cloud images as the input in later daily use, which is ideal for popularisation in buildings.

Finally, the comparative tests of nowcasting performance based on different datasets lead to two main findings. In the first place, based on 8 identical testing days, there is no significant difference in the performance of solar irradiance nowcasting models trained with 34 days of data from April to July and 48 days of data from April to September, which may be due to the lack of drastic changes in the sun and clouds from the end of spring to the beginning of fall. However, it is worth noting adding the same amount of winter data to the training set of the above models may result in decreases in nowcasting accuracy, as the position of the sun and the state of the clouds will be very different in winter compared to the period from April to September. In addition, while the solar irradiance nowcasting models trained with 48 days of data perform well for the GHI and DHI nowcasting of 4 testing days in December, they do not achieve ideal performance for the DNI nowcasting, especially compared to the DNI nowcasting of 12 testing days from April to September. The reason for the above finding may be the drastic changes in DNI due to the sun's lower position and

increased heavy cloudy sky conditions in winter. Based on the above, the impact of the expansion of training set on nowcasting accuracy needs to be further explored. Still, the effect of the seasonality of testing set on nowcasting accuracy is evident. Thus, using the same month's data to train and test the solar irradiance nowcasting models could theoretically result in optimal accuracy. However, considering the total number of nowcasting models to be trained, using the data from the same season with similar sun positions and the state of clouds to train and test solar irradiance nowcasting models might be a more practical way to obtain the ideal nowcasting accuracy. In summary, the construction of seasonal nowcasting models might be more conducive to enhancing the building applicability of the proposed solar irradiance nowcasting method.

5.1.3 Comparison with Contemporary State-of-the-Art Methods

In this section, the nowcasting performance of the developed solar irradiance nowcasting method has been compared with state-of-the-art methods, and the results are presented as follow. In general, NWP methods and Top-down forecast methods are significantly less suitable for buildings than the proposed method according to spatial-temporal resolution. In addition, Statistic and Learning methods are also rarely used for the nowcasting with nowcasting horizons less than 30 minutes because it usually lacks minute-scale weather data sources, which provide GHI, temperature, humidity, etc., as model input. In this case, the proposed method is mainly compared with Bottom-up forecast methods and Hybrid methods.

- Comparison with Bottom-up Forecast Methods

  [250] is a representative Bottom-up forecast method published in 2021, which utilised very complex image processing techniques. Due to the difference in the definition of cloudy sky conditions between this research and [250], the optimal and worst solutions of [250] under cloudy sky condition is chosen for comparison. In terms of MAE and RMSE, the 1-min GHI nowcasting

performance of proposed method demonstrates significantly lower errors under most sky conditions including cloudy and overcast sky conditions compared to [250]. Due to the nowcasting under cloudy and overcast sky conditions tends to be the most difficult, the reliability of proposed method is apparent. However, it is worth noting that MAE and RMSE are absolute indicators, so this difference may be induced by different datasets.

Table 5.1 Comparison of 1-min GHI nowcasting performance with article [250].

Sky Conditions	MAE	MAE ([250])	RMSE	RMSE ([250])
Clear (1-min)	52.53	27	91.94	30
Cloudy (1-min)	52.14	62	90.15	110
Cloudy (1-min)	86.46	100	133.75	167
Overcast (1-min)	44.14	127	66.85	177

- Comparison with Hybrid Methods

  [307] published in 2022 proposed a hybrid method which integrates Bottom-up methods with Data-driven methods. First of all, the definitions of the sky conditions in this research and [307] are similar. Light cloudy, heavy cloudy and overcast in this research respectively corresponds to thin cloud, thick cloud and blocking cloud [307]. ABC corresponding to the Since both this research and [307] used MAPE as evaluation metric, it is straightforward to compare their nowcasting performance under different weather conditions. According to MAPE, the proposed method outperforms evidently than the method used in [307]. Therefore, the reliability of this research is comparable to that of complex hybrid methods.

Table 5.2 Comparison of GHI nowcasting performance with article [307].

Sky Conditions	MAPE	MAPE ([307])
Light Cloudy (Thin Cloud)	52.14	62
Heavy Cloudy (Thick Cloud)	86.46	100
Overcast (Blocking Cloud)	44.14	127

Another hybrid method developed by [283] is also compared with this research. In terms of MAE and RMSE, there are comparatively large gaps in 5-min GHI nowcasting performance between this research and [283]. As mentioned above, however, these evaluation metrics are absolute indicators and, therefore, may not accurately reflect the difference between these two studies. In this case, r, as a relative indicator, is more appropriate to respond to their difference. In general, the r of these two studies is close. In addition, the r of this research is close to 0.9, which implies the proposed method can accurately predict the trends of GHI. Thus, the proposed method remains generally reliable.

Table 5.3 Comparison of 5-min GHI nowcasting performance with article [283].

Method	MAE	RMSE	r
Proposed Method	94.39	144.36	0.8839
ASI1 Model **([283])**	29.1	64.4	0.94
ASI2 Model **([283])**	29.2	63.4	0.94
ASI3 Model **([283])**	36.2	68.0	0.93
ASI4 Model **([283])**	35.5	66.2	0.94
ASI5 Model **([283])**	37.5	65.9	0.94

In general, the r of these two studies is close. In addition, the r of this research is close to 0.9, which implies the proposed method can accurately predict the trends of GHI. Thus, the proposed method remains generally reliable.

To sum up, the proposed method can achieve similar or better nowcasting performance compared to Bottom-up forecast methods. Additionally, although some advanced Hybrid methods show better performance than the proposed method in terms of absolute indicators. Their difference is not obvious according to relative indicator. Consequently, the developed solar irradiance nowcasting is generally reliable.

5.2 Limitations of the Research

Apart from the contributions of this research, the limitations of this research need to be articulated. To sum up, the limitations of this research mainly involve:

- Amount of Data and Diversity of Datasets.

  Although a total of about 12 months of cloud images and solar irradiance data were collected in Cardiff and Shanghai during the research period, only 60 days of data collected in Shanghai were used in this research, taking into account a range of factors such as the quality, integrity and diverse sky conditions represented by these data. In this case, more high-quality, integrated data with more diverse characteristics, such as territoriality, seasonality and sky conditions, need to be collected to expand the volume and characteristics of datasets. In addition, more combinations of datasets with larger amounts of data and more diverse characteristics need to be tested to verify the generalisability of the proposed solar irradiance nowcasting method. Consequently, this research has been limited by the amount of data and the diversity of datasets.

- Image Processing Techniques.

  To ensure that the proposed solar irradiance nowcasting method achieves reliable accuracy and reduced the time consumption of computation, this research relies heavily on the machine learning of cloud image by the nowcasting model. Thus, only two technologies, including High Dynamic Range (HDR) Synthesis and Masking are used for image processing. However, more image processing techniques related to distortion calibration of images, image binarization, colour threshold adjustment, pixel recognition of the sky and clouds, etc, can be used to optimise the processing of cloud images to obtain more ideal input for the proposed solar irradiance nowcasting model. In this case, it is necessary to find the right balance between the

degree of image processing and the time consumption of computation in the future. Thus, this research has been limited by image processing techniques. Nevertheless, a more advanced image processing technique has been developed and published in a journal article by the author but not presented in this research since the integration of that image processing approach and the proposed method in this research will take time to explore.

- Training Time.

  Due to the large number of high-resolution cloud images that need to be processed, a significant amount of training time is needed by the proposed solar irradiance nowcasting model. In this research, the training time for a single nowcasting model was several hours or even a couple of days. Moreover, the time consumption of model training in different comparative tests for various purposes, including parameter adjustment, model optimisation, various model comparisons, etc, will increase exponentially. In this case, this research has been limited by the training time.

- Nowcasting Model.

  Although the proposed solar irradiance nowcasting model can provide reliable nowcasting of GHI, DNI and DHI, there is still much room for its optimisation. First, the accuracy of the nowcasting model is impacted by a series of model parameters, such as the number of hidden layers, activation functions, the number of nodes in each layer, learning rate, weights, the number of iterations, etc. In general, these parameters are usually set to default values. However, it is necessary to find their optimal values for optimising the performance of the nowcasting model. Secondly, a series of various architectures of ResNet are available, such as ResNet-18, ResNet-50, ResNet-1202, etc. Various architectures of ResNet imply different nowcasting accuracy, computational ability and training time. Thus, it is worth conducting more comparative tests to explore the optimal architecture according to different specific purposes.

Thirdly, the training and optimization of the nowcasting model need to collect data from the same location over a long period of time that is not conducive to locations or buildings where data is difficult to obtain. In this case, additional data processing approaches need to be explored and integrated with the nowcasting model to generalise beyond the model training location in data-scarce conditions. To sum up, more exploration of model parameters, architectures of ResNet and data processing approaches is needed to optimise the nowcasting model.

- Stability of Equipment Operation.

  The stability of the equipment operation affects the continuity and quality of data collection. Due to the epidemic control of COVID-19 and the administrative policy of Tongji University, the Raspberry Pi camera used in this research must be reinstalled daily and thus is not equipped with fixed rain protection, which adds a significant amount of additional movement and installation labour, affecting the efficiency and quality of data collection. Thus, this research has been limited by the stability of the equipment operation.

- Design of Comparative Tests.

  There is still a lot of room for improving the design of comparative tests in this research. Firstly, a larger number of diverse datasets and more varied nowcasting horizons need to be used to test the effect of time intervals on solar irradiance nowcasting and find an optimal time interval. In addition, more comparative tests for longer nowcasting horizons need to be conducted to explore the maximum nowcasting horizon of the proposed solar irradiance nowcasting. Moreover, data from more days under different sky conditions need to be used to validate the accuracy of the nowcasting model further. Besides, the proposed solar irradiance forecasting model needs to be compared with other advanced forecasting models to verify its strength. Additionally, more datasets of different magnitudes and different seasons

need to be used to explore the influence of dataset selection on nowcasting performance. In the end, the impact of the setup parameters or different architectures of the nowcasting model could be investigated through more comparative tests.

- Research for Practical Building Applications.

  The main concern of this research is to develop a solar irradiance nowcasting method to provide reliable GHI, DNI and DHI, which are very unpredictable critical weather data for building applications. As a result, although the study of the practical building applications of the proposed solar irradiance nowcasting method is already underway, it is not presented in this research.

5.3 Current and Potential Applications of Solar Irradiance Nowcasting Method in Buildings

This research has developed a solar irradiance nowcasting method to achieve the nowcasting of GHI, DNI and DHI for buildings. Based on a series of comparative tests, the nowcasting GHI, DNI and DHI at various time intervals (10-sec, 1-min, 5-min and 10-min) for different nowcasting horizons (10-sec, 1-min, 5-min and 10-min) have been proven to be reliable. These very short-term GHI, DNI and DHI nowcasting with high spatial-temporal resolution will be valuable weather data for buildings and their future development. Specifically, the nowcasting of GHI, DNI and DHI can be applied to diverse aspects of buildings, such as energy management, energy system protection, lighting and shading system regulation, intelligent building facade control, etc, to optimise the operational efficiency and safety of building systems, occupant comfort and the design of building. Based on the above, several current and potential applications are discussed to articulate the value and perspective of the developed solar irradiance nowcasting method for buildings that will provide initial sights for subsequent research.

5.3.1 Current Applications of Solar Irradiance Nowcasting Method in Buildings

This section presents current applications of solar irradiance nowcasting method in buildings, mainly involving energy management and energy system protection.

- Energy Management.

  Reliable solar irradiance nowcasting is significant for building energy management. Nowadays, a single large commercial or industrial building, an individual small intelligent building or a cluster of buildings, such as a campus, forms an individual micro-gird in fact. In this case, the integrated Energy Management System (EMS) of buildings can utilise solar irradiance nowcasting to optimise energy rationing between the solar panels of micro-

girds and the grid. In specific, EMS can reduce the amount of electricity purchased from the grid and rely on the electricity generated by solar panels to meet most of the building's needs. This not only reduces energy costs but also reduces the impact on the environment. In addition, solar irradiance nowcasting can be used to ensure the stability of micro-girds equipped with PV panels. A Battery Energy Storage System (BESS) can be charged with solar energy when the amount of energy generation in a building exceeds its demand. It can be discharged at moments when the building load is at its peak or when energy system issues happen. In this case, BESS can be used in conjunction with solar irradiance nowcasting to maintain the stability of micro-girds by discharging energy during the fluctuations of solar energy. A series of studies have demonstrated current applications of solar irradiance nowcasting for energy management, involving operational planning, electricity market transaction, peak load matching, load following, etc [355-361]. According to the survey responses in [362], the majority of respondents believe very short-term solar irradiance forecasting can enable an increase in PV penetration in a microgrid. The 1-min, 5-min and 10-min nowcasting of GHI, DNI and DHI acquired in this research are all very suitable for this type of application.

- Energy System Protection.

  Rapid transitions of clouds create a great deal of dramatic fluctuations in very short-term PV power variations that cause "Ramp Events". These "ramp events" can damage grid transient stability, leading to voltage flickers or even blackouts, which increase wear and tear on generation and transmission equipment, shortening equipment life and increasing maintenance costs. For example, for those girds equipped with fixed PV panels, although "Ramp Events" do not directly cause physical damage to PV panels, they can affect certain equipment in the system, such as inverter. An inverter is a device that

converts direct current (DC) generated by photovoltaic (PV) panels into alternating current (AC). During “Ramp Events”, inverters need to rapidly respond to drastic changes in power output. This can lead to frequent adjustments in output, increasing the operational burden and wear on the inverter. In addition, “Ramp Events” also lead to negative impact to PV panels equipped with trackers. When “Ramp Events” happen, frequent adjustments of the tracking system to cope with rapidly changing solar radiation conditions may increase the wear and tear of mechanical parts and the probability of failure, thus affecting the long-term reliability of the system and increasing maintenance costs. Moreover, although auto-tracking PV panels can adjust its orientation to maximise sunlight reception, under the influence of rapidly changing cloud cover during “Ramp Events”, the system may not be able to respond quickly enough to adjust to the optimal angle in time and accurately, resulting in energy loss. According to the above, the benefits of solar irradiance nowcasting for the grids and PV panels are obvious. Using solar irradiance nowcasting, solar systems can take measures in advance to adjust system operation, power production and distribution to protect the equipment of solar systems. In conclusion, utilising solar irradiance nowcasting to protect solar systems is valuable and thus some studies related to spinning reserve and ramp rates control have been executed [363, 364]. The 1-min nowcasting of GHI, DNI and DHI are the optimal choice for this type of application because of the high-frequency variations of solar irradiance.

5.3.2 Potential Applications of Solar Irradiance Nowcasting Method in Buildings

Potential applications of solar irradiance nowcasting method in buildings, including lighting and shading system regulation, pre-conditioned HVAC systems, and intelligent building surface design, are demonstrated in this section.

- Lighting and Shading System Regulation.

  Solar irradiance nowcasting is also very valuable for lighting and shading system regulation. Firstly, solar irradiance nowcasting can be integrated into intelligent lighting systems, enabling the system to automatically adjust the brightness and colour temperature of indoor lighting based on predicted changes in solar irradiance. For example, when strong solar irradiance is predicted, the system can automatically dim indoor lights to reduce energy consumption and maintain a comfortable visual environment. Secondly, buildings can be assembled with smart shading systems, such as automatic blinds, smart glass or motorised curtains. These devices can be linked to a centralised control system that automatically adjusts to solar irradiance nowcasting. Specifically, when solar irradiance nowcasting indicates imminent high-intensity solar irradiance, a smart shading system can automatically regulate shading devices to block sunlight, reducing indoor temperature rise and air-conditioning load. At moments of low solar irradiance, smart shading devices can adjust to allow more natural light in, increasing heat utilisation and reducing lighting requirements. In conjunction with this research, the 1-min and 5-min nowcasting of DNI and DHI are ideal for the sensitive regulation of lighting and shading systems.

- Pre-conditioned HVAC Systems.

  Heating, Ventilation, and Air Conditioning (HVAC) systems in buildings often include thermostats and automated control units that receive and analyse solar irradiance data. In this case, HVAC systems can utilise solar irradiance nowcasting to adjust the operating modes in advance. For instance, before the indoor temperature is predicted to rise due to the increase in solar irradiance, an HVAC system can lower the indoor temperature to prevent sudden increases in temperature that could cause discomfort. Conversely, if a decrease in solar irradiance is predicted, the system can slightly raise the

indoor temperature to maintain comfort without overly relying on heating equipment. In addition, the ventilation system can be pre-adjusted in response to expected changes in indoor temperature and air quality based on solar irradiance nowcasting. For example, if enhanced solar irradiance is predicted, the ventilation system can automatically open windows or vents to increase the flow of fresh air in advance, preventing excessive indoor temperatures and adjusting air quality. Due to the changes in thermal and air environments taking longer to occur, the 10-min nowcasting of GHI and DNI achieved in this research is more likely to be used for the abovementioned applications in some special scenarios, such as greenhouses, rooms with solar chimneys or extensive glass coverage, etc, where risk of overheating exists.

- Intelligent Building Surface Design.

  Solar irradiance nowcasting can also be used in conjunction with intelligent interactive systems for buildings and environments to affect the design of intelligent building surfaces. The 10-min nowcasting of GHI, DNI and DHI obtained in this research has potential to be used for this application considering the response time of building operations.

To sum up, the above building applications of solar irradiance nowcasting can more accurately control the energy consumption, operation cost and indoor environment of buildings, optimising operational efficiency and safety of building systems as well as enhancing the comfort of the living or working environment. Although only some of the above applications are used actually and many building-related software have not yet well supported the utilisation of high-resolution solar irradiance, other potential applications will, in turn, drive the development of building-related software and building intelligence in the future. Most importantly, it is worth noting that when these applications do not operate separately but together, a whole intelligent building system will be formed, where the solar irradiance nowcasting will demonstrate its maximum application value.

5.3.3 Case Study on The Application of Solar Radiation Nowcasting in Buildings

Since this research focuses on a very narrow subject, the nowcasting of solar irradiance data, the relationship between solar irradiance nowcasting and buildings has hardly been discussed specifically at current research. However, it is not difficult to find the value of this research from many studies.

[365] explores short-term forecasting photovoltaic solar power for home energy management systems. In this article, the significance of DNI for architecture and energy management, particularly in Concentrated Photovoltaic (CPV) systems, is extensively discussed. In addition, this article developed a short-term photovoltaic solar power forecasting method based on an ANN and GHI is one of the four key variables used to train the forecasting model. In this study, historical GHI obtained from the database of Honda Smart Home (HSH) US is be used as input of the forecasting model after a series of pre-processing steps, finally achieving a 15-minute solar power forecasting. Based on the above, it is evident that accurate minute-scale nowcasting of GHI are more suitable for the forecasting model than historical data, because the timestamp of historical GHI and predicted solar power do not match, while the timestamps of predicted GHI can be kept consistent.

In [366], an effective energy management approach is designed to systematically regulate energy usage in residential areas, aiming to reduce the peak to reduce electricity costs and pressure, optimise the scheduling of smart appliances and electric vehicles, lower electricity costs, and enhance user comfort. According to the article, the prediction of solar irradiance is the foundation for accurate power generation estimation, which plays a key role in microgrids and home energy management systems (HEMS).

In summary, although the primary focus of the above studies is not on solar irradiance nowcasting, the role of solar irradiance nowcasting is critical to them. To

more intuitively illustrate the impact the application of solar irradiance nowcasting on buildings, a practical case is demonstrated below.

[28] explores the relationship between weather forecasting, specifically nowcasting, and building performance. In specific, the article discusses how accurate weather nowcasting, especially the nowcasting of solar irradiance, can impact the precision of dynamic building simulations. These simulations can predict indoor temperature variations and heating loads, which are essential for maintaining energy efficiency and comfort in buildings. Three buildings from BESTEST case studies are used to conduct dynamic building energy simulations base on simulation engine EnergyPlus. The findings of this study suggest that weather nowcasting (including solar irradiance nowcasting) can lead to accurate building performance simulations, especially in buildings without significant south-facing glazing. For buildings with large south-facing windows, however, the variance in solar irradiance nowcasting can lead to discrepancies, indicating the need for further improvement of solar irradiance nowcasting techniques for these specific scenarios. Some relevant results of building simulation of this study are displayed in Figure 5.1-5.5. Based on the above, the application of solar irradiance nowcasting has an evident impact on buildings that proves the value of this research.

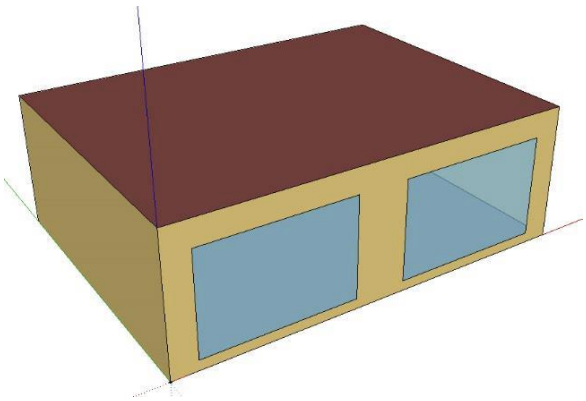

Figure 5.1 A single zone building with large glazing - Case 640/940/900FF defined within ANSI/ASHRAE Standard 140-2014

(Resource: H. Du, C.F. Bandera, L. Chen, Nowcasting methods for optimising building performance, (2019).)

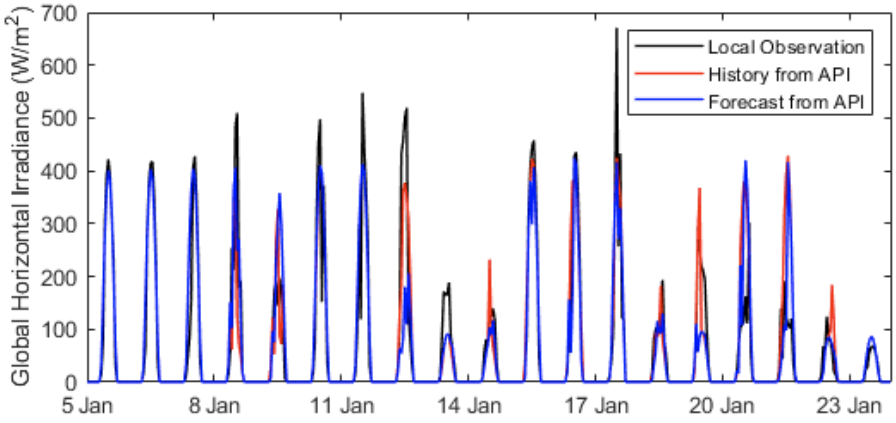

Figure 5.2 Global radiation forecast vs observation

(Resource: H. Du, C.F. Bandera, L. Chen, Nowcasting methods for optimising building performance, (2019).)

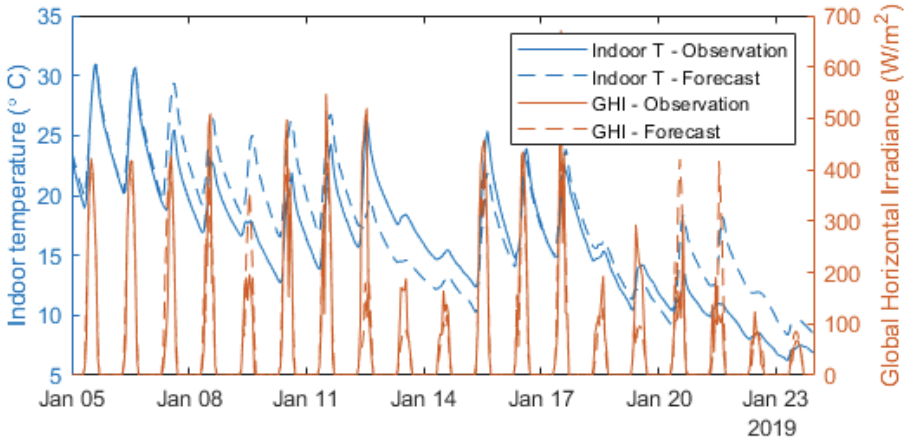

Figure 5.3 Indoor temperature prediction on building with south facing glazing

(Resource: H. Du, C.F. Bandera, L. Chen, Nowcasting methods for optimising building performance, (2019).)

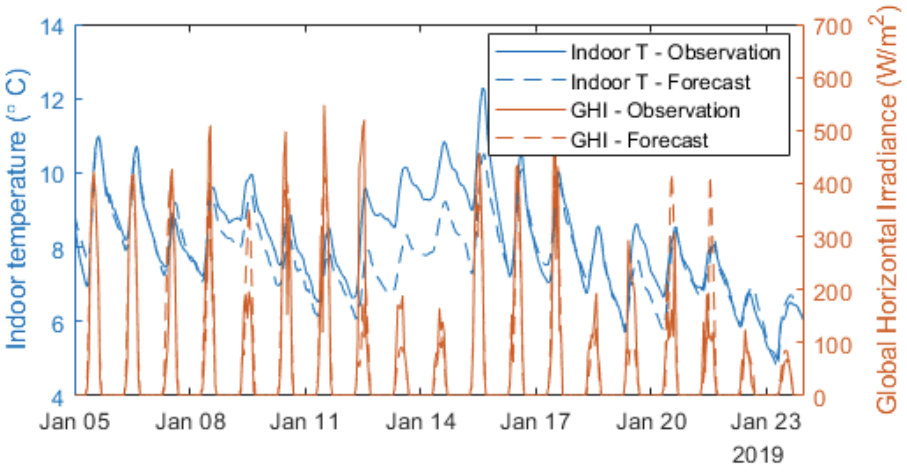

Figure 5.4 Indoor temperature prediction on building with north facing glazing

(Resource: H. Du, C.F. Bandera, L. Chen, Nowcasting methods for optimising building performance, (2019).)

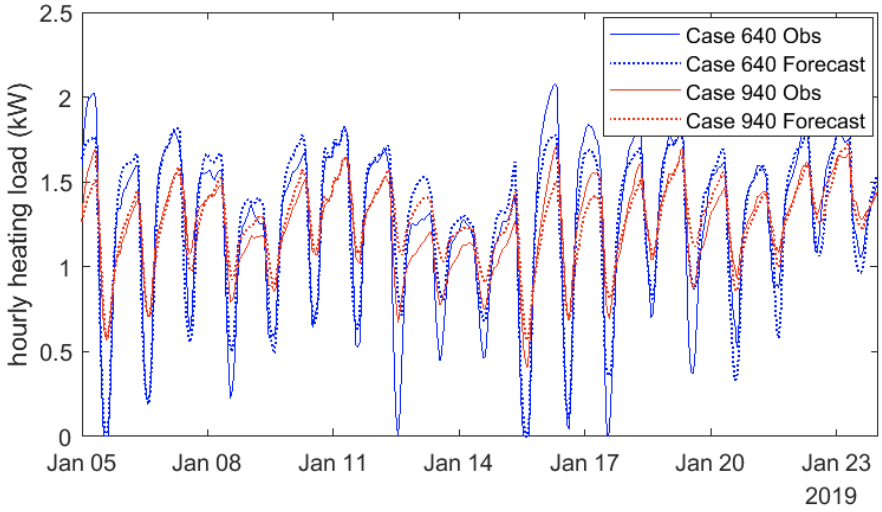

Figure 5.5 Heating load for building with north facing glazing

(Resource: H. Du, C.F. Bandera, L. Chen, Nowcasting methods for optimising building performance, (2019).)

5.4 Implications of The Research

Based on the discussion above, this research carries profound implications for both academic community and practical applications. It not only addresses existing gaps in the field of solar irradiance forecasting but also suggests consequential impact on society and economy. This section explores these implications in detail, highlighting how they contribute to advancing knowledge and promoting potential social and economic development.

5.4.1 Academic Implication - Systematic Literature Review.

The critical value of the systematic literature review in this research is that it provides a well-defined review methodology that includes a series of benefits.

- Comprehensiveness and Objectivity.

  The developed systematic review methodology requires a thorough search of all potentially relevant literature to minimise the risk of missing important studies. In this case, the comprehensiveness and objectivity of research are increased through explicit criteria for selecting and assessing literature.

- Reproducibility.

  The developed systematic review methodology clearly defines the approaches and processes of different steps, involving identification, screening, eligibility, inclusion and analysis. This well-defined approaches and processes ensure the transparency and reproducibility of the research.

- Evidence Synthesis.

  The developed systematic review methodology help synthesise the results of numerous studies, providing stronger evidence to support or refute a hypothesis. Thus, it is particularly suited for evaluating and comparing results across different studies.

- Identifying Research Gaps.

  Based on the developed systematic review methodology, the research gaps

are identified more objectively and efficiently, guiding future research directions.

- Knowledge Updating.

  As new research continually emerges, the developed systematic review methodology is conductive to regularly update the review, providing the latest research trends and findings.

- Decision Support.

  The high-quality evidence provided by systematic literature reviews can help policymakers and practitioners make evidence-based decisions.

In summary, a systematic literature review is a comprehensive research method that systematically collects, assesses, and synthesises all relevant research findings to answer a specific research question. Currently, systematic literature reviews are widely used in fields such as medicine, social sciences, and environmental science, and are considered one of the highest levels of evidence sources. Based on references to other systematic literature reviews, the systematic review methodology developed in this research can help relevant researchers, practitioners and the public quickly and comprehensively understand the field of solar irradiance forecasting. In addition, the well-defined review methodology not only address the limitations of current literature review, but also provides a methodological paradigm of literature review for researcher, especially individual researcher.

5.4.2 Academic Implication - Solar Irradiance Nowcasting Method.

The crucial contribution of the proposed solar irradiance nowcasting method lies in the integration of diverse approaches and techniques across different stages of solar irradiance forecasting. Based on the proposed nowcasting method, the nowcasting of three critical solar irradiance components - GHI, DHI and DNI - with high spatial-temporal resolution are achieved, which is the most significant contribution of this research to the field of solar irradiance forecasting. That is because

there are small amounts of studies can achieve minute-scale nowcasting with very high spatial-temporal resolution (1 metre to 2 kilometres, 10 seconds to 10 minutes), and even less of them simultaneously predict three critical solar irradiance components - GHI, DHI and DNI, especially DNI.

Similar to common studies, this research also makes considerable efforts in the development and optimisation of solar irradiance nowcasting models - ResNet-152, which mainly involves the following aspects:

- Model Selection.

  The selection of ResNet-152 is critical to the development of solar irradiance nowcasting models. Although ResNet-152 performs better than most CNNs according to accuracy, computational time consumption and number of parameters and has been extensively applied in different fields, it has also hardly been used in research on solar radiation forecasting. Besides, ResNet-152 has obvious advantages for the crucial task of this study - cloud images recognition, as demonstrated in section 3.3.1.1. Therefore, it is very valuable to explore the application of ResNet-152 in the field of solar irradiance nowcasting.

- Data Preprocessing.

  As a typical data-driven model, data preprocessing is also a crucial part to the development of ResNet-152. In this research, the data preprocessing method is adjusted according to the capabilities of ResNet-152. Relying on the powerful image recognition capabilities of ResNet-152, this research simplifies the conventional flow of data preprocessing. In this research, only two crucial image preprocessing techniques, HDR Synthesis and Masking, are used, which efficiently reduces the time consumption required for model training and testing, making it more conducive to practical applications.

- Model Optimisation.

  The utilisation of L2 functions and the adjustment of hyperparameters are the

main means for the optimisation of ResNet-152 in this research. For deep neural networks such as ResNet-152, the L2 function has obvious advantages in preventing overfitting and optimising the training stability and generalisation ability of the network. In this research, the selection of L2 function efficiently helps the ResNet-152 converge faster to a lower error rate. In addition, a series of key hyperparameters, such as learning rate, epochs, are manually and constantly adjusted to compare the nowcasting performance of ResNet-152. In this case, the effect of hyperparameters is evaluated and the optimal configuration for ResNet-152 is finally selected in iterative processes.

- Evaluation Methods.

  Diverse verification metrics and designs of tests are also important to the optimisation of ResNet-152. By applying various verification metrics, the nowcasting performance of the ResNet-152 in different circumstances, including time intervals, nowcasting horizons, sky conditions, benchmark models, and datasets, are compared from various perspectives.

In summary, the contributions of this research to the development and optimisation of solar irradiance nowcasting models encompass everything from proposing the use of the ResNet-152, simplifying data preprocessing to tuning model, and then implementing and evaluating the model.

However, unlike common studies that focus on the development or optimisation of forecasting models, this research constructs a systematic research methodology that not only focuses on the forecasting models, but also involves the processing and optimisation of model input data, the selection of low-cost equipment and user-friendly programming, as well as diverse comparative tests and validation methods. These efforts are beneficial for subsequent researchers to follow and increase the applicability of the proposed nowcasting method. Additionally, the collection of solar irradiance data with high spatial-temporal resolution, the settings and parameters for model training are also significant contributions of this research, especially for data-

driven methods that have become increasingly popular in recent years due to the development of artificial intelligence. In general, the contribution of this research is more in the collection of specific solar irradiance data and application of diverse forecasting approaches and techniques than in the development of forecasting model.

5.4.3 Practical Implication - Low-cost Equipment and User-friendly Programming.

According to the Table 3.1-3.2 in section 3.2.2, the nowcasting method proposed in this research only requires the temporary use of a BF5 Sunshine Sensor worth £3,200 at an early stage. Thus, it can be rented at a low cost instead of being purchased. In long-term practical use, the method merely requires equipment worth around £300, including a Raspberry Pi computer, a mobile phone tripods and other accessories. Therefore, the practical application of the proposed nowcasting method is very low-cost. In contrast, representative equipment, such as a SPN1 Sunshine Pyranometer, usually costs around £7,000. The huge difference in cost between the above devices is self-evident, which is usually determined by the following reasons.

- Material Costs.

  Expensive devices use higher-quality materials that are more durable and stable.

- Research and Development Investment.

  Expensive devices are often based on substantial research and development investments, both in terms of time and money. These investments need to be recovered through the selling price of the product.

- Technology, Accuracy and Functions.

  Expensive devices use advanced technologies, such as more sophisticated sensors and processors, to improve measurement accuracy and provide more functions. These technologies are more expensive. For example, SPN1 Sunshine Pyranometer can directly achieve the measurements of GHI, DHI

and DNI, While BF5 Sunshine Sensor can merely measure GHI and DHI.

- Production Scale.

  Currently, the measurements of solar irradiance are only required by a few professional institutions and companies, which determines the expensive devices is produced in smaller quantities. In this case, its production costs are usually higher because economies of scale cannot be achieved.

- Market Positioning.

  The manufacturers of expensive devices position their products in the high-end market, mainly targeting professional institutions and companies and offer additional features or services, which results in higher pricing.

Based on the above reasons, the prices of these expensive devices are unlikely to decrease in the short term. In this case, the value of the low-cost equipment developed in this research is obvious. In addition to the low-cost equipment, the programming of this research is based on Python, which have many significant benefits for the ordinary researchers and public.

- Lowering Entry Barriers.

  Python is a high-level programming language with simple, readable syntax, making it ideal for beginners. In addition, Python has an extensive range of learning resources, tutorials, and community support, making it easy for self-learners.

- Promoting Technology Accessibility.

  As an open-source programming language, Python is free to use and can be modified and distributed by anyone. This makes it accessible to people from all over the world, promoting the widespread use and innovation of technology.

- Encouraging Community Collaboration and Innovation.

  Python allows developers and users to contribute to the codebase, constantly improving projects. Community members help each other increase productivity by sharing code and tools.

- Enhancing Interdisciplinary Collaboration.

  Python is widely used in various disciplines and industries, such as environmental science, healthcare, architecture, and finance. Its simple syntax and powerful libraries make it easier for experts from different fields and regions to collaborate, promoting knowledge sharing and technology development worldwide.

- Reducing Development Costs.

  Python are typically free and has a vast array of third-party libraries and tools (e.g., NumPy, Pandas, TensorFlow), which users can directly utilise to implement various functionalities. Compared to expensive proprietary software, open-source programming significantly lowers development and deployment costs.

- Supporting Sustainable Development and Environmental Protection.

  Python encourages code reuse and sharing, avoiding unnecessary resource waste and repetitive work, which has a positive impact on environmental and resource conservation.

- Increasing Technological Self-Sufficiency.

  Python allows users to tailor solutions according to their needs, without relying on commercial software vendors' services and pricing strategies. This is important for researchers, individuals, and small businesses.

In summary, this research combines low-cost equipment with user-friendly programming to replace expensive equipment, providing the public and ordinary researchers with convenient, efficient, and low-cost means to apply solar irradiance nowcasting on the buildings where they work and live every day.

5.4.4 Potential Social and Economic Impacts.

Based on the academic and practical implications discussed above, the potential social and economic Impacts of the proposed solar irradiance nowcasting method is

discussed below.

- Potential Social Impacts.

  c) Improving Occupant Comfort.

  More precise indoor environmental control can create a more comfortable environment for occupants by adjusting indoor temperature and lighting in advance according to the nowcasting of solar irradiance. This improvement in comfort can have a positive impact on social well-being by increasing employee productivity and occupant quality of life.

  d) Reducing Carbon Footprint.

  By using solar irradiance nowcasting, buildings can optimise energy use to reduce carbon emissions, thereby mitigating the urban heat island effect and improving air quality. This is significant for improving public health and promoting environmental sustainability, which is conducive to creating a more liveable urban environment.

  e) Supporting the Sustainable Development Goals (SDGs).

  The use of solar irradiance nowcasting in building energy systems can make important contributions to several specific SDGs.

  Goal 7: Affordable and Clean Energy.

  Solar irradiance nowcasting can further promote the development of solar energy systems in buildings, thereby raising public awareness of clean energy, reducing their cost of using clean energy, and finally facilitating the popularisation of clean energy.

  Goal 11: Sustainable Cities and Communities.

  Solar irradiance nowcasting can help buildings optimise the energy management, reducing the need for HVAC systems, lowering energy consumption. This promotes the development of more environmentally-friendly and energy-saving construction of cities and communities.

  Goal 13: Climate Action.

Solar irradiance nowcasting can enable buildings to use solar energy more efficiently, thereby reducing greenhouse gas emissions. This directly supports the goal of combating climate change and promotes global climate action.

- Potential Economic Impacts.

  a) Cost Savings.

  By using solar irradiance nowcasting to precisely control the energy use, unnecessary electricity, heat consumption and equipment operation in buildings can be reduced, directly lowering operating costs. In addition, energy conservation and emission reduction can also reduce investment in facility maintenance and potential fines or taxes due to increasingly rigor environmental regulations.

  b) Improving Energy Efficiency.

  Using solar irradiance nowcasting and energy management system, buildings can achieve higher energy efficiency, which means maximising resource use, reducing energy consumption, and lessening dependence on traditional energy sources, supporting energy diversification strategies.

  c) Long-term Financial Benefits.

  The use of solar irradiance nowcasting can bring significant long-term financial benefits for buildings.

  Benefit 1: Long-term Cost Savings.

  As mentioned above, solar irradiance nowcasting can promote buildings improving energy efficiency, reducing the use of traditional energy, extending equipment life. In this case, the cost of energy use, system operation and equipment maintenance can be effectively reduced, especially in the long term.

  Benefit 2: Return on investment (ROI).

  Base on solar irradiance nowcasting, solar energy system optimisation in

buildings can provide a high ROI for buildings in the long term. As the application of solar radiation nowcasting in buildings becomes increasingly widespread, its application cost will gradually decrease, while energy efficiency will constantly improve. In this case, investors can recover the investment costs more quickly, thereby achieving long-term financial benefits.

Benefit 3: Industry Development and Job Opportunities.

Applying solar irradiance nowcasting to optimise solar energy system optimisation in buildings can also facilities the development of advanced technologies and job creation in related fields, positively impacting economic restructuring and the growth of emerging industries.

In conclusion, solar irradiance nowcasting has far-reaching impacts on both society and economy. It can improve the comfort of the living and working environment, support sustainable development goals, while improving energy efficiency and long-term financial benefits.

5.5 Chapter Summary

In summary, this chapter first provides an in-depth interpretation for the results of solar irradiance nowcasting. At the beginning, five groups of comparative tests are briefly reintroduced. Then, the major findings of this research, the reasons for the findings and the potential effects of the findings are articulated to deliver a comprehensive understanding of the research results. In the end, the results of the proposed method are compared with those of contemporary state-of-the-art methods to demonstrate the reliability of the proposed method.

Based on the interpretation of research results, a series of limitations of the research is presented, involving an amount of data and diversity of datasets, image processing techniques, training time, nowcasting model, stability of equipment operation, design of comparative tests, and research for practical building applications. The elaboration of research limitations will provide future research.

Most importantly, current and potential building applications of solar irradiance nowcasting and the Implications of the research are discussed at the end of this chapter to emphasise the value and prospective of this research for building operational efficiency and safety, occupant comfort and design.

Chapter Six

6 Conclusion

The above chapters thoroughly describe the literature review, research methodology, results verification and analysis, discussion of this research. Thus, the purpose of this chapter is to conclude this research.

An overview of the research is first presented to reiterate the background, importance, aim, questions of the research and demonstrates the relationship between research questions and chapters. Then, the major findings of the research are articulated again. After that, the main contributions of the research are demonstrated. Ultimately, all research activities, contributions, limitations, future works, and the significance of the research are concluded at the end of this chapter.

6.1 Overview of the Research

Solar energy, as one of the most promising renewable energies, has been widely used in recent decades to reduce carbon emissions in human living and production, which is the cause of the growth of global greenhouse gases. Although solar energy is abundant and widespread, its instability - caused by a series of factors such as the movement of the sun, changing cloud cover, water vapour, and air pollution - presents significant challenges in its effective utilisation. Therefore, anticipating fluctuations in solar energy, especially the changing pattern of solar irradiance, can contribute to the effectiveness of solar applications. In this case, a large number of solar irradiance forecasting methods have been developed to achieve reliable solar irradiance forecasting.

Buildings, which are fundamental to human living and production, consume substantial energy while generating a vast amount of carbon emissions. Consequently, employing solar irradiance forecasting methods to enhance the efficient utilisation of solar energy in buildings holds significant importance. However, most solar irradiance forecasting methods are usually not customised for buildings and do not meet the needs of future building intelligence. Fortunately, a range of emerging opportunities, including the recent development of building intelligence, the 5G internet, and the emerging solar irradiance nowcasting methods with high spatial-temporal resolution, bring the possibility to the development of solar forecasting methods suitable for buildings.

The importance of this research is to explore the solar irradiance nowcasting methods appropriate for buildings from an architectural perspective. In this context, this research mainly includes three significant tasks. At first, this research needs to explore what solar irradiance forecasting methods are more applicable and reliable to buildings. Then, this research needs to develop an interdisciplinary research methodology for solar irradiance nowcasting by integrating knowledge of meteorology,

imagery, computer science, and architecture. Finally, this research needs to discuss the potential value of solar irradiance nowcasting to buildings and the development of future buildings that provide initial inspiration for subsequent research.

Based on the above, the aim of this research is to develop a solar irradiance nowcasting method with high spatial-temporal resolution based on low-cost equipment and user-friendly programming to achieve reliable nowcasting of GHI, DNI and DHI for buildings and discuss its current and potential applications in buildings.

In response to a series of research gaps, five critical research questions were proposed and answered by the main research activities of this research.

1. How can a literature review be conducted based on a clear methodology to screen the solar irradiance forecasting methods appropriate for buildings?

   This research question was answered in Chapter 2 - Literature Review.

   In Chapter 2, this research applied a clear methodology of systematic review to identify the solar irradiance forecasting methods appropriate for buildings according to a series of different characteristics, including forecasting horizons, spatial-temporal resolution, data acquisition ways, forecasting parameters, equipment and programming, etc.

2. How can a solar irradiance nowcasting method appropriate for buildings be developed?

   This research question was answered in Chapter 3 - Research Methodology.

   In Chapter 3, this research developed a solar irradiance nowcasting method with very short-term forecasting horizons and high spatial-temporal resolution to achieve the nowcasting of GHI, DNI and GHI appropriate for buildings by utilising low-cost equipment, user-friendly programming and a promising Residual Neural Network (ResNet-152) model.

   A clear workflow of research methodology with three main stages, including data collection and processing, solar irradiance nowcasting, comparative tests and verification, was demonstrated in Chapter 3. Specifically, the first stage of

the research methodology showed the collection approaches of consecutive cloud images, GHI and DHI, and the procedures of data processing involving image processing and data alignment. Then, the second stage of the research methodology demonstrated the procedures of solar irradiance nowcasting, including dataset collation, the training of the ResNet-152 nowcasting model, the nowcasting of GHI and DHI, the calculation of DNI from the nowcasting of GHI and DHI. Finally, the third stage of the research methodology described a series of comparative tests aimed at exploring the effect of different factors, including time interval, nowcasting horizons, sky conditions, forecasting models and datasets, on the performance of the developed solar irradiance nowcasting method and the setup of these comparative tests.

3. How can the results of solar irradiance nowcasting be generated?

   This research question was initially answered in Chapter 3 - Methodology and mainly responded Chapter 4 - Results Verification and Analysis of Solar Irradiance Nowcasting.

   At the end of Chapter 3, the setup of a series of comparative tests is demonstrated. These setups involve the selection of time intervals and forecasting horizons, the classification of sky conditions, comparative models and the selection of evaluation metrics. Based on the developed methodology of solar irradiance nowcasting and the above test setups, a series of comparative tests were specifically executed in Chapter 4, which generated the nowcasting results of GHI, DNI, and DHI.

4. How can the reliability of solar irradiance nowcasting be verified?

   This research question was initially responded to in Chapter 3 - Methodology and mainly answered in Chapter 4 - Results Verification and Analysis of Solar Irradiance Nowcasting.

   At the end of Chapter 3, this research first assessed the characteristics and popularity of different evaluation metrics, such as MAE, RMSE, MAE, nRMSE,

etc, according to the literature review in Chapter 2. Then, several appropriate evaluation metrics were selected to evaluate the reliability of solar irradiance nowcasting from various perspectives. Based on the abovementioned comparative tests and selected evaluation metrics, Chapter 4 specifically demonstrated the reliability of solar irradiance nowcasting under the influence of different factors.

5. What current or potential building applications can the proposed solar irradiance nowcasting method be applied to?

   This research question was answered in Chapter 5 - Discussion.

   In Chapter 5, this research discussed current applications of the proposed solar irradiance nowcasting method in buildings based on current building applications of solar irradiance nowcasting methods and potential applications of the proposed solar irradiance nowcasting method in buildings based on the future trends in building development.

6.2 Summary of Major Findings

In this research, a series of comparative tests were conducted to explore the effect of different factors, including time interval, nowcasting horizons, sky conditions, forecasting models and datasets, on the performance of the developed solar irradiance nowcasting method that verified its reliability. According to section 5.1.2, the major findings from the above comparative tests and their significance are summarised as follows:

- The effect of various time intervals on nowcasting performance.

  The crucial finding of this set of comparative tests is that 1-min time interval is likely to be the optimal temporal resolution for solar irradiance nowcasting because the nowcasting of GHI, DNI and DHI at 1-min time interval always achieves the best performance no matter what the nowcasting horizon is. In practice, 1-min time interval is ideal considering the time consumption of computer operation, data transmission, system response and other factors, but requiring a certain amount of device computing power and stability. Nevertheless, solar irradiance nowcasting at 1-min time interval is still valuable for buildings and their future development, as it meets more accurate requirements of building operation and control.

- The effect of various nowcasting horizons on nowcasting performance.

  The main finding of this set of comparative tests is that the nowcasting performance is negatively correlated with nowcasting horizon. The GHI, DNI and DHI nowcasting for 10-sec, 1-min, 5-min and 10-min nowcasting horizons demonstrated reliable accuracy, especially 10-sec and 1-min. In practice, solar irradiance nowcasting for 1-min nowcasting horizon and solar irradiance nowcasting for 5-min and 10-min nowcasting horizons can respectively meet the requirements of different building applications.

- The effect of different sky conditions on nowcasting performance.

  The critical finding of this set of comparative tests is that the nowcasting of GHI and DNI performs well under clear, light, cloudy and overcast sky conditions, and the nowcasting of DHI performs well regardless of any sky conditions. In other words, heavy cloudy is the only sky condition that has an impact on the performance of the proposed solar irradiance nowcasting method, especially for DNI nowcasting. Despite this, the overall trend of the DNI can still be successfully predicted even under heavy cloudy sky conditions. Thus, the proposed solar irradiance nowcasting method is reliable under different sky conditions, which is beneficial for building applications.

- The influence of different models on nowcasting performance.

  The key finding of this set of comparative tests is that the proposed solar irradiance nowcasting model, ResNet-152, always achieves the best performance compared to the baseline model - Multilayer Perceptron (MLP) and the benchmark model - Persistence Model (PM), apart from performing worse than PM 1-min nowcasting horizon. Nevertheless, ResNet-152 is better than PM in practical applications of buildings because the utilisation of ResNet-152 can greatly reduce the cost of equipment and maintenance and the difficulty of the equipment operation. Based on the above, the proposed solar irradiance nowcasting model is very appropriate for buildings.

- The influence of different datasets on nowcasting performance.

  Two major findings are obtained in this set of comparative tests. First, the influence of the expansion of training set on nowcasting accuracy is still uncertain because the performance of solar irradiance nowcasting models trained with 34 days of data from April to July and 48 days of data from April to September is close for 8 identical testing days. Thus, the effect of the data range of training set on the nowcasting accuracy still needs further research. In contrast, the influence of the seasonality of testing set on nowcasting

accuracy is obvious because the DNI nowcasting of 4 testing days in December performs apparently worse than the DNI nowcasting of 12 testing days from April to September based on the solar irradiance nowcasting models trained with 48 days of data. Therefore, constructing seasonal nowcasting models might be more beneficial to the application of the proposed solar irradiance nowcasting method on buildings.

To sum up, the reliability of the developed solar irradiance nowcasting method is evident according to the above findings.

6.3 Contributions of the Research

The aim of this research is to develop an appropriate solar irradiance nowcasting method to achieve reliable GHI, DNI and DHI nowcasting for buildings and their future development. In this case, a series of research activities were carried out, involving the systematic literature review of solar irradiance forecasting methods, the study of the forecasting horizons and spatial-temporal resolutions, the exploration of nowcasting models, the investigation of low-cost equipment and user-friendly programming, the nowcasting of GHI, DNI and DHI, the results verification and analysis of GHI, DNI and DHI nowcasting, the discussion of current and potential nowcasting applications on buildings. Based on the above research activities, the main contributions of the research are summarised as follows:

- Systematic Review from An Architectural Perspective.

  At first, this research conducts a systematic literature review of solar irradiance forecasting methods over the past 20 years and then specifically reviews and analyses emerging solar irradiance nowcasting methods from an architectural perspective. In contrast to other literature reviews of solar irradiance forecasting methods, this review is based on a methodology of systematic review, contributing to a comprehensive and in-depth investigation of the state-of-the-art solar irradiance forecasting methods. More importantly, this review starts with a consideration of the nowcasting horizons and spatial-temporal resolution suitable for buildings to review current solar irradiance nowcasting methods applicable to buildings and their future development, which is the most critical difference from other literature reviews. In summary, this review fills the research gap in current literature reviews of solar irradiance forecasting methods, as current literature reviews often lack a clear review methodology and do not provide a targeted review from an architectural perspective.

- Development of A Solar Irradiance Nowcasting Method.

  In addition, the critical contribution of this research is the development of a solar irradiance nowcasting method with high spatial-temporal resolution by using a promising deep residual network model - ResNet-152, low-cost equipment and user-friendly programming to achieve the reliable nowcasting of GHI, DNI and DHI for buildings and their future development.

  First of all, the developed solar irradiance nowcasting method achieves a very short-term nowcasting horizon, high spatial resolution (2 km) and high temporal resolution (10 seconds, 1 minute, 5 minutes and 10 minutes), which are appropriate for the applications of buildings. This fills the research gap in the study of the nowcasting horizon and spatial-temporal resolution suitable for buildings.

  Secondly, the proposed solar irradiance nowcasting method applies a promising deep residual network model - ResNet-152 as the nowcasting model, which is well suited for complex image recognition and categorisation tasks and has rarely been used in the field of solar irradiance forecasting.

  Thirdly, low-cost equipment and user-friendly programming are utilised in the proposed solar irradiance nowcasting method, which contributes to popularising the nowcasting method for the daily applications of buildings. In practical operation, the time consumption of this nowcasting method, from capturing a cloud image to generating a nowcasting value of solar irradiance, is less than 20 seconds, which is evidently faster than most studies in the same field. Less time consumption of solar irradiance nowcasting means more possible applications of buildings can be developed. In a word, the utilisation of low-cost equipment and user-friendly programming effectively reduces the cost, complexity, and time consumption of building applications. Also, the organisation and installation of a range of equipment are articulated, and a lot of programming work for each research step is ready to be open-sourced in

the future. These efforts will both provide a valuable foundation for subsequent researchers.

At last, unlike most studies that focus on the forecasting of GHI or DNI, the proposed solar irradiance nowcasting method achieves the nowcasting of three critical components of solar irradiance, including GHI, DNI, and DHI, that fills the gap in the studies of DHI forecasting.

- Comparative Tests of the Effect of Different Factors on Solar Irradiance Nowcasting.

  Moreover, this research articulates the effect of different factors involving time interval, nowcasting horizons, sky conditions, forecasting models and datasets on solar irradiance nowcasting using a series of comparative tests that are seldom completed by others.

  At first, the results of the comparative tests of nowcasting performance at various time intervals indicate that 1-min time interval is likely to be the optimal time interval for solar irradiance nowcasting based on accuracy and building practicality. The effect of time intervals has hardly been studied by others, and thus, the findings in this group of comparative tests are valuable and fill the research gap in the study of the effect of time intervals on solar irradiance nowcasting.

  Secondly, the negative correlation between nowcasting horizon and nowcasting performance is demonstrated based on the results of comparative tests of nowcasting performance for various nowcasting, as well as the proposed solar irradiance nowcasting method in very short-term nowcasting can achieve a comparable performance compared with most advanced studies.

  Thirdly, comparative tests of nowcasting performance under different sky conditions are conducted to explore both the effect of sky conditions at different dates and at different moments on a representative date on solar

irradiance nowcasting. The results show that the accuracy of the proposed solar irradiance nowcasting method under clear, light cloudy and overcast sky conditions is higher than many studies, but like most studies, the nowcasting accuracy of DNI under heavy cloudy sky conditions is not ideal enough. In other word, heavy cloudy is the only sky condition negatively affect the nowcasting accuracy, especially for DNI nowcasting. Despite this, the performance of the proposed solar irradiance nowcasting method is reliable in most sky conditions that demonstrates its practicality for buildings.

Fourthly, the comparative tests of nowcasting performance among different models compare the proposed nowcasting model - ResNet-152 with a benchmark model - PM and a baseline model – MLP, which are commonly used for comparison in many studies. Although the nowcasting accuracy of PM is extremely high in very short-term nowcasting horizons, the nowcasting accuracy of ResNet-152 achieves the close level for 1-min nowcasting horizon and even better for 5-min and 10-min nowcasting horizons. Compared to MLP, the superiority of ResNet-152 for solar irradiance nowcasting is very clear. Thus, the proposed nowcasting model - ResNet-152, is verified better than a benchmark model - PM and a baseline model - MLP, according to accuracy and building practicality that demonstrates the promise of ResNet-152 as a nowcasting model.

Finally, this research innovatively explores the effect of the data range of training set and the influence of the seasonality of testing set on nowcasting accuracy that achieve opposite findings, which gives insight into the dataset selection for solar irradiance nowcasting.

- Verification of The Nowcasting Results based on Various Evaluation Metrics.

  Furthermore, this research investigates the characteristics and popularity of evaluation metrics, including MAE, RMSE, nMAE, nRMSE, skill score (SS), r, etc. and selects appropriate evaluation metrics to evaluate the nowcasting

performance from various perspectives. That fills the research gap in the study of evaluation metrics for solar irradiance forecasting methods.

Based on the comparative tests and verification, the performance of the developed solar irradiance nowcasting method is proven to be reliable under the impact of different factors. In contrast to some Bottom-up forecast methods, those applying complex image processing techniques, the developed solar irradiance nowcasting method demonstrates similar or higher accuracy. In addition, although the developed solar irradiance nowcasting method presents a relatively low accuracy in terms of absolute indicators compared to some advanced Hybrid methods, their difference is not significant according to relative indicators. Thus, the overall reliability of the developed solar irradiance nowcasting is evident.

- Discussion of Current and Potential Building Applications of Solar Irradiance Nowcasting Method.

  Finally, this research discusses the current and potential applications of solar irradiance nowcasting method in current or future buildings, which fills the research gap in the discussion about application of solar irradiance nowcasting method on buildings and provides a foundation and future research directions for the application of the nowcasting method on buildings.

6.4 Future Works

Based on all research activities, research findings and limitations of the research, a range of promising future works is listed as follows:

- Optimisation of Image Processing Techniques

  Optimising image processing techniques is one major direction for future research. At first, the preprocessing procedures of the image can be improved. For instance, the application of thresholding techniques to meticulously recognize image pixels, followed by the simplification of the recognised image data through grayscale conversion and binarization may significantly enhance the processing efficiency of nowcasting models. Furthermore, the utilization of advanced deep learning models for the preliminary classification of images allows these categorised groups of images to serve as training data for different nowcasting models, which can potentially enhance the accuracy and relevance of the models. Diverse image processing techniques can be used individually or in combination to solve specific image processing tasks.

- Optimisation of Nowcasting Model

  The optimisation of nowcasting model is pivotal for future research. Firstly, the performance of nowcasting model can be improved by adjusting the model training parameters, such as learning rate, batch size, epochs, loss function, etc. For example, the learning rate of nowcasting model can be strategically adjusted to prevent overfitting or underfitting. More importantly, different deep learning models, such as CNN, RNN, LSTM, can be applied in combination to optimise performance of nowcasting model. For instance, a Hybrid method using ResNet and LSTM is well suited for processing those tasks that require an understanding of both spatial and temporal dynamics, such as the machine learning of consecutive cloud images or cloud movement videos. Thus, the Hybrid method can potentially improve the nowcasting performance.

- Exploration of Nowcasting Impact Factors

  In addition to the optimisation of nowcasting method, more exploration of nowcasting impact factors is essential to future research because they are related to the generalisation of nowcasting method. First, the impact of more diverse datasets from various locations, months, and seasons needs to be studied. Moreover, the nowcasting performance for longer forecasting horizons, such as 15 to 20 minutes. Furthermore, more popular deep learning models, including LSTM, SVM, ANN, etc. can be compared with the developed nowcasting model to explore the influence of models on nowcasting accuracy.

- Improvements in Hardware and Software

  Improvements in hardware and software are also needed in future research. In terms of hardware, the proposed nowcasting method heavily relies on the low-cost ground-based sky camera and thus faces system maintenance issues induced by environmental effects on the camera, including rain, frosting, insects, etc. With respect to software, some building simulation programs are not compatible with very high temporal resolution nowcasting (such as 1 minute) and therefore need to be improved.

- Optimisation of Building Performance

  Utilising the developed solar irradiance nowcasting method to optimise building performance involving operational efficiency, safety and occupant comfort is the ultimate goal of future research. At first, future research can apply 1 to 5-minute nowcasting to optimise building energy management and protect solar systems because very short-term nowcasting horizons can help buildings respond effectively to “Ramp Events”. In addition, with the development of integrated smart building systems in the future, 5 to 30-minute nowcasting can be combined with the control of HVAC, lighting and shading systems to adjust the thermal and visual comfort in buildings.

6.5 Conclusion

This research begins with concerns about the concern of environmental problems, global greenhouse gas emissions and building carbon emissions and goes on to the development of a solar irradiance nowcasting method appropriate for buildings and their future development.

The main research activities started with a systematic literature review of solar irradiance forecasting methods, which comprehensively reviewed the current state of research and identified the forecasting methods appropriate for buildings according to the characteristics of these methods. Then, based on the study of previous research, a solar irradiance nowcasting method with high spatial-temporal resolution based on low-cost equipment and user-friendly programming was developed to achieve reliable nowcasting of GHI, DNI and DHI. After that, a series of comparative experiments were conducted to explore the impact of different factors, including time intervals, forecasting horizons, sky conditions, forecasting models and datasets, on nowcasting performance and a range of evaluation metrics were used to verify the reliability of the nowcasting. Finally, the current and potential applications of solar irradiance nowcasting method in buildings were discussed to demonstrate the profound value of this research.

Based on the above, the main contributions of this research include the systematic review of solar irradiance forecasting methods from an architectural perspective, the development of a solar irradiance nowcasting method, the comparative tests of the effect of different factors on solar irradiance nowcasting, the verification of the nowcasting results based on various evaluation metrics and the discussion of current and potential building applications of the nowcasting method.

The main limitations of this research relate to the amount of data and diversity of datasets, image processing techniques, training time, nowcasting model, stability of equipment operation, design of comparative tests, and research for practical building

applications. In this case, the promising future works mainly involve optimisation of image processing techniques, optimisation of nowcasting model, exploration of nowcasting impact factors, improvements in hardware and software, and optimisation of building performance.

In conclusion, the significance of this research is to innovatively explore a solar irradiance nowcasting method from an architectural perspective and achieve reliable nowcasting of GHI, DNI and DHI, which are foundations for applying solar irradiance nowcasting to optimise the operational efficiency and safety, occupant comfort and design of buildings. In addition, the development of solar irradiance nowcasting method establishes an interdisciplinary research methodology integrating the knowledge of meteorology, imagery, computer science and architecture, which can increase interdisciplinary communication and cooperation, as well as provide more research directions. Furthermore, the specific approaches, tools and outcomes of the research, as well as the discussion of the possible applications of solar irradiance nowcasting on buildings, provide initial inspiration for future research and the future development of buildings. Ultimately, from a broader perspective, this research is not only of significance to the academic community and practical applications, but also has profound social and economic impacts, including improving the comfort of the living and working environment, supporting sustainable development goals, enhancing energy efficiency and long-term financial benefits.

Bibliography

[1] W.M.O. (WMO), The World Meteorological Organization's (WMO) Provisional Statement of Global Climate 2023, (2023). https://wmo.int/publication-series/provisional-state-of-global-climate-2023

[2] X. Chen, Solar Photovoltaic Power Intermittency Under Passing Clouds: Control, Forecasting, and Emulation, The University of Liverpool (United Kingdom), 2021.

[3] I. Dincer, Renewable energy and sustainable development: a crucial review, Renewable and sustainable energy reviews, 4(2) (2000) 157-175.

[4] T. Blaschke, M. Biberacher, S. Gadocha, I. Schardinger, 'Energy landscapes': Meeting energy demands and human aspirations, Biomass and Bioenergy, 55 (2013) 3-16.

[5] Q. Schiermeier, J. Tollefson, T. Scully, A. Witze, O. Morton, Energy alternatives: Electricity without carbon, Nature, 454(7206) (2008) 816-823.

[6] R. Foster, M. Ghassemi, A. Cota, Solar energy: renewable energy and the environment, CRC press, 2009.

[7] V. Devabhaktuni, M. Alam, S. Shekara Sreenadh Reddy Depuru, R.C. Green, D. Nims, C. Near, Solar energy: Trends and enabling technologies, Renewable and Sustainable Energy Reviews, 19 (2013) 555-564.

[8] D.R. Myers, K. Emery, T. Stoffel, Uncertainty estimates for global solar irradiance measurements used to evaluate PV device performance, Solar Cells, 27(1-4) (1989) 455-464.

[9] L. Chen, Y. Li, H. Du, Y. Lai, Solar radiation nowcasting through advanced CNN model integrated with ResNet structure, Building Simulation 2021, (2021).

[10] D. Yang, J. Kleissl, C.A. Gueymard, H.T.C. Pedro, C.F.M. Coimbra, History and trends in solar irradiance and PV power forecasting: A preliminary assessment and review using text mining, Solar Energy, 168 (2018) 60-101.

[11] S. Sobri, S. Koohi-Kamali, N.A. Rahim, Solar photovoltaic generation forecasting methods: A review, Energy Conversion and Management, 156 (2018) 459-497.

[12] M. Diagne, M. David, P. Lauret, J. Boland, N. Schmutz, Review of solar irradiance forecasting methods and a proposition for small-scale insular grids, Renewable and Sustainable Energy Reviews, 27 (2013) 65-76.

[13] U.N.E. Programme, 2021 Global Status Report for Buildings and Construction: Towards a Zero-emission, Efficient and Resilient Buildings and Construction Sector, (2021).

[14] X. Sun, Z. Gou, S.S.-Y. Lau, Cost-effectiveness of active and passive design strategies for existing building retrofits in tropical climate: Case study of a zero energy building, Journal of Cleaner Production, 183 (2018) 35-45.

[15] Q. Ha, M.D. Phung, IoT-enabled dependable control for solar energy harvesting in smart buildings, IET Smart Cities, 1(2) (2019) 61-70.

[16] G. Notton, G.A. Faggianelli, C. Voyant, S. Ouedraogo, G. Pigelet, J.-L. Duchaud, Solar radiation forecasting for smart building applications, in: Computational Intelligence Techniques for Green Smart Cities, Springer, 2022, pp. 229-247.

[17] A. Manur, M. Marathe, A. Manur, A. Ramachandra, S. Subbarao, G. Venkataramanan, Smart solar home system with solar forecasting, 2020 IEEE International Conference on Power Electronics, Smart Grid and Renewable Energy (PESGRE2020), (2020) 1-6.

[18] B.J. Martins, A. Cerentini, S.L. Mantelli, T.Z.L. Chaves, N.M. Branco, A. von Wangenheim, R. Rüther, J.M. Arrais, Systematic review of nowcasting approaches for solar energy production based upon ground-based cloud imaging, Solar Energy Advances, 2 (2022) 100019.

[19] D. Lazos, A.B. Sproul, M. Kay, Optimisation of energy management in commercial buildings with weather forecasting inputs: A review, Renewable and Sustainable Energy Reviews, 39 (2014) 587-603.

[20] C. Fan, F. Xiao, S. Wang, Development of prediction models for next-day building energy consumption and peak power demand using data mining techniques, Applied Energy, 127 (2014) 1-10.

[21] M. Diagne, M. David, P. Lauret, J. Boland, N. Schmutz, Review of solar irradiance forecasting methods and a proposition for small-scale insular grids, Renewable & Sustainable Energy Reviews, 27 (2013) 65-76.

[22] H.B. Tolabi, M.H. Moradi, S.B.M. Ayob, A review on classification and comparison of different models in solar radiation estimation, International Journal of Energy Research, 38(6) (2014) 689-701. 10.1002/er.3161

[23] E.W. Law, A.A. Prasad, M. Kay, R.A. Taylor, Direct normal irradiance forecasting and its application to concentrated solar thermal output forecasting–A review, Solar Energy, 108 (2014) 287-307.

[24] P. Kumari, D. Toshniwal, Deep learning models for solar irradiance forecasting: A comprehensive review, Journal of Cleaner Production, 318 (2021) 128566.

[25] R. Samu, M. Calais, G.M. Shafiullah, M. Moghbel, M.A. Shoeb, B. Nouri, N. Blum, Applications for solar irradiance nowcasting in the control of microgrids: A review, Renewable and Sustainable Energy Reviews, 147 (2021) 111187.

[26] S. Etxebarria Berrizbeitia, E. Jadraque Gago, T. Muneer, Empirical Models for the Estimation of Solar Sky-Diffuse Radiation. A Review and Experimental Analysis, Energies, 13(3) (2020).

[27] E.S.M.A. Program, Global photovoltaic power potential by country, World Bank, 2020.

[28] H. Du, C.F. Bandera, L. Chen, Nowcasting methods for optimising building performance, (2019).

[29] B. Dong, K.P. Lam, A real-time model predictive control for building heating and cooling systems based on the occupancy behavior pattern detection and local weather forecasting, Building Simulation, (2014) 89-106.

[30] R. Enríquez, M.J. Jiménez, M. del Rosario Heras, Solar forecasting requirements for buildings MPC, Energy Procedia, 91 (2016) 1024-1032.

[31] F. Oldewurtel, A. Parisio, C.N. Jones, D. Gyalistras, M. Gwerder, V. Stauch, B. Lehmann, M. Morari, Use of model predictive control and weather forecasts for energy efficient building climate control, Energy and buildings, 45 (2012) 15-27.

[32] F. Ozgen, M. Esen, H. Esen, Experimental investigation of thermal performance of a double-flow solar air heater having aluminium cans, Renewable Energy, 34(11) (2009) 2391-2398.

[33] R.H. Inman, H.T.C. Pedro, C.F.M. Coimbra, Solar forecasting methods for renewable energy integration, Progress in Energy and Combustion Science, 39(6) (2013) 535-576.

[34] J. Antonanzas, N. Osorio, R. Escobar, R. Urraca, F.J. Martinez-de-Pison, F. Antonanzas-Torres, Review of photovoltaic power forecasting, Solar energy, 136 (2016) 78-111.

[35] F. Lin, Y. Zhang, J. Wang, Recent advances in intra-hour solar forecasting: A review of ground-based sky image methods, International Journal of Forecasting, 39(1) (2023) 244-265.

[36] J. Tian, R. Ooka, D. Lee, Multi-scale solar radiation and photovoltaic power forecasting with machine learning algorithms in urban environment: A state-of-the-art review, Journal of Cleaner Production, (2023) 139040.

[37] R.H. Inman, H.T. Pedro, C.F. Coimbra, Solar forecasting methods for renewable energy integration, Progress in energy and combustion science, 39(6) (2013) 535-576.

[38] P.A. Jimenez, J.P. Hacker, J. Dudhia, S.E. Haupt, J.A. Ruiz-Arias, C.A. Gueymard, G. Thompson, T. Eidhammer, A. Deng, WRF-Solar: Description and clear-sky assessment of an augmented NWP model for solar power prediction, Bulletin of the American Meteorological Society, 97(7) (2016) 1249-1264.

[39] P. Mathiesen, J. Kleissl, Evaluation of numerical weather prediction for intra-day solar forecasting in the continental, Weather and Forecasting, 8(4) (1984) 401-411.

[40] H. Yang, J. Kleissl, Preprocessing WRF initial conditions for coastal stratocumulus forecasting, Solar Energy, 133 (2016) 180-193.

[41] P. Mathiesen, C. Collier, J. Kleissl, A high-resolution, cloud-assimilating numerical weather prediction model for solar irradiance forecasting, Solar Energy, 92 (2013) 47-61. 10.1016/j.solener.2013.02.018

[42] V. Lara-Fanego, J.A. Ruiz-Arias, A.D. Pozo-Vazquez, C.A. Gueymard, J. Tovar-Pescador, Evaluation Of DNI Forecast Based On The WRF Mesoscale Atmospheric Model For CPV Applications, in: F. Dimroth, F. Rubio, I. Anton (Eds.) 8th International Conference on Concentrating Photovoltaic Systems, Vol. 1477, 2012, pp. 317-322.

[43] J.C. Cao, S. Cao, Study of forecasting solar irradiance using neural networks with preprocessing sample data by wavelet analysis, Energy, 31(15) (2006) 3435-3445.

[44] V. Sharma, D. Yang, W. Walsh, T. Reindl, Short term solar irradiance forecasting using a mixed wavelet neural network, Renewable Energy, 90 (2016) 481-492. 10.1016/j.renene.2016.01.020

[45] Y. Chu, C.F.M. Coimbra, Short-term probabilistic forecasts for Direct Normal Irradiance, Renewable Energy, 101 (2017) 526-536. 10.1016/j.renene.2016.09.012

[46] H. Jiang, Y. Dong, A nonlinear support vector machine model with hard penalty function based on glowworm swarm optimization for forecasting daily global solar radiation, Energy conversion and management, 126 (2016) 991-1002.

[47] S. Al-Alawi, H. Al-Hinai, An ANN-based approach for predicting global radiation in locations with no direct measurement instrumentation, Renewable Energy, 14(1-4) (1998) 199-204.

[48] A. Mellit, H. Eleuch, M. Benghanem, C. Elaoun, A.M. Pavan, An adaptive model for predicting of global, direct and diffuse hourly solar irradiance, Energy Conversion and Management, 51(4) (2010) 771-782.

[49] D. Yang, V. Sharma, Z. Ye, L.I. Lim, L. Zhao, A.W. Aryaputera, Forecasting of global horizontal irradiance by exponential smoothing, using decompositions, Energy, 81 (2015) 111-119. 10.1016/j.energy.2014.11.082

[50] C. Join, C. Voyant, M. Fliess, M. Muselli, M. Nivet, C. Paoli, F. Chaxel, Short-term solar irradiance and irradiation forecasts via different time series techniques: A preliminary study, 3rd International Symposium on Environmental Friendly Energies and Applications (EFEA), (2014) 1-6.

[51] A.S. Dorvlo, J.A. Jervase, A. Al-Lawati, Solar radiation estimation using artificial neural networks, Applied Energy, 71(4) (2002) 307-319.

[52] C. Chen, S. Duan, T. Cai, B. Liu, Online 24-h solar power forecasting based on weather type classification using artificial neural network, Solar energy, 85(11) (2011) 2856-2870.

[53] C. Renno, F. Petito, A. Gatto, ANN model for predicting the direct normal irradiance and the global radiation for a solar application to a residential building, Journal of Cleaner Production, 135 (2016) 1298-1316.

[54] A. Sfetsos, A.H. Coonick, Univariate and multivariate forecasting of hourly solar radiation with artificial intelligence techniques, Solar Energy, 68(2) (2000) 169-178.

[55] H. Jiang, Y. Dong, A Novel Model Based on Square Root Elastic Net and Artificial Neural Network for Forecasting Global Solar Radiation, Complexity, (2018).

[56] Y. Chu, C.F. Coimbra, Short-term probabilistic forecasts for direct normal irradiance, Renewable Energy, 101 (2017) 526-536.

[57] A. Hammer, D. Heinemann, E. Lorenz, B. Lückehe, Short-term forecasting of solar radiation: a statistical approach using satellite data, Solar Energy, 67(1-3) (1999) 139-150.

[58] E. Lorenz, A. Hammer, D. Heinemann, Short term forecasting of solar radiation based on satellite data, EUROSUN2004 (ISES Europe Solar Congress), (2004) 2004.

[59] R. Perez, S. Kivalov, J. Schlemmer, K. Hemker, D. Renné, T.E. Hoff, Validation of short and medium term operational solar radiation forecasts in the US, Solar Energy, 84(12) (2010) 2161-2172.

[60] L. Nonnenmacher, C.F.M. Coimbra, Streamline-based method for intra-day solar forecasting through remote sensing, Solar Energy, 108 (2014) 447-459.

[61] M. Cervantes, H. Krishnaswami, W. Richardson, R. Vega, Utilization of Low Cost, Sky-Imaging Technology for Irradiance Forecasting of Distributed Solar Generation, 2016 IEEE Green Technologies Conference (GreenTech), (2016) 142-146.

[62] W. Richardson Jr, H. Krishnaswami, R. Vega, M. Cervantes, A low cost, edge computing, all-sky imager for cloud tracking and intra-hour irradiance forecasting, Sustainability, 9(4) (2017) 482.

[63] R. Marquez, C.F. Coimbra, Intra-hour DNI forecasting based on cloud tracking image analysis, Solar Energy, 91 (2013) 327-336.

[64] W. Richardson, H. Krishnaswami, Jr., R. Vega, M. Cervantes, A Low Cost, Edge Computing, All-Sky Imager for Cloud Tracking and Intra-Hour Irradiance Forecasting, Sustainability, 9(4) (2017). 10.3390/su9040482

[65] D. Bernecker, C. Riess, E. Angelopoulou, J. Hornegger, Continuous short-term irradiance forecasts using sky images, Solar Energy, 110 (2014) 303-315. 10.1016/j.solener.2014.09.005

[66] H. Yang, B. Kurtz, D. Nguyen, B. Urquhart, C.W. Chow, M. Ghonima, J. Kleissl, Solar irradiance forecasting using a ground-based sky imager developed at UC San Diego, Solar Energy, 103 (2014) 502-524.

[67] Z. Peng, D. Yu, D. Huang, J. Heiser, S. Yoo, P. Kalb, 3D cloud detection and tracking system for solar forecast using multiple sky imagers, Solar Energy, 118 (2015) 496-519.

[68] C. Voyant, M. Muselli, C. Paoli, M.-L. Nivet, Numerical weather prediction (NWP) and hybrid ARMA/ANN model to predict global radiation, Energy, 39(1) (2012) 341-355.

[69] Y. Chu, H.T.C. Pedro, C.F.M. Coimbra, Hybrid intra-hour DNI forecasts with sky image processing enhanced by stochastic learning, Solar Energy, 98 (2013) 592-603. 10.1016/j.solener.2013.10.020

[70] F.J.L. Lima, F.R. Martins, E.B. Pereira, E. Lorenz, D. Heinemann, Forecast for surface solar irradiance at the Brazilian Northeastern region using NWP model and artificial neural networks, Renewable Energy, 87 (2016) 807-818.

[71] R. Marquez, H.T.C. Pedro, C.F.M. Coimbra, Hybrid solar forecasting method uses satellite imaging and ground telemetry as inputs to ANNs, Solar Energy, 92 (2013) 176-188.

[72] W. Ji, K.C. Chee, Prediction of hourly solar radiation using a novel hybrid model of ARMA and TDNN, Solar Energy, 85(5) (2011) 808-817.

[73] C. Voyant, G. Notton, S. Kalogirou, M.-L. Nivet, C. Paoli, F. Motte, A. Fouilloy, Machine learning methods for solar radiation forecasting: A review, Renewable Energy, 105 (2017) 569-582. 10.1016/j.renene.2016.12.095

[74] M.Q. Raza, M. Nadarajah, C. Ekanayake, On recent advances in PV output power forecast, Solar Energy, 136 (2016) 125-144.

[75] J. Kleissl, Solar energy forecasting and resource assessment, Academic Press, 2013.

[76] D. Wang, L. Hu, H. Du, Y. Liu, J. Huang, Y. Xu, J. Liu, Classification, experimental assessment, modeling methods and evaluation metrics of Trombe walls, Renewable and Sustainable Energy Reviews, 124 (2020) 109772.

[77] R.M. Pereira, C. Silva Santos, A. Rocha, Solar irradiance modelling using an offline coupling procedure for the Weather Research and Forecasting (WRF) model, Solar Energy, 188 (2019) 339-352. 10.1016/j.solener.2019.06.020

[78] V.E. Larson, Chapter 12 - Forecasting Solar Irradiance with Numerical Weather Prediction Models, in: J. Kleissl (Ed.) Solar Energy Forecasting and Resource Assessment, Academic Press, Boston, 2013, pp. 299-318.

[79] I.I. Prado-Rujas, A. García-Dopico, E. Serrano, M.S. Pérez, A Flexible and Robust Deep Learning-Based System for Solar Irradiance Forecasting, IEEE Access, 9 (2021) 12348-12361. 10.1109/ACCESS.2021.3051839

[80] M. Diagne, M. David, J. Boland, N. Schmutz, P. Lauret, Post-processing of solar irradiance forecasts from WRF model at Reunion Island, Solar Energy, 105 (2014) 99-108. 10.1016/j.solener.2014.03.016

[81] R.A. Verzijlbergh, P.W. Heijnen, S.R. de Roode, A. Los, H.J.J. Jonker, Improved model output statistics of numerical weather prediction based irradiance forecasts for solar power applications, Solar Energy, 118 (2015) 634-645. 10.1016/j.solener.2015.06.005

[82] J.A. Lee, S.E. Haupt, P.A. Jimenez, M.A. Rogers, S.D. Miller, T.C. McCandless, Solar Irradiance Nowcasting Case Studies near Sacramento, Journal of Applied Meteorology and Climatology, 56(1) (2017) 85-108. 10.1175/jamc-d-16-0183.1

[83] S.D. Miller, M.A. Rogers, J.M. Haynes, M. Sengupta, A.K. Heidinger, Short-term solar irradiance forecasting via satellite/model coupling, Solar Energy, 168 (2018) 102-117. 10.1016/j.solener.2017.11.049

[84] A. Rincón, O. Jorba, M. Frutos, L. Alvarez, F.P. Barrios, J.A. González, Bias correction of global irradiance modelled with weather and research forecasting model over Paraguay, Solar Energy, 170 (2018) 201-211.

[85] J. Dersch, M. Schroedter-Homscheidt, K. Gairaa, N. Hanrieder, T. Landelius, M. Lindskog, S.C. Mueller, L.R. Santigosa, T. Sirch, S. Wilbert, Impact of DNI nowcasting on annual revenues of CSP plants for a time of delivery based feed in tariff, Meteorologische Zeitschrift, 28(3) (2019) 235-253.

[86] F. Kurzrock, H. Nguyen, J. Sauer, F.C. Ming, S. Cros, W.L. Smith, Jr., P. Minnis, R. Palikonda, T.A. Jones, C. Lallemand, L. Linguet, G. Lajoie, Evaluation of WRF-DART (ARW v3.9.1.1 and DART Manhattan release) multiphase cloud water path assimilation for short-term solar irradiance forecasting in a tropical environment, Geoscientific Model Development, 12(9) (2019) 3939-3954.

[87] S. Gentile, F. Di Paola, D. Cimini, D. Gallucci, E. Geraldi, S. Larosa, S.T. Nilo, E. Ricciardelli, E. Ripepi, M. Viggiano, F. Romano, 3D-VAR Data Assimilation of SEVIRI Radiances for the Prediction of Solar Irradiance in Italy Using WRF Solar Mesoscale Model-Preliminary Results, Remote Sensing, 12(6) (2020).

[88] J.E. Sanchez-Lopez, J. Solís-García, J.C. Riquelme, Semi-real-time decision tree ensemble algorithms for very short-term solar irradiance forecasting, International Journal of Electrical Power & Energy Systems, 158 (2024) 109947.

[89] T. Han, R. Li, X. Wang, Y. Wang, K. Chen, H. Peng, Z. Gao, N. Wang, Q. Peng, Intra-hour solar irradiance forecasting using topology data analysis and physics-driven deep learning, Renewable Energy, 224 (2024) 120138.

[90] X. Huang, Q. Li, Y. Tai, Z. Chen, J. Zhang, J. Shi, B. Gao, W. Liu, Hybrid deep neural model for hourly solar irradiance forecasting, Renewable Energy, 171 (2021) 1041-1060.

[91] M. Demirtas, M. Yesilbudak, S. Sagiroglu, I. Colak, Prediction of solar radiation using meteorological data, 2012 International Conference on Renewable Energy Research and Applications (ICRERA), (2012) 1-4. 10.1109/ICRERA.2012.6477329

[92] G.M. Tina, S. De Fiore, C. Ventura, Analysis of forecast errors for irradiance on the horizontal plane, Energy Conversion and Management, 64 (2012) 533-540.

[93] S. Basterrech, L. Zjavka, L. Prokop, S. Mišák, Irradiance prediction using Echo State Queueing Networks and Differential polynomial Neural Networks, 2013 13th International Conference on Intellient Systems Design and Applications, (2013) 271-276.

[94] U. Nalina, V. Prema, K. Smitha, K.U. Rao, Multivariate regression for prediction of solar irradiance, 2014 International Conference on Data Science & Engineering (ICDSE), (2014) 177-181.

[95] T. Zhu, H. Wei, X. Zhao, C. Zhang, K. Zhang, Clear-sky model for wavelet forecast of direct normal

irradiance, Renewable Energy, 104 (2017) 1-8.

[96] A. Takilalte, S. Harrouni, J. Mora, Forecasting global solar irradiance for various resolutions using time series models-case study: Algeria, Energy Sources Part a-Recovery Utilization and Environmental Effects, (2019).

[97] I. Lillo-Bravo, M. Larrañeta, E. Núñez-Ortega, R. González-Galván, Simplified model to correct thermopile pyranometer solar radiation measurements for photovoltaic module yield estimation, Renewable Energy, 146 (2020) 1486-1497.

[98] H. Wang, R. Cai, B. Zhou, S. Aziz, B. Qin, N. Voropai, L. Gan, E. Barakhtenko, Solar irradiance forecasting based on direct explainable neural network, Energy Conversion and Management, 226 (2020) 113487.

[99] F. Rodríguez, F. Martín, L. Fontán, A. Galarza, Ensemble of machine learning and spatiotemporal parameters to forecast very short-term solar irradiation to compute photovoltaic generators' output power, Energy, 229 (2021) 120647.

[100] M. Jaihuni, J.K. Basak, F. Khan, F.G. Okyere, T. Sihalath, A. Bhujel, J. Park, D.H. Lee, H.T. Kim, A novel recurrent neural network approach in forecasting short term solar irradiance, ISA Transactions, 121 (2022) 63-74.

[101] V. Voicu, D. Petreus, R. Etz, Solar Irradiance Nowcasting using IoT with LSTM-RNN, 2022 IEEE 28th International Symposium for Design and Technology in Electronic Packaging (SIITME), (2022) 82-86.

[102] D. Yang, C. Gu, Z. Dong, P. Jirutitijaroen, N. Chen, W.M. Walsh, Solar irradiance forecasting using spatial-temporal covariance structures and time-forward kriging, Renewable Energy, 60 (2013) 235-245.

[103] R. Dambreville, P. Blanc, J. Chanussot, D. Boldo, Very short term forecasting of the Global Horizontal Irradiance using a spatio-temporal autoregressive model, Renewable Energy, 72 (2014) 291-300.

[104] I. Zliobaite, J. Hollmen, H. Junninen, Regression models tolerant to massively missing data: a case study in solar-radiation nowcasting, Atmospheric Measurement Techniques, 7(12) (2014) 4387-4399.

[105] H.T.C. Pedro, C.F.M. Coimbra, Short-term irradiance forecastability for various solar micro-climates, Solar Energy, 122 (2015) 587-602.

[106] J. Li, J.K. Ward, J. Tong, L. Collins, G. Platt, Machine learning for solar irradiance forecasting of photovoltaic system, Renewable Energy, 90 (2016) 542-553.

[107] T.A. Fathima, V. Nedumpozhimana, Y.H. Lee, S. Winkler, S. Dev, A Chaotic Approach on Solar Irradiance Forecasting, 2019 Photonics & Electromagnetics Research Symposium - Fall (PIERS - Fall), (2019) 2724-2728.

[108] S. Gbémou, H. Tolba, S. Thil, S. Grieu, Global horizontal irradiance forecasting using online sparse Gaussian process regression based on quasiperiodic kernels, 2019 IEEE International Conference on Environment and Electrical Engineering and 2019 IEEE Industrial and Commercial Power Systems Europe (EEEIC / I&CPS Europe), (2019) 1-6.

[109] H. Tolba, N. Dkhili, J. Nou, J. Eynard, S. Thil, S. Grieu, GHI forecasting using Gaussian process

regression: kernel study, Ifac Papersonline, 52(4) (2019) 455-460.

[110] J. Huertas-Tato, R. Aler, I.M. Galván, F.J. Rodríguez-Benítez, C. Arbizu-Barrena, D. Pozo-Vázquez, A short-term solar radiation forecasting system for the Iberian Peninsula. Part 2: Model blending approaches based on machine learning, Solar Energy, 195 (2020) 685-696.

[111] D. Cannizzaro, A. Aliberti, L. Bottaccioli, E. Macii, A. Acquaviva, E. Patti, Solar radiation forecasting based on convolutional neural network and ensemble learning, Expert Systems with Applications, 181 (2021) 115167.

[112] M. Castangia, A. Aliberti, L. Bottaccioli, E. Macii, E. Patti, A compound of feature selection techniques to improve solar radiation forecasting, Expert Systems with Applications, 178 (2021) 114979.

[113] A. Bhatt, W. Ongsakul, N.M. M, J.G. Singh, Sliding window approach with first-order differencing for very short-term solar irradiance forecasting using deep learning models, Sustainable Energy Technologies and Assessments, 50 (2022) 101864.

[114] S.M. Ruffing, G.K. Venayagamoorthy, Short to Medium Range Time Series Prediction of Solar Irradiance Using an Echo State Network, 2009 15th International Conference on Intelligent System Applications to Power Systems, (2009) 1-6.

[115] L. Mora-Lopez, J. Mora, M. Piliougine, M. Sidrach-de-Cardona, An Intelligent Memory Model for Short-Term Prediction: An Application to Global Solar Radiation Data, in: N. GarciaPedrajas, F. Herrera, C. Fyfe, J.M. Benitez, M. Ali (Eds.) Trends in Applied Intelligent Systems, Pt Iii, Proceedings, Vol. 6098, 2010, pp. 596-+.

[116] J.M. Gomes, P.M. Ferreira, A.E. Ruano, Implementation of an intelligent sensor for measurement and prediction of solar radiation and atmospheric temperature, 2011 IEEE 7th International Symposium on Intelligent Signal Processing, (2011) 1-6.

[117] Z. Wang, F. Wang, S. Su, Solar Irradiance Short-Term Prediction Model Based on BP Neural Network, Energy Procedia, 12 (2011) 488-494.

[118] T. Khatib, A. Mohamed, K. Sopian, M. Mahmoud, Assessment of Artificial Neural Networks for Hourly Solar Radiation Prediction, International Journal of Photoenergy, (2012).

[119] K.A. Baharin, H.A. Rahman, M.Y. Hassan, G.C. Kim, Hourly irradiance forecasting for Peninsular Malaysia using dynamic neural network with preprocessed data, 2013 IEEE Student Conference on Research and Developement, (2013) 191-197.

[120] S. Wang, Y. Xu, C. Fan, Short-term PV Generation System Forecasting Model without Solar Radiation Based on Improved Wavelet Neural Network, in: X. Tang, X. Chen, Y. Dong, X. Wei, Q. Yang (Eds.) Advances in Energy Science and Technology, Pts 1-4, Vol. 291-294, 2013, pp.83-88.

[121] A. Alzahrani, J.W. Kimball, C. Dagli, Predicting Solar Irradiance Using Time Series Neural Networks, Procedia Computer Science, 36 (2014) 623-628.

[122] K.A. Baharin, H.A. Rahman, M.Y. Hassan, C.K. Gan, Hourly irradiance forecasting in Malaysia using support vector machine, 2014 IEEE Conference on Energy Conversion (CENCON), (2014) 185-190.

[123] I. Colak, M. Yesilbudak, N. Genc, R. Bayindir, Multi-period Prediction of Solar Radiation Using ARMA and ARIMA Models, 2015 IEEE 14th International Conference on Machine Learning and

Applications (ICMLA), (2015) 1045-1049.

[124] P. Lauret, C. Voyant, T. Soubdhan, M. David, P. Poggi, A benchmarking of machine learning techniques for solar radiation forecasting in an insular context, Solar Energy, 112 (2015) 446-457.

[125] T.C. McCandless, S.E. Haupt, G.S. Young, A model tree approach to forecasting solar irradiance variability, Solar Energy, 120 (2015) 514-524.

[126] L.A. Teixeira Júnior, R.M.d. Souza, M.L.d. Menezes, K.M. Cassiano, J.F.M. Pessanha, R.C. Souza, ARTIFICIAL NEURAL NETWORK AND WAVELET DECOMPOSITION IN THE FORECAST OF GLOBAL HORIZONTAL SOLAR RADIATION, Pesquisa Operacional, 35(1) (2015) 73-90.

[127] S.L. Arun, M.P. Selvan, Very short term prediction of solar radiation for residential load scheduling in smartgrid, 2016 National Power Systems Conference (NPSC), (2016) 1-5.

[128] F.-V. Gutierrez-Corea, M.-A. Manso-Callejo, M.-P. Moreno-Regidor, M.-T. Manrique-Sancho, Forecasting short-term solar irradiance based on artificial neural networks and data from neighboring meteorological stations, Solar Energy, 134 (2016) 119-131.

[129] C.R. Hamilton, F. Maier, W.D. Potter, Hourly Solar Radiation Forecasting Through Model Averaged Neural Networks and Alternating Model Trees, in: H. Fujita, M. Ali, A. Selamat, J. Sasaki, M. Kurematsu (Eds.) Trends in Applied Knowledge-Based Systems and Data Science, Vol. 9799, 2016, pp. 737-750.

[130] L. Mazorra Aguiar, B. Pereira, P. Lauret, F. Diaz, M. David, Combining solar irradiance measurements, satellite-derived data and a numerical weather prediction model to improve intra-day solar forecasting, Renewable Energy, 97 (2016) 599-610.

[131] T.C. McCandless, S.E. Haupt, G.S. Young, A regime-dependent artificial neural network technique for short-range solar irradiance forecasting, Renewable Energy, 89 (2016) 351-359. 10.1016/j.renene.2015.12.030

[132] T.C. McCandless, G.S. Young, S.E. Haupt, L.M. Hinkelman, Regime-Dependent Short-Range Solar Irradiance Forecasting, Journal of Applied Meteorology and Climatology, 55(7) (2016) 1599-1613.

[133] A.A. Sharma, Univariate short term forecasting of solar irradiance using modified online backpropagation through time, 2016 International Computer Science and Engineering Conference (ICSEC), (2016) 1-6.

[134] K.Y. Bae, H.S. Jang, D.K. Sung, Hourly Solar Irradiance Prediction Based on Support Vector Machine and Its Error Analysis, Ieee Transactions on Power Systems, 32(2) (2017) 935-945.

[135] C.L. Dewangan, S.N. Singh, S. Chakrabarti, Solar irradiance forecasting using wavelet neural network, 2017 IEEE PES Asia-Pacific Power and Energy Engineering Conference (APPEEC), (2017) 1-6. 1

[136] I.A. Ibrahim, T. Khatib, A novel hybrid model for hourly global solar radiation prediction using random forests technique and firefly algorithm, Energy Conversion and Management, 138 (2017) 413-425.

[137] R. Jovanovic, L.M. Pomares, Y.E. Mohieldeen, D. Perez-Astudillo, D. Bachour, An evolutionary method for creating ensembles with adaptive size neural networks for predicting hourly solar

irradiance, 2017 International Joint Conference on Neural Networks (IJCNN), (2017) 1962-1967.

[138] C.-C. Wei, Predictions of Surface Solar Radiation on Tilted Solar Panels using Machine Learning Models: A Case Study of Tainan City, Taiwan, Energies, 10(10) (2017).

[139] N. Zemouri, H. Bouzgou, C.A. Gueymard, Gaussian process with linear discriminant analysis for predicting hourly global horizontal irradiance in Tamanrasset, Algeria, 2017 5th International Conference on Electrical Engineering - Boumerdes (ICEE-B), (2017) 1-5.

[140] M. Abu Zalata, I. Robandi, D.C. Riawan, Ieee, New Model for Hourly Solar Radiation Forecasting using ANN for Java Island, Indonesia, 2018.

[141] R. Caballero, L.F. Zarzalejo, A. Otero, L. Pinuel, S. Wilbert, Short Term Cloud Nowcasting for a Solar Power Plant based on Irradiance Historical Data, Journal of Computer Science & Technology, 18(3) (2018) 186-192.

[142] Z. Dong, D. Yang, J. Yan, C. Yu, Ieee, Deep learning solution for intra-day solar irradiance forecasting in tropical high variability regions, in: 2018 Ieee 7th World Conference on Photovoltaic Energy Conversion, 2018, pp. 2736-2741.

[143] G.M.d. Paiva, S.P. Pimentel, S. Leva, M. Mussetta, Assessment of Exogenous Variables on Intra-Day Solar Irradiance Forecasting Models, 2018 IEEE International Conference on Environment and Electrical Engineering and 2018 IEEE Industrial and Commercial Power Systems Europe (EEEIC / I&CPS Europe), (2018) 1-6.

[144] A. Shakya, S. Michael, C. Saunders, D. Armstrong, P. Pandey, S. Chalise, R. Tonkoski, Solar Irradiance Forecasting in Remote Microgrids Using Markov Switching Model, 2018 IEEE Power & Energy Society General Meeting (PESGM), (2018) 1-1.

[145] X. Shi, Q. Huang, J. Li, X. Lei, Study on Short-Term Predictions about Photovoltaic Output Power from Plants Lacking in Solar Radiation Data, 2018 11th International Conference on Intelligent Computation Technology and Automation (ICICTA), (2018) 75-78.

[146] Z. Wang, C. Tian, Q. Zhu, M. Huang, Hourly Solar Radiation Forecasting Using a Volterra-Least Squares Support Vector Machine Model Combined with Signal Decomposition, Energies, 11(1) (2018).

[147] R.B. Ammar, M.B. Ammar, A. Oualha, Photovoltaic power forecasting through temperature and solar radiation estimation, 2019 16th International Multi-Conference on Systems, Signals & Devices (SSD), (2019) 691-699.

[148] K. Basaran, A. Ozcift, D. Kilinc, A New Approach for Prediction of Solar Radiation with Using Ensemble Learning Algorithm, Arabian Journal for Science and Engineering, 44(8) (2019) 7159-7171.

[149] L. Benali, G. Notton, A. Fouilloy, C. Voyant, R. Dizene, Solar radiation forecasting using artificial neural network and random forest methods: Application to normal beam, horizontal diffuse and global components, Renewable Energy, 132 (2019) 871-884.

[150] K. Benmouiza, A. Cheknane, Clustered ANFIS network using fuzzy c-means, subtractive clustering, and grid partitioning for hourly solar radiation forecasting, Theoretical and Applied Climatology, 137(1-2) (2019) 31-43.

[151] H. Bouzgou, C.A. Gueymard, Fast short-term global solar irradiance forecasting with wrapper

mutual information, Renewable Energy, 133 (2019) 1055-1065.

[152] X. Huang, J. Shi, B. Gao, Y. Tai, Z. Chen, J. Zhang, Forecasting Hourly Solar Irradiance Using Hybrid Wavelet Transformation and Elman Model in Smart Grid, Ieee Access, 7 (2019) 139909-139923.

[153] J.B. Ki, K. Lee, K. Eui-Jong, Development of a Prediction Model of Solar Irradiances Using LSTM for use in Building Predictive Control, Journal of The Korean Solar Energy Society, 39(5) (2019) 41-52.

[154] M.G.A. Saumyamala, N.V. Chandrasekara, HOURLY SOLAR RADIATION FORECASTING USING ARTIFICIAL NEURAL NETWORK MODEL FOR COLOMBO, SRI LANKA, Advances and Applications in Statistics, 56(2) (2019) 143-151.

[155] S. Theocharides, M. Kynigos, M. Theristis, G. Makrides, G.E. Georghiou, Intra-day Solar Irradiance Forecasting Based on Artificial Neural Networks, 2019 IEEE 46th Photovoltaic Specialists Conference (PVSC), (2019) 1628-1631.

[156] W. Wang, Z. Zhen, K. Li, K. Lv, F. Wang, An Ultra-short-term Forecasting Model for High-resolution Solar Irradiance Based on SOM and Deep Learning Algorithm, 2019 IEEE Sustainable Power and Energy Conference (iSPEC), (2019) 1090-1095.

[157] J. Wojtkiewicz, M. Hosseini, R. Gottumukkala, T.L. Chambers, Hour-Ahead Solar Irradiance Forecasting Using Multivariate Gated Recurrent Units, Energies, 12(21) (2019).

[158] Z. Zarkov, L. Stoyanov, I. Draganovska, V. Lazarov, The Comparison of different approaches for solar radiation forecasting using Artificial Neural Network, 2019 11th Electrical Engineering Faculty Conference (BulEF), (2019) 1-6.

[159] D. Chandola, H. Gupta, V.A. Tikkiwal, M.K. Bohra, Multi-step ahead forecasting of global solar radiation for arid zones using deep learning, Procedia Computer Science, 167 (2020) 626-635.

[160] A. Eschenbach, G. Yepes, C. Tenllado, J.I. Gómez-Pérez, L. Piñuel, L.F. Zarzalejo, S. Wilbert, Spatio-Temporal Resolution of Irradiance Samples in Machine Learning Approaches for Irradiance Forecasting, IEEE Access, 8 (2020) 51518-51531.

[161] B. Gao, X. Huang, J. Shi, Y. Tai, J. Zhang, Hourly forecasting of solar irradiance based on CEEMDAN and multi-strategy CNN-LSTM neural networks, Renewable Energy, 162 (2020) 1665-1683.

[162] X. Huang, C. Zhang, Q. Li, Y. Tai, B. Gao, J. Shi, A Comparison of Hour-Ahead Solar Irradiance Forecasting Models Based on LSTM Network, Mathematical Problems in Engineering, 2020(1) (2020) 4251517.

[163] M.A. Jallal, S. Chabaa, A. Zeroual, A new artificial multi-neural approach to estimate the hourly global solar radiation in a semi-arid climate site, Theoretical and Applied Climatology, 139(3-4) (2020) 1261-1276.

[164] J. Lee, W. Wang, F. Harrou, Y. Sun, Reliable solar irradiance prediction using ensemble learning-based models: A comparative study, Energy Conversion and Management, 208 (2020). 10.1016/j.enconman.2020.112582

[165] M. Marzouq, H. El Fadili, K. Zenkouar, Z. Lakhliai, M. Amouzg, Short term solar irradiance forecasting via a novel evolutionary multi-model framework and performance assessment for sites

with no solar irradiance data, Renewable Energy, 157 (2020) 214-231.

[166] T. Mutavhatsindi, C. Sigauke, R. Mbuvha, Forecasting Hourly Global Horizontal Solar Irradiance in South Africa Using Machine Learning Models, IEEE Access, 8 (2020) 198872-198885.

[167] M.C. Sorkun, O. Durmaz Incel, C. Paoli, Time series forecasting on multivariate solar radiation data using deep learning (LSTM), Turkish Journal of Electrical Engineering and Computer Sciences, 28(1) (2020) 211-223.

[168] T. Watanabe, H. Takenaka, D. Nohara, Framework of Forecast Verification of Surface Solar Irradiance From a Numerical Weather Prediction Model Using Classification With a Gaussian Mixture Model, Earth and Space Science, 7(11) (2020) e2020EA001260.

[169] M. Abdel-Nasser, K. Mahmoud, M. Lehtonen, HIFA: Promising Heterogeneous Solar Irradiance Forecasting Approach Based on Kernel Mapping, IEEE Access, 9 (2021) 144906-144915.

[170] H. Ali-Ou-Salah, B. Oukarfi, K. Bahani, M. Moujabbir, A New Hybrid Model for Hourly Solar Radiation Forecasting Using Daily Classification Technique and Machine Learning Algorithms, Mathematical Problems in Engineering, 2021(1) (2021) 6692626.

[171] P. Kumari, D. Toshniwal, Extreme gradient boosting and deep neural network based ensemble learning approach to forecast hourly solar irradiance, Journal of Cleaner Production, 279 (2021) 123285.

[172] P. Kumari, D. Toshniwal, Long short term memory–convolutional neural network based deep hybrid approach for solar irradiance forecasting, Applied Energy, 295 (2021) 117061.

[173] C.S. Lai, C. Zhong, K. Pan, W.W.Y. Ng, L.L. Lai, A deep learning based hybrid method for hourly solar radiation forecasting, Expert Systems with Applications, 177 (2021) 114941.

[174] C.N. Obiora, A.N. Hasan, A. Ali, N. Alajarmeh, Forecasting Hourly Solar Radiation Using Artificial Intelligence Techniques, IEEE Canadian Journal of Electrical and Computer Engineering, 44(4) (2021) 497-508.

[175] C. Zhong, C.S. Lai, W.W.Y. Ng, Y. Tao, T. Wang, L.L. Lai, Multi-view deep forecasting for hourly solar irradiance with error correction, Solar Energy, 228 (2021) 308-316.

[176] H. Acikgoz, A novel approach based on integration of convolutional neural networks and deep feature selection for short-term solar radiation forecasting, Applied Energy, 305 (2022) 117912.

[177] H. Ali-Ou-Salah, B. Oukarfi, T. Mouhaydine, Short-term solar radiation forecasting using a new seasonal clustering technique and artificial neural network, International Journal of Green Energy, 19(4) (2022) 424-434.

[178] S. Belaid, A. Mellit, H. Boualit, M. Zaiani, Hourly global solar forecasting models based on a supervised machine learning algorithm and time series principle, International Journal of Ambient Energy, 43(1) (2022) 1707-1718.

[179] S.A. Haider, M. Sajid, H. Sajid, E. Uddin, Y. Ayaz, Deep learning and statistical methods for short- and long-term solar irradiance forecasting for Islamabad, Renewable Energy, 198 (2022) 51-60.

[180] S. Shan, X. Xie, T. Fan, Y. Xiao, Z. Ding, K. Zhang, H. Wei, A deep-learning based solar irradiance forecast using missing data, IET Renewable Power Generation, 16(7) (2022) 1462-1473.

[181] J. Tong, L. Xie, S. Fang, W. Yang, K. Zhang, Hourly solar irradiance forecasting based on encoder–decoder model using series decomposition and dynamic error compensation, Energy Conversion and Management, 270 (2022) 116049.

[182] Y. Chen, M. Bai, Y. Zhang, J. Liu, D. Yu, Proactively selection of input variables based on information gain factors for deep learning models in short-term solar irradiance forecasting, Energy, 284 (2023) 129261.

[183] J. Liu, X. Huang, Q. Li, Z. Chen, G. Liu, Y. Tai, Hourly stepwise forecasting for solar irradiance using integrated hybrid models CNN-LSTM-MLP combined with error correction and VMD, Energy Conversion and Management, 280 (2023) 116804.

[184] Neeraj, P. Gupta, A. Tomar, Multi-model approach applied to meteorological data for solar radiation forecasting using data-driven approaches, Optik, 286 (2023) 170957.

[185] M. Neshat, M.M. Nezhad, S. Mirjalili, D.A. Garcia, E. Dahlquist, A.H. Gandomi, Short-term solar radiation forecasting using hybrid deep residual learning and gated LSTM recurrent network with differential covariance matrix adaptation evolution strategy, Energy, 278 (2023) 127701.

[186] J. Munkhammar, Very short-term probabilistic and scenario-based forecasting of solar irradiance using Markov-chain mixture distribution modeling, Solar Energy Advances, 4 (2024) 100057.

[187] G. Reikard, C. Hansen, Forecasting solar irradiance at short horizons: Frequency and time domain models, Renewable Energy, 135 (2019) 1270-1290.

[188] A.W. Aryaputera, D. Yang, W.M. Walsh, Day-Ahead Solar Irradiance Forecasting in a Tropical Environment, Journal of Solar Energy Engineering-Transactions of the Asme, 137(5) (2015).

[189] D. Yang, Z. Ye, L.H.I. Lim, Z. Dong, Very short term irradiance forecasting using the lasso, Solar Energy, 114 (2015) 314-326.

[190] A. Moncada, W. Richardson, Jr., R. Vega-Avila, Deep Learning to Forecast Solar Irradiance Using a Six-Month UTSA SkyImager Dataset, Energies, 11(8) (2018).

[191] Â. Frimane, J. Munkhammar, D. van der Meer, Infinite hidden Markov model for short-term solar irradiance forecasting, Solar Energy, 244 (2022) 331-342.

[192] S.A. Fatemi, A. Kuh, Solar radiation forecasting using zenith angle, 2013 IEEE Global Conference on Signal and Information Processing, (2013) 523-526.

[193] A.T. Lorenzo, W.F. Holmgren, M. Leuthold, C.K. Kim, A.D. Cronin, E.A. Betterton, Short-term PV power forecasts based on a real-time irradiance monitoring network, 2014 IEEE 40th Photovoltaic Specialist Conference (PVSC), (2014) 0075-0079.

[194] P.S. Loh, J.V. Chua, A.C. Tan, C.I. Khaw, Data-driven short-term forecasting of solar irradiance profile, Energy Procedia, 143 (2017) 572-578.

[195] T.A. Fathima, V. Nedumpozhimana, Y.H. Lee, S. Winkler, S. Dev, Predicting Solar Irradiance in Singapore, 2019 Photonics & Electromagnetics Research Symposium - Fall (PIERS - Fall), (2019) 3164-3167.

[196] M. Paulescu, E. Paulescu, Short-term forecasting of solar irradiance, Renewable Energy, 143 (2019) 985-994.

[197] M. Jaihuni, J.K. Basak, F. Khan, F.G. Okyere, E. Arulmozhi, A. Bhujel, J. Park, L.D. Hyun, H.T. Kim, A Partially Amended Hybrid Bi-GRU-ARIMA Model (PAHM) for Predicting Solar Irradiance in

Short and Very-Short Terms, Energies, 13(2) (2020).

[198] S. Das, Short term forecasting of solar radiation and power output of 89.6kWp solar PV power plant, Materials Today: Proceedings, 39 (2021) 1959-1969.

[199] P. Lauret, M. David, P.-J. Trombe, F. Ramahatana-Andriamasomanana, STATISTICAL MODELS TO PREDICT SOLAR RADIATION AT HIGH RESOLUTIONS, 2015.

[200] W. Ji, C. Chan, J. Loh, F. Choo, L. Chen, Solar radiation prediction using statistical approaches, 2009 7th International Conference on Information, Communications and Signal Processing (ICICS), (2009) 1-5.

[201] C. Ching-Tsan, L. Yung-Sheng, L. Xiao Ru, L. Chiung-Chou, A RSCMAC based forecasting for Solar Irradiance from local weather information, The 2012 International Joint Conference on Neural Networks (IJCNN), (2012) 1-7.

[202] D. Yang, P. Jirutitijaroen, W.M. Walsh, Hourly solar irradiance time series forecasting using cloud cover index, Solar Energy, 86(12) (2012) 3531-3543.

[203] D. Yang, P. Jirutitijaroen, W.M. Walsh, The Estimation of Clear Sky Global Horizontal Irradiance at the Equator, in: J. Luther (Ed.) Pv Asia Pacific Conference 2011, Vol. 25, 2012, pp. 141-148.

[204] E. Akarslan, F.O. Hocaoğlu, R. Edizkan, A novel M-D (multi-dimensional) linear prediction filter approach for hourly solar radiation forecasting, Energy, 73 (2014) 978-986.

[205] S.M. Lurwan, N. Mariun, H. Hizam, M.A.M. Radzi, A. Zakaria, Predicting power output of photovoltaic systems with solar radiation model, 2014 IEEE International Conference on Power and Energy (PECon), (2014) 304-308.

[206] M. Brabec, M. Paulescu, V. Badescu, Tailored vs black-box models for forecasting hourly average solar irradiance, Solar Energy, 111 (2015) 320-331.

[207] A.T. Lorenzo, W.F. Holmgren, A.D. Cronin, Irradiance forecasts based on an irradiance monitoring network, cloud motion, and spatial averaging, Solar Energy, 122 (2015) 1158-1169.

[208] A. Bao, S. Fei, M. Zhong, Short-Term Solar Irradiance Forecasting Using Neural Network and Genetic Algorithm, in: Y. Jia, J. Du, W. Zhang, H. Li (Eds.) Proceedings of 2016 Chinese Intelligent Systems Conference, Vol Ii, Vol. 405, 2016, pp. 619-627. 10.1007/978-981-10-2335-4_57

[209] O. Ceylan, M. Starke, P. Irminger, B. Ollis, D. King, K. Tomsovic, Hourly Day Ahead Solar Irradiance Forecasting Model in LabVIEW Using Cloud Cover Data, Istanbul University-Journal of Electrical and Electronics Engineering, 16(2) (2016) 2047-2054.

[210] J. Huang, R.J. Davy, Predicting intra-hour variability of solar irradiance using hourly local weather forecasts, Solar Energy, 139 (2016) 633-639. 10.1016/j.solener.2016.10.036

[211] M. Schroedter-Homscheidt, G. Gesell, Verification of Sectoral Cloud Motion Based Direct Normal Irradiance Nowcasting from Satellite Imagery, in: V. Rajpaul, C. Richter (Eds.) Solarpaces 2015: International Conference on Concentrating Solar Power and Chemical Energy Systems, Vol. 1734, 2016.

[212] E. Scolari, F. Sossan, M. Paolone, Irradiance prediction intervals for PV stochastic generation in microgrid applications, Solar Energy, 139 (2016) 116-129.

[213] D. Torregrossa, J.Y. Le Boudec, M. Paolone, Model-free computation of ultra-short-term prediction intervals of solar irradiance, Solar Energy, 124 (2016) 57-67.

[214] E. Akarslan, F.O. Hocaoglu, A novel adaptive approach for hourly solar radiation forecasting, Renewable Energy, 87 (2016) 628-633.

[215] H. Al-Saadi, R. Zivanovic, S. Al-Sarawi, Uncertainty Model for Total Solar Irradiance Estimation on Australian Rooftops, in: W.E. Alnaser, A.A. Sayigh (Eds.) World Renewable Energy Congress-17, Vol. 23, 2017.

[216] Z. Chen, A. Troccoli, Urban solar irradiance and power prediction from nearby stations, Meteorologische Zeitschrift, 26(3) (2017) 277-290.

[217] Y. Hirata, K. Aihara, Improving time series prediction of solar irradiance after sunrise: Comparison among three methods for time series prediction, Solar Energy, 149 (2017) 294-301.

[218] M. Olama, A. Melin, J. Dong, S. Djouadi, Y. Zhang, Stochastic short-term high-resolution prediction of solar irradiance and photovoltaic power output, 2017 North American Power Symposium (NAPS), (2017) 1-6.

[219] T. Sirch, L. Bugliaro, T. Zinner, M. Moehrlein, M. Vazquez-Navarro, Cloud and DNI nowcasting with MSG/SEVIRI for the optimized operation of concentrating solar power plants, Atmospheric Measurement Techniques, 10(2) (2017) 409-429.

[220] E. Akarslan, F.O. Hocaoglu, R. Edizkan, Novel short term solar irradiance forecasting models, Renewable Energy, 123 (2018) 58-66.

[221] S. Dev, T. AlSkaif, M. Hossari, R. Godina, A. Louwen, W.v. Sark, Solar Irradiance Forecasting Using Triple Exponential Smoothing, 2018 International Conference on Smart Energy Systems and Technologies (SEST), (2018) 1-6.

[222] A. Alfadda, S. Rahman, M. Pipattanasomporn, Solar irradiance forecast using aerosols measurements: A data driven approach, Solar Energy, 170 (2018) 924-939.

[223] D. Gallucci, F. Romano, A. Cersosimo, D. Cimini, F. Di Paola, S. Gentile, E. Geraldi, S. Larosa, S.T. Nilo, E. Ricciardelli, M. Viggiano, Nowcasting Surface Solar Irradiance with AMESIS via Motion Vector Fields of MSG-SEVIRI Data, Remote Sensing, 10(6) (2018).

[224] A. Jadidi, R. Menezes, N. de Souza, A.C. de Castro Lima, A Hybrid GA-MLPNN Model for One-Hour-Ahead Forecasting of the Global Horizontal Irradiance in Elizabeth City, North Carolina, Energies, 11(10) (2018).

[225] L. Laiti, L. Giovannini, D. Zardi, G. Belluardo, D. Moser, Estimating Hourly Beam and Diffuse Solar Radiation in an Alpine Valley: A Critical Assessment of Decomposition Models, Atmosphere, 9(4) (2018).

[226] Y. Dong, H. Jiang, Global Solar Radiation Forecasting Using Square Root Regularization-Based Ensemble, Mathematical Problems in Engineering, 2019 (2019).

[227] M. Paulescu, E. Paulescu, V. Badescu, Chapter 9 - Nowcasting solar irradiance for effective solar power plants operation and smart grid management, in: R. Deo, P. Samui, S.S. Roy (Eds.) Predictive Modelling for Energy Management and Power Systems Engineering, Elsevier, 2021, pp. 249-270.

[228] L. Yang, X. Gao, J. Hua, P. Wu, Z. Li, D. Jia, Very Short-Term Surface Solar Irradiance Forecasting Based on FengYun-4 Geostationary Satellite, Sensors, 20(9) (2020).

[229] J. Alonso-Montesinos, J. Polo, J. Ballestrín, F.J. Batlles, C. Portillo, Impact of DNI forecasting

on CSP tower plant power production, Renewable Energy, 138 (2019) 368-377.

[230] L. Yang, X. Gao, Z. Li, D. Jia, J. Jiang, Nowcasting of Surface Solar Irradiance Using FengYun-4 Satellite Observations over China, Remote Sensing, 11(17) (2019).

[231] R. Dambreville, P. Blanc, J. Chanussot, D. Boldo, S. Dubost, Very short term forecasting of the Global Horizontal Irradiance through Helioclim maps, 2014 5th International Renewable Energy Congress (IREC), (2014) 1-6.

[232] J. Alonso-Montesinos, F.J. Batlles, Solar radiation forecasting in the short- and medium-term under all sky conditions, Energy, 83 (2015) 387-393.

[233] J. Alonso-Montesinos, F.J. Batlles, C. Portillo, Solar irradiance forecasting at one-minute intervals for different sky conditions using sky camera images, Energy Conversion and Management, 105 (2015) 1166-1177.

[234] E. Duverger, C. Penin, P. Alexandre, F. Thiery, D. Gachon, T. Talbert, Irradiance forecasting for microgrid energy management, 2017 IEEE PES Innovative Smart Grid Technologies Conference Europe (ISGT-Europe), (2017) 1-6.

[235] Y.-Y. Kim, A Study on Prediction of Solar Access and Irradiance by Calculating the Area of a Shaded Region, journal of the regional association of architectural institute of korea, 19(4) (2017) 137-144.

[236] A. Ayet, P. Tandeo, Nowcasting solar irradiance using an analog method and geostationary satellite images, Solar Energy, 164 (2018) 301-315.

[237] J. Lago, K. De Brabandere, F. De Ridder, B. De Schutter, Short-term forecasting of solar irradiance without local telemetry: A generalized model using satellite data, Solar Energy, 173 (2018) 566-577.

[238] M. Schroedter-Homscheidt, N. Killius, D.M. Guevara, T. Sirch, N. Hanrieder, S. Wilbert, Z. Yasser, Satellite-based DNI Nowcasting Based on a Sectoral Atmospheric Motion Approach, in: R. Mancilla, C. Richter (Eds.) International Conference on Concentrating Solar Power and Chemical Energy Systems, Vol. 2033, 2018.

[239] J. Wojtkiewicz, S. Katragadda, R. Gottumukkala, A Concept-Drift Based Predictive-Analytics Framework: Application for Real-Time Solar Irradiance Forecasting, 2018 IEEE International Conference on Big Data (Big Data), (2018) 5462-5464.

[240] M. André, R. Perez, T. Soubdhan, J. Schlemmer, R. Calif, S. Monjoly, Preliminary assessment of two spatio-temporal forecasting technics for hourly satellite-derived irradiance in a complex meteorological context, Solar Energy, 177 (2019) 703-712.

[241] V. Kallio-Myers, A. Riihelä, P. Lahtinen, A. Lindfors, Global horizontal irradiance forecast for Finland based on geostationary weather satellite data, Solar Energy, 198 (2020) 68-80.

[242] R. Marquez, C.F.M. Coimbra, Intra-hour DNI forecasting based on cloud tracking image analysis, Solar Energy, 91 (2013) 327-336. 10.1016/j.solener.2012.09.018

[243] B. Nouri, S. Wilbert, N. Blum, Y. Fabel, E. Lorenz, A. Hammer, T. Schmidt, L.F. Zarzalejo, R. Pitz-Paal, Probabilistic solar nowcasting based on all-sky imagers, Solar Energy, 253 (2023) 285-307.

[244] E. Saade, D.E. Clough, A.W. Weimer, Use of Image-Based Direct Normal Irradiance Forecasts

in the Model Predictive Control of a Solar-Thermal Reactor, Journal of Solar Energy Engineering-Transactions of the Asme, 136(1) (2014).

[245] S.R. West, D. Rowe, S. Sayeef, A. Berry, Short-term irradiance forecasting using skycams: Motivation and development, Solar Energy, 110 (2014) 188-207. 10.1016/j.solener.2014.08.038

[246] L. Magnone, F. Sossan, E. Scolari, M. Paolone, Cloud Motion Identification Algorithms Based on All-Sky Images to Support Solar Irradiance Forecast, 2017 IEEE 44th Photovoltaic Specialist Conference (PVSC), (2017) 1415-1420.

[247] H. Zhang, C. Zhang, W. Li, Short-term DNI forecasting using cloud history patterns matching, 2017 Seventh International Conference on Information Science and Technology (ICIST), (2017) 57-63. 10.1109/ICIST.2017.7926492

[248] M. Caldas, R. Alonso-Suárez, Very short-term solar irradiance forecast using all-sky imaging and real-time irradiance measurements, Renewable Energy, 143 (2019) 1643-1658.

[249] F. Wang, Z. Xuan, Z. Zhen, Y. Li, K. Li, L. Zhao, M. Shafie-khah, J.P.S. Catalão, A minutely solar irradiance forecasting method based on real-time sky image-irradiance mapping model, Energy Conversion and Management, 220 (2020) 113075.

[250] L.H. Dissawa, R.I. Godaliyadda, P.B. Ekanayake, A.P. Agalgaonkar, D. Robinson, J.B. Ekanayake, S. Perera, Sky Image-Based Localized, Short-Term Solar Irradiance Forecasting for Multiple PV Sites via Cloud Motion Tracking, International Journal of Photoenergy, 2021(1) (2021) 9973010.

[251] B. Nouri, N. Blum, S. Wilbert, L.F. Zarzalejo, A Hybrid Solar Irradiance Nowcasting Approach: Combining All Sky Imager Systems and Persistence Irradiance Models for Increased Accuracy, Solar RRL, 6(5) (2022) 2100442.

[252] P.K. Ray, H.B. Gooi, Chapter 3 - Short-term solar irradiance forecasting using ground-based sky images, in: B. Subudhi, P.K. Ray (Eds.) Microgrid Cyberphysical Systems, Elsevier, 2022, pp. 67-88.

[253] J. Liu, H. Zang, L. Cheng, T. Ding, Z. Wei, G. Sun, A Transformer-based multimodal-learning framework using sky images for ultra-short-term solar irradiance forecasting, Applied Energy, 342 (2023) 121160.

[254] S. Quesada-Ruiz, Y. Chu, J. Tovar-Pescador, H.T.C. Pedro, C.F.M. Coimbra, Cloud-tracking methodology for intra-hour DNI forecasting, Solar Energy, 102 (2014) 267-275.

[255] Y. Chu, M. Li, C.F.M. Coimbra, Sun-tracking imaging system for intra-hour DNI forecasts, Renewable Energy, 96 (2016) 792-799.

[256] M. Li, Y. Chu, H.T.C. Pedro, C.F.M. Coimbra, Quantitative evaluation of the impact of cloud transmittance and cloud velocity on the accuracy of short-term DNI forecasts, Renewable Energy, 86 (2016) 1362-1371.

[257] T. Schmidt, J. Kalisch, E. Lorenz, D. Heinemann, Evaluating the spatio-temporal performance of sky-imager-based solar irradiance analysis and forecasts, Atmospheric Chemistry and Physics, 16(5) (2016) 3399-3412.

[258] P. Blanc, P. Massip, A. Kazantzidis, P. Tzoumanikas, P. Kuhn, S. Wilbert, D. Schueler, C. Prahl, Short-Term Forecasting of High Resolution Local DNI Maps with Multiple Fish-Eye Cameras in

Stereoscopic Mode, in: A. AlObaidli, N. Calvet, C. Richter (Eds.) International Conference on Concentrating Solar Power and Chemical Energy Systems, Vol. 1850, 2017.

[259] M. Chang, Y. Yao, G. Li, Y. Tong, P. Tu, Cloud tracking for solar irradiance prediction, 2017 IEEE International Conference on Image Processing (ICIP), (2017) 4387-4391.

[260] H.-Y. Cheng, Cloud tracking using clusters of feature points for accurate solar irradiance nowcasting, Renewable Energy, 104 (2017) 281-289.

[261] P. Kuhn, S. Wilbert, D. Schuler, C. Prahl, T. Haase, L. Ramirez, L. Zarzalejo, A. Meyer, L. Vuilleumier, P. Blanc, J. Dubrana, A. Kazantzidis, M. Schroedter-Homscheidt, T. Hirsch, R. Pitz-Paal, Validation of Spatially Resolved All Sky Imager Derived DNI Nowcasts, in: A. AlObaidli, N. Calvet, C. Richter (Eds.) International Conference on Concentrating Solar Power and Chemical Energy Systems, Vol. 1850, 2017.

[262] J. Nou, R. Chauvin, J. Eynard, S. Thil, S. Grieu, Towards the intrahour forecasting of direct normal irradiance using sky-imaging data, Heliyon, 4(4) (2018).

[263] B. Nouri, P. Kuhn, S. Wilbert, C. Prahl, R. Pitz-Paal, P. Blanc, T. Schmidt, Z. Yasser, L.R. Santigosa, D. Heineman, Nowcasting of DNI Maps for the Solar Field Based on Voxel Carving and Individual 3D Cloud Objects from All Sky Images, in: R. Mancilla, C. Richter (Eds.) International Conference on Concentrating Solar Power and Chemical Energy Systems, Vol. 2033, 2018.

[264] Y. Ai, Y. Peng, W. Wei, A Model of Very Short-term Solar Irradiance Forecasting Based on Low-cost Sky Images, in: Z. You, J. Xiao, Z. Tan (Eds.) Materials Science, Energy Technology, and Power Engineering I, Vol. 1839, 2017.

[265] C. Arbizu-Barrena, J.A. Ruiz-Arias, F.J. Rodríguez-Benítez, D. Pozo-Vázquez, J. Tovar-Pescador, Short-term solar radiation forecasting by advecting and diffusing MSG cloud index, Solar Energy, 155 (2017) 1092-1103.

[266] C. Feng, M. Cui, M. Lee, J. Zhang, B. Hodge, S. Lu, H.F. Hamann, Short-term global horizontal irradiance forecasting based on sky imaging and pattern recognition, 2017 IEEE Power & Energy Society General Meeting, (2017) 1-5.

[267] V. Bone, J. Pidgeon, M. Kearney, A. Veeraragavan, Intra-hour direct normal irradiance forecasting through adaptive clear-sky modelling and cloud tracking, Solar Energy, 159 (2018) 852-867.

[268] B. Nouri, S. Wilbert, P. Kuhn, N. Hanrieder, M. Schroedter-Homscheidt, A. Kazantzidis, L. Zarzalejo, P. Blanc, S. Kumar, N. Goswami, R. Shankar, R. Affolter, R. Pitz-Paal, Real-Time Uncertainty Specification of All Sky Imager Derived Irradiance Nowcasts, Remote Sensing, 11(9) (2019).

[269] S. Pereira, P. Canhoto, R. Salgado, Development and assessment of artificial neural network models for direct normal solar irradiance forecasting using operational numerical weather prediction data, Energy and AI, 15 (2024) 100314.

[270] G. Narvaez, L.F. Giraldo, M. Bressan, A. Pantoja, Machine learning for site-adaptation and solar radiation forecasting, Renewable Energy, 167 (2021) 333-342.

[271] P. Manandhar, M. Temimi, Z. Aung, Short-term solar radiation forecast using total sky imager via transfer learning, Energy Reports, 9 (2023) 819-828.

[272] M. Ajith, M. Martínez-Ramón, Deep learning based solar radiation micro forecast by fusion of infrared cloud images and radiation data, Applied Energy, 294 (2021) 117014.

[273] H.-Y. Cheng, C.-C. Yu, Multi-model solar irradiance prediction based on automatic cloud classification, Energy, 91 (2015) 579-587.

[274] Y. Chu, H.T.C. Pedro, M. Li, C.F.M. Coimbra, Real-time forecasting of solar irradiance ramps with smart image processing, Solar Energy, 114 (2015) 91-104.

[275] C.M. Fernández Peruchena, M. Gastón, M. Schroedter-Homscheidt, M. Kosmale, I. Martínez Marco, J.A. García-Moya, J.L. Casado-Rubio, Dynamic Paths: Towards high frequency direct normal irradiance forecasts, Energy, 132 (2017) 315-323.

[276] J. Du, Q. Min, P. Zhang, J. Guo, J. Yang, B. Yin, Short-Term Solar Irradiance Forecasts Using Sky Images and Radiative Transfer Model, Energies, 11(5) (2018).

[277] E.F.M. Abreu, P. Canhoto, M.J. Costa, Prediction of diffuse horizontal irradiance using a new climate zone model, Renewable & Sustainable Energy Reviews, 110 (2019) 28-42.

[278] S. Tiwari, R. Sabzehgar, M. Rasouli, Short Term Solar Irradiance Forecast Using Numerical Weather Prediction (NWP) with Gradient Boost Regression, 2018 9th IEEE International Symposium on Power Electronics for Distributed Generation Systems (PEDG), (2018) 1-8.

[279] X. Zhao, H. Wei, H. Wang, T. Zhu, K. Zhang, 3D-CNN-based feature extraction of ground-based cloud images for direct normal irradiance prediction, Solar Energy, 181 (2019) 510-518.

[280] T. Zhu, H. Zhou, H. Wei, X. Zhao, K. Zhang, J. Zhang, Inter-hour direct normal irradiance forecast with multiple data types and time-series, Journal of Modern Power Systems and Clean Energy, 7(5) (2019) 1319-1327.

[281] T. Leelaruji, N. Teerakawanich, Short Term Prediction of Solar Irradiance Fluctuation Using Image Processing with ResNet, 2020 8th International Electrical Engineering Congress (iEECON), (2020) 1-4.

[282] X. Zhao, L. Xie, H. Wei, H. Wang, K. Zhang, Fuzzy inference systems based on multi-type features fusion for intra-hour solar irradiance forecasts, Sustainable Energy Technologies and Assessments, 45 (2021) 101061.

[283] S.-A. Logothetis, V. Salamalikis, S. Wilbert, J. Remund, L.F. Zarzalejo, Y. Xie, B. Nouri, E. Ntavelis, J. Nou, N. Hendrikx, L. Visser, M. Sengupta, M. Pó, R. Chauvin, S. Grieu, N. Blum, W. van Sark, A. Kazantzidis, Benchmarking of solar irradiance nowcast performance derived from all-sky imagers, Renewable Energy, 199 (2022) 246-261.

[284] L. Zhang, R. Wilson, M. Sumner, Y. Wu, Advanced multimodal fusion method for very short-term solar irradiance forecasting using sky images and meteorological data: A gate and transformer mechanism approach, Renewable Energy, 216 (2023) 118952.

[285] N.Y. Hendrikx, K. Barhmi, L.R. Visser, T.A. de Bruin, M. Pó, A.A. Salah, W.G.J.H.M. van Sark, All sky imaging-based short-term solar irradiance forecasting with Long Short-Term Memory networks, Solar Energy, 272 (2024) 112463.

[286] R. Sarkis, I. Oguz, D. Psaltis, M. Paolone, C. Moser, L. Lambertini, Intraday solar irradiance forecasting using public cameras, Solar Energy, 275 (2024) 112600.

[287] W. Kong, Y. Jia, Z.Y. Dong, K. Meng, S. Chai, Hybrid approaches based on deep whole-sky-

image learning to photovoltaic generation forecasting, Applied Energy, 280 (2020) 115875.

[288] S.T. Sarena, L. Kuo-Lung, C. Tsai-Hsiang, H. Tai-Di, T. Kuan-Sheng, C. Yung-Ruei, Y.D. Lee, H. Yuan-Hsiang, Very short term Solar Irradiance Prediction for a microgrid system in Taiwan based on Hybrid of Support Vector Regression and Grey Theory, 2013 3rd International Conference on Electric Power and Energy Conversion Systems, (2013) 1-6.

[289] Y. Chu, H.T.C. Pedro, L. Nonnenmacher, R.H. Inman, Z. Liao, C.F.M. Coimbra, A Smart Image-Based Cloud Detection System for Intrahour Solar Irradiance Forecasts, Journal of Atmospheric and Oceanic Technology, 31(9) (2014) 1995-2007.

[290] J. Li, J.K. Ward, Irradiance forecasting for the photovoltaic systems, Proceedings of 2014 International Conference on Modelling, Identification & Control, (2014) 346-350.

[291] Z. Qu, B. Gschwind, M. Lefevre, L. Wald, Improving HelioClim-3 estimates of surface solar irradiance using the McClear clear-sky model and recent advances in atmosphere composition, Atmospheric Measurement Techniques, 7(11) (2014) 3927-3933.

[292] H.T.C. Pedro, C.F.M. Coimbra, Nearest-neighbor methodology for prediction of intra-hour global horizontal and direct normal irradiances, Renewable Energy, 80 (2015) 770-782.

[293] J. Xu, S. Yoo, D. Yu, H. Huang, D. Huang, J. Heiser, P. Kalb, A Stochastic Framework for Solar Irradiance Forecasting Using Condition Random Field, in: T. Cao, E.P. Lim, Z.H. Zhou, T.B. Ho, D. Cheung, H. Motoda (Eds.) Advances in Knowledge Discovery and Data Mining, Part I, Vol. 9077, 2015, pp. 511-524.

[294] J. Xu, S. Yoo, D. Yu, D. Huang, J. Heiser, P. Kalb, Solar Irradiance Forecasting using Multi-layer Cloud Tracking and Numerical Weather Prediction, 2015.

[295] M. André, S. Dabo-Niang, T. Soubdhan, H. Ould-Baba, Predictive spatio-temporal model for spatially sparse global solar radiation data, Energy, 111 (2016) 599-608.

[296] J. Nou, R. Chauvin, J. Eynard, S. Thil, S. Grieu, Towards the short-term forecasting of direct normal irradiance using a sky imager, Ifac Papersonline, 50(1) (2017) 14137-14142.

[297] T. Taomae, L. Lim, D. Stevens, D. Nakafuji, 30 min-Ahead Gridded Solar Irradiance Forecasting Using Satellite Data, in: J. Wang, G. Cong, J. Chen, J. Qi (Eds.) Databases Theory and Applications, Adc 2018, Vol. 10837, 2018, pp. 186-198.

[298] A. Kumler, Y. Xie, Y. Zhang, A Physics-based Smart Persistence model for Intra-hour forecasting of solar radiation (PSPI) using GHI measurements and a cloud retrieval technique, Solar Energy, 177 (2019) 494-500.

[299] A. Ryu, M. Ito, H. Ishii, Y. Hayashi, Preliminary Analysis of Short-term Solar Irradiance Forecasting by using Total-sky Imager and Convolutional Neural Network, 2019 IEEE PES GTD Grand International Conference and Exposition Asia (GTD Asia), (2019) 627-631.

[300] J. Dong, M.M. Olama, T. Kuruganti, A.M. Melin, S.M. Djouadi, Y. Zhang, Y. Xue, Novel stochastic methods to predict short-term solar radiation and photovoltaic power, Renewable Energy, 145 (2020) 333-346.

[301] T. McCandless, S. Dettling, S.E. Haupt, Comparison of Implicit vs. Explicit Regime Identification in Machine Learning Methods for Solar Irradiance Prediction, Energies, 13(3) (2020).

[302] K. Yan, H. Shen, L. Wang, H. Zhou, M. Xu, Y. Mo, Short-Term Solar Irradiance Forecasting

Based on a Hybrid Deep Learning Methodology, Information, 11(1) (2020).

[303] Z. Zhen, J. Liu, Z. Zhang, F. Wang, H. Chai, Y. Yu, X. Lu, T. Wang, Y. Lin, Deep Learning Based Surface Irradiance Mapping Model for Solar PV Power Forecasting Using Sky Image, IEEE Transactions on Industry Applications, (2020) 1-1.

[304] O. El Alani, M. Abraim, H. Ghennioui, A. Ghennioui, I. Ikenbi, F.-E. Dahr, Short term solar irradiance forecasting using sky images based on a hybrid CNN–MLP model, Energy Reports, 7 (2021) 888-900.

[305] E. Pérez, J. Pérez, J. Segarra-Tamarit, H. Beltran, A deep learning model for intra-day forecasting of solar irradiance using satellite-based estimations in the vicinity of a PV power plant, Solar Energy, 218 (2021) 652-660.

[306] R. Gallo, M. Castangia, A. Macii, E. Macii, E. Patti, A. Aliberti, Solar radiation forecasting with deep learning techniques integrating geostationary satellite images, Engineering Applications of Artificial Intelligence, 116 (2022) 105493.

[307] S. Song, Z. Yang, H. Goh, Q. Huang, G. Li, A novel sky image-based solar irradiance nowcasting model with convolutional block attention mechanism, Energy Reports, 8 (2022) 125-132.

[308] E. Ogliari, M. Sakwa, P. Cusa, Enhanced Convolutional Neural Network for solar radiation nowcasting: All-Sky camera infrared images embedded with exogeneous parameters, Renewable Energy, 221 (2024) 119735.

[309] J. Huertas-Tato, R. Aler, F.J. Rodriguez-Benitez, C. Arbizu-Barrena, D. Pozo-Vazquez, I.M. Galvan, Predicting Global Irradiance Combining Forecasting Models Through Machine Learning, in: F.J.D. Juez, J.R. Villar, E.A. DeLaCal, A. Herrero, H. Quintian, J.A. Saez, E. Corchado (Eds.) Hybrid Artificial Intelligent Systems, Vol. 10870, 2018, pp. 622-633.

[310] F. Nomiyama, J. Asai, T. Murakami, H. Takano, J. Murata, A study on global solar radiation forecasting models using meteorological data and their application to wide area forecast, 2012 IEEE International Conference on Power System Technology (POWERCON), (2012) 1-6.

[311] S.X. Chen, H.B. Gooi, M.Q. Wang, Solar radiation forecast based on fuzzy logic and neural networks, Renewable Energy, 60 (2013) 195-201. 10.1016/j.renene.2013.05.011

[312] J. Huang, M. Korolkiewicz, M. Agrawal, J. Boland, Forecasting solar radiation on an hourly time scale using a Coupled AutoRegressive and Dynamical System (CARDS) model, Solar Energy, 87 (2013) 136-149.

[313] V.P.A. Lonij, A.E. Brooks, A.D. Cronin, M. Leuthold, K. Koch, Intra-hour forecasts of solar power production using measurements from a network of irradiance sensors, Solar Energy, 97 (2013) 58-66. 10.

[314] Z. Peng, S. Yoo, D. Yu, D. Huang, Solar irradiance forecast system based on geostationary satellite, 2013 IEEE International Conference on Smart Grid Communications (SmartGridComm), (2013) 708-713.

[315] A. Anvari-Moghaddam, H. Monsef, A. Rahimi-Kian, H. Nance, Feasibility study of a novel methodology for solar radiation prediction on an hourly time scale: A case study in Plymouth, United Kingdom, Journal of Renewable and Sustainable Energy, 6(3) (2014).

[316] H.-Y. Cheng, C.-C. Yu, S.-J. Lin, Bi-model short-term solar irradiance prediction using support

vector regressors, Energy, 70 (2014) 121-127.

[317] Z. Dong, D. Yang, T. Reindl, W.M. Walsh, Satellite image analysis and a hybrid ESSS/ANN model to forecast solar irradiance in the tropics, Energy Conversion and Management, 79 (2014) 66-73.

[318] A. Saaban, L. Zainudin, M.N. Abu Bakar, On Piecewise Interpolation Techniques for Estimating Solar Radiation Missing Values in Kedah, in: H. Ibrahim, J. Zulkepli, N. Aziz, N. Ahmad, S.A. Rahman (Eds.) International Conference on Quantitative Sciences and Its Applications, Vol. 1635, 2014, pp. 217-221.

[319] C. Voyant, C. Darras, M. Muselli, C. Paoli, M.-L. Nivet, P. Poggi, Bayesian rules and stochastic models for high accuracy prediction of solar radiation, Applied Energy, 114 (2014) 218-226.

[320] M. Fidan, F.O. Hocaoğlu, Ö.N. Gerek, Harmonic analysis based hourly solar radiation forecasting model, IET Renewable Power Generation, 9(3) (2015) 218-227.

[321] M. Ghayekhloo, M. Ghofrani, M.B. Menhaj, R. Azimi, A novel clustering approach for short-term solar radiation forecasting, Solar Energy, 122 (2015) 1371-1383.

[322] G.A. Licciardi, R. Dambreville, J. Chanussot, S. Dubost, Spatiotemporal Pattern Recognition and Nonlinear PCA for Global Horizontal Irradiance Forecasting, Ieee Geoscience and Remote Sensing Letters, 12(2) (2015) 284-288.

[323] L. Mazorra Aguiar, B. Pereira, M. David, F. Díaz, P. Lauret, Use of satellite data to improve solar radiation forecasting with Bayesian Artificial Neural Networks, Solar Energy, 122 (2015) 1309-1324.

[324] L.M. Aguiar, B. Pereira, P. Lauret, F. Díaz, M. David, Combining solar irradiance measurements, satellite-derived data and a numerical weather prediction model to improve intra-day solar forecasting, Renewable Energy, 97 (2016) 599-610.

[325] M. David, F. Ramahatana, P.J. Trombe, P. Lauret, Probabilistic forecasting of the solar irradiance with recursive ARMA and GARCH models, Solar Energy, 133 (2016) 55-72.

[326] M. Gaston, C. Fernandez-Peruchena, H. Kornich, T. Landelius, A Combination of HARMONIE Short Time Direct Normal Irradiance Forecasts and Machine Learning: The #hashtdim Procedure, in: A. AlObaidli, N. Calvet, C. Richter (Eds.) International Conference on Concentrating Solar Power and Chemical Energy Systems, Vol. 1850, 2017.

[327] F.O. Hocaoglu, F. Serttas, A novel hybrid (Mycielski-Markov) model for hourly solar radiation forecasting, Renewable Energy, 108 (2017) 635-643.

[328] J. Ma, H. Jiang, K. Huang, Z. Bi, K.L. Man, Novel Field-Support Vector Regression-Based Soft Sensor for Accurate Estimation of Solar Irradiance, Ieee Transactions on Circuits and Systems I-Regular Papers, 64(12) (2017) 3183-3191.

[329] S. Monjoly, M. André, R. Calif, T. Soubdhan, Hourly forecasting of global solar radiation based on multiscale decomposition methods: A hybrid approach, Energy, 119 (2017) 288-298.

[330] G. Reikard, S.E. Haupt, T. Jensen, Forecasting ground-level irradiance over short horizons: Time series, meteorological, and time-varying parameter models, Renewable Energy, 112 (2017) 474-485.

[331] C. Crisosto, M. Hofmann, R. Mubarak, G. Seckmeyer, One-Hour Prediction of the Global Solar

Irradiance from All-Sky Images Using Artificial Neural Networks, Energies, 11(11) (2018).

[332] M. David, M.A. Luis, P. Lauret, Comparison of intraday probabilistic forecasting of solar irradiance using only endogenous data, International Journal of Forecasting, 34(3) (2018) 529-547.

[333] H. Verbois, R. Huva, A. Rusydi, W. Walsh, Solar irradiance forecasting in the tropics using numerical weather prediction and statistical learning, Solar Energy, 162 (2018) 265-277.

[334] F. Wang, Y. Yu, Z. Zhang, J. Li, Z. Zhen, K. Li, Wavelet Decomposition and Convolutional LSTM Networks Based Improved Deep Learning Model for Solar Irradiance Forecasting, Applied Sciences-Basel, 8(8) (2018).

[335] Y. Ge, Y. Nan, L. Bai, A Hybrid Prediction Model for Solar Radiation Based on Long Short-Term Memory, Empirical Mode Decomposition, and Solar Profiles for Energy Harvesting Wireless Sensor Networks, Energies, 12(24) (2019).

[336] C. Huang, L. Wang, L.L. Lai, Data-Driven Short-Term Solar Irradiance Forecasting Based on Information of Neighboring Sites, Ieee Transactions on Industrial Electronics, 66(12) (2019) 9918-9927.

[337] W. Richardson, Jr., D. Canadillas, A. Moncada, R. Guerrero-Lemus, L. Shephard, R. Vega-Avila, H. Krishnaswami, Validation of All-Sky Imager Technology and Solar Irradiance Forecasting at Three Locations: NREL, San Antonio, Texas, and the Canary Islands, Spain, Applied Sciences-Basel, 9(4) (2019).

[338] T.A. Siddiqui, S. Bharadwaj, S. Kalyanaraman, A Deep Learning Approach to Solar-Irradiance Forecasting in Sky-Videos, 2019 IEEE Winter Conference on Applications of Computer Vision (WACV), (2019) 2166-2174.

[339] I. Urbich, J. Bendix, R. Mueller, The Seamless Solar Radiation (SESORA) Forecast for Solar Surface Irradiance-Method and Validation, Remote Sensing, 11(21) (2019).

[340] P. Wang, R. van Westrhenen, J.F. Meirink, S. van der Veen, W. Knap, Surface solar radiation forecasts by advecting cloud physical properties derived from Meteosat Second Generation observations, Solar Energy, 177 (2019) 47-58.

[341] T. Watanabe, D. Nohara, Prediction of time series for several hours of surface solar irradiance using one-granule cloud property data from satellite observations, Solar Energy, 186 (2019) 113-125.

[342] F.J. Rodríguez-Benítez, C. Arbizu-Barrena, J. Huertas-Tato, R. Aler-Mur, I. Galván-León, D. Pozo-Vázquez, A short-term solar radiation forecasting system for the Iberian Peninsula. Part 1: Models description and performance assessment, Solar Energy, 195 (2020) 396-412.

[343] Z. Wu, Q. Li, X. Xia, Multi-timescale forecast of solar irradiance based on multi-task learning and echo state network approaches, IEEE Transactions on Industrial Informatics, (2020) 1-1.

[344] G.M. Yagli, D. Yang, O. Gandhi, D. Srinivasan, Can we justify producing univariate machine-learning forecasts with satellite-derived solar irradiance?, Applied Energy, 259 (2020).

[345] A.F. Zambrano, L.F. Giraldo, Solar irradiance forecasting models without on-site training measurements, Renewable Energy, 152 (2020) 557-566.

[346] H. Zang, L. Liu, L. Sun, L. Cheng, Z. Wei, G. Sun, Short-term global horizontal irradiance

forecasting based on a hybrid CNN-LSTM model with spatiotemporal correlations, Renewable Energy, (2020).

[347] A.H. Nielsen, A. Iosifidis, H. Karstoft, IrradianceNet: Spatiotemporal deep learning model for satellite-derived solar irradiance short-term forecasting, Solar Energy, 228 (2021) 659-669.

[348] B. Schulz, M. El Ayari, S. Lerch, S. Baran, Post-processing numerical weather prediction ensembles for probabilistic solar irradiance forecasting, Solar Energy, 220 (2021) 1016-1031.

[349] A.H. Eşlik, E. Akarslan, F.O. Hocaoğlu, Short-term solar radiation forecasting with a novel image processing-based deep learning approach, Renewable Energy, 200 (2022) 1490-1505.

[350] J.O. Kamadinata, T.L. Ken, T. Suwa, Sky image-based solar irradiance prediction methodologies using artificial neural networks, Renewable Energy, 134 (2019) 837-845.

[351] T. Mertens, J. Kautz, F.V. Reeth, Exposure Fusion, 15th Pacific Conference on Computer Graphics and Applications (PG'07), (2007) 382-390. 10.1109/PG.2007.17

[352] M.A. Robertson, S. Borman, R.L. Stevenson, Dynamic range improvement through multiple exposures, Proceedings 1999 international conference on image processing (Cat. 99CH36348), (1999) 159-163.

[353] K. He, X. Zhang, S. Ren, J. Sun, Deep Residual Learning for Image Recognition, 2016 IEEE Conference on Computer Vision and Pattern Recognition (CVPR, (2016) 770-778.

[354] A. Canziani, A. Paszke, E. Culurciello, An analysis of deep neural network models for practical applications, arXiv preprint arXiv:1605.07678, (2016).

[355] A. Heydari, D.A. Garcia, F. Keynia, F. Bisegna, L. De Santoli, A novel composite neural network based method for wind and solar power forecasting in microgrids, Applied Energy, 251 (2019) 113353.

[356] D.H. Alamo, R.N. Medina, S.D. Ruano, S.S. García, K.P. Moustris, K.K. Kavadias, D. Zafirakis, G. Tzanes, E. Zafeiraki, G. Spyropoulos, An advanced forecasting system for the optimum energy management of island microgrids, Energy procedia, 159 (2019) 111-116.

[357] T. Bogaraj, J. Kanakaraj, Intelligent energy management control for independent microgrid, Sādhanā, 41(7) (2016) 755-769.

[358] J. Pascual, J. Barricarte, P. Sanchis, L. Marroyo, Energy management strategy for a renewable-based residential microgrid with generation and demand forecasting, Applied Energy, 158 (2015) 12-25.

[359] W. Shi, E.-K. Lee, D. Yao, R. Huang, C.-C. Chu, R. Gadh, Evaluating microgrid management and control with an implementable energy management system, 2014 IEEE International Conference on Smart Grid Communications (SmartGridComm), (2014) 272-277.

[360] S. Mohammadi, S. Soleymani, B. Mozafari, Scenario-based stochastic operation management of microgrid including wind, photovoltaic, micro-turbine, fuel cell and energy storage devices, International Journal of Electrical Power & Energy Systems, 54 (2014) 525-535.

[361] Y. Zhang, B. Liu, T. Zhang, B. Guo, An intelligent control strategy of battery energy storage system for microgrid energy management under forecast uncertainties, International Journal of Electrochemical Science, 9(8) (2014) 4190-4204.

[362] R. Samu, M. Calais, G. Shafiullah, M. Moghbel, M.A. Shoeb, B. Nouri, N. Blum, Applications for

solar irradiance nowcasting in the control of microgrids: A review, Renewable and Sustainable Energy Reviews, 147 (2021) 111187.

[363] G. Liu, M. Starke, B. Xiao, X. Zhang, K. Tomsovic, Microgrid optimal scheduling with chance-constrained islanding capability, Electric Power Systems Research, 145 (2017) 197-206.

[364] S. Sukumar, H. Mokhlis, S. Mekhilef, M. Karimi, S. Raza, Ramp-rate control approach based on dynamic smoothing parameter to mitigate solar PV output fluctuations, International Journal of Electrical Power & Energy Systems, 96 (2018) 296-305.

[365] K. Bot, A. Ruano, M.d.G. Ruano, Short-term forecasting photovoltaic solar power for home energy management systems, Inventions, 6(1) (2021) 12.

[366] S. Aslam, A. Khalid, N. Javaid, Towards efficient energy management in smart grids considering microgrids with day-ahead energy forecasting, Electric Power Systems Research, 182 (2020) 106232.

Publications from This Research

- Chen, Lei, and Yangluxi Li. “A state-of-art method for solar irradiance forecast via using fisheye lens.” International Journal of Low-Carbon Technologies,16.2 (2020): 555-569.

- Chen, Lei, Yangluxi Li, Hu Du, and Yu-kun Lai. “Solar radiation nowcasting through advanced CNN model integrated with ResNet structure.” Building Simulation conference 2021, Bruges, Belgium. IBPSA Publishing, 2021.

- Chen, Lei, Hu Du, and Yangluxi Li. “Scoping Low-Cost Measures to Nowcast Sub-Hourly Solar Radiations for Buildings.” IOP Conference Series: Earth and Environmental Science. Vol. 329. No. 1. IOP Publishing, 2019.

- Du, Hu, C.F. Bandera, and Lei Chen. “Nowcasting methods for optimising building performance”, 2019.

Appendix A: Other Nowcasting Results

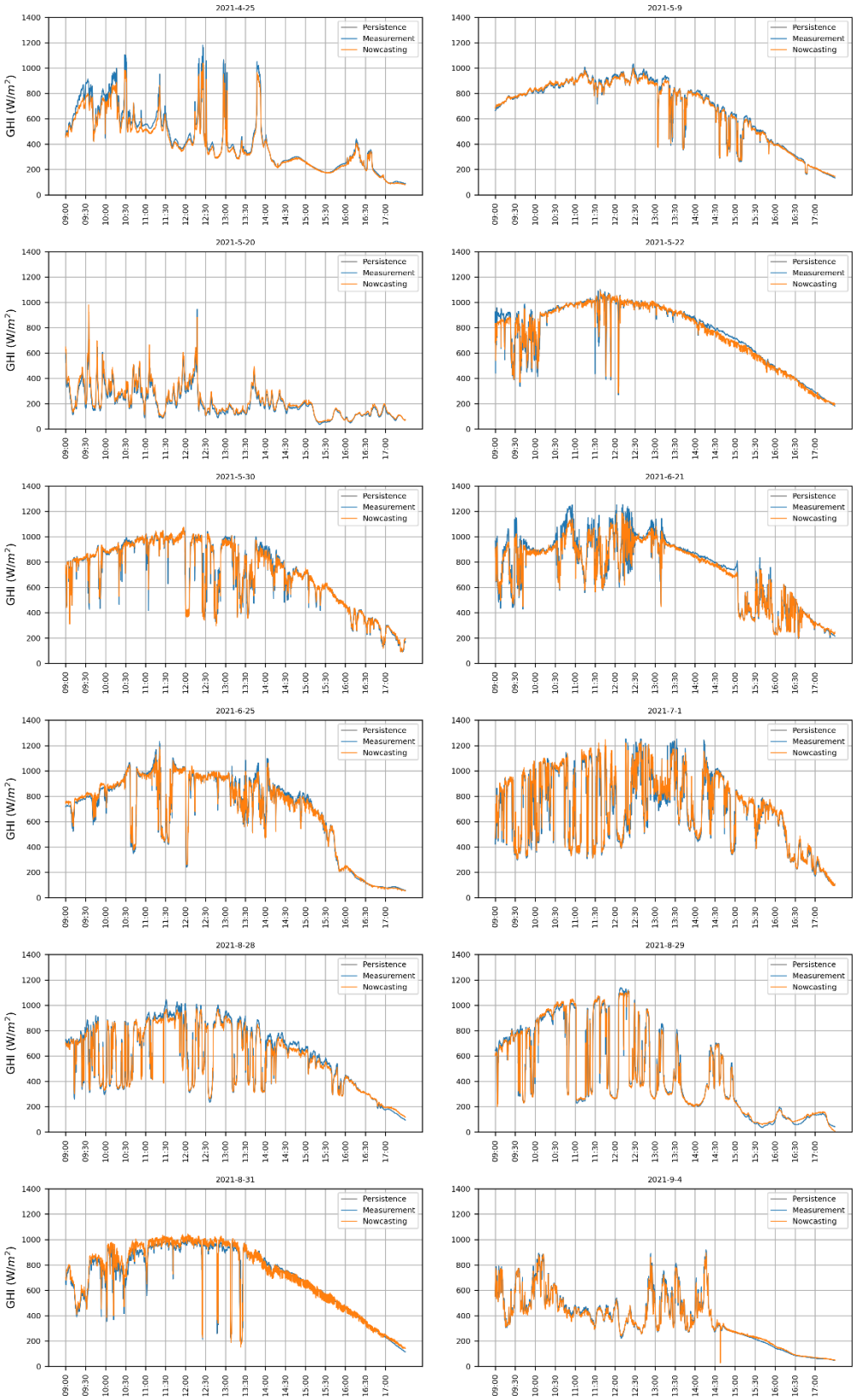

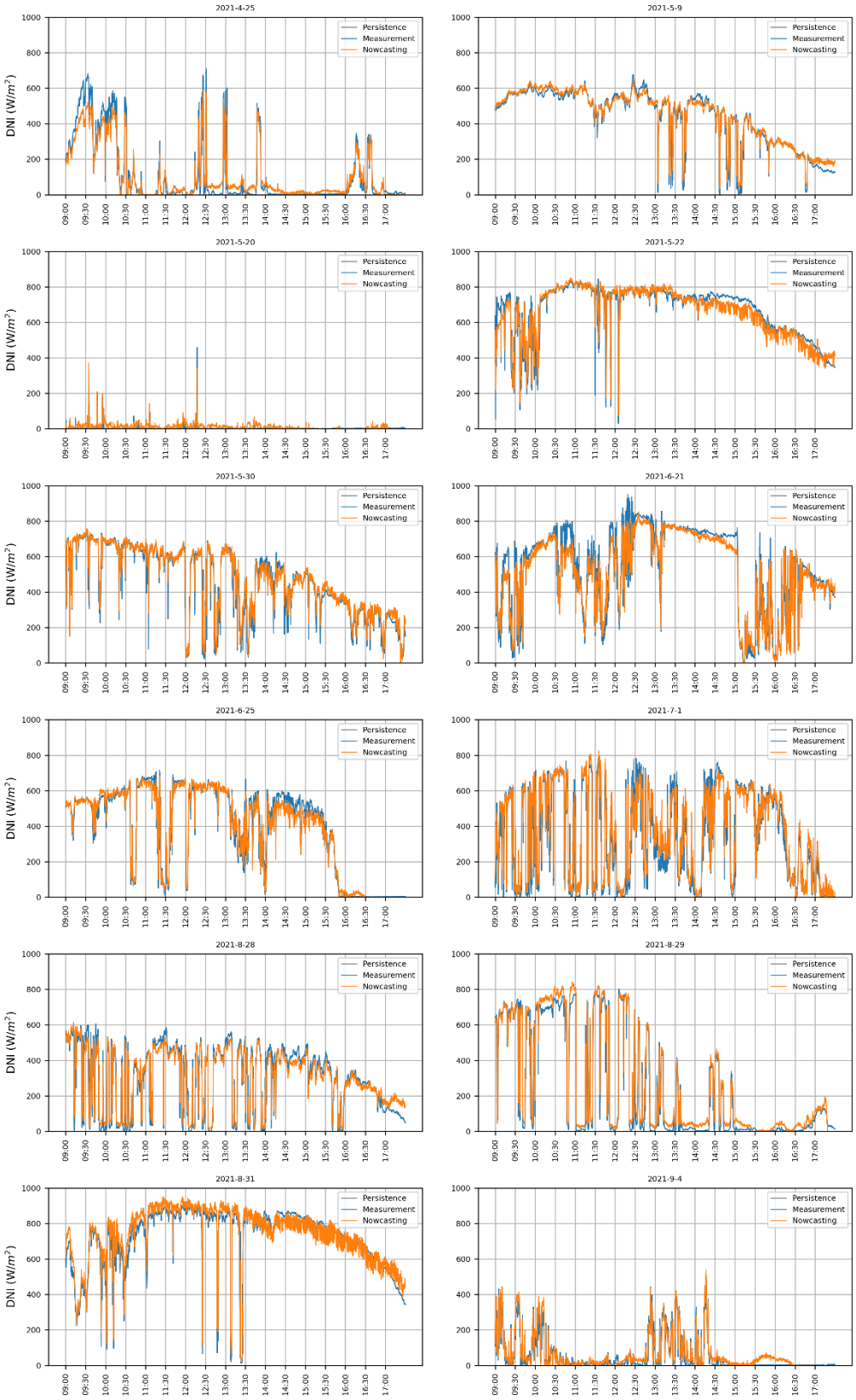
2021-4-25
2021-5-9
2021-5-20
2021-5-22
2021-5-30
2021-6-21
2021-6-25
2021-7-1
2021-8-28
2021-8-29
2021-8-31
2021-9-4
Persistence
Measurement
Nowcasting
DNI (W/m²)

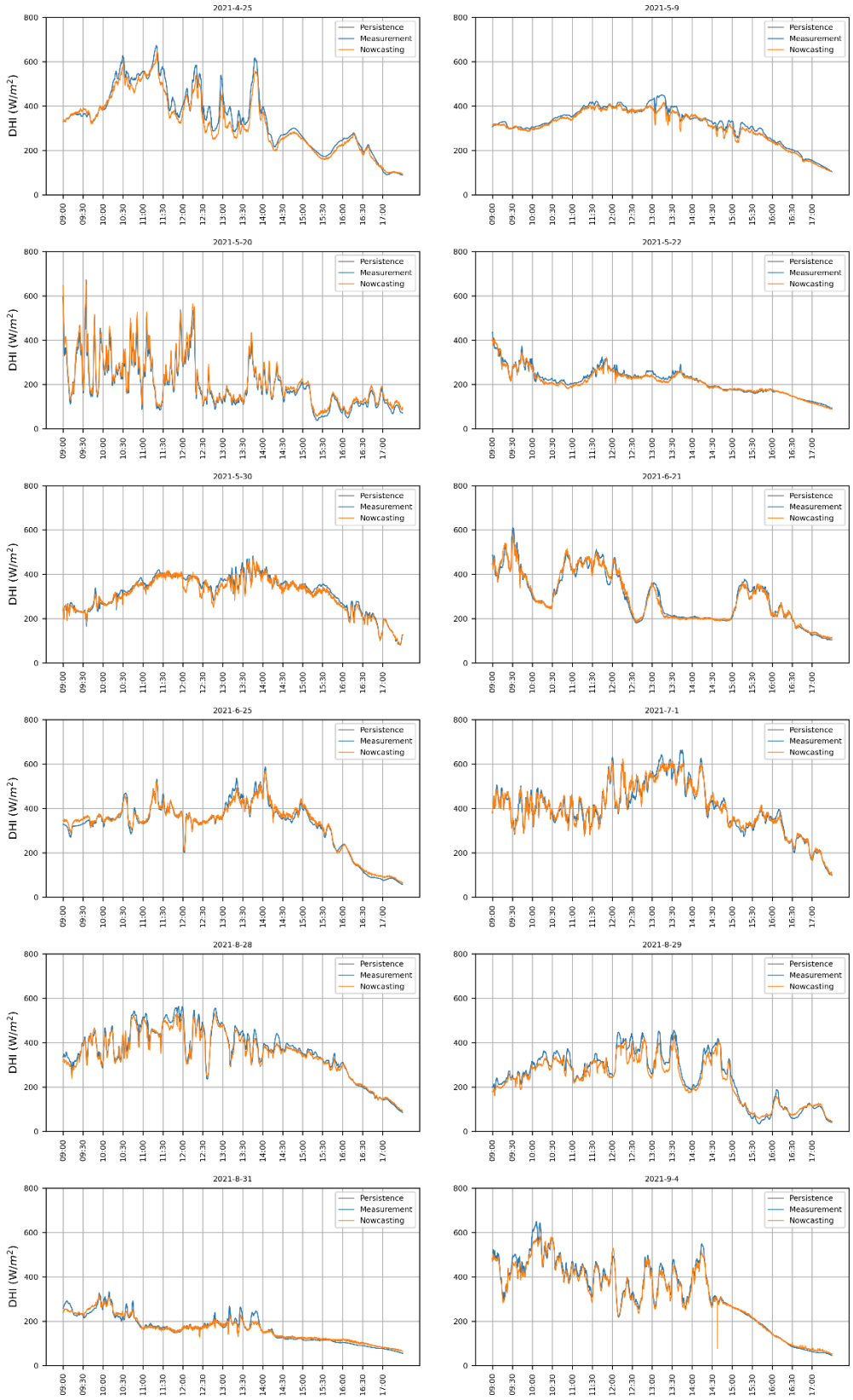

Nowcasting Performance at 10-sec time intervals for 10-sec nowcasting horizon

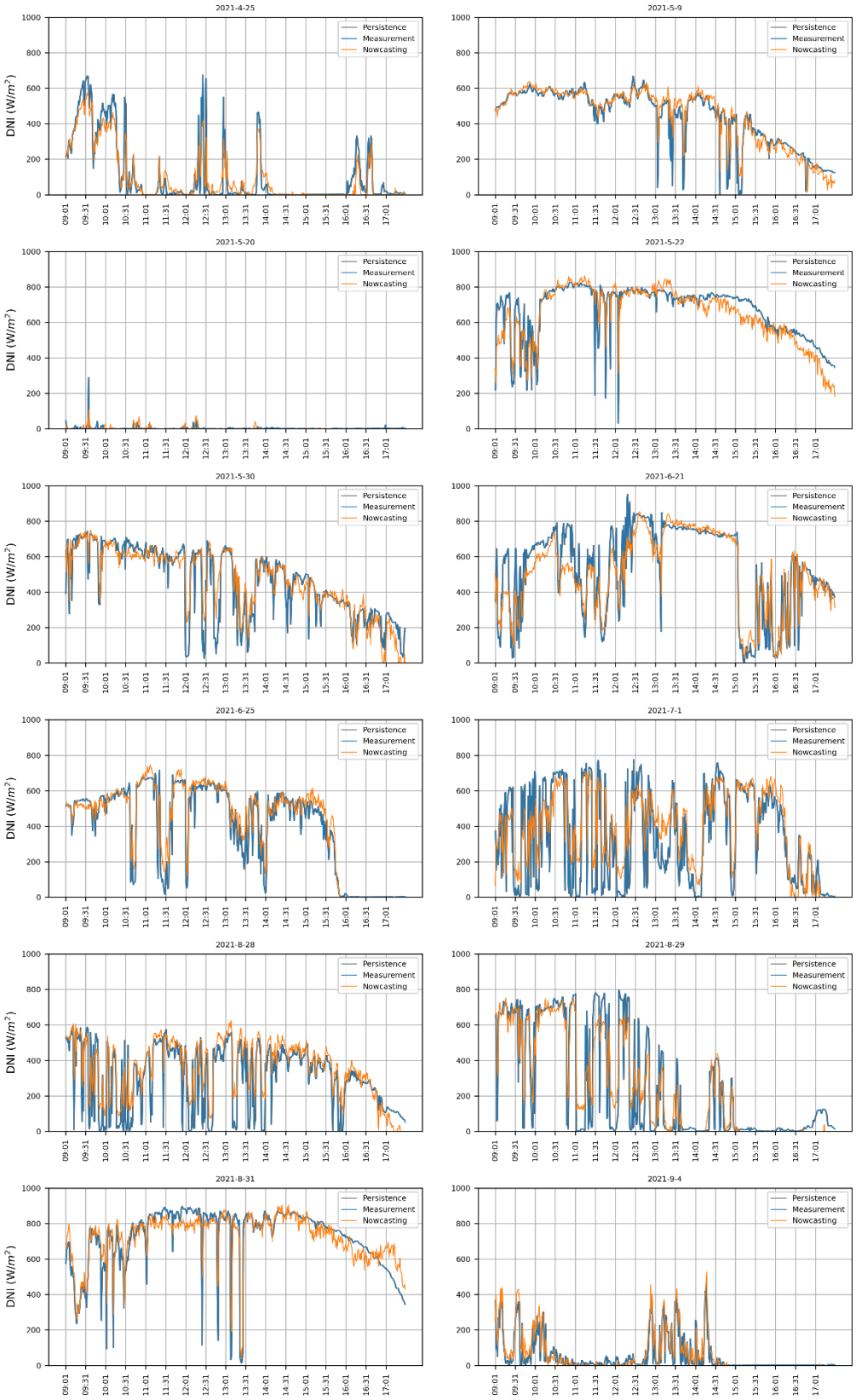
2021-4-25
2021-5-9
2021-5-20
2021-5-22
2021-5-30
2021-6-21
2021-6-25
2021-7-1
2021-8-28
2021-8-29
2021-8-31
2021-9-4
Persistence
Measurement
Nowcasting
DNI (W/m²)

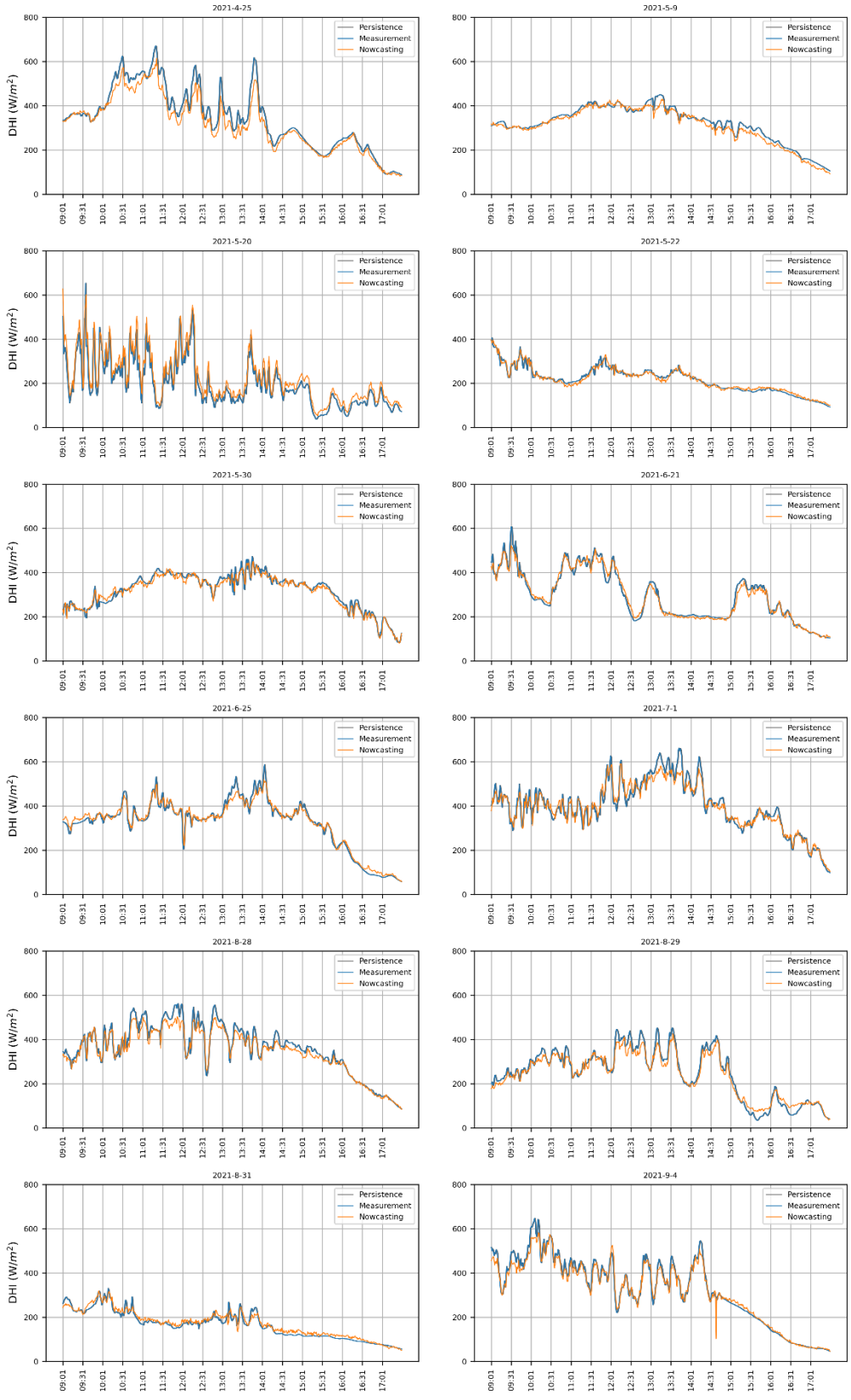

Nowcasting Performance at 1-min time intervals for 1-min nowcasting horizon

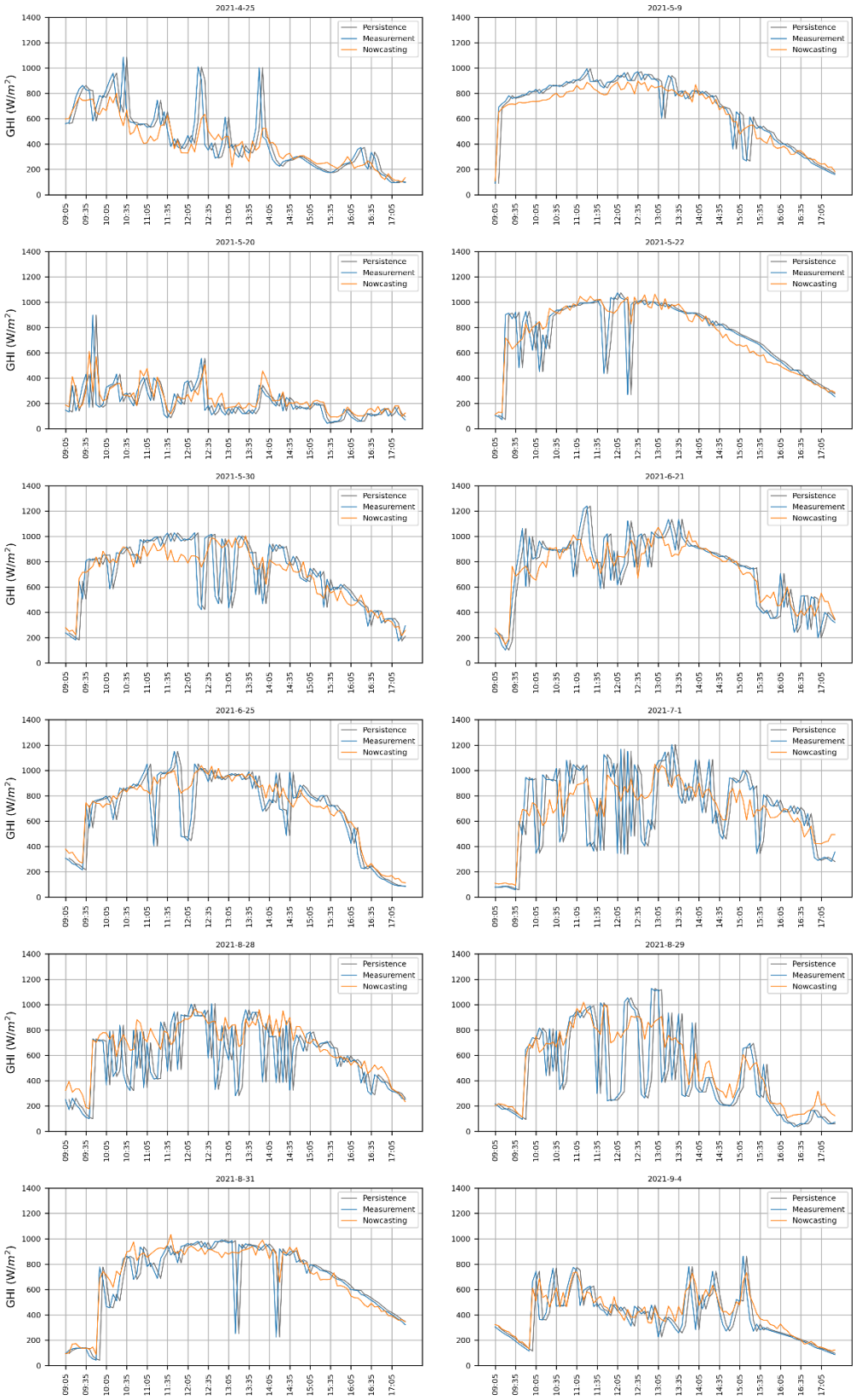
2021-4-25
2021-5-9
2021-5-20
2021-5-22
2021-5-30
2021-6-21
2021-6-25
2021-7-1
2021-8-28
2021-8-29
2021-8-31
2021-9-4
Persistence
Measurement
Nowcasting
GHI (W/m²)

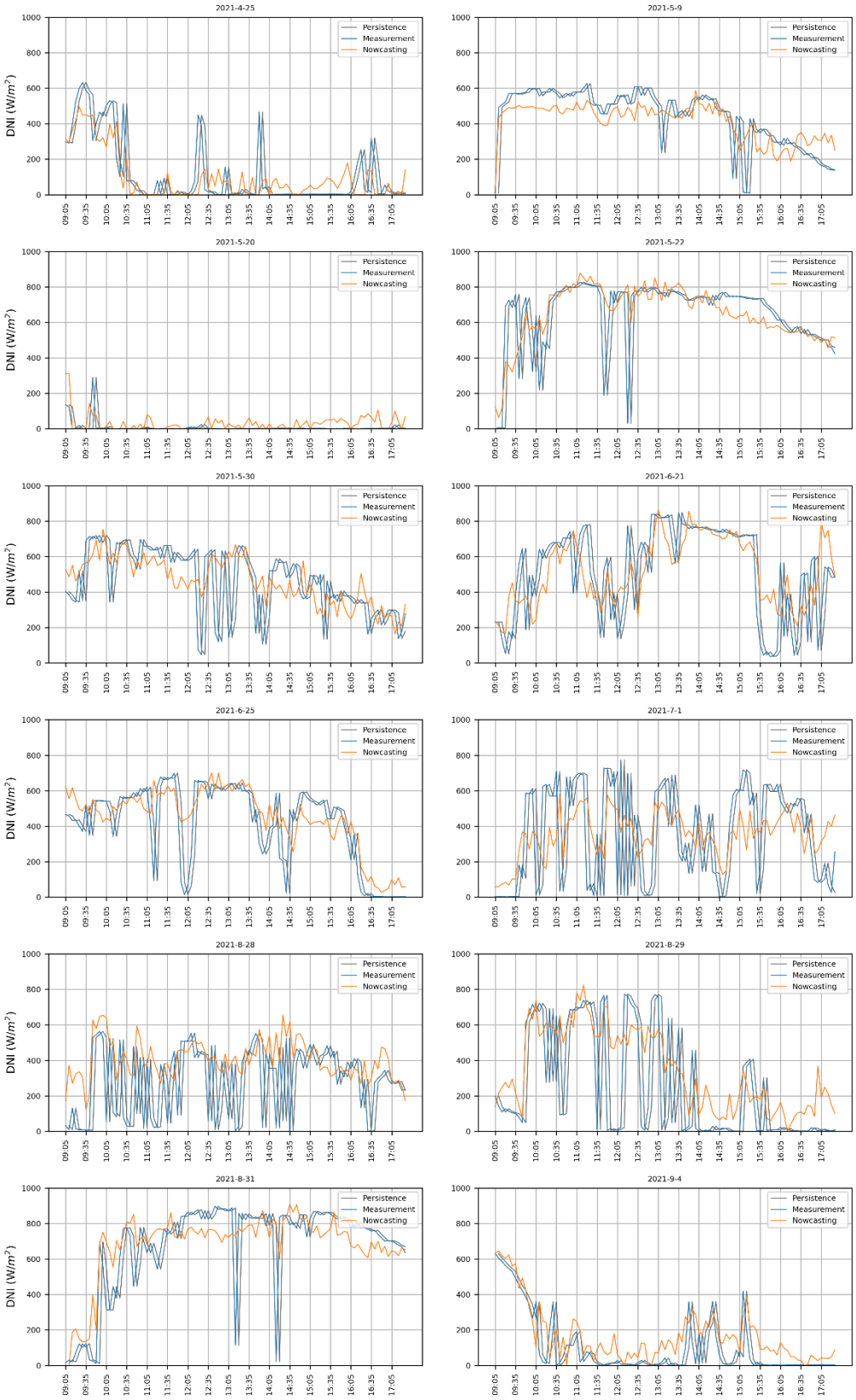
2021-4-25
2021-5-9
2021-5-20
2021-5-22
2021-5-30
2021-6-21
2021-6-25
2021-7-1
2021-8-28
2021-8-29
2021-8-31
2021-9-4
Persistence
Measurement
Nowcasting
DNI (W/m²)

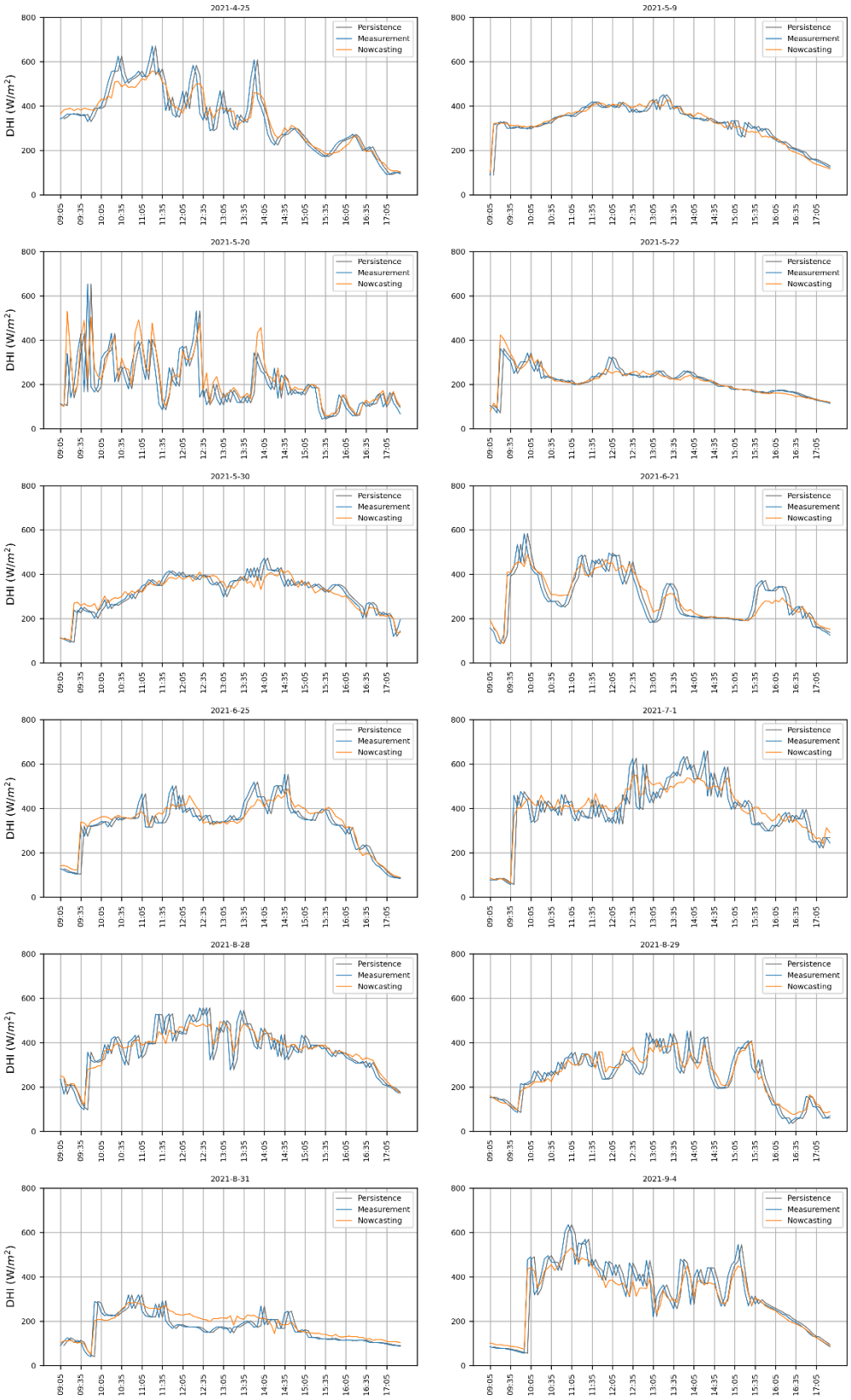

Nowcasting Performance at 5-min time intervals for 5-min nowcasting horizon

Appendix B：Data and Data Collection Process

All collected data of the research are shared on GitHub:

https://github.com/ChenL61/Collected-Data-of-Solar-Irradiance-Nowcasting-Research.git

The instruction of data collection process is presented below.

- The Collection of Cloud Images
    1. Installing WAVESHARE OV5647 fisheye lens on a Raspberry Pi.
    2. Connecting the Raspberry Pi to the 10000mAh power bank.
    3. Connecting the Raspberry Pi to Wi-Fi and logging into Raspberry Pi OS.
    4. Ensuring the system time of Raspberry Pi is correctly synchronized (Due to the system time stops when Raspberry Pi is turn off. While the program relies on the correct time to take photos, and incorrect synchronization can prevent the program from taking photos.)
    5. Running the data collection program written in python on the Raspberry Pi desktop.
    6. Fixing the Raspberry Pi camera on a tripod.
    7. Placing the tripod on the site for data collection.
    8. Collecting cloud images according to the time required.
    9. Using network transmission transferring the collected cloud images from Raspberry Pi.
- The Collection of GHI and DHI
    1. Connecting the BF5 Sunshine Sensor with a datalogger.
    2. Turning on the BF5 Sunshine Sensor.
    3. Fixing the Raspberry Pi camera on a tripod and placing the tripod on the site for data collection.
    4. Placing the BF5 Sunshine Sensor within 5 meters of the Raspberry Pi.
    5. Collecting GHI and DHI according to the time required.
    6. Connecting the datalogger to a computer and collecting GHI and DHI data.

Raspberry Pi Camera

BF5 Sunshine Sensor

Appendix C：Programming Work

- **Data Collection**

1.1 Pi_takeimage

```
from time import sleep
import time
from picamera import PiCamera
import datetime
import os

    pi take the images

    Args:
        LR_or_HR: type
        interval: interval time
        count: number of images
        save_path:  destination data
        exposures:  exposure
        log:  log of the images
    Returns:


save_path = "/home/pi/Desktop/"
camera = PiCamera()
count = 0
exposures = [100, 450, 700]
LR_or_HR = "LR"
resolutions = [(1600, 1200)] if LR_or_HR == "HR" else [(640, 480)]
archives = ['/HR']
interval = 10  # Unit: second
log = save_path+'/' + LR_or_HR + 'log.txt'

def takeImagesWithTime(iso_values,st_time, save_path):
        global count, save_path
        for exposure in exposures:
                # Set ISO to the desired value
                camera.iso = iso_values
                # Wait for the automatic gain control to settle
                sleep(1)
                # Now fix the values
                camera.saturation = 0
                camera.sharpness = 0
                camera.brightness = 50
                camera.contrast = 0
```

```
                camera.shutter_speed = exposure
                camera.exposure_mode = 'off'
                g = camera.awb_gains
                camera.awb_mode = 'off'
                camera.awb_gains = g

                img_time = st_time.strftime("(%Y-%m-%d %H-%M-%S)")
                for i, resolu in enumerate(resolutions):
                        camera.resolution = resolu
                        path =  + archives[i]
                        # Finally, take several photos with the fixed settings
                        camera.capture('%s/id%d_iso%d_expo%d_%s.jpg' %(path, count,
iso_values, exposure, img_time)) # image 名称
        count += 1

def main():
        iso = 100
        signal = False
        record = False
        print("hello! Begin getting data")

        Time = datetime.datetime.now()
        Time = time.strftime('%Y%m%d')
        save_path += Time
        if os.path.exists(save_path)==False:
                os.mkdir(save_path)
                for i in range(len(archives)):
                        os.mkdir(save_path + archives[i])
                print("create DIR path")
        f = open(log, 'a+')  # logs
        while True:
                time_now = datetime.datetime.now()
                # print('\rTime: %s' %(time_now.strftime('%Y/%m/%d %H:%M:%S')), end='',
flush=True)
                if time_now.hour == 8 and time_now.minute == 59 and time_now.second ==
58:
                        record = True
                        print('\nStart Record')
                        break

        while record:
                time_now = datetime.datetime.now()
                if time_now.hour == 17 and time_now.minute == 30:
                        record = False
                if(time_now.second % interval == 0):
                        signal = True
```

```
                if signal:
                        #S = time.time()
                        takeImagesWithTime(iso, time_now)
                        f.write('%s\n' %(time_now.strftime('%Y/%m/%d %H:%M:%S')))
                        signal = False
                        #E = time.time()
                        #print(E - S)
        f.flush()
        f.close()
        camera.close()
        print('Today is Done, have a rest.')


if __name__ == '__main__':
        main()
```

1.2 Pi_main

```
import os
import re
import time
import shutil
import datetime
import subprocess
import psutil
import urllib
import threading
import paramiko

from bs4 import BeautifulSoup
from urllib.parse import urlparse
from time import sleep
import logging
from pi_upload_config import *

time = time.strftime('%Y%m%d', time.localtime(time.time()))
download_path = os.path.join(download_path, time)
print(download_path)

import time


class PIload:
    def __init__(self, host, port, username, password):
        self.host = host
        self.port = port
```

```
            self.username = username
            self.password = password
            self.transport = None
            self.client = None
            self.init_logger()


    def init_logger(self):
        self.logger = logging.getLogger('efuseload')
        self.logger.setLevel('INFO')
        console = logging.StreamHandler()
        console.setLevel("INFO")
        formatter = logging.Formatter("%(asctime)s - %(name)s - %(levelname)s
- %(message)s")
        console.setFormatter(formatter)
        self.logger.addHandler(console)
        handler =
logging.FileHandler("/home/pi/Desktop/log/{}.txt".format(time.strftime('%Y%m%d',
time.localtime(time.time()))))
        handler.setLevel('INFO')
        handler.setFormatter(formatter)
        self.logger.addHandler(handler)

    def create_sftp_client(self):
        try:
            self.transport = paramiko.Transport((self.host, self.port))
            self.transport.connect(username=self.username, password=self.password)
            self.client = paramiko.SFTPClient.from_transport(self.transport)
            self.logger.info("create_sftp_client PASS")
        except Exception as e:
            self.logger.error(e)
            raise Exception(e)

    def stop_sftp_client(self):
        try:
            self.transport.close()
        except Exception as e:
            self.logger.error(e)
            raise Exception(e)

    def remove_file(self,file_path):
        files = os.listdir(file_path)
        for file in files:
            remove_file_path = os.join(file_path, file)
            os.remove(remove_file_path)

    def execute_efuse(self):  # execute
```

```
        for i in range(1):
            try:
                self.upload() #local_upload_path
                break
            except Exception as  ex :
                if i >= 0 :
                    raise Exception(ex)
                else:
                    self.logger.info("Update ftp fail times:{}".format(i+1))
                pass
        self.trans_file()
        self.logger.info("Update efuse PASS")

    def kill(self,proc_pid):
        parent_proc = psutil.Process(proc_pid)
        for child_proc in parent_proc.children(recursive=True):
            child_proc.kill()
        parent_proc.kill()


    def generate_url(self,command = 'generate_url.sh'):
        """ execute commands and judge result of returns
            Args:
            command: generate rul
            retest_allowed: false or true
        """
        url = ''
        bflag = False

        try:
            wpath = os.path.split(os.path.abspath(__file__))[0]
            cmd = "{}/{} ".format(wpath,command)
            proc = subprocess.Popen(args=[cmd],
                                    shell=True,
                                    stdout=subprocess.PIPE,
                                    stderr=subprocess.STDOUT,
                                    bufsize=1)

            while proc.poll() is None:
                for line in iter(proc.stdout.readline, b''):
                    line = line.decode('UTF-8')
                    self.logger.info("generate_url:{}".format(line))
                    if line.find("https://artifactory-cn.nevint.com:443/artifactory/firmware-all-
local/adc/fuse/") >= 0:
                        bflag = True
                        self.kill(proc.pid)
                        url_message = line.split("")
```

```
                    url = url_message[3]
                    self.logger.info("url message is: {}".format(line))
                    break
            self.logger.info("generate url is {}".format(url))

        except subprocess.CalledProcessError as e:
            self.logger.error(e)
            raise Exception(e)

        if bflag:
            self.logger.info("{} success".format(cmd))
            return url
        else:
            self.logger.info("{} fail".format(cmd))
            raise Exception("generate_url fail")
            return ' '

        try:
            is_existence = False
            self.logger.info(host)
            self.logger.info(port)
            self.logger.info("sftp connect pass")

             # private = paramiko.RSAKey.from_private_key_file('/Users/root/.ssh/id_rsa')
            # tran.connect(username="root", pkey=private)
            self.logger.info("sftp from_transport pass")

            #while not is_existence:
            #    is_existence = True if "request" in self.client.listdir(communicate_path) else
False
            #    if not is_existence:
            #        self.logger.info("upload pause")

            self.logger.info("start upload")

            is_existence = True if "running" in self.client.listdir(base_remote_path) else
False
            self.logger.info(self.client.listdir(base_remote_path))
            self.logger.info(is_existence)

            if not is_existence:
                self.client.mkdir(remote_path)

            files = os.listdir(download_path)
            for file in files:
                local_path = os.path.join(download_path, file)
                remote_upload_path = os.path.join(remote_path, file)
```

```
                self.logger.info(local_path)
                self.logger.info(remote_upload_path)
                self.client.put(local_path, remote_upload_path)
                self.logger.info("sftp put pass")

            except Exception as e:
                self.stop_sftp_client()
                self.logger.error(e)
                raise Exception(e)


        def renameftpdone(self):
            try:
                is_existence = False
                newfilepath = ""
                newfilepath = base_remote_path +"done_"+
    datetime.datetime.now().strftime('%Y%m%d%H%M%S')

                is_existence = True if "running" in self.client.listdir(base_remote_path) else
    False
                self.logger.info(self.client.listdir(base_remote_path))

                if is_existence:
                    self.logger.info(newfilepath)
                    self.client.rename(remote_path,newfilepath)
            except Exception as e:
                self.logger.error(e)
                raise Exception(e)
            self.logger.info("Renameftpdone PASS")


        def callbackfunc(self,blocknum, blocksize, totalsize):


            percent = 100.0 * blocknum * blocksize / totalsize
            if percent > 100:
                percent = 100
            print("%.2f%%" % percent)


        def trans_file(self):
            filename_list = os.listdir(download_path)
            for file in filename_list:
                used_name = os.path.join(download_path, file)
                new_name = os.path.join(local_save_path, file)
                self.logger.info("{} ==> {}".format(used_name, new_name))
                shutil.move(used_name, new_name)
```

```
def main():
    start_time = time.time()
    fuse_obj = PIload(host, port, sftp_username, sftp_password)
    fuse_obj.create_sftp_client()

    j = 1
    for i in range(efusenumber):
        fuse_obj.execute_efuse()
        if j == perfusenumber or i == efusenumber -1 :
            fuse_obj.renameftpdone()
            j = 0
        j = j + 1

    end_time = time.time()
    print("cost time is {}".format(end_time - start_time))
    fuse_obj.delete_files()
    fuse_obj.stop_sftp_client()
    #end_time = time.time()
    #print("cost time is {}".format(end_time - start_time))


if __name__ == '__main__':
    main()
```

- **Data Processing**

1. Masking

```
import numpy as np
import cv2


def make_mask(src_picture, th_num):
    image = cv2.imread(src_picture)
    gray_image = cv2.cvtColor(image, cv2.COLOR_BGR2GRAY)
    (T, mask_image) = cv2.threshold(gray_image, th_num, 255,
cv2.THRESH_BINARY)
    cv2.imshow("mask", mask_image)
    cv2.waitKey(0)
    cv2.imwrite("generated_template.jpg", mask_image)
    return mask_image

def mask_process(template, src_picture):
    src_picture = cv2.imread(src_picture)
    masked = cv2.bitwise_and(src_picture, src_picture, mask=template)
    cv2.imshow("ans", masked)
    cv2.imwrite("after_process.jpg", masked)
    cv2.waitKey(0)

def mask_dataset(template, img):
    cv2_img = cv2.imread(img)
    masked = cv2.bitwise_and(cv2_img, cv2_img, mask=template)
    return Image.fromarray(cv2.cvtColor(masked, cv2.COLOR_BGR2RGB))

def main():
    source_picture = "LR.jpg"
    threshold_number = 140
    template = make_mask(source_picture, threshold_number)
    mask_process(template, source_picture)


if __name__ == '__main__':
    main()
```

2. HDR

```
# encoding:utf8
import threading

import cv2
import numpy as np
import os
from natsort import ns, natsorted

index = 0
resolution = ['LR', 'HR']
date = '20210520'

#win
dir_path = r"D:\solar\solar"

root_path = os.path.join(dir_path, date)
save_path = root_path
print(save_path)



def robertson(img_fn, imgs_path, save_path, count):


    # img_fn = ['1tl.jpeg', '2tr.jpeg', '3bl.jpeg', '4br.jpeg']
    img_list = [cv2.imread(os.path.join(imgs_path, fn)) for fn in img_fn]
    expo = [100, 450, 700]
    exposure_times = np.array([1 / i for i in expo], dtype=np.float32)
    # exposure_times = np.array([15.0, 2.5, 0.25, 0.0333], dtype=np.float32)
    merge_robertson = cv2.createMergeRobertson()
    hdr_robertson = merge_robertson.process(img_list, times=exposure_times.copy())
    tonemap2 = cv2.createTonemapDrago(gamma=1.3)
    tonemap2.process(hdr_robertson.copy())

    merge_mertens = cv2.createMergeMertens()
    res_mertens = merge_mertens.process(img_list)

    # Convert datatype to 8-bit and save


    res_mertens_8bit = np.clip(res_mertens * 255, 0, 255).astype('uint8')

    cv2.imwrite(os.path.join(save_path , "%d.jpg" % count), res_mertens_8bit)
    pass
```

```
"""
Read the images in the files and do the HDR
input image format: id0_iso100_expo450_(2020-12-25 09-00-00).jpg
output image format: <n>.jpg
"""
if __name__ == '__main__':
    # combine every 3 images
    for day in date:
        total = 0
        dst_path = save_path + resolution[index] + '-HDR/'
        dst_path = os.path.join(save_path, resolution[index]+'-HDR')
        os.mkdir(dst_path)
        img_path = root_path + resolution[index] + '/'
        img_path = os.path.join(root_path, resolution[index])
        imgs = os.listdir(img_path)
              #  id0_iso100_expo450_(2020-12-21 09-00-00).jpg
        # for img in imgs:
                            #     if img[-19:-17] == "12":
        #         imgs.remove(img)
        imgs = natsorted(imgs)
        img_num = len(imgs)
        #print(imgs)
        for j in range(0, img_num, 3):
            thread = threading.Thread(target=robertson, args=(imgs[j:min(j + 3, img_num)],
img_path, dst_path, total))
            thread.run()
            total += 1
        print("%s ,count is %d" % (day, total))
```

- **Solar Irradiance Nowcasting**

1. Config

```
import argparse


def parsers():
    # Parameter setting
    parser = argparse.ArgumentParser("irradiance prediction")

    # Whether to add mask
    parser.add_argument('--mask', type=int, default=0, help='add mask ?')

    # Calculate the mean and standard deviation of the original training set
    parser.add_argument('--cal_mean_std_path', type=str,
default='/home/sda4/data/0min-300s-regular/DNI/LR/train',
                        help='path for calculating mean and standard deviation')

    # The original data set is divided into training, verification and test sets
    parser.add_argument('--source_train_path', type=str,
default='/home/sda4/data/0min-300s-regular/DNI/LR/train',
                        help='path of original training set')
    parser.add_argument('--source_test_path', type=str, default='/home/sda4/data/0min-
300s-regular/DNI/LR/test',
                        help='path of original test set')
    parser.add_argument('--target_train_path', type=str, default='data/train', help='target
path of train dataset')
    parser.add_argument('--target_val_path', type=str, default='data/val', help='target
path of validation dataset')
    parser.add_argument('--target_test_path', type=str, default='data/test', help='target
path of test dataset')

    # Set the path of training set, verification set and test set
    parser.add_argument('--train_path', type=str, default='data/train', help='path of train
dataset')
    parser.add_argument('--val_path', type=str, default='data/val', help='path of
validation dataset')
    parser.add_argument('--test_path', type=str, default='data/test', help='path of test
dataset')

    # Set the tag types of training and testing (GHI, DHI, DNI)
    parser.add_argument('--data_type', type=str, default='ghi', help='data type')

    # Name of the model
    parser.add_argument('--model_name', type=str, default='ResNet152', help='model
name that will be used')
```

```
        # Model and result saving path
        parser.add_argument('--save_path', type=str, default='result', help="the save path of
result")

        # Model loading path
        parser.add_argument('--load_model', type=str,
default='result/ResNet152_model_86.pt', help='the load model path')

        # Training settings
        parser.add_argument('--epoch', type=int, default=100, help='train epoches')
        parser.add_argument('--batch_size', type=int, default=16, help='batch size')
        parser.add_argument('--num_workers', type=int, default=0, help='number of cpus to
train')

        # Optimizer settings
        parser.add_argument('--lr', type=float, default=0.001, help='learning rate of model')
        parser.add_argument('--momentum', type=float, default=0.90, help='momentum of
learning')
        parser.add_argument('--weight_decay', type=float, default=0.01, help='regularization
parameter')

        args = parser.parse_args()
        return args
```

2. Cal_mean_std

```
import os
import numpy as np
import torch
import time
from torchvision import transforms
from PIL import Image
from config import parsers
import gc
import cv2

'''
Add a mask to an image
'''
def mask(img, mask_image):
    cv2_img = cv2.imread(img)
    masked = cv2.bitwise_and(cv2_img, cv2_img, mask=mask_image)
    return Image.fromarray(cv2.cvtColor(masked, cv2.COLOR_BGR2RGB))
```

```
if __name__ == '__main__':
    opt = parsers()
    train_path = opt.cal_mean_std_path
    add_mask = opt.mask
    image_mask = cv2.imread("LR.jpg")
    gray_image = cv2.cvtColor(image_mask, cv2.COLOR_BGR2GRAY)
    (T, mask_image) = cv2.threshold(gray_image, 140, 255, cv2.THRESH_BINARY)

    imgs = [os.path.join(train_path, i) for i in os.listdir(train_path)]
    # Crop the center of the picture to 480 * 480
    trans = transforms.Compose([
        transforms.CenterCrop(480),
        transforms.ToTensor()
    ])
    img_num = float(len(imgs))
    mean_tmp = np.array([0.0, 0.0, 0.0])
    std_tmp = np.array([0.0, 0.0, 0.0])
    cal_num = 0.0
    data = []

    # Take 2000 pictures as the unit, calculate mean and std respectively,
    # and finally take the average value
    for i in range(len(imgs)):
        if add_mask == 0:
            tmp = trans(Image.open(imgs[i])).numpy()
        else:
            tmp = trans(mask(imgs[i], mask_image)).numpy()
        mean_tmp[0] = mean_tmp[0] + np.mean(tmp[0, :, :])
        mean_tmp[1] = mean_tmp[1] + np.mean(tmp[1, :, :])
        mean_tmp[2] = mean_tmp[2] + np.mean(tmp[2, :, :])
        if ((i + 1) % 2000 == 0) or ((i + 1) == len(imgs)):
            cal_num = cal_num + 1.0
            data.append(tmp)
            data = np.array(data)
            std_tmp[0] = std_tmp[0] + np.std(data[:, 0, :, :])
            std_tmp[1] = std_tmp[1] + np.std(data[:, 1, :, :])
            std_tmp[2] = std_tmp[2] + np.std(data[:, 2, :, :])
            del data
            gc.collect()
            data = []
        else:
            data.append(tmp)

    mean_tmp = mean_tmp / img_num
    std_tmp = std_tmp / cal_num
    # Output calculation results of mean and standard deviation
    print('mean:')
```

```
    print(mean_tmp)
    print('std:')
    print(std_tmp)
```

3. Split Dataset

```
import numpy as np
import os
from shutil import copy
import random
from config import parsers

'''
The original training set is divided into training set and verification set by 8:2
    source_path: the path of the original data set
'''
def split_file_list(source_path):
    imgs = [os.path.join(source_path, i) for i in os.listdir(source_path)]
    random.shuffle(imgs)
    img_num = len(imgs)
    return imgs[:int(img_num * 0.8)], imgs[int(img_num * 0.8):]


if __name__ == '__main__':
    opt = parsers()
    # The dataset is divided into training set, verification set and test set

    # The training set and the verification set are divided from the original training set,
    # and the test set is the original test set。
    file_path = opt.source_train_path
    test_path = opt.source_test_path
    train_path = opt.target_train_path
    val_path = opt.target_val_path
    test_target_path = opt.target_test_path
    train_files, val_files = split_file_list(file_path)
    test_files = [os.path.join(test_path, i) for i in os.listdir(test_path)]
    for i in range(len(train_files)):
        copy(train_files[i], train_path)
    for i in range(len(val_files)):
        copy(val_files[i], val_path)
    for i in range(len(test_files)):
        copy(test_files[i], test_target_path)

    print('Data set partition completed!')
```

4. Dataset

```
import numpy as np
import os
import cv2
import torch
from torch.utils.data import Dataset
from torchvision import transforms
from PIL import Image


class MyDataSet(Dataset):
    """
    Data processing and loading of training sets and validation sets

        img_path: data set path
        train: true is the training set, false is the verification set
        target_label: labels requiring training and prediction (GHI, DHI, DNI)
        add_mask: whether to add a mask to the picture (0 is not added, 1 is added)
    """

    def __init__(self, img_path, train=True, transform=None, target_label='ghi',
add_mask=0):
        self.label = target_label
        self.add_mask = add_mask
        self.file_path = img_path
        self.imgs = [os.path.join(self.file_path, i) for i in os.listdir(self.file_path)]
        self.img_num = len(self.imgs)

        self.image_mask = cv2.imread("LR.jpg")
        self.gray_image = cv2.cvtColor(self.image_mask, cv2.COLOR_BGR2GRAY)
        (T, self.mask_image) = cv2.threshold(self.gray_image, 140, 255,
cv2.THRESH_BINARY)

        # Standardize data sets
        self.normalize = transforms.Normalize(
            mean=[0.4922, 0.5424, 0.5440],
            std=[0.2952, 0.3117, 0.3254]
        )
        if train:
            self.trans = transforms.Compose([
                transforms.CenterCrop(480),
                transforms.RandomHorizontalFlip(),
                transforms.ToTensor(),
                self.normalize
            ])
        else:
```

```
            self.trans = transforms.Compose([
                transforms.CenterCrop(480),
                transforms.ToTensor(),
                self.normalize
            ])

        self.date_list = []
        for i in range(self.img_num):
            date = ""
            date_arr = (self.imgs[i].split('/')[-1].split('-')[1:6])
            n = len(date_arr)
            for j in range(n):
                date += date_arr[j]
                if (j == 0 or j == 1):
                    date += "-"
                if (j == 2 or j == 3):
                    date += ":"
                self.date_list.append(date)


    def mask(self, img, mask_image):
        # Function to add mask
        cv2_img = cv2.imread(img)
        masked = cv2.bitwise_and(cv2_img, cv2_img, mask=mask_image)
        return Image.fromarray(cv2.cvtColor(masked, cv2.COLOR_BGR2RGB))


    def __getitem__(self, index):
        if self.add_mask == 0:
            data_tmp = self.trans(Image.open(self.imgs[index]))
        else:
            data_tmp = self.trans(self.mask(self.imgs[index], self.mask_image))

        target_tmp = None
        # Process tags that need to be predicted
        if self.label == 'ghi':
            target_tmp = float(self.imgs[index].split('/')[-1].split('-')[6]) / 1000.0
            target_tmp = torch.tensor(target_tmp)
        elif self.label == 'dhi':
            target_tmp = float(self.imgs[index].split('/')[-1].split('-')[7]) / 600.0
            target_tmp = torch.tensor(target_tmp)
        elif self.label == 'dni':
            target_tmp = float(self.imgs[index].split('/')[-1].split('-')[8]) / 800.0
            target_tmp = torch.tensor(target_tmp)

        date_tmp = self.date_list[index]
```

```
            return data_tmp, target_tmp, date_tmp

        def __len__(self):
            return self.img_num


    class MyDataSetTest(Dataset):
        """
        Data processing and loading of test set

            img_path: data set path
            target_label: labels requiring prediction (GHI, DHI, DNI)
            add_mask: whether to add a mask to the picture (0 is not added, 1 is added)
        """

        def __init__(self, img_path, transform=None, target_label='ghi', add_mask=0):
            self.label = target_label
            self.file_path = img_path
            self.add_mask = add_mask
            self.imgs = [os.path.join(self.file_path, i) for i in os.listdir(self.file_path)]
            #self.imgs = sorted(self.imgs, key=lambda x: int(x.split('/')[-1].split('-
')[0].split('\\')[1]))
            self.imgs = sorted(self.imgs, key=lambda x: int(x.split('/')[-1].split('-')[0]))
            self.img_num = len(self.imgs)

            self.image_mask = cv2.imread("LR.jpg")
            self.gray_image = cv2.cvtColor(self.image_mask, cv2.COLOR_BGR2GRAY)
            (T, self.mask_image) = cv2.threshold(self.gray_image, 140, 255,
cv2.THRESH_BINARY)


            # Standardize data sets
            self.normalize = transforms.Normalize(
                mean=[0.4922, 0.5424, 0.5440],
                std=[0.2952, 0.3117, 0.3254]
            )
            self.trans = transforms.Compose([
                transforms.CenterCrop(480),
                transforms.ToTensor(),
                self.normalize
            ])


            self.date_list = []
            for i in range(self.img_num):
                date = ""
                date_arr = (self.imgs[i].split('/')[-1].split('-')[1:6])
```

```
            n = len(date_arr)
            for j in range(n):
                date += date_arr[j]
                if (j == 0 or j == 1):
                    date += "-"
                if (j == 2 or j == 3):
                    date += ":"
            self.date_list.append(date)


    def mask(self, img, mask_image):
        # Function to add mask
        cv2_img = cv2.imread(img)
        masked = cv2.bitwise_and(cv2_img, cv2_img, mask=mask_image)
        return Image.fromarray(cv2.cvtColor(masked, cv2.COLOR_BGR2RGB))


    def __getitem__(self, index):
        if self.add_mask == 0:
            data_tmp = self.trans(Image.open(self.imgs[index]))
        else:
            data_tmp = self.trans(self.mask(self.imgs[index], self.mask_image))
        target_tmp = None
        # Process tags that need to be predicted
        if self.label == 'ghi':
            target_tmp = float(self.imgs[index].split('/')[-1].split('-')[6]) / 1000.0
            target_tmp = torch.tensor(target_tmp)
        elif self.label == 'dhi':
            target_tmp = float(self.imgs[index].split('/')[-1].split('-')[7]) / 600.0
            target_tmp = torch.tensor(target_tmp)
        elif self.label == 'dni':
            target_tmp = float(self.imgs[index].split('/')[-1].split('-')[8]) / 800.0
            target_tmp = torch.tensor(target_tmp)

        date_tmp = self.date_list[index]

        return data_tmp, target_tmp, date_tmp

    def __len__(self):
        return self.img_num
```

5. ResNet-50

```
from torch import nn
import torchvision


# Model architecture of resnet50
class ResNet50(nn.Module):
    def __init__(self):
        super(ResNet50, self).__init__()
        self.resnet50 = torchvision.models.resnet50(pretrained=True)
        self.fc3 = nn.Linear(1000, 1)

    def forward(self, x):
        x = self.resnet50(x)
        x = self.fc3(x)
        return x
```

6. ResNet-152

```
from torch import nn
import torchvision


# Model architecture of resnet152
class ResNet152(nn.Module):
    def __init__(self):
        super(ResNet152, self).__init__()
        self.resnet152 = torchvision.models.resnet152(pretrained=True)
        self.fc3 = nn.Linear(1000, 1)

    def forward(self, x):
        x = self.resnet152(x)
        x = self.fc3(x)
        return x
```

7. Model Training

```
import torch
from torch import nn
import time
from dataset import MyDataSet
from torch.utils.data import DataLoader
import numpy as np
from config import parsers
```

```
from ResNet50 import ResNet50
from ResNet152 import ResNet152


"""
Function for model training

    net: Model used
    train_loader: Training set
    val_loader: Validation set
    num_epochs: Training rounds
    lr: learning rate
    device: Equipment used in the training (CPU or GPU)
    save_file: File to store training information
    net_name: Model name used
    momentum: Momentum value
    weight_decay: Parameters for weight decay
    save_file_path: Path to save training results
"""
def train_model(net, train_loader, val_loader, num_epochs, lr, device, save_file,
net_name,
                momentum, weight_decay, save_file_path):
    net.to(device)
    optimizer = torch.optim.SGD(net.parameters(), lr=lr, momentum=momentum,
weight_decay=weight_decay)
    # Learning rate decay
    milestones = [15, 50, 80]
    torch.optim.lr_scheduler.MultiStepLR(optimizer=optimizer, milestones=milestones,
gamma=0.1, last_epoch=-1)
    best_loss = 1e8

    # Using mean square error loss
    loss = nn.MSELoss()
    for epoch in range(num_epochs):
        time_start = time.time()
        train_loss = 0.0
        all_num = 0.0
        net.train()
        for i, (X, y, date) in enumerate(train_loader):
            optimizer.zero_grad()
            X, y = X.to(device), y.to(device)
            y = y.reshape(-1, 1)
            y_hat = net(X)
            l = loss(y_hat, y)
            l.backward()
            optimizer.step()
            with torch.no_grad():
```

```
                train_loss = train_loss + l * X.shape[0]
                all_num = all_num + X.shape[0]
            train_loss = train_loss / all_num
            epoch_time = time.time() - time_start

            # Use the validation set to evaluate the training result
            mae_loss, mbe_loss, mse_loss, rmse_loss, mape_loss, corr_loss =
evaluate_valloss(net, val_loader, device=device)

            # Store the best performing model parameters in the validation set
            if best_loss > mae_loss:
                best_loss = mae_loss
                model_name = save_file_path + '/' + net_name + "_model_{}".format(epoch + 1)
+ ".pt"
                torch.save(net.state_dict(), model_name)
            print("epoch: {} train loss: {} epoch_time: {} MAE: {} MBE: {} MSE: {} RMSE: {}
MAPE: {} Corr: {}".format(
                epoch+1, train_loss, epoch_time, mae_loss[0], mbe_loss[0], mse_loss[0],
rmse_loss[0], mape_loss[0], corr_loss
            ))
            save_file.write("epoch: {} train loss: {} epoch_time: {} MAE: {} MBE: {} MSE: {}
RMSE: {} MAPE: {} Corr: {}\n".format(
                epoch+1, train_loss, epoch_time, mae_loss[0], mbe_loss[0], mse_loss[0],
rmse_loss[0], mape_loss[0], corr_loss
            ))



    """
        The tag value predicted by the model is compared with the real value
        to calculate each evaluation index

            net: Model used
            data_iter: Data sets to be evaluated
            device: Equipment used in the evaluation (CPU or GPU)
    """
    def evaluate_valloss(net, data_iter, device=None):
        if isinstance(net, nn.Module):
            net.eval()  # Set to evaluation mode
            if not device:
                device = next(iter(net.parameters())).device
        net.eval()
        mse_loss = 0.0
        mae_loss = 0.0
        mbe_loss = 0.0
        mape_loss = 0.0
        all_num = 0.0
```

```
        predict = None
        target_all = None
        with torch.no_grad():
            for X, y, date in data_iter:
                X = X.to(device)
                y = y.to(device)
                y = y.reshape(-1, 1)
                all_num = all_num + y.numel()
                y_hat = net(X)
                if predict is None:
                    predict = y_hat
                    target_all = y
                else:
                    predict = torch.cat((predict, y_hat))
                    target_all = torch.cat((target_all, y))
                y = y.cpu().numpy()
                y_hat = y_hat.cpu().numpy()
                y = y
                y_hat = y_hat
                mae_loss = mae_loss + sum(abs(y-y_hat))
                mbe_loss = mbe_loss + sum(y-y_hat)
                mse_loss = mse_loss + sum((y - y_hat)**2)
                mape_loss = mape_loss + sum(abs((y - y_hat) / y))
        mae_loss = mae_loss / all_num
        mbe_loss = mbe_loss / all_num
        mse_loss = mse_loss / all_num
        rmse_loss = np.sqrt(mse_loss)
        mape_loss = (mape_loss / all_num) * 100.0
        mean_p = predict.mean()
        mean_g = target_all.mean()
        sigma_p = predict.std()
        sigma_g = target_all.std()
        correlation = ((predict - mean_p) * (target_all - mean_g)).mean(axis=0) / (sigma_p *
sigma_g)
        index = (sigma_g != 0)
        correlation = (correlation[index]).mean()
        return mae_loss, mbe_loss, mse_loss, rmse_loss, mape_loss, correlation


    if __name__ == "__main__":
        torch.cuda.set_device(0)
        opt = parsers()
        # Parameter setting
        train_info_file = opt.save_path + '/' + 'train_info.txt'
        file_to_write = open(train_info_file, 'a')

        # Training with GPU
```

```
        device = torch.device("cuda" if torch.cuda.is_available() else "cpu")
        time_pre = time.time()

        # Data acquisition and data division
        train_dataset = MyDataSet(img_path=opt.train_path, train=True,
target_label=opt.data_type, add_mask=opt.mask)
        val_dataset = MyDataSet(img_path=opt.val_path, train=False,
target_label=opt.data_type, add_mask=opt.mask)
        train_loader = DataLoader(train_dataset, batch_size=opt.batch_size, shuffle=True,
num_workers=opt.num_workers)
        val_loader = DataLoader(val_dataset, batch_size=opt.batch_size, shuffle=False,
num_workers=opt.num_workers)

        net = None
        # Select model architecture
        if opt.model_name == 'ResNet152':
            net = ResNet152()
        elif opt.model_name == 'ResNet50':
            net = ResNet50()

        # Start training
        train_model(net=net, train_loader=train_loader, val_loader=val_loader,
num_epochs=opt.epoch, lr=opt.lr, device=device,
                    save_file=file_to_write, net_name=opt.model_name,
momentum=opt.momentum, weight_decay=opt.weight_decay,
                    save_file_path=opt.save_path)
        file_to_write.close()
        time_all = time.time() - time_pre
        print("Run time is {}".format(time_all))
```

8. GHI and DHI Nowcasting

```
import torch
from config import parsers
from ResNet152 import ResNet152
from ResNet50 import ResNet50
from torch.utils.data import DataLoader
from dataset import MyDataSetTest
import numpy as np
from torch import nn
import pandas as pd
import os
os.environ["CUDA_VISIBLE_DEVICES"] = "1"

"""
Function to load the model
```

```
    model_path: Path of model storage
    model_name: Model name used
    device: Equipment used in the prediction (CPU or GPU)
"""
def load_model(model_path, model_name, device):
    if model_name == "ResNet50":
        net = ResNet50()
    elif model_name == "ResNet152":
        net = ResNet152()

    net.load_state_dict(torch.load(model_path))
    net = net.to(device)
    net.eval()
    return net


# Convert timestamp to date type
def dateparse(timestamp):
    time = pd.datetime.strptime(timestamp, "%Y-%m-%d %H:%M:%S")
    return time


"""
Use the model to predict the label of the test set
and compare it with the real value to calculate various indicators

        net: Loaded model
        data_iter: the test set
        label_type: Label type to be predicted (GHI, DHI, DNI)
        save_path: Save path of predicted results and indicators
        device: Equipment used in the evaluation (CPU or GPU)
"""
def evaluate_valloss(net, data_iter, label_type, save_path, device=None):
    if isinstance(net, nn.Module):
        net.eval()  # Set to evaluation mode
        if not device:
            device = next(iter(net.parameters())).device
    net.eval()
    mse_loss = 0.0
    mae_loss = 0.0
    mbe_loss = 0.0
    mape_loss = 0.0
    all_num = 0.0
    df_result = pd.DataFrame()
    date_list = []
    predict = None
```

```
        target_all = None
        with torch.no_grad():
            for X, y, date in data_iter:
                X = X.to(device)
                y = y.to(device)
                if label_type == 'ghi':
                    y = y.reshape(-1, 1) * 1000.0
                    all_num = all_num + y.numel()
                    y_hat = net(X) * 1000.0
                elif label_type == 'dhi':
                    y = y.reshape(-1, 1) * 600.0
                    all_num = all_num + y.numel()
                    y_hat = net(X) * 600.0
                elif label_type == 'dni':
                    y = y.reshape(-1, 1) * 800.0
                    all_num = all_num + y.numel()
                    y_hat = net(X) * 800.0
                if predict is None:
                    predict = y_hat
                    target_all = y
                else:
                    predict = torch.cat((predict, y_hat))
                    target_all = torch.cat((target_all, y))
                date_tmp = list(date)
                date_list = date_list + date_tmp
                y = y.cpu().numpy()
                y_hat = y_hat.cpu().numpy()
                y = y
                y_hat = y_hat
                mae_loss = mae_loss + sum(abs(y-y_hat))
                mbe_loss = mbe_loss + sum(y-y_hat)
                mse_loss = mse_loss + sum((y - y_hat)**2)
                mape_loss = mape_loss + sum(abs((y - y_hat) / y))
        mae_loss = mae_loss / all_num
        mbe_loss = mbe_loss / all_num
        mse_loss = mse_loss / all_num
        rmse_loss = np.sqrt(mse_loss)
        mape_loss = (mape_loss / all_num) * 100.0
        mean_p = predict.mean()
        mean_g = target_all.mean()
        sigma_p = predict.std()
        sigma_g = target_all.std()
        correlation = ((predict - mean_p) * (target_all - mean_g)).mean(axis=0) / (sigma_p *
sigma_g)
        index = (sigma_g != 0)
        correlation = (correlation[index]).mean()
        predict = predict.cpu().numpy().reshape(-1, )
```

```
        target_all = target_all.cpu().numpy().reshape(-1, )
        df_result['Time'] = date_list
        df_result['Time'] = df_result['Time'].map(dateparse)
        if label_type == 'ghi':
            df_result['ghi_target'] = target_all
            df_result['ghi_predict'] = predict
            save_result = save_path + '/' + 'ghi_result.csv'
            df_result.to_csv(save_result, index=None)
        elif label_type == 'dhi':
            df_result['dhi_target'] = target_all
            df_result['dhi_predict'] = predict
            save_result = save_path + '/' + 'dhi_result.csv'
            df_result.to_csv(save_result, index=None)
        elif label_type == 'dni':
            df_result['dni_target'] = target_all
            df_result['dni_predict'] = predict
            save_result = save_path + '/' + 'dni_result.csv'
            df_result.to_csv(save_result, index=None)

        return mae_loss, mbe_loss, mse_loss, rmse_loss, mape_loss, correlation


    if __name__ == "__main__":
        opt = parsers()
        # Parameter setting
        batch_size = opt.batch_size
        eval_epochs = opt.epoch
        eval_path = opt.test_path
        model_name = opt.model_name
        model_path = opt.load_model
        device = torch.device("cuda" if torch.cuda.is_available() else "cpu")
        #device = torch.device("cpu")

        # Load the test dataset
        test_dataset = MyDataSetTest(img_path=eval_path, target_label=opt.data_type,
add_mask=opt.mask)
        test_loader = DataLoader(test_dataset, batch_size=batch_size, shuffle=False,
num_workers=opt.num_workers)

        # Load the model and use it for prediction and indicator calculation
        net = load_model(model_path=model_path, model_name=model_name,
device=device)
        mae_loss, mbe_loss, mse_loss, rmse_loss, mape_loss, correlation =
evaluate_valloss(net=net,
                                                    data_iter=test_loader,
                                                    label_type=opt.data_type,
                                                    save_path=opt.save_path,
```

```
                                                    device=device)
        test_info_file = opt.save_path + '/' + 'test_info.txt'
        # Save indicator information
        file_to_write = open(test_info_file, 'a')
        print("MAE: {} MBE: {} MSE: {} RMSE: {} MAPE: {} Corr: {}".format(
            mae_loss[0], mbe_loss[0], mse_loss[0], rmse_loss[0], mape_loss[0], correlation
        ))
        file_to_write.write("MAE: {} MBE: {} MSE: {} RMSE: {} MAPE: {} Corr: {}\n".format(
            mae_loss[0], mbe_loss[0], mse_loss[0], rmse_loss[0], mape_loss[0], correlation
        ))
        file_to_write.close()
```

9. DNI Calculation

```
    import time
    import os
    import pandas as pd
    import numpy as np
    import pytz

    import math


    dir_path=r"D:\solar\solar\class_res\60I-300H152"

    def dateparse(timestamp):
        return pd.datetime.strptime(timestamp, '%Y-%m-%d %H:%M:%S')

    def read_csv(file):
        # os.chdir(path)
        # filename_list = os.listdir(path)
        data = pd.read_csv(file, encoding = 'gbk', date_parser=dateparse) # Read the
corresponding column from the CSV file
        data.columns = ['TIME', 'measured value', 'predicted value']
        return data


    def ephemeris(time, latitude, longitude, pressure=101325, temperature=12):
        """
        Python-native solar position calculator.
        The accuracy of this code is not guaranteed.
        Consider using the built-in spa_c code or the PyEphem library.

        Parameters
        ----------
        time : pandas.DatetimeIndex
```

```
    Must be localized or UTC will be assumed.
latitude : float
    Latitude in decimal degrees. Positive north of equator, negative
    to south.
longitude : float
    Longitude in decimal degrees. Positive east of prime meridian,
    negative to west.
pressure : float or Series, default 101325
    Ambient pressure (Pascals)
temperature : float or Series, default 12
    Ambient temperature (C)

Returns
-------

DataFrame with the following columns:

    * apparent_elevation : apparent sun elevation accounting for
      atmospheric refraction.
    * elevation : actual elevation (not accounting for refraction)
      of the sun in decimal degrees, 0 = on horizon.
      The complement of the zenith angle.
    * azimuth : Azimuth of the sun in decimal degrees East of North.
      This is the complement of the apparent zenith angle.
    * apparent_zenith : apparent sun zenith accounting for atmospheric
      refraction.
    * zenith : Solar zenith angle
    * solar_time : Solar time in decimal hours (solar noon is 12.00).

References
----------

.. [1] Grover Hughes' class and related class materials on Engineering
   Astronomy at Sandia National Laboratories, 1985.

See also
--------
pyephem, spa_c, spa_python

"""

# Added by Rob Andrews (@Calama-Consulting), Calama Consulting, 2014
# Edited by Will Holmgren (@wholmgren), University of Arizona, 2014

# Most comments in this function are from PVLIB_MATLAB or from
# pvlib-python's attempt to understand and fix problems with the
# algorithm. The comments are *not* based on the reference material.
```

```
# This helps a little bit:
# http://www.cv.nrao.edu/~rfisher/Ephemerides/times.html

# the inversion of longitude is due to the fact that this code was
# originally written for the convention that positive longitude were for
# locations west of the prime meridian. However, the correct convention (as
# of 2009) is to use negative longitudes for locations west of the prime
# meridian. Therefore, the user should input longitude values under the
# correct convention (e.g. Albuquerque is at -106 longitude), but it needs
# to be inverted for use in the code.

Latitude = latitude
Longitude = -1 * longitude

Abber = 20 / 3600.
LatR = np.radians(Latitude)

# the SPA algorithm needs time to be expressed in terms of
# decimal UTC hours of the day of the year.

# if localized, convert to UTC. otherwise, assume UTC.
try:
   time_utc = time.tz_convert('UTC')
except TypeError:
   time_utc = time

# strip out the day of the year and calculate the decimal hour
DayOfYear = time_utc.dayofyear
DecHours = (time_utc.hour + time_utc.minute/60. + time_utc.second/3600. +
         time_utc.microsecond/3600.e6)

# np.array needed for pandas > 0.20
UnivDate = np.array(DayOfYear)
UnivHr = np.array(DecHours)

Yr = np.array(time_utc.year) - 1900
YrBegin = 365 * Yr + np.floor((Yr - 1) / 4.) - 0.5

Ezero = YrBegin + UnivDate
T = Ezero / 36525.

# Calculate Greenwich Mean Sidereal Time (GMST)
GMST0 = 6 / 24. + 38 / 1440. + (
   45.836 + 8640184.542 * T + 0.0929 * T ** 2) / 86400.
GMST0 = 360 * (GMST0 - np.floor(GMST0))
GMSTi = np.mod(GMST0 + 360 * (1.0027379093 * UnivHr / 24.), 360)
```

```
# Local apparent sidereal time
LocAST = np.mod((360 + GMSTi - Longitude), 360)

EpochDate = Ezero + UnivHr / 24.
T1 = EpochDate / 36525.

ObliquityR = np.radians(
   23.452294 - 0.0130125 * T1 - 1.64e-06 * T1 ** 2 + 5.03e-07 * T1 ** 3)
MlPerigee = 281.22083 + 4.70684e-05 * EpochDate + 0.000453 * T1 ** 2 + (
   3e-06 * T1 ** 3)
MeanAnom = np.mod((358.47583 + 0.985600267 * EpochDate - 0.00015 *
            T1 ** 2 - 3e-06 * T1 ** 3), 360)
Eccen = 0.01675104 - 4.18e-05 * T1 - 1.26e-07 * T1 ** 2
EccenAnom = MeanAnom
E = 0

while np.max(abs(EccenAnom - E)) > 0.0001:
   E = EccenAnom
   EccenAnom = MeanAnom + np.degrees(Eccen)*np.sin(np.radians(E))

TrueAnom = (
   2 * np.mod(np.degrees(np.arctan2(((1 + Eccen) / (1 - Eccen)) ** 0.5 *
         np.tan(np.radians(EccenAnom) / 2.), 1)), 360))
EcLon = np.mod(MlPerigee + TrueAnom, 360) - Abber
EcLonR = np.radians(EcLon)
DecR = np.arcsin(np.sin(ObliquityR)*np.sin(EcLonR))

RtAscen = np.degrees(np.arctan2(np.cos(ObliquityR)*np.sin(EcLonR),
                     np.cos(EcLonR)))

HrAngle = LocAST - RtAscen
HrAngleR = np.radians(HrAngle)
HrAngle = HrAngle - (360 * (abs(HrAngle) > 180))

SunAz = np.degrees(np.arctan2(-np.sin(HrAngleR),
                    np.cos(LatR)*np.tan(DecR) -
                    np.sin(LatR)*np.cos(HrAngleR)))
SunAz[SunAz < 0] += 360

SunEl = np.degrees(np.arcsin(
   np.cos(LatR) * np.cos(DecR) * np.cos(HrAngleR) +
   np.sin(LatR) * np.sin(DecR)))

SolarTime = (180 + HrAngle) / 15.

# Calculate refraction correction
Elevation = SunEl
```

```
    TanEl = pd.Series(np.tan(np.radians(Elevation)), index=time_utc)
    Refract = pd.Series(0, index=time_utc)

    Refract[(Elevation > 5) & (Elevation <= 85)] = (
       58.1/TanEl - 0.07/(TanEl**3) + 8.6e-05/(TanEl**5))

    Refract[(Elevation > -0.575) & (Elevation <= 5)] = (
       Elevation *
       (-518.2 + Elevation*(103.4 + Elevation*(-12.79 + Elevation*0.711))) +
       1735)

    Refract[(Elevation > -1) & (Elevation <= -0.575)] = -20.774 / TanEl

    Refract *= (283/(273. + temperature)) * (pressure/101325.) / 3600.

    ApparentSunEl = SunEl + Refract

    # make output DataFrame
    DFOut = pd.DataFrame(index=time_utc)
    DFOut['apparent_elevation'] = ApparentSunEl
    DFOut['elevation'] = SunEl
    DFOut['azimuth'] = SunAz
    DFOut['apparent_zenith'] = 90 - ApparentSunEl
    DFOut['zenith'] = 90 - SunEl
    DFOut['solar_time'] = SolarTime
    DFOut.index = time
    return DFOut

def calculate_dni(time, ghi, dhi):
    ghi_data = pd.DataFrame()
    dhi_data = pd.DataFrame()


    ghi_data['TIME']= pd.to_datetime(time)
    ghi_data['measured value'] = ghi
    dhi_data['measured value'] = dhi

    timezone = pytz.timezone('Asia/Shanghai')


    t1=pd.DatetimeIndex(ghi_data['TIME'], tz = timezone)

    latitude = 31.29
    longitude = 121.2085
    #time = '2021-07-01 17:29:30'

    apparent_elevation = ephemeris(t1, latitude, longitude, pressure=101325.0,
```

```
temperature=16.0)

        print(apparent_elevation)

        degree = (90 - np.array(apparent_elevation['apparent_elevation'])) * np.pi/180 #转化为弧度


        dni_m = np.true_divide(np.array(ghi_data['measured value'] - dhi_data['measured value']), np.cos(degree))
        dni_m = np.around(dni_m, decimals = 2)
        print(dni_m)

        return dni_m


    def calculate_dni_from_twofile(path, save_flag=False, measure_flag=False):  # 从分别的 ghi_file.csv 和 dhi_file.csv 生成 dhi_file.csv
        os.chdir(path)
        filename_list = os.listdir(path)
        ghi_file = ''
        dhi_file = ''
        for file in filename_list:
            if file.find('ghi') >= 0:
                ghi_file = file
            elif file.find('dhi') >= 0:
                dhi_file = file
        print("{}, {}".format(ghi_file, dhi_file))
        # name = csv_to_xls(os.path.join(path, file))
        ghi_data = read_csv(ghi_file)
        dhi_data = read_csv(dhi_file)

        dni_m = calculate_dni(ghi_data['TIME'], ghi_data['measured value'], dhi_data['measured value'])

        dni_p  = calculate_dni(ghi_data['TIME'], ghi_data['predicted value'], dhi_data['predicted value'])


        result = pd.DataFrame()
        result['Time'] = ghi_data['TIME']
        result['dni_target'] = dni_m
        result['dni_predict'] = dni_p
        if save_flag == True:
            file_name = ghi_file.replace('ghi', 'dni')
            #如果想要保存 dni 文件 去掉下一行注释
```

```
            result.to_csv(file_name, index=0)

        if measure_flag==False:
            return ghi_data['TIME'], ghi_data['predicted value'], dhi_data['predicted value'],
result['dni_predict']
        else:
            return ghi_data['TIME'], ghi_data['measured value'], dhi_data['measured value'],
result['dni_target']


    def calculate_dni_from_onefile(file_path, save_flag=False):
        GHI = 'total_Avg'
        DHI = 'diffuse_Avg'
        TIME = 'TMSTAMP'

        data = pd.read_csv(file_path, encoding = 'gbk', usecols = [TIME, GHI,
DHI],parse_dates=[TIME], date_parser=dateparse, header = 1

        ghi_data = pd.DataFrame()
        dhi_data = pd.DataFrame()

        ghi_data['TIME']= pd.to_datetime(data[TIME])
        ghi_data['measured value'] = data[GHI]
        dhi_data['measured value'] = data[DHI]

        print(ghi_data['TIME'])
        dni_m = calculate_dni(data[TIME], data[GHI], data[DHI])

        result = pd.DataFrame()
        result['Time'] = ghi_data['TIME']

        result['dhi_measure'] = ghi_data['measured value']
        result['dhi_measure'] = dhi_data['measured value']
        result['dni_measure'] = dni_m

        if save_flag == True:
            file_name = "dni.csv"

            result.to_csv(file_name, index=0)

        return ghi_data['TIME'], ghi_data['measured value'], dhi_data['measured value'],
result['dni_measure']


    def main():
        os.chdir(dir_path)
        calculate_dni_from_twofile(dir_path, True)
```

```
    # dir_path = r"D:/solar/solar/20211018/20211018.csv"
    # calculate_dni_from_onefile(dir_path, True)


if __name__ == "__main__":
    main()
```

- **Verification**

```
import datetime

import re
import pandas as pd
import numpy as np
import csv
import os
from sklearn.metrics import mean_squared_error, mean_absolute_error
from soupsieve import select

# dir_path = r"D:\PythonWorks\solar_project\Result_8-12" ## win format
dir_path = "/Users/cirtus/Desktop/solar/test/solar/data/" ## 300-300
dir_path = r"D:\solar\solar\class_res" ## 300-300


def dateparse(timestamp):
    #   07/21/21 下午 06 时 34 分 00
    # print(type(timestamp))
    if timestamp.find('-') >= 0:
        time = pd.datetime.strptime(timestamp, "%Y-%m-%d %H:%M:%S")
    else:
        time = pd.datetime.strptime(timestamp, '%Y/%m/%d %H:%M')
    return time


def nRMSE(y, y_hat):
    return np.sqrt(mean_squared_error(y, y_hat)) / np.mean(y)


def RMSE(y, y_hat):
    return np.sqrt(mean_squared_error(y, y_hat))


def nMAE(y, y_hat):
    return mean_absolute_error(y, y_hat) / np.mean(y)


def MAE(y, y_hat):
    return mean_absolute_error(y, y_hat)


def MBE(y, y_hat):
    return np.mean((y_hat - y))
```

```
def MAPE(y, y_hat):
    return np.mean(np.abs(y_hat - y) / y) * 100


def R(y, y_hat):
    mean_p = y_hat.mean()
    mean_g = y.mean()
    sigma_p = y_hat.std()
    sigma_g = y.std()
    correlation = ((y_hat - mean_p) * (y - mean_g)).mean(axis=0) / (sigma_p * sigma_g)

    return correlation

# SS-MAE SS-RMSE
def SS_MAE(y, y_hat, p):
    p_mae = MAE(y, p)
    f_mae = MAE(y, y_hat)
    print("SSMAE :{} {}".format(p_mae, f_mae))
    ss_mae = 1 - (f_mae / p_mae)
    return ss_mae * 100

def SS_RMSE(y, y_hat, p):
    p_rmse = RMSE(y, p)
    f_rmse = RMSE(y, y_hat)
    ss_rmse = 1 - (f_rmse / p_rmse)
    return ss_rmse * 100

def indicators(y, y_hat):
    mae = MAE(y, y_hat)
    nmae = nMAE(y, y_hat)
    rmse = RMSE(y, y_hat)
    nrmse = nRMSE(y, y_hat)
    r = R(y, y_hat)
    mape = MAPE(y, y_hat)
    mbe = MBE(y, y_hat)
    return mae, nmae, rmse, nrmse, r, mape, mbe


def main():
    os.chdir(dir_path)

    dirlist = os.listdir(dir_path)
    # print(dirlist)

    for dir in dirlist:
        file_path = os.path.join(dir_path, dir)
```

```
            filename_list = os.listdir(file_path)
            # os.chdir(file_path)
            print(file_path)

            select_file = []
            for file in filename_list:
                if file.find("ghi") >= 0 and file.find("result") >= 0:
                    select_file.append(file)

            for file in filename_list:
                if file.find("dhi") >= 0 and file.find("result") >= 0:
                    select_file.append(file)

            for file in filename_list:
                if file.find("dni") >= 0 and file.find("result") >= 0:
                    select_file.append(file)

            # print(select_file)
            # exit()

            for file in select_file:
                if file.find("ghi") >= 0 or file.find("dhi") >= 0 or file.find("dni") >= 0:  #
                    file_tag = dir + ' ' + file
                    file = os.path.join(file_path, file)
                    # if file.find("dni") >=0:
                    # head = ["Time", "Measurement", "Nowcasting", "WeightForecst"]
                    print("file \n")
                    print(file)
                    head = ["Time", "Measurement", "Nowcasting"]
                    f = pd.read_csv(file, header=0)
                    f.columns = head
                    print("f \n")
                    print(f)

                    # idx = 0
                    # for ind, date in enumerate(f["Time"]):
                    #     if datetime.datetime.strptime(date, "%Y-%m-%d %H:%M:%S").month >
9:
                    #         idx = ind
                    #         break

                    f['Time'] = f['Time'].map(dateparse)
                    f["month"] = f["Time"].map(lambda x: x.month)
                    f["day"] = f["Time"].map(lambda x: x.day)
                    # print(f["month"].month)

                    # criteria = (f["Time"].month< 8760) & (df.index%2 == 0)
```

```
                # criteria = ((f["month"] == 5 ) & (f["day"] == 30))
                # criteria = ((f["month"] == 5 ) & (f["day"] == 22)) | ((f["month"] == 6 ) &
(f["day"] == 21))
                # criteria = ((f["month"] == 5 ) & (f["day"] == 9)) | ((f["month"] == 5 ) & (f["day"]
== 30)) | ((f["month"] == 6 ) & (f["day"] == 25)) | ((f["month"] == 7 ) & (f["day"] == 1))
                # criteria = ((f["month"] == 4 ) & (f["day"] == 25)) | ((f["month"] == 5 ) &
(f["day"] == 20))
                # f = f[criteria]
                print(dir)
                number = re.findall("\d+",dir)
                print(number)
                late = int(number[1]) // int(number[0])
                print(late)

                y = f['Measurement'].to_numpy()
                # y_hat = f['WeightForecst'].to_numpy()
                y_hat = f['Nowcasting'].to_numpy()
                p = f['Measurement'].shift(late).to_numpy()
                # p = f['Nowcasting'].shift(1).to_numpy()
                # y_hat = p

                # y = np.where(y, y, 1)
                # y_hat = np.where(y_hat, y_hat, 1)
                y_hat = np.where(y_hat >= 0, y_hat, 0)
                print("three")
                ## late



                mae, nmae, rmse, nrmse, r, mape, mbe = indicators(y[late:], y_hat[late:])
                # mae, nmae, rmse, nrmse, r, mape, mbe = indicators(y[late:], p[late:])


                ss_mae = SS_MAE(y[late:], y_hat[late:], p[late:])
                ss_rmse = SS_RMSE(y[late:], y_hat[late:], p[late:])
                print("MAE: {}\n"
                    "nMAE: {}\n"
                    "RMSE: {}\n"
                    "nRMSE: {}\n"
                    "R: {}\n"
                    "MAPE: {} %\n"
                    "MBE: {} \n"
                    "SS_MAE: {} %\n"
                    "SS_RMSE: {} %".format(mae, nmae, rmse, nrmse, r, mape, mbe,
ss_mae, ss_rmse))

                mae = round(mae, 2)
```

```
                nmae = round(nmae, 2)
                rmse = round(rmse, 2)
                nrmse = round(nrmse, 2)
                r = round(r, 4)
                mape = round(mape, 2)
                mape = str(mape) + "%"
                mbe = round(mbe, 2)
                ss_mae = str(round(ss_mae, 2)) + "%"
                ss_rmse = str(round(ss_rmse, 2)) + "%"

                # file_name = "3_another_result.csv"
                file_name = "result.csv"
                file_name = os.path.join(dir_path, file_name)

                if os.path.isfile(file_name) == True:
                    with open(file_name, 'a+', encoding="utf-8", newline='') as csvfile:
                        writer = csv.writer(csvfile)
                        writer.writerow([file_tag, mae, nmae, rmse, nrmse, r, mape, mbe,
ss_mae, ss_rmse])
                        csvfile.close()

                else:
                    field_order = ["file_name", "MAE", "nMAE", "RMSE", "nRMSE", "R",
"MAPE", "MBE", "SS-MAE", "SS-RMSE"]
                    with open(file_name, 'w', encoding="utf-8", newline='') as csvfile:
                        writer = csv.writer(csvfile)
                        writer.writerow(field_order)
                        writer.writerow([file_tag, mae, nmae, rmse, nrmse, r, mape, mbe,
ss_mae, ss_rmse])
                        csvfile.close()


    if __name__ == '__main__':
        main()
```